A Methodology for the Design of Greenhouses with Semi-Transparent Photovoltaic Cladding and Artificial Lighting

James Bambara

A Thesis
In the Department
of
Building, Civil and Environmental Engineering

Presented in Partial Fulfillment of the Requirements
For the Degree of
Doctor of Philosophy (Building Engineering) at
Concordia University
Montreal, Quebec, Canada

August 2018

CONCORDIA UNIVERSITY

SCHOOL OF GRADUATE STUDIES

This is to certify that the thesis prepared

By: James Bambara

Entitled: A Methodology for the Design of Greenhouses with Semi-Transparent Photovoltaic Cladding and Artificial Lighting

and submitted in partial fulfillment of the requirements for the degree of

Doctor Of Philosophy (Building Engineering)

complies with the regulations of the University and meets the accepted standards with respect to originality and quality.

Signed by the final examining committee:

_____ Chair

Dr. Leila Kosseim

_____ External Examiner

Dr. Soteris Kaogirou

_____ External to Program

Dr. Marius Paraschivoiu

_____ Examiner

Dr. Radu Grigore Zmeureanu

_____ Examiner

Dr. Catherine Mulligan

_____ Thesis Supervisor

Dr. Andreas Athienitis

Approved by _____

Dr. Fariborz Haghighat, Graduate Program Director

Friday October 12, 2018 _____

Dr. Amir Asif, Dean

Gina Cody School of Engineering and Computer Science

ABSTRACT

A Methodology for the Design of Greenhouses with Semi-Transparent Photovoltaic Cladding and Artificial Lighting

James Bambara, Ph.D.
Concordia University, 2018

Greenhouse construction is on the rise in response to a growing demand for fresh local produce and the need for a climate resilient food web. In mid-to-high latitude locations, greenhouses that control light to a consistent daily integral can produce crops year-round by employing heating, horticultural lighting and movable screens. Their energy consumption represents a major production cost and is largely dictated by the envelope design. As an increasing number of envelope materials (including energy generating photovoltaic cladding) become available, methods for determining the most efficient design are needed.

A methodology was developed to assist in identifying the most suitable envelope design from a set of alternatives. First, the energy performance was assessed by conducting integrated thermal-daylighting analysis using building energy simulation software. Then, life cycle cost analysis was employed to determine the most cost-effective design. The methodology was applied to the following three case studies for a mid-latitude (Ottawa (45.4°N), Canada) and a high-latitude location (Whitehorse (60.7°N), Canada): 1) semi-transparent photovoltaic cladding (STPV) applied to the roof; 2) comparison of a glass, polycarbonate and opaque insulation on the walls and roof; and 3) design of ground thermal insulation.

For Ottawa, the STPV cladding caused internal shading that was counteracted by augmenting supplemental lighting by as much as 84%, which in turn reduced heating energy use by up to 12%. Although STPV cladding increased lighting electricity use, it generated 44% of the electricity that was consumed for supplemental lighting in the present study and 107% in the future projection study. Currently, STPV cladding is not an economically attractive investment unless time-of-use (TOU) electricity pricing is available. However, in the future, a 23% and 37% reduction in life cycle cost (LCC) was achieved for constant and TOU electricity pricing, respectively. STPV will increasingly become a promising cladding alternative for improving

energy efficiency and economics of greenhouse operations. By reflecting light onto the crops, an insulated and reflective opaque north wall can lower both lighting electricity and heating energy consumption, while reducing the LCC by 2.6%. The use of ground insulation had a positive albeit negligible impact on energy and economic performance.

ACKNOWLEDGEMENTS

Thanks to my supervisor, Dr. Andreas Athienitis, for giving me the opportunity to work on this interesting and challenging multidisciplinary project. I would like to thank Dr. Catherine Mulligan, Dr. Andreas Athienitis, Dr. Marius Paraschivoiu, Dr. Pragasen Pillay, Dr. Fariborz Haghighat, Priyanka Pandey and the other co-researchers involved in the Concordia Institute for Water, Energy and Sustainable Systems (CIWESS) for the opportunity to participate in innovative projects and exchange inspiring thoughts during the various network events. In addition, I would like to thank Dr. Paul Fazio and Dr. Radu Zmeureanu for their kind advice and support throughout my undergraduate and graduate studies, the solar lab colleages, Laurence Miall, and all the other great people in the Building, Civil, and Environmental Engineering department.

The scholarships awarded by Concordia University and the Natural Sciences and Engineering Research Council of Canada (NSERC) Alexander Graham Bell Canada Graduate Scholarship, the J.W. McConnell family, Professeur Hugh McQueen, and funding from the NSERC Smart Net Zero Energy Buildings Strategic Research Network and the CIWESS were very much appreciated and motivating. Thanks to Mitacs and industrial partner s2e Technologies Inc. for the research internship under the Accelerate Grant. My appreciation goes to Lynn Dee, Jiwu Rao, Jaime Yeargans, Joe Rhib, Jacques Payer, Konstantinos Kapsis and William Gagnon for their help with the experimental work and to Laura Bambara, Shawn Katz, Gerald Parnis and Bruno Marcotte for editing.

I am also very grateful for my supportive family and friends!

“The world has enough for everyone's needs, but not everyone's greed.”

— Mahatma Gandhi

DEDICATION

To my grandfather Salvatore who loved growing plants

CONTENTS

LIST OF FIGURES

LIST OF TABLES

NOMENCLATURE

Symbols

A	area (m^2); greenhouse footprint (m^2)
a	coefficient for temperature-dependent CHTC calculations (dimensionless)
ACH	air change per hour of ventilation or infiltration air (hr^{-1})
Amp	amplitude of temperature fluctuation (°C)
AR	annually recurring cost ($)
ARNU	annually recurring non-uniform cost ($)
ARU	annually recurring uniform cost ($)
B	base date (calendar yr)
b	coefficient for temperature-dependent CHTC calculations (dimensionless)
C	cost ($); cost per unit ($ $unit^{-1}$); thermal conductance (W m^{-2} °C^{-1})
c	specific heat (kJ kg^{-1} °C^{-1}); speed of light (m s^{-1})
COP	coefficient of performance of electric chiller
CO2	carbon dioxide mass transfer rate (kg hr^{-1})
CV	control volume size (m)
D	nominal discount rate (%); depth (m)
d	real discount rate (%)
D_h	hydraulic diameter (m)
DLI	daily light integral (mol m^{-2} day^{-1})
E	energy cost ($CAD); electric power generated (W)
e	escalation rate (dimensionless)
E_{AL}	electric energy consumption for lighting (W m^{-2})
E_{AL_r}	electric power rating of light fixture (W)
E_{AL_yr}	annual electricity consumption for lighting (kWh yr^{-1})
EC	annual energy consumption (electricity kWh yr^{-1}, nat. gas m^3 yr^{-1}, propane L yr^{-1})
EF	location-specific emission factor (kg eCO_2 kWh^{-1} or kg eCO_2 m^{-3})
ET_{cst}	latent heat flux constant due to air movement and vapor pressure deficit (W m^{-2})
EV	fuel energy value (MJ m^{-3})
f_{dry}	dryness of the waste (dimensionless)
f_{solids}	waste solids:minerals ratio (dimensionless)
F	fraction (dimensionless); view factor (dimensionless)
GHG	equivalent GHG emissions by source (kg eCO_2 yr^{-1})
G_m	measured incident shortwave radiation (W m^{-2})
h	convective heat transfer coefficient (W m^{-2} °C^{-1})
h_p	Planck's constant (J s)
h_v	latent heat of vaporization of water (kJ kg^{-1})
HW	hourly wage ($ hr^{-1})
I	incident solar radiation (W m^{-2}); inflation rate (%); current (A)
Inv	initial investment cost ($)
k	thermal conductivity (W m^{-1} K^{-1})
L	length (m)
l	thickness (mm)
LCC	life cycle cost ($)

L_w	wiring loss (dimensionless)
m	water mass transfer rate (kg hr^{-1})
M	quantity of organic waste (tonnes yr^{-1})
n	study period for life cycle cost analysis (yr)
N	Avogadro's constant (photons $mole^{-1}$); number of years (yr)
Nb	item quantity (dimensionless)
NFR	net financial results ($ m^{-2} yr^{-1})
NS	net savings ($)
Nu	Nusselt number (dimensionless)
OM&R	operations, maintenance and replacement cost ($)
p	labor time needed to replace a light fixture (hr)
P	lifespan (yr); perimeter (m)
P_{AL}	artificial light lifespan (hr)
P_{AL_max}	maximum period before artificial light replacement is needed (yr)
P_{AL_repl}	period before artificial light replacement is needed (yr)
PE	photon efficiency (μmol J^{-1})
P_{op}	light fixture annual operating period (hr yr^{-1})
PP	photoperiod (hr day^{-1})
PPF	photosynthetic photon flux of the light fixture (μmol s^{-1})
PPFD	photosynthetic photon flux density (μmol m^{-2} s^{-1})
PV	present value cost ($)
Q	energy flux (W)
Q_{heat}	energy consumption for heating (kJ hr^{-1} or W)
Q_{heat_yr}	annual energy consumption for heating (GJ yr^{-1})
R	thermal resistance (m^2 °C W^{-1})
Re	Reynolds number (dimensionless)
Repl	replacement cost ($)
Res	residual value ($)
$S_{destroyed}$	anaerobic digestion efficiency (dimensionless)
S_t	savings in operational costs ($)
t	year from base date (yr)
T	temperature (°C)
TLI	light integral supplemented per simulation timestep (mol m^{-2})
ts	time shift (d)
U	U-value (W m^{-2} $°C^{-1}$)
V	greenhouse volume (m^3); voltage (V); volumetric flow rate (m^3 hr^{-1})
V_{avg}	speed of recirculating water (m s^{-1})
V_{wind}	wind speed (m s^{-1})
W	water cost ($); width (m)
WCH	water change per hour (hr^{-1})
X	capacitance multiplication factor (dimensionless)
y	year from base date (yr)
Y	revenue from crop sales ($)
$Y_{methane}$	theoretical yield of methane (Nm^3 CH_4 kg^{-1} dry organic solids degraded)
α	shortwave radiation absorptance (dimensionless)
β_{PV}	PV module temperature coefficient (% $°C^{-1}$)

Δ	change in value (dimensionless); measurement error
δT	rate of change of temperature (°C)
δt	rate of change of time (s)
Δt	timestep (hr)
$\delta\omega$	rate of change of air humidity ratio ($kg_{water}\ kg_{dry\_air}^{-1}$)
ε	emissivity of surface (dimensionless)
η	efficiency (dimensionless); change in value (%)
θ	incidence angle (°)
λ	wavelength (nm)
μ	dynamic viscosity ($kg\ m^{-1}\ s^{-1}$)
ρ	shortwave radiation reflectance (dimensionless); density ($kg\ m^{-3}$)
σ	Stefan-Boltzmann constant ($W\ m^{-2}\ K^{-4}$)
τ	shortwave radiation transmittance (dimensionless)
ω	air humidity ratio ($kg_{water}\ kg_{dry\_air}^{-1}$)

Subscripts

0	initial
a	air
AGH	alternative greenhouse
AL	artificial light; artificial light fixture
ar	arable soil layer
ARNU	annually recurring non-uniform
ARU	annually recurring uniform
aux	auxiliary
BCGH	base case greenhouse
boil	boiler
c	crop surface
cds	condensation
con	concrete
cond	conduction
conv	convection
cool	cooling
cpl	coupling between thermal zones
crop	crop; crop photosynthesis
de	deep earth
dehum	dehumidification
dep	depreciation
e	effective
E	energy
el	electricity
elec	electrical
ET	evapotranspiration
f	floor
fan	air mixing fan
fert	fertilization

FF	forecasted future value
fr	window frame
g	clear-glazed portion
gains	internal heat gains
gas	natural gas; methane
GH	greenhouse
glass	glass
gnd	ground
heat	heating; heating system
hum	humidification
HVAC	heating, ventilation and air conditioning
i	greenhouse air; surface or element i
inf	infiltration
ins	insulation
inst	installation
int	interest
inv	inverter; investment
j	surface j
lab	labor
l	lower
lwr	longwave radiation
m	moisture; measured value
maint	maintenance
mat	material
max	maximum
min	minimum
mov	movable insulation
NIR	near infrared radiation
o	outside air
p	constant pressure; peak; thermal output of boiler that satisfies the peak demand
PAR	photosynthetically active radiation
poly	twin-wall polycarbonate
pv	photovoltaic (module); portion of STPV covered by PV cells
PVGH	photovoltaic greenhouse
refl	reflected portion
repl	replacement
SATE	surplus air thermal energy
si	inside surface; inside surface i
sink	light fixture heat sink
sj	inside surface j
so	outside surface
soil	soil
sol	solar
sp	setpoint
STC	standard testing conditions
stor	storage

STPV	semi-transparent photovoltaic glazing
struc	structure
swr	absorbed shortwave radiation
t	transmitted
tax	tax
th	thermal
top	top airnode (zone above TSS)
tot	total
TSS	thermal shading screen
u	upper
var	variable
vent	ventilation
w	water
yr	year

Abbreviations

1D	1-dimensional
2D	2-dimensional
3D	3-dimensional
AD	anaerobic digester/digestion
AL	artificial light
AGH	alternative greenhouse
ASHRAE	American society of heating, refrigerating and air conditioning engineers
BCGH	base case greenhouse
CAD	Canadian dollar
CFD	computational fluid dynamics
CHP	combined heat and power
CHTC	convective heat transfer coefficient
CO_2	carbon dioxide
DC	direct current
DLI	daily light integral
D-PE	double inflated polyethylene film
E	east
eCO_2	equivalent carbon dioxide emissions
EC	environmental chamber
EPS	expanded polystyrene
ETFE	Ethylene tetrafluoroethylene
GES	greenhouse energy simulation
GHG	greenhouse gas
HID	high intensity discharge
HVAC	heating, ventilation and air conditioning
ins.	insulation
LCC	life cycle cost
LCCA	life cycle cost analysis
LED	light emitting diode

LWR	longwave radiation
MH	metal halide
N	north
NFR	net financial result
NIR	near-infrared radiation
NPV	net present value
NSERC	Natural sciences and engineering research council of Canada
OM&R	operations, maintenance and replacement
PAR	photosynthetically active radiation
PE	polyethylene
poly	polycarbonate
PPF	photosynthetic photon flux
PPFD	photosynthetic photon flux density
PV	photovoltaic
PVB	polyvinyl butyral
PVGH	photovoltaic greenhouse
S	south
SSEC	solar simulator - environmental chamber
STC	standard testing conditions
STPV	semi-transparent photovoltaics
SWR	shortwave radiation
TMY	typical meteorological year
TOU	time-of-use
TRNSYS	transient system simulation tool
TSS	thermal shading screen
USD	United Stated dollar
UV	ultraviolet
W	west

CHAPTER 1: INTRODUCTION

1.1 Motivation

Crops can be grown in greenhouses to increase yields, provide protection from the elements (e.g. thunder storms, hail, pests), prolong the growing season and provide fresh local produce during the winter period. Fig. 1.1 shows how there has been a steady rise in greenhouse production area in Canada. As the human population continues to increase and the weather becomes more extreme and unpredictable, there will be a growing need for protected cultivation in greenhouses. Growing crops in greenhouses is also an essential component of national food security policy, especially in mid-to-high latitude locations where a cold winter season makes it impossible to grow crops outdoors. Greenhouses can be designed to provide fresh produce year-round near the consumer in all locations of the world by employing heating and supplemental lighting. However, Canada still imports a majority of its produce, especially during the winter (Mukezangango, 2017). This is mainly explained by the fact that exporting countries such as Mexico have lower operating costs (e.g. more sunlight, low cost labor) and the low-tech greenhouse used do not require significant initial capital investments. Meanwhile, technology for advanced greenhouse has been constantly improving thanks to pioneers in countries such as the Netherlands, which were the top exporter of fresh produce in 2013 (Darrach, 2014). These new age greenhouses allow more to be produced with less by employing advanced envelopes, heating and lighting technologies, integrated pest management, automation/robotization, amongst others.

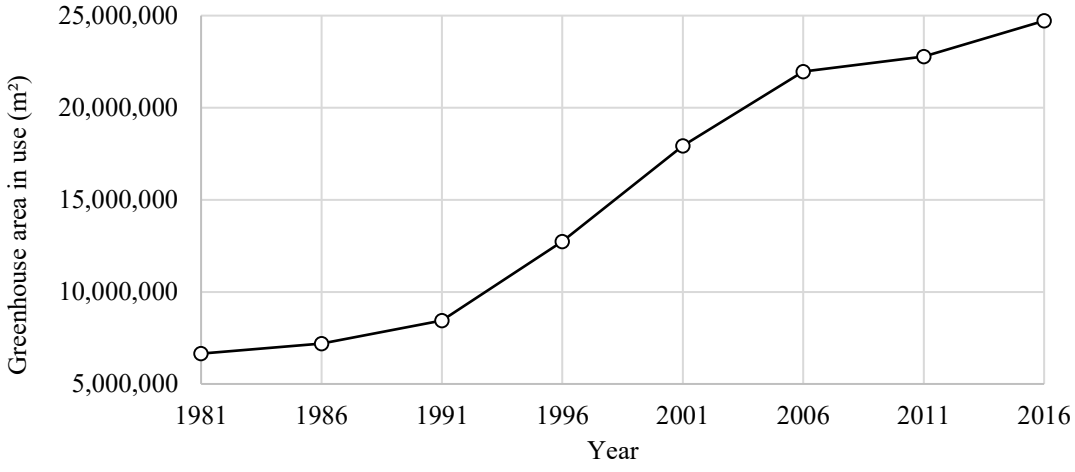

Figure 1.1: Evolution of greenhouse cultivation area in Canada (Statistics Canada, 2018).

Leafy green vegetables (e.g. kale, spinach, swiss chard) are particularly suitable for local production in mid-to-high latitude locations because they require low energy inputs (lower light and temperature requirements) compared to fruiting crops. In addition, these crops perish quickly and can loose a significant amount of their nutrients during transport. This is being further pushed by increased public awareness and the local agriculture movement whereby consumers are demanding higher quality produce (i.e. taste, nutritional value, organic, chemical free), with reduced waste and transport-related environmental emissions. Therefore, there will be an increased need for energy efficient greenhouses to grow these crops near the consumer.

Leafy green crops can be produced consistently throughout the year in colder climates by providing the adequate temperature and controlling the light to a consistent daily integral. A basic assumption of this control strategy is that once the initial investment for a horticultural lighting system has been made, they should be designed to provide its maximum benefit. That is, the lighting system and indoor microclimate are controlled to provide consistent crop yield and quality to meet market demand independently of the exterior environmental conditions (e.g. contract growing). This strategy involves carefully controlling the daily light integral by activating supplemental lighting when there is insufficient daylight and using screens when excess insolation exists. These high-performance greenhouses have been investigated by Albright (2000, 2005) to produce leafy green vegetables such as lettuce and spinach in floating raft hydroponic systems that enable high levels of automation (Fig. 1.2).

(a) **(b)**

Figure 1.2: (a) Lettuce production in a greenhouse that controls light to a consistent daily integral in Mirabel, Canada; (b) semi-automated harvesting method (Hydronov, 2018).

The energy consumed for greenhouse climate control represents a major portion of overall production costs in mid-to-high latitude locations. Most of these energy costs are related to heating, ventilation, and air conditioning (HVAC) and lighting requirements, which is greatly dictated by the greenhouse envelope design (i.e. heat and light transmission that occurs through the building envelope greatly influence the thermal energy consumed for heating and the electricity used for lighting). Therefore, it is important to have methods for comparing conventional and innovative (e.g. energy generating photovoltaic cladding) greenhouse envelope design options at the early stages before they are built. This work aims to facilitate the decision-making process for envelope design so that production costs are minimized over the lifespan of the infrastructure and economic viability of the greenhouse operation is enhanced.

1.2 Problem Statement

Technological advances are providing greenhouse owners with an increasing number of cladding options and methods for determining the most suitable design for a given climate and local economic conditions are necessary. Greenhouse envelope design is a challenging task because it must simultaneously consider the interaction between many design elements and weight the impact on key decision-making factors (e.g. indoor climate control, crop growth, economics). Strategic greenhouse envelope design should follow a systematic approach which integrates physical, biological and economic models. However, most prior work focuses on evaluating the performance of alternative designs with respect to energy use or crop yield, for a single design element and climatic location, with economic considerations often omitted from the decision-making process. As an example, Berroug et al. (2011) performed a simulation study to quantify the improvement in thermal performance that can be achieved by covering the north wall of a greenhouse with phase change material. In another numerical study, Carlini et al. (2012) calculated that using photovoltaic modules on the south-facing slope of a greenhouse roof can reduce heating and cooling by approximately 10% and 30%, respectively. However, to decide whether these are cost-effective retrofits, the additional initial, operating and maintenance costs associated with the phase change material and photovoltaic module retrofits must be weighed against energy cost savings/revenues and the potential impact on crop yield over the lifespan of the greenhouse.

Vanthoor (2011) provided a methodology for greenhouse design based on climatic, crop yield and economic models. The methodology was applied to design greenhouses for growing tomatoes in Spain and Netherlands using the annual net financial result as a method for economic assessment. The envelope design alternatives were applied to all the surfaces of the greenhouse and consisted of single and double polyethylene film, seasonal whitewash, outdoor shade screen and indoor thermal screen. The indoor climate was predicted using a custom model based on the work of De Zwart (1996). However, the analysis does not cover greenhouse with artificial lighting and the method needed to consider the daylight, lighting and thermal energy domains.

There is a need to build upon the work of Vanthoor (2011) and extend the analysis to the design of greenhouses with artificial lighting. The use of an alternative cladding for these greenhouses will usually change the daylight that is available for photosynthesis, and the amount of artificial light must be adjusted to counteract this effect. For instance, replacing glass with twin-wall polycarbonate would result in higher lighting electricity consumption (due to the lower light transmittance of polycarbonate) and lower heating energy use (due to the higher thermal resistance of polycarbonate). Therefore, the domains of heating/cooling and lighting are interconnected and must be considered together for the holistic envelope design of greenhouses that control light to a consistent daily integral. The climate model must be able to control the artificial light based on daylight availability while considering their effect on the thermal energy consumption. Furthermore, daylight and artificial light provide different spectrums and light conversion efficiencies, and this must be considered by the design method because they are combined to achieve a target daily light integral, which is expressed in number of photosynthetically active photons intercepted by the canopy per square meter per day.

The use of building energy simulation (BES) software such as TRNSYS (Klein et al., 2014) and EnergyPlus (DOE, 2014) for greenhouse climate modeling offers several advantages over the more tedious and less universal process of creating a custom model. The modeling process can build upon previous work that has enabled detailed energy transfer calculations (e.g. shortwave radiation calculations based on view factor matrices, geometric distribution, multiple reflections and transmission of sunlight back outside) and benefit from pre-existing models (e.g. HVAC equipment). It is also convenient for modeling custom multilayered glazing

where the effective optical and thermal properties may be determined using software such as WINDOW (DOE, 2015). However, several shortcomings exist when greenhouses are modeled using BES software and some adaptations of the model are required. For example, an evapotranspiration model is required to account for the process whereby plants convert a fraction of absorbed solar radiation into moisture.

Once the annual energy performance of the greenhouse has been obtained, the economic analysis must be conducted to determine whether a design permutation is viable from an investor's perspective. The annual net financial result provides useful information regarding the potential revenues from operating a greenhouse and payback analysis provides insight into how fast an investment can be recovered. However, these methods are not ideal because they fail to compare design options based on their long-term viability. For instance, the payback period may be shorter for one option but the alternative design (that has a longer payback) may provide a lower cost over the lifespan of the infrastructure. Life cycle cost analysis (LCCA) provides a better assessment of the long-term cost effectiveness of a project because it considers all costs arising from owning, operating, maintaining and ultimately disposing of a project. Furthermore, LCCA can reduce the time and effort needed to compare between alternatives by requiring only the economic items that change between designs to be considered as inputs.

Finally, there is a need for more efficient systems capable of combining renewable energy generation and agricultural production. One such solution is the photovoltaic (PV) greenhouse in which both crop and solar electricity are produced by the same building. Semi-transparent photovoltaics (STPV) can be employed as a greenhouse cladding material as a means to transmit a fraction of sunlight while producing electricity. Most studies on PV greenhouses have focused on daylight (Cossu et al., 2017), energy consumption (Carlini et al., 2012), energy generation (Emmott et al., 2015) or the effect on crop growth (Minuto et al., 2009). However, there is no previously published work regarding the analysis of greenhouses equipped with STPV cladding and artificial lighting. When STPV is applied to greenhouses that control light to a consistent daily integral, shading occurs that is counteracted by increasing supplemental lighting, which in turn will presumably reduce heating energy use. Therefore, the incremental cost for STPV cladding must be weighed against changes in the cost associated with electrical and thermal energy consumption and revenues from the sale of generated solar electricity.

1.3 Objectives

The aim of this research is to assist designers in the process of selecting between conventional and solar optimized envelope options so that the energy efficiency and economic viability of the greenhouse operation is improved. The specific objectives include:

- **Develop an integrated thermal-daylight modeling methodology** for greenhouses with artificial lighting using BES software. This process requires the identification of necessary adaptations for modeling greenhouses using the software and discussion of limitations regarding their use. For a given greenhouse design and climate, the modeling method must be able to quantify the amount of photosynthetically active radiation from sunlight that is received by the crop canopy, control the supply of artificial lighting to achieve the target daily light integral, and translate its effects to the thermal energy model.
- **Develop a methodology for the envelope design of greenhouses** with artificial lighting by combining the integrated energy analysis with life cycle cost analysis. The methodology should be able to determine the most cost-effective design from a set of discrete envelope design alternatives that may be applied to each surface of the greenhouse (walls, roof and ground).
- **Identify and compare methods for modeling STPV cladding** using BES, whereby temperature-dependent electrical efficiency calculations and the thermal response of the greenhouse to PV electricity generation are considered.
- **Establish methods for modeling detailed ground heat transfer** in greenhouses characterized by separate crop and floor zones.
- **Demonstrate the use of the proposed design methodology** through relevant case studies in a mid-latitude and high-latitude location. The first case study will evaluate the potential for replacing a glass roof with single-sided and bifacial STPV cladding, for various fractions of PV coverage, using two electricity pricing scenarios and, current and future efficiency of PV and horticultural lighting technology. In the second case study, conventional glass will be compared to twin-wall polycarbonate and opaque reflective insulation installed on the walls and roof. The third case study evaluates the benefit of various ground insulation configurations.

1.4 Scope

The methodology is intended to assist with the envelope design of greenhouses that control light to a consistent daily integral. These greenhouses are suitable for mid-to-high latitude locations where winter daylight levels are not compatible with consistent crop yields. The methodology can be applied to any greenhouse geometry, orientation, and glazing/screen configuration. For practical purposes, the cases studies consider a single greenhouse geometry and orientation for two designs locations that represent average (mid-latitude) and extreme (high-latitude) weather conditions. The evaluation of whether artificial lighting should be used in the first place, and which type of horticultural lighting technology and screen control strategies are most suitable is beyond the scope of this analysis. The methodology can be applied to greenhouses that employ other types of supplemental lighting control strategies but potential changes in crop yield should be accounted for in the economic analysis.

1.5 Outline

This thesis follows the manuscript-based format. Chapter 2 provides the relevant background knowledge and a review of literature and technology pertaining to the design, modeling, energy efficiency, and integrated energy systems for greenhouses. The methodology that was developed for the envelope design of greenhouses that control light to a consistent daily integral is presented in Chapter 3. In Chapter 4, the design methodology was applied to evaluate the potential for replacing a conventional glass roof with crystalline silicone STPV cladding in Ottawa Ontario, Canada (45.4°N, mid-latitude). Various PV area ratios (10-50%) and present and future efficiencies of photovoltaic and horticultural lighting technology were assessed. A study for determining the most cost-effective envelope design between glass, twin-wall polycarbonate and opaque insulation for each surface of a greenhouse located in Ottawa is presented in Chapter 5. Chapter 6 presents the modeling approach for calculating detailed ground heat transfer and the analysis for determining the most cost-effective ground insulation design configuration (vertical perimeter and horizontal configurations applied to greenhouses with a concrete slab, unfinished soil and a raft hydroponic system) for Ottawa. The conclusion presented in Chapter 7 summarizes the results and the main contributions of this work and provides recommendations for future research in this field. The values of greenhouse design and economic parameters used for the case studies are presented in Appendix A and B, respectively.

A comparison of two approaches for modeling STPV cladding using BES software and experimental calibration is provided in Appendix C. Appendix D extends the analysis of Chapter 4 to evaluate the potential for bifacial STPV cladding and the impact of time-of-use electricity pricing for Ottawa. The analyses of Chapter 4, 5 and 6 was repeated for Whitehorse, Yukon, Canada (60.7°N, high-latitude) and presented in Appendix E, G and J, respectively. Appendix I presents the analysis for a ground consisting of a raft hydroponic growing system for both locations. The sensitivity analysis of net savings to energy model, operation and economic parameters for Chapter 4, 5 and 6 are presented in Appendix F, H and K, respectively. Appendix L compares of the energy performance of a greenhouse and vertical farm equipped with STPV cladding. Appendix M presents a study which highlights the potential for integrating organic waste recycling and greenhouse agriculture in Canada.

CHAPTER 2: BACKGROUND AND LITERATURE/TECHNOLOGY REVIEW

2.1 Commercial Greenhouses

For commercial greenhouse owners to generate a profit, the revenue from crop sales must exceed the total operating expenses. The initial investment cost for greenhouses mainly includes the cost of the land, building and machinery/equipment. The choice of the structure and envelope materials is a major component of the building's upfront cost and greatly influences the crop yield and energy consumption because it is through the envelope that heat and light transmission occur. Therefore, the greenhouse envelope should be designed for the specific crop type, local climate and economic conditions. The major production costs for greenhouses are described by Laate (2013) and listed below:

- **Capital interest:** Interest a sum paid for the use of capital. It is charged for the use of investment capital. Had the capital not been invested to buy a specific asset, it could have been used elsewhere and would have provided some alternative revenue.
- **Depreciation:** This represents the loss in value of an asset over time, mainly because of obsolescence. For buildings and equipment, it is that portion of the decrease in value resulting from the passage of time.
- **Property and business taxes:** Taxes on real estate include payments made on the assessed value of the greenhouse operation less any assessment for the greenhouse operator's residence or operations other than the greenhouse. There is a business tax on greenhouses located in urban municipalities.
- **Labour costs:** Hired labour costs include the amount of wages and any benefits received by the hired workers.
- **Production materials and supplies:** Expenses for the purchase of seeds, fertilizers, chemicals, growth media, etc.
- **Heating costs:** The cost for proving heating using fuels (natural gas, biomass, etc.) or electricity (for heat pumps).
- **Electricity costs:** The electricity consumed for artificial lighting, fans, pumps, controllers, refrigeration, etc.
- **Water costs:** The water consumed for irrigation, cleaning, evaporative cooling, etc.

- **Transportation expenses:** Expenses for trucks or other vehicles owned or transport services utilized for the greenhouse operation.
- **Repairs and maintenance costs:** Maintenance costs included repairs to greenhouse structures, equipment (e.g, boilers), tractors and all other machinery and equipment associated with the greenhouse operation.
- **Marketing charges:** Amount paid by each greenhouse operator for having their products marketed.
- **Miscellaneous costs:** This may include legal and accounting fees, office supplies, membership fees, insurance costs and other costs incurred in a greenhouse operation, but not reported under any other heading.

As an example, the breakdown of production costs for growing cucumber in Alberta, Canada are illustrated in Fig. 2.1. For this mid-latitude location, the labor (26%) and energy costs (23%) are nearly equal and represent the largest components of total production costs. Year-round crop production in greenhouses located at mid-to-high latitudes typically entails high energy costs due to the cold climate and low water costs because it is relatively plentiful. Energy efficient greenhouse design can play an important role in lowering operating costs and enhancing the profitability of greenhouse operations. The greenhouse management must evaluate all the production processes and their cost and evaluate methods to improve efficiency. A major barrier for the expansion of greenhouse operations that are located at mid-to-high latitudes in developed countries is the cost of energy and labor. For example, when comparing the cost of tomatoes grown in Mexico with Canada, the labor costs is significantly lower, and the greenhouses do not require heating or artificial lighting. The additional transport cost for importation is small compared to the lower operating expenses. For this reason, greenhouse operators are constantly seeking ways to improve production efficiency (for instance, by reducing energy use and amount of growing supplies, increasing production efficiency and crop yield, reducing labor costs through automation/robotization). Fortunately, domestic greenhouse operations are benefiting from the growing demand for local produce due to its improved quality/taste, higher nutritional value and fair-trade standards.

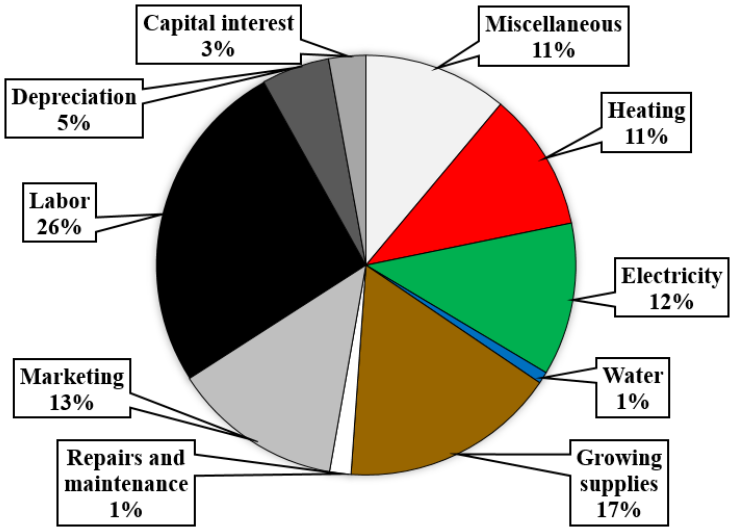

Figure 2.1: Breakdown of cucumber production costs in Alberta, Canada (Laate, 2013).

2.2 Climate Control

Depending on the desired crop growth performance, there can be many environmental parameters that need to be controlled in a greenhouse. The most significant are the air temperature and irrigation/fertilization. More advanced greenhouses will also control the humidity, carbon dioxide (CO_2) and lighting levels. The desired climate inside a greenhouse is maintained by using the appropriate equipment, sensors and controllers. A description of the key environmental parameters and equipment that is commonly used to control them is discussed next.

2.2.1 Temperature

An unheated greenhouse will have large fluctuations in air temperature because the envelope transmits a lot of solar radiation during the day (air temperature rises above outside) and looses heat quickly at night. The comfort air temperature for most plants is 18-24°C and growth is improved when the nighttime temperature is lower than the daytime (Climax Conseils, 2014). To avoid damaging the crops, heating is employed when the air temperature drops below approximately 10°C. Some winter hardy crops (e.g. kale) can grow until the temperature drops below freezing. During the day, the sunlight can cause the air temperature to rise above the comfort level of plants (above 28°C is generally not desirable). Ventilation (replacing inside air with outside air) is the main method for removing the excess solar gains. This can be achieved

using natural or forced ventilation. In the case of natural ventilation, the flow of air through the openings in the greenhouse structure is induced by pressure difference. Forced ventilation systems are indispensable when the rate at which heat is generated inside the greenhouse is higher than the rate of heat removal through natural ventilation. In this case, a mechanical device must be used (e.g. a fan or a blower) to increase the rate of air exchange. The ventilation rate may be increased to as high as 60 air changes per hour (ACH) during warm sunny periods (Jackson and Darby, 2006).

Greenhouse temperature control is achieved by using various types of HVAC equipment and ensuring that it is distributed to the proper location. Unit heaters have been the heater of choice for many growers because of their low capital and installation costs, reliability and ease of staging. The heat is commonly produced by burning natural gas because of its low cost. When the combustion takes place inside the greenhouse, it also produces CO_2 which can improve crop growth. For large greenhouses, a central hot water boiler is a popular choice. The heat can be distributed into the greenhouse using water-to-air heat exchangers, radiant heat pipes or through floor heating. Cooling of the greenhouse air is usually achieved by evaporative cooling, whereby heat is removed from the air by evaporation of water (converting sensible heat into latent heat).

2.2.2 Humidity

Humidity is another important climate factors in a greenhouse influencing the processes of plant photosynthesis and transpiration. Both too low and too high humidity levels negatively affect plant growth and the development/quality of the greenhouse crops. Water that is absorbed by the roots moves upward through a transport tissue (xylem). This flow enables the distribution of nutrients required for the proper growth of a plant. Water that is not retained by the plant and not used in various chemical processes is lost through the transpiration to the atmosphere. Water vapour is expelled mainly through the stomata (pores in the leaf and stem surface). The amount of water that is transpired is regulated by the opening and closing of the stomata. Relative humidity in the range of 60-90% is optimal for the growth of many greenhouse plant species (Kittas et al., 2012). To ensure that the relative humidity is maintained at a desired level both heating and ventilation are commonly used. In some cases, humidification and dehumidification are also used to control the inside humidity. During the day, excess humidity from evapotranspiration is commonly removed by ventilating. At night, several ways can be used to

reduce the humidity. Certain types of envelopes enable sufficient condensation for controlling humidity. As the thermal resistance of the envelope increases, the need to rely on humidity control via heating the inside air, ventilation or mechanical dehumidification increases (Campen et al., 2003). Ventilating increases the need for heating whereas dehumidification requires electricity. Therefore, optimal designs should evaluate the choice of the envelope and heating and humidity control systems together. At night, for single-glazed greenhouses, ventilation could be stopped or reduced to approximately 1 ACH, whereas for double-glazed covers, up to 4 ACH may be required to remove humidity and compensate for reduced condensation on the glazing (Jackson and Darby, 2006; Climax Conseils, 2014).

2.2.3 CO_2

During photosynthesis, crops utilize the lights energy to combine water and CO_2 and produce food (carbohydrates) while releasing oxygen. The generic formula of photosynthesis is:

$$6\,H_2O\ +\ 6\,CO_2 + light\ energy\ \rightarrow\ C_6H_{12}O_6 + 6\,O_2 \tag{2.1}$$

Crop growth is affected when CO_2 levels are too low. The CO_2 in the air is replenished through ventilation and/or CO_2 fertilization. In a closed greenhouse concept, there is no ventilation and therefore humidity, temperature and CO_2 are controlled using an external source of energy and CO_2 fertilization (Adams et al., 2007).

2.2.4 Air circulation

Plants require some air movement to remove heat and humidity (prevents disease) and provide CO_2 to the leaves. Air circulation also helps plants to build strength. Mixing of the inside air also helps to reduce the problem of air stratification. Air circulation is commonly achieved using horizontal airflow fans (for horizontal airflow) and/or ceiling fans (for vertical mixing).

2.2.5 Light

Natural light: The solar energy flux (shortwave radiation) at earth level is within the wavelength region between 300 and 2500 nm. As illustrated in Fig. 2.2, it consists of an ultraviolet (UV, 300–400 nm), a portion that is mainly active for living organisms (~400–700 nm) and an near-infrared (NIR, 700–2500 nm) portion.

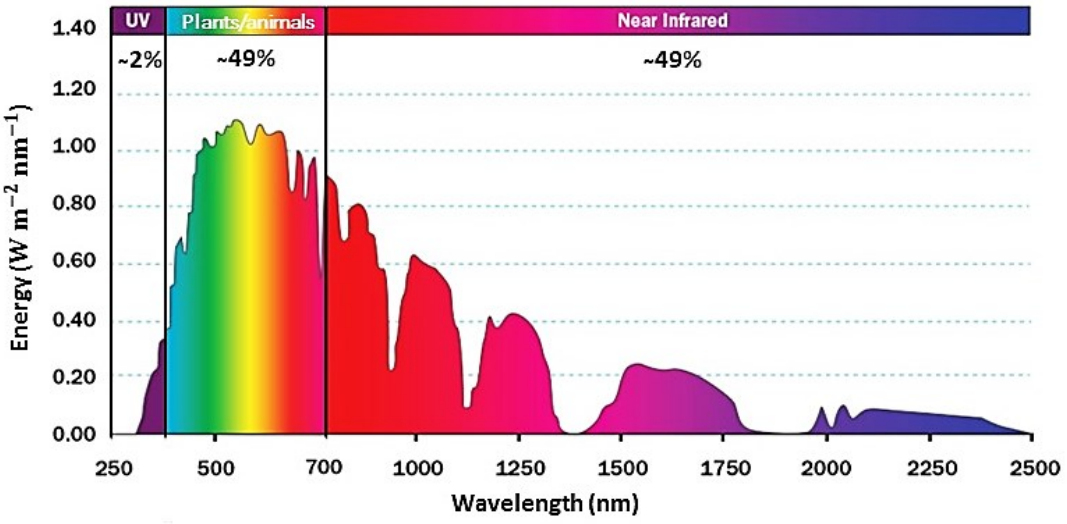

Figure 2.2: Solar spectrum (ASTM E 891) divided into an ultraviolet (UV) portion, a portion that is mainly active for living organisms, and a near-infrared (NIR) portion (Ewing, 2018).

Plants and humans perceive light very differently from one another. Humans and many other animals use something called photopic vision in well-lit conditions to perceive color and light. Lumens are a unit of measurement based on a model of human eye sensitivity in well-lit conditions, which is why the model is called the photopic response curve (Fig. 2.3). As you can see, the photopic response curve is bell shaped and shows how humans are much more sensitive to green light, than blue or red light. Humans may not be efficient at perceiving light in these regions, but plants are highly efficient at using red and blue light to drive photosynthesis (Fig. 2.3). As shown in Table 2.1, the shortwave radiation is measured in irradiance and is commonly used in thermal energy computations whereas daylight requirements for humans is measured in illuminance and in photosynthetic photon flux density (PPFD) for plants.

The photosynthetically active radiation (PAR) measure of radiant power is important in evaluating the effect of light on plant growth. McCree (1972) showed that the photosynthetic response correlates better with the number of photons than with energy. This is expected because photosynthesis is a photochemical conversion where each molecule is activated by the absorption of one photon in the primary photochemical process. PAR is defined in terms of photon flux, specifically, the number of moles of photons in the radiant energy between 400 nm and 700 nm. One mole of photons is 6.0222 x 10^{23} photons (Avagadro's Number). Some plant scientists want a conversion for the photon flux in the 400 nm to 800 nm band although it is currently not the standard PAR metric.

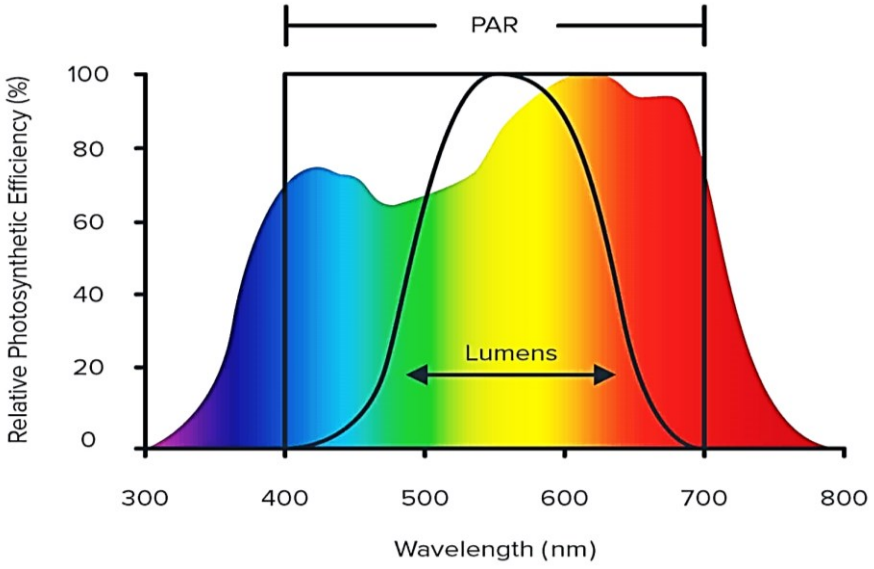

Figure 2.3: Effect of wavelength on relative photosynthesis compared to human response curves in the radiant energy between 300 nm and 800 nm (Crazy-leds, 2018).

Table 2.1: Comparison of terminology for sunlight and its perception by humans and plants

	Sunlight spectrum	Light for humans	Light for plants
Radiant power (~400-700 nm)	-	Lumens	Photosynthetically active radiation (PAR)
Incident light on surface	Irradiance	Illuminance	Photosynthetic photon flux density (PPFD)
Units	W m^{-2}	lux	µmol of photons m^{-2} s^{-1}

In general, plants development depends on the quantity, duration and spectral quality of light that is available. A lot of research is being conducted to understand the effect of the PAR spectrum on crop growth, yield and health (Pinho et al., 2012; Dzakovich et al., 2015; Hernández and Kubota, 2014). This knowledge can be used to design artificial lights whose spectral power distribution matches the crop growth needs and avoids wasting energy. For instance, it has been found that chlorophylls have maximum sensitivities in the blue and red regions, around 300-400 nm and 600-700 nm, respectively (Pinho et al., 2012). Consequently, the design of light emitting diode (LED) horticultural lighting has focused on delivering this spectrum, amongst others, for crop growth (Fig. 2.4c). A plant in vegetative stages requires more blue light whereas fruiting and flowering stages require more red light. However, some crops (e.g. a study for tomatoes by Dzakovich et al., 2015) are more efficient than others (e.g. baby leafy greens) at making use of all the PAR radiant energy (i.e. light quantity is more important than quality).

Light requirements: A suitable measure for quantifying the amount of sunlight received by crops is the daily light integral (DLI), defined as the number of photons intercepted by the canopy per square meter per day (mol m^{-2} day^{-1}), which represents the cumulative PAR radiant energy impinging on a crop over a day. This measure is more appropriate than the amount of total shortwave radiation (expressed in J m^{-2} day^{-1}) because DLI only considers the light that can be used by plants. Furthermore, it is the most suitable measure for quantifying the total light when it is provided from different sources (e.g. sunlight and artificial lighting). The amount of light may also be controlled based on the amount of incident sunlight per week rather than per day. The daily light integral in a greenhouse varies between 1 and 35 mol m^{-2} day^{-1} (Dorais, 2013). However, leafy greens need DLI of 8-22 mol m^{-2} day^{-1} and the harvest stages of fruiting vegetables (e.g. tomatoes, peppers, cucumbers) require as least 25 mol m^{-2} day^{-1} (Dorais, 2003; Albright, 2000). Artificial lighting may be used in greenhouses to provide high quality products year-round in mid-to-high latitude locations but is energy and capital intensive. Therefore, high yield must be maintained to justify its use. For instance, Albright (2000) has demonstrated that the yield of lettuce harvested after 35 days can be increased by 86% by controlling light to 17 mol m^{-2} day^{-1} instead of 8 mol m^{-2} day^{-1}.

Artificial lighting: The amount of sunlight that is received by the crops depends on the envelope design. Depending on the crop lighting requirements, artificial lighting and shading screens may be required. Shading systems are typically employed when the accumulated sunlight is above the desired DLI, when the intensity it too high, or to prevent overheating. Historically, supplemental lighting has been achieved using high intensity discharge lights (HID) such as high-pressure sodium (HPS) and metal halide (MH). The most commonly used artificial light source in greenhouses is HPS lamps that are available as 400, 600 and 1000 W fixtures. Modern single-ended HPS lights have electronic ballasts (Fig. 2.4a). The next generation HID lights are double-ended (Fig. 2.4b). HPS lamps emit a wide peak at green-orange wavelengths but emit very little blue and violet light (Fig. 2.5a). Metal halide light emit more blue light are often used for vegetative growth in the absence of sunlight (e.g. cannabis) (Fig. 2.5b). MH lights are less efficient than HPS and have a shorter lifespan. High intensity LED have many advantages over conventional HID fixtures, such as the ability to control the output spectrum, dimmable control, higher energy efficiency and longer lifespan. HID fixtures produce both PAR and NIR (wasted energy) radiant energy whereas LED fixtures are designed to provide only PAR (Fig. 2.5c). The

high cost of LED has restricted their use to specific applications (e.g. space-based plant growth facilities, plant factories), but rapidly decreasing cost and efficiency improvements will presumably increase the market for LED in greenhouses in the near future. One disadvantage of high intensity LED lamps is that the entire fixture requires replacement whereas only the light bulb is replaced for HID fixtures (ballasts need replacement approximately every decade).

Supplemental lighting can be applied during the day or at night, provided that the photoperiod (lite hours per day) remains at the appropriate value. In general, photoperiods of 12-24 hr day^{-1} can be used for leafy greens whereas fruiting crops prefer 14-20 hr day^{-1}. For HID lights, on/off cycling can reduce bulb lifespan and therefore low amount of light (50-300 µmol m^{-2} s^{-1}) may be supplemented either all day, in the early morning or late afternoon periods, or after sunset until the desired DLI is obtained. The optimal control of the shading screens and lighting system has been extensively researched by Albright (2000). LED are suitable for dimmable lighting whereby the light intensity can be adjusted (Pinho et al., 2013).

(a) **(b)** **(c)**

Figure 2.4: Three types of fixtures for greenhouse applications: (a) single-ended HID fixture with electronic ballast and MH (left) and HPS (right) bulbs (Grow lights, 2018); (b) double-ended HPS fixture (Gravita, 2018); (c) high intensity LED fixture (Illumitex, 2016).

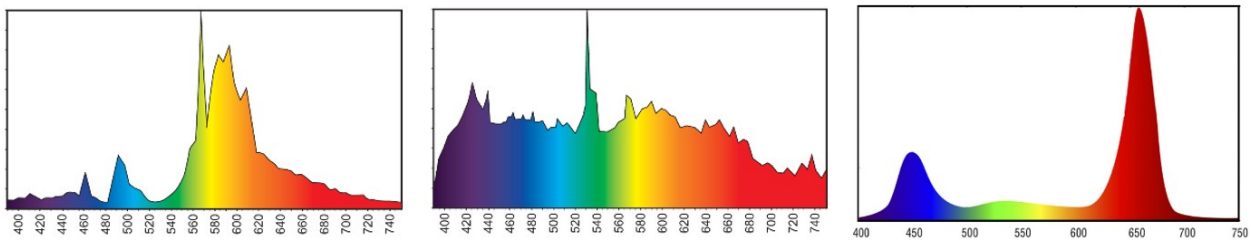

(a) **(b)** **(c)**

Figure 2.5: Spectral power distribution provided by a: (a) HPS bulb (Hortilux, 2018); (b) MH bulb (Hortilux, 2018); (c) LED fixture, F3 spectrum (Illumitex, 2016).

As shown in Table 2.1, the performance of artificial lighting fixtures can be evaluated using the photon efficiency (ratio between the total emitted number of moles photons in the PAR region per second and the total input power), the electrical efficiency (ratio between the total radiant power within the PAR region and the total input power), the bulb/fixture lifespan (the lifespan provided for HID fixtures is for the bulbs – ballasts also require periodic replacement – whereas presently for LEDs, the entire fixture needs replacement), and the initial, operation, and maintenance costs. It is important to consider the lifecycle cost when comparing fixtures because they have different efficiencies (affects electrical and HVAC energy use) and bulb/fixture lifespans. The fact that they have different spectral power distributions can further complicate the performance comparison. For instance, LEDs may be designed to deliver photons in the PAR spectrum only whereas HID lamps provide both PAR and NIR photons. Therefore, the initial cost of the fixture expressed in price per Watt is somewhat misleading because it does not consider the relative usefulness of the output photons. Nelson and Bugbee (2014) performed an economic analysis to compare LED and HID fixtures for greenhouses applications. The five-year electric plus fixture cost per mole of photons was 2.3 times higher for LED fixtures, due to high capital costs. LED horticultural fixtures are still in their early stages of deployment and have the most potential for efficiency gains (Pinho et al., 2012). The unique ability of LED fixtures to efficiently focus photons on specific areas can be used to improve the photon capture by plant canopies. To make most use of the emitted light, manufacturer's use lighting software (e.g. Calculux by Philips, 2018) to determine the optimal fixture spacing and height above the canopy so that the PPFD is as uniform as possible. Specifications for several types of horticultural lighting fixtures are provided in Table 2.2.

Table 2.2: Specifications of greenhouse light fixtures (Grow lights, 2018; Pinho et al., 2012; Dorais, 2013; Gravita, 2016; Ushio, 2018; Illumitex, 2016, 2018).

	Photon efficiency ($\mu mol\ J^{-1}$)	Electrical efficiency (%)	Lifespan (hr)	Initial cost ($\$\ \mu mol^{-1}$)
Single-ended HPS	1.7-2.1	30%	5,000-24,000	0.16-0.19
Double-ended HPS	2.1	N/A	10,000	0.13-0.17
Single-ended MH	1.25	25%	5,000-12,000	0.21
Double-ended MH	1.8	N/A	6,000	0.19
LED	1.8-2.3	35-45%	50,000	1.00-1.30

Crop production cycles: The amount of light may also be varied depending on the desired crop production cycle (to maximize yield) and the stage of crop growth (to reduce energy use). It is

desirable to supplement daylight with enough light to provide the optimal DLI and photoperiod. To maximize production cycles and enable a cleanup period, the seedling stages is commonly performed in propagation facilities and delivered to the greenhouse at 2-6 weeks old. Fig. 2.6 illustrates the production periods and Table 2.3 provides the DLI and photoperiod for lettuce (12 cycles yr^{-1}), tomatoes (summer and winter harvest cycle, 1 cycle yr^{-1} with potentially more by intercropping) and cannabis (4 cycles yr^{-1}) that may be achieved by using artificial lighting and the appropriate screens in greenhouse agriculture.

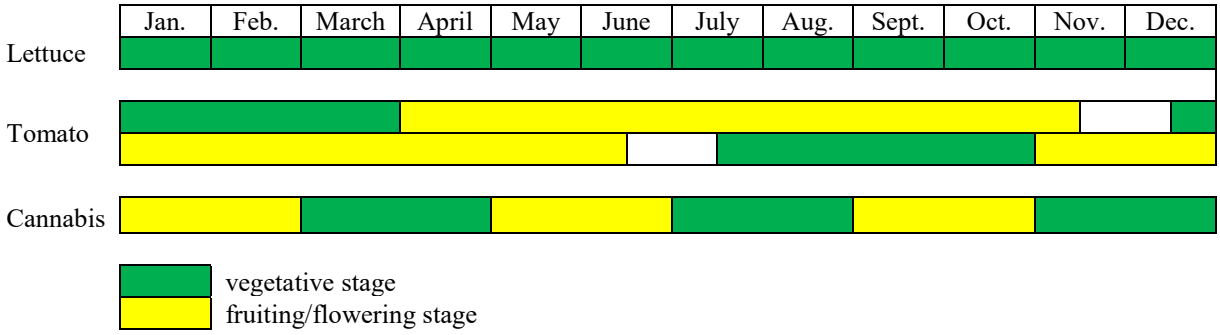

Figure 2.6: Production periods for leafy green, fruiting and flowering crops (Brechner et al., 1996; Elmhirst, 2006; Gravita, 2016).

Table 2.3: DLI and photoperiod for leafy green, fruiting and flowering crops (Gravita, 2016; Lumigrow, 2018).

	DLI vegetative stage (mol m^{-2} day^{-1})	DLI fruiting/ flowering stage (mol m^{-2} day^{-1})	Photoperiod vegetative stage (hr day^{-1})	Photoperiod fruiting/ flowering stage (hr day^{-1})
Lettuce	17	-	18-24	-
Tomatoes	15	25-40	18-20	18-20
Cannabis	42	42	18-24	12

2.2.6 Irrigation/fertilization

In addition to light and CO_2, plants require water and nutrients for growth. The main parameters to be monitored at the root zone include humidity, temperature, pH, oxygen level, carbon, plant available nutrients and microbial activity. There are several techniques for irrigating crops and this can influence the evaporation rate from the growth medium. The lowest cost option is planting directly in the ground with water and nutrients provided by soaker hoses or by drip irrigation. For soilless agriculture, irrigation and fertilization techniques consist mainly of nutrient film technique, drip irrigation, ebb and flow and aeroponics. Industrial agriculture

fertilization has been performed by adding synthetic fertilizer and using pesticides, which largely destroys soil microbiology. Fortunately, awareness is growing on the benefits of organic agriculture and healthy soil microbiology. The concept of feeding the microorganisms (instead of the plants directly, which in turn improves soil health while unlocking nutrients needed for optimal plant growth) addresses our need for a sustainable food web (Ingham, 1985).

2.3 Types of Greenhouses

There are many types of greenhouse designs available, depending on the available investment capital, the type of crop produced, and the desired growth period and crop yield. The main types that are suitable for mid-to-high latitude locations will be presented next.

2.3.1 Greenhouses for three-season cultivation

Low-cost crop shelters: These greenhouses have a lightweight structure typically covered with a single layer of translucent polyethylene film (Fig. 2.7a). Their purpose is mainly to protect the crops against the elements (e.g. heavy rains, high intensity solar radiation, wind) and improve the growth conditions in spring and fall. Natural ventilation is provided through large openings and usually, there is no heating, artificial lighting (crop growth according to the seasonal daylight availability) or screen employed.

Extended season greenhouses: These greenhouses also grow crops according to the natural light cycle (no supplemental lighting) but utilize some heating or night insulation to extend the growing season by seedlings seedlings in the late winter or early spring and finishing in the late fall or early winter. They are generally used to prolong the growing season for fruiting vegetables (e.g. tomatoes) (Fig. 2.7b). They are typically covered with low cost single or double inflated polyethylene films. Ventilation can be provided by either natural or mechanical means.

2.3.2 Greenhouse for year-round agriculture

Without supplemental lighting: In Canada, it is difficult to harvest fruiting crops during the winter without supplemental lighting. However, the cold period is suitable for growing fruiting crops in the vegetative stage (e.g. conventional production cycle for harvesting tomatoes from April to November, Fig. 2.6). Certain leafy greens (e.g. kale, mustard greens) can be grown in greenhouses throughout the year by maintaining the greenhouse air temperature above freezing.

Therefore, the purpose of these greenhouse it mainly to enable growth in the vegetative stages for fruiting crops and to produce slow growing winter hardy crops using the available daylight and minimal heating, rather than constant high crop yield and speed/number of production cycles. Passive solar design principles are often employed to store solar gains and improve nighttime growing temperature.

With supplemental lighting: In mid-to-high latitude locations, crops can be produced throughout the year using artificial lights. A basic assumption of this control strategy is that once the initial investment for a horticultural lighting system has been made, they should be designed to provide its maximum benefit. That is, the lighting system and indoor environment are controlled to provide consistent crop yield and quality to meet market demand independently of the exterior environmental conditions (e.g. contract growing with target growth cycles). For leafy green vegetables, this strategy involves carefully controlling the DLI by activating supplemental lighting when there is insufficient daylight and using movable screens when excess insolation exists (Fig. 2.7c). For fruiting and flowering crops, supplemental lighting is usually delivered constantly throughout the day (or in the early morning and late afternoon periods) and may be varied according to the stage of growth (Fig. 2.7d). Insolation above the DLI is generally permitted for these crops. Due to the superior level of environmental control, these greenhouses have the highest initial cost and energy consumption. Heating is supplied to maintain adequate growth temperature and evaporative cooling is commonly used to prevent overheating in summer. Humidification, dehumidification and CO_2 fertilization are also used when appropriate.

Indoor cultivation: These grow operations are lite 100% using artificial lighting and have opaque insulated wall constructions. Common designs include warehouse types building and shipping container systems. In general, the plants are grown in a stacked shelve configuration (plant factory) and lite with fluorescent (T8 or T5) and more recently LED grow lights (Fig. 2.7e). Plant factories are advantageous for growing plants that require lower temperature (e.g. microgreens, baby leafy greens) because mechanical cooling of the insulated building can be more effective than cooling all the solar gains inside a greenhouse. They are also an effective way to produce large amount of produce near the consumer in densely populated urban areas (e.g. Japan, Singapore). They can be completely sealed (no ventilation) by dehumidifying the air (which also provides the opportunity for water recovery) and by employing CO_2 fertilization for

optimal growth. A promising application for plant factories include production of temperature sensitive crops such as microgreens in the extreme climates such as the desert (extreme heat and water scarcity). Kozai (2015) has demonstrated that plant factories can be used to produce robust transplants that provide improved growth when moved into a greenhouse compared to plants started directly in a greenhouse. The main barrier for the adoption of plant factories is the initial and operating cost of lighting and HVAC equipment (Harbick and Albright, 2016). Historically, most cannabis operations have been grown in plant factories for security purposes and superior control over growth conditions (typically MH lights are used for vegetative growth and HPS lights for flowering stage), but this consumes enormous amount of energy. Fortunately, competition will progressively move cannabis production towards greenhouses and outdoor production. The concept of growing plants in a multi-story building (vertical farm) to save space has been proposed by Despommier (2011). A simulation by Bambara and Athienitis (2015a) revealed that a four-story vertical farm with STPV cladding in Montreal, Canada generates 49% less solar electricity and consumes up to 31% less heating than a greenhouse of equivalent surface area, whereas their cooling energy demand is approximately equal (Appendix L).

Building-integrated greenhouses: Crops can be grown within the built environment in rooftop and façade-integrated greenhouse concepts (Sun Works, 2007). The heat loss from the underlying building is recovered by the rooftop greenhouse, while the warmer floor temperature can improve thermal comfort in winter. Moreover, rooftop greenhouses are particularly beneficial as they make good use of an otherwise unproductive space that is located near the consumer. The commercial viability of urban rooftop agriculture has been demonstrated by Lufa Farms in Montreal, Canada (Lufa Farms, 2018) (Fig. 2.7f). Grocery stores are an ideal candidate for rooftop greenhouses because they can sell the crops directly on-site, thereby maximizing freshness and minimizing transport costs, which is particularly important for leafy green vegetables. Whole Foods market in Brooklyn, USA, was the first to install a rooftop greenhouse which was designed, constructed and owned by Gotham Greens (Gotham Greens, 2018). Moreover, several synergies exist between the building-integrated greenhouse and the building itself. The greenhouse can supply food, energy (solar and biomass), rainwater, and oxygen to the building, while the building can provide CO_2, moist air and waste heat to the greenhouse. Unfortunately, the deployment of rooftop greenhouses is slow due to high construction costs and stringent regulations.

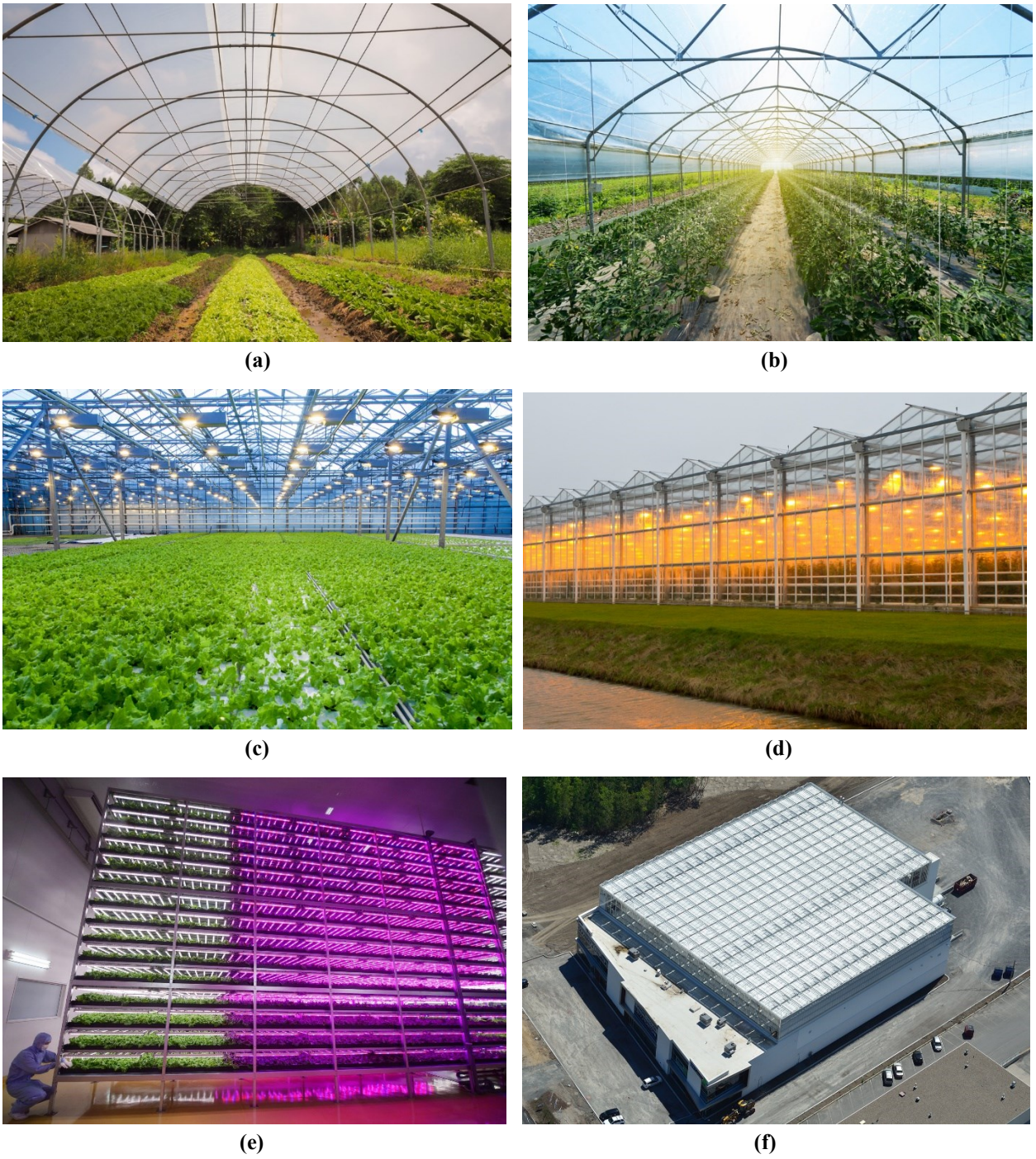

Figure 2.7: Types of greenhouses: (a) low cost hoop house (Shutterstock, 2018); (b) three-season greenhouse for tomato production (Shutterstock, 2018); (c) year-round lettuce production in a high-tech greenhouse that controls light to a consistent daily integral (Shutterstock, 2018); (d) high-tech greenhouse with HPS lighting for year-round tomato production (Shutterstock, 2018); (e) plant factory for growing baby leafy greens and microgreens (National geographic, 2018); (f) rooftop greenhouse (Lufa Farms, 2018).

2.4 Energy Conservation

The factors affecting the energy use in greenhouses are as follows:

- **Location:** The main variables include the outside air temperature and humidity, solar radiation, wind speed, cloud cover and precipitation.
- **Type of crop:** Control of the indoor climate depends on the type of crop produced and the main parameters include the inside air temperature and humidity, light and CO_2 concentration.
- **Crop production cycle:** The production cycles vary according to the level of technology employed to control the indoor environment. The most energy intensive being year-round crop production with ambitious targets for harvest cycles.
- **Design:** The construction parameters that can be varied include the size and shape, construction type, envelope designs (cover materials, screens and ground insulation), condition of the greenhouse cover (cleanliness, age and condensation) and space utilization.
- **Orientation:** This influences the amount of transmitted solar radiation and wind speed.

Greenhouses in mid-to-high latitude locations consume large amounts of energy for HVAC and artificial lighting. Their energy consumption profile depends mainly on the location and the type of crops produced. At low latitude locations, the cost of water can represent one of the highest variable costs. Increasingly, water may be viewed as another component of energy use since it is often treated (waste water treatment plants, desalination) and piped to the farm. For northern climates, the heating energy consumption can represent up to 85% of total energy demand (Runkle and Both, 2011). The innovative seawater greenhouse concept uses 1-5 kWh of electricity to produce one cubic meter of water by humidifying the air intake and condensing the water contained in the exhaust air using relatively cool seawater (Sablani et al., 2003). The rising price of energy has driven much of the research in energy efficiency for buildings. Some of the energy efficiency measures that have been studied for greenhouse are presented next.

2.4.1 Crop production cycle

All crops that do not need to be fresh (e.g. dried, extractions, canning, fermenting) could be grown outdoors or in three-season greenhouses using minimal energy inputs. For instance,

cannabis can be dried and grown outdoors during the summer season rather than year-round production indoors or in greenhouse where it consumes enormous amounts of energy. For fresh produce that must be produced year-round near the consumer, several energy conservation strategies have been developed and are discussed next.

2.4.2 Shape and structure

The shape specifies the area and orientation for heat and light transmission and influences energy use and crop growth. Numerous studies have been conducted to study the shape of single span greenhouses (Lawand et al., 1975; Beshada et al., 2006; Tiwari and Gupta, 2002). Multi-span greenhouses are used for large scale production. These gutter-connected greenhouses reduce heat transmission compared to single span and is easier for workers to maintain the plants. For large scale greenhouses, there is less flexibility in the design of wall and roof configurations. Von Elsner (2000) provided a review of common designs for multi-span greenhouse. Typical roof designs include straight sloped (Venlo, wide-span), tunnel, arched and gothic. The wall height may range from 2-7 meters (Von Elsner, 2000; De Cloet, 2018). Higher walls help to reduce the air temperature at the crop level by ensuring that the solar gains rise and are often accompanied by heating systems (forced air or water pipes) that deliver heat beneath and/or between the crop canopy. Multi-span greenhouses can have a varying degree of openings at the roof for maximizing sunlight penetration and natural ventilation using gutter vents, single ridge and double ridge vents (Westbooke, 2018). The snow load is an important factor to consider when designing the roof so that it may be shed and melted as needed. For high latitude locations where snow is an issue, greenhouse such as the gothic are ideal (Harnois, 2018). A pitch slope with a ratio of at least 1: 2 (26.5°) is common to guarantee proper slippage of snow (Von Elsner, 2000). Generally, lightweight structure made of galvanized steel or aluminum are selected for their long lifespan and to minimize shading. An aspect ratio (the length of a building divided by its width) of 1.2 to 1.3 is often recommended or passive solar houses (Athienitis, 2007). However, such rules of thumb are nor reported for greenhouses.

2.4.3 Orientation

Generally, it's best to orient a greenhouse so that the length runs in the east-west orientation. Harnett (1975) measured 7.4%-10.5% higher solar radiation transmission throughout the year in an east-west greenhouse compared to the same north-south oriented greenhouse,

located in England. Sethi (2009) concluded that an east-west orientation should be preferred at all latitudes except near the equator because a greenhouse with this orientation receives more radiation in winter, when it is most needed.

2.4.4 Heating system

Heating is most commonly achieved using natural gas systems (unit heaters or boilers) or biomass boilers. According to Chau et al. (2009), the installation of a wood pellet boiler in a greenhouse to supply up to 60% of the total heat demand is economical for average or large greenhouses (7.5-15 hectares) in Canada. As flue gas from natural gas boilers is often injected inside greenhouses for CO_2 enrichment (to enhance crop growth), the authors assumed that displacing all natural gas heating with wood pellets would require buying liquid CO_2 for enrichment, which may not be economically feasible. A condensing boiler can convert natural gas into heat at efficiencies of up to 96% (Viessmann, 2017). Heat pump technology is another promising option and units that can operate at low temperatures are being developed. However, grid electricity is subject to power outages whereas fuel and on-site renewable energy generation offers greater grid independency and reliability. Ozgener (2010) investigated a greenhouse heating system consisting of a solar-assisted geothermal heat pump combined with a small wind turbine. Moreover, a promising technology for grid-independent electricity generation are combined heat and power (CHP) engines, whereby the by-products of natural gas combustion, including heat, CO_2, and water, can all be used within the greenhouse (Modak, 2011). The excess heat from the CHP engine can be used to drive absorption chillers to provide cooling (Fig. 2.8a). Other studies have investigated the use of waste heat from power plants or industrial processes (Andrews and Pearce, 2011; Pietzsch and Meyer, 2008).

Providing the heat where it is needed can reduce heating energy use and increase growth by improving the climate around the plants. According to Garzoli (1989), temperature stratification is a major problem in greenhouses. To alleviate this problem, he suggested to supply heat directly to the roots of plants which would allow to reduce the air temperature by 4-5°C. Innovative HVAC distribution systems deliver conditioned air to using flexible plastic ducts that run beneath the plants (Fig. 2.8b). Other designs include floor heating and heated pipes located between the crop canopy.

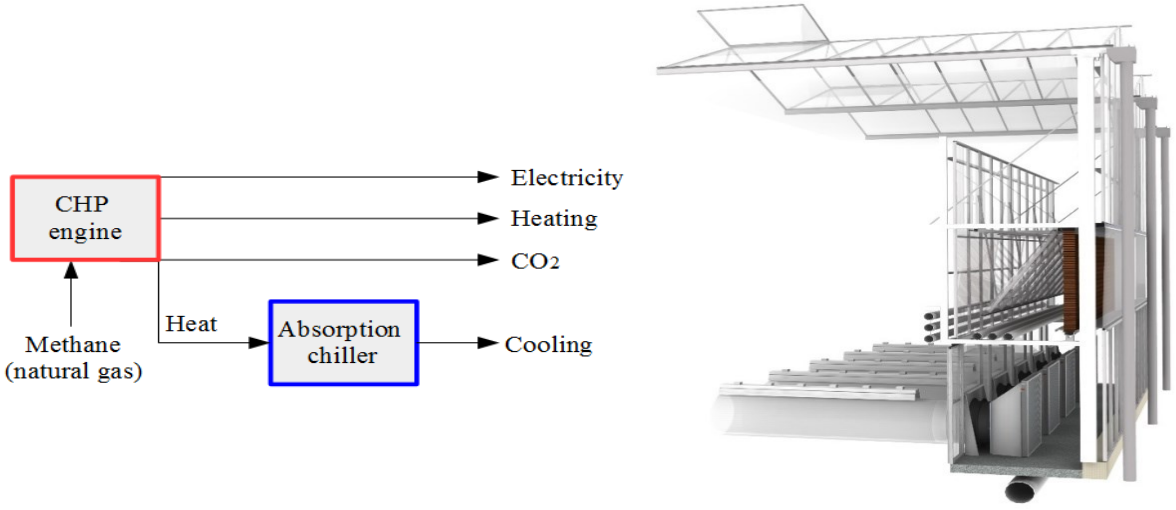

Figure 2.8: (a) Combined heat and power and absorption chiller system; (b) air is centrally conditioned and delivered directly beneath crops using polyethylene ducts (Kubo, 2018).

2.4.5 Lighting

The electricity consumed for lighting can be reduced using high efficiency lighting systems and ensuring that a maximum amount of light is intercepted by the canopy (Table 2.1). However, the benefit of an improved lighting system is less at higher latitudes because the excess heat from the lights can serve to reduce heating energy use. It was estimated the supplemental lighting with HPS lamps contributed about 25–41% of the total heating requirement of a double inflated polyethylene film greenhouse located in Quebec City (Brault et al., 1989). Since Canadian greenhouses are most frequently heated with natural gas, displacing its use for heating by electricity (waste heat from lighting) can reduce carbon dioxide emissions when hydroelectricity is used.

2.4.6 Screens

Most of the energy that is consumed for heating occurs at night, so reducing nighttime heat loss can have a large impact on reducing energy costs. To reduce longwave radiation and conduction heat transfer, movable thermal screens are commonly installed on the interior of the greenhouse envelope and closed from sunset to sunrise. An airtight thermal screen system has an energy savings potential comparable to double glazing at night, and it produces nearly no reduction of light transmittance during the day (Tantau et al., 2011). It is common practice to use a thermal shading screen (TSS), which serves the dual purpose a thermal screen and a shading

screen for blocking excess solar radiation. Hundreds of different screens are available from various manufacturers although most are made from woven aluminum strips and some include a plastic film. They are designed to have a low solar absorptance, high emissivity and typical have a shortwave radiation transmittance of 40-60% (Cohen and Fuchs, 1999).

2.4.7 Glazing

A greenhouse designer can choose from many different glazing materials (section 2.6). They are characterized by their optical and thermal properties. Low iron glass has a very high solar transmittance but a low thermal resistance. Glazing materials with higher thermal resistance generally suffer from reduced light transmission. Hemming et al. (2011) developed a double glazing with anti-reflective coatings that has a similar light transmission as a single glazing but has the advantage of higher thermal resistance. Other double glazings were produced using a combination of anti-reflection and modern low-emissivity coatings, reaching an even higher thermal resistance. The choice of the glazing must be carefully evaluated by considering its effect on energy use, crop yield and economic over the lifespan of the greenhouse.

2.4.8 Ventilation

Selecting openings that promote natural airflow (manually or mechanically operated wall and gutter/ridge openings) is a common method for reducing electricity consumed for mechanical ventilation. The electricity consumed by ventilation fans can be reduced and the microclimate improved by selecting high efficiency motors with variable frequency drives (Teitel et al., 2008). In addition, several techniques can be employed to reduce the amount of heat that is lost3 due to ventilation. The humidity in the greenhouse can be minimized (thereby reducing the need to ventilate for moisture control) by reducing the transpiration level of plants (e.g. by removing the excess leaves) or by dehumidifying with heat recovery. In some instances, selecting a glazing with lower thermal resistance can promote condensation and avoid the need for nighttime ventilation altogether but this increases the heat loss through the envelope (Climax Conseils, 2014). Energy recovery ventilation consists of using heat exchangers to transfer energy between the air exhaust and supply streams, and it is practical in climates with significant heating needs. Rousse et al. (2000) built a counter-flow heat exchanger designed for Quebec greenhouses using thin film polyethylene tubes, and they measured an efficiency of up to 84% with a payback

of three years. The heat exchanger was inexpensive, easy to assemble and maintain, could resist corrosion and mold propagation and could operate satisfactorily even at sub zero temperatures. It is important to weigh the energetic and economic benefits of energy recovery ventilation because of their additional cost, and because pressure drops through the heat exchangers increases fan energy consumption.

2.4.9 Infiltration

The heat loss by air infiltration can be minimized by properly sealing the construction joints and by reducing the air circulation around the greenhouse using wind breaks.

2.4.10 Passive solar design

All greenhouses use passive solar energy, but some greenhouses are designed and constructed to minimize the use of energy for heating/cooling. Common passive solar design principles include having a large glazing exposed to the south, a thermally massive north wall, and collecting/storing the excess solar gains in various forms of thermal mass (water, rock, brick, concrete, sand, phase change materials) for passive or active release. Moreover, greenhouses constructed beneath the ground or using earth-to-air heat exchangers can reduce the need for cooling (ventilation fans or evaporative cooling).

2.4.11 Temperature

In general, plant growth is enhanced when the nighttime temperature is lower than the daytime and this may be used to conserve energy. Using computer models, Elings et al. (2005) investigated several energy conservation measures that were implemented in a representative tomato greenhouse in the Netherlands. One of the eleven tested solutions was to decrease the day and night setpoints of temperature by 2°C. Another was to increase the setpoint of relative humidity from 85% up to 90%. The results showed that the reduction of the temperature setpoint allowed for energy savings of the order of 16%, when compared to the reference case. The increased setpoint of relative humidity resulted in lower energy savings (roughly 5%).

2.4.11 Space utilization

The more plants can be fit into a greenhouse, the lower the energy per unit produced will be. The use of movable benches can increase the available crop production area to 84% as

opposed to 64-70% for traditional longitudinal and peninsular layouts (Sanford, 2011). The use of hanging baskets can also provide additional growing space for plants that require a lot of light, with low light crops positioned in the shaded area beneath.

2.5 Envelope Design

Technological advances are providing greenhouse owners with an increasing number of cladding options and methods for determining the most suitable design for a given climate and economic conditions are needed. The choice of the envelope design affects the physical (e.g. transmitted daylight and associated heating energy use), biological (e.g. light availability and associated crop yield) and economic (e.g. incremental investment cost for alternative cladding) and therefore all aspects must be considered together to obtain an optimal design. Table 2.4 provides a list of the main experimental and numerical investigations that have been conducted to determine the influence of greenhouse envelope design on the crop yield and/or the energy performance. Although these studies provide useful design information, most of them do not result in optimal solutions because the greenhouse design is approached as a single factorial problem whereby economic analysis is often not included in the analysis. There are only a few studies which have attempted to optimize greenhouse design based on crop growth, energy and economic models (Table 2.4). These studies are intended to optimize the design of greenhouses for a specific location or one single construction parameter. A research team in the Netherlands developed a model for optimizing greenhouse design for a broad range of climatic conditions (Vanthoor, 2011). Their model performs a modified controlled random search using parallel computing for maximizing the annual net financial result for growing tomatoes. This design method selects the best alternative for maximizing the economic performance for eight design elements: 1) the type of greenhouse structure; 2) the cover material; 3) the type of exterior shading screen; 4) the whitewash type; 5) the type of interior shading screen; 6) the type and capacity of the heating system; 7) the type and capacity of the cooling system; and 8) the type and capacity of CO_2 enrichment. Each design element is represented by an array of discrete options ranging from three to twelve. For instance, the cover material design element consisted only of a single polyethylene (PE) film, double inflated (D-PE) film and single glass. Their optimization algorithm was applied to design a greenhouse in Spain and the Netherlands.

Table 2.4: Main research activities on greenhouse envelope design.

Type of study	Country	Ref.	Envelope design	Approach	Highlights
Impact of envelope design on energy performance.	Netherlands	Hemming et al. (2006a)	NIR reflecting coatings.	Experimental	• Transmission measured with spectrophotometer. • Wavelengths from 800-1100 nm should be reflected out of the greenhouse. • The best NIR-filtering material has still not been found. • NIR-filtering is not desirable during winter-time.
	Morocco	Berroug et al. (2011)	Phase change material (PCM) applied to north wall.	Numerical	• Simulation for January with 32.4 $kg_{PCM}\,m^{-2}$. • Temperature of plants and air increased by 6-12°C. • Air humidity decreased by 10-15%.
	Germany	Max et al. (2012)	Glazing design comprised of combination of anti-reflection coated glass and ethylene tetrafluoroethylene film.	Experimental	• Hot box system used to measure heat transfer coefficients. • The glass-film concept reduced heat transfer by 38% compared to float glass.
Impact of envelope design on crop yield.	Netherlands	Hemming et al. (2006b)	Use of light diffusing glazings.	Numerical	• Dynamic climate model calculations with INTKAM. • Diffuse light is able to penetrate deeper into the crop canopy. • Sweet pepper production can potentially be increased by 5-6% during summer months due to the use of diffuse greenhouse covering materials.
	Japan	Kadowaki et al. (2012)	Amorphous silicon PV modules were applied to south-oriented side of roof.	Experimental	• Straight-line and checkerboard PV-array configurations covering 12.9% of roof area were tested. • The fresh and dry weight of onion cultivated under the PVs array shadow were significantly less than

					those cultivated in the control greenhouse.
Impact of envelope design on economics.	Spain	Emmott et al. (2015)	Organic PV modules were applied to south-oriented side of roof.	Numerical	• Economic analysis suggests there could be a huge potential for PV greenhouses if aggressive cost targets can be met. • Semi-transparent organic PV devices may struggle to perform better than opaque crystalline silicon with partial coverage.
Impact of envelope design on energy performance and crop yield.	Canada	Papadopoulos and Hao (1997)	Comparison of D-PE, twin wall acrylic panels and glass glazings.	Experimental	• Glazing were applied to separate identical greenhouses for assessing tomato growth over two spring seasons. • Final marketable yield in the D-PE and acrylic greenhouses was similar to that of glass. • The D-PE and acrylic greenhouses decreased heating energy use by 30% compared to the glass.
	Italy	Minuto et al. (2009)	Multilayered copper indium diselenide PV modules partially cover both spans of the roof.	Experimental	• The yield of basil and zucchini crops were not significantly affected when 19% of the roof area was covered with PV modules. • During a four-month period from May to October, solar electricity production was nearly 1300 kWh compared to electricity use of under 100 kWh.
Impact of envelope design on energy performance , crop yield and economics.	Netherlands	Hemming et al. (2010)	Glass versus PE film	Numerical	• The climate and tomato growth inside a greenhouse in Taiwan are simulated using KASPRO. • A glass cover was selected. • The application of a thermal screen is recommended.
	Netherlands	Hemming et al. (2011)	Several prototype glazing (single and	Numerical	• The climate and tomato growth inside a greenhouse are

			double glass) were produced and covered with different coatings (anti-reflection and low-emission).		simulated using KASPRO. • Economic calculations for tomato showed that single and double glasses with anti-reflection coating currently have the highest potentials. • The use of low-emission coatings does not seem to be attractive.
	Netherlands	Speetjens et al. (2012)	Glass, two types of ethylene-vinyl acetate films and two types of PE films.	Numerical	• The climate and tomato growth inside a greenhouse in Taiwan are simulated using KASPRO and INKTAM. • The greenhouse should be covered with a plastic film that is diffuse and has a high transmission of light. • It should also have a high transmission of infra-red radiation.
	Netherlands	Vanthoor (2011)	Glass, PE and D-PE film.	Numerical	• A model-based method to design greenhouses for a broad range of climatic and economic conditions was described. • Glass was selected as cover material, more for its lower annual costs than the slightly higher light transmission. • The Spanish greenhouse benefited most from a seasonal whitewash whereas the Dutch climate favors the use of a thermal screen.
	Italy	Barbera et al. (2017)	Mono-crystalline silicon PV modules installed on upper half of south-oriented roof.	Numerical	• Greenhouse climate was simulated and microalgal yield was calculated based on a validated growth model. • Economic analysis was carried out showing a reduction of biomass production costs when PV is present.

2.6 Envelope Materials

The heat and light transmission that occurs with the outside environment is dictated by the thermal and optical properties of the building envelope (walls, roof and floor). Ideally, in mid-to-high latitude locations, it is desirable to have glazing with a high transmittance to shortwave radiation, a high thermal resistance and a low emissivity/transmittance to longwave radiation. In practice, conventional glazings do not have all these properties and the optimal design can only be identified by conducting energy, crop yield and economic analysis. Many different materials can be used as greenhouse covers. Traditionally, clear glass was the only material available, but plastic materials are now widely used. Glass is the most durable and expensive cover material while flexible films are the least expensive and durable materials. While increasing the insulation of greenhouse cover materials conserves energy, it also decreases condensation and therefore humidity management (which itself consumes energy) becomes more important. This section is divided into three sub-sections which describe different greenhouse cover types: glass, rigid plastics and flexible plastic films (Table 2.5).

Table 2.5: Comparison of glazing material properties (Bartok, 2001; AGC, 2018).

Material	Light transmission (%)	Thermal resistance (m^2 °C W^{-1})	Longwave radiation transmittance (%)	Lifespan (yr)
Glass				
Single	88-93	0.9	3	25+
Double	75-80	1.4	< 3	25+
Acrylic				
Single	90	0.9	< 5	30+
Double	84	1.8-2.0	< 3	30+
Polycarbonate (poly)				
Single	90	0.9	< 3	10-15
Double	78-82	1.6-1.9	< 3	10-20
Triple	74-76	1.9-2.4	< 3	10-20
Polyethylene (PE) film				
Single	87	0.8	50	3-4
Double	78	1.4	50	3-4
Double, with IR	78	2	< 20	3-4
Ethylene tetrafluoroethylene (ETFE) film				
Single	94	0.8	N/A	10-25

2.6.1 Roof and wall envelope

Glass: In Canada, 34% of greenhouses are covered by glass, but only 28% and 13% in the provinces of Ontario and Québec, respectively (Statistics Canada, 2010). Typically, single glass is used for greenhouses, but with rising energy prices, double glass is now sometimes being considered. While it may decrease heating energy consumption, double glass will reduce light transmission unless anti-reflective coatings are used (Hemming et al., 2011). Glass has a high sunlight transmittance (up to 93% for low iron glass), a low thermal resistance and transmittance, a long lifespan, and is easy to clean. However, it is more susceptible to damage by hail than plastic alternatives.

Rigid plastic: In Canada and Ontario, rigid plastics covers 7% of greenhouses while this number rises to 9% for Québec (Statistics Canada, 2010). Polycarbonate panels are available as single layer corrugated sheet and as double or triple multilayered cross sections for improved strength and insulation. Polycarbonate is lightweight making it ideal for rooftop greenhouses and is resistant to hail. Acrylic is available as flat or corrugated sheet and double multilayered cross sections. Its transmittance is slightly lower than glass and is characterized by a high coefficient of thermal expansion and low fire resistance.

Plastic films: In Canada, Ontario and Québec, as much as 60%, 65% and 78% of greenhouse area is covered by plastic film, respectively (Statistics Canada, 2010). Three-season greenhouses typically employ single PE film whereas D-PE is employed for added thermal resistance in heated greenhouses. PE has a relatively high solar transmittance but also the highest transmittance to longwave radiation of all cover materials. It is the lowest cost glazing material and its light weight allows for a low-cost structure, but it has a short lifespan due to degradation by UV radiation. ETFE has the dual advantages of high light transmission and long lifespan.

Opaque/reflective walls: Opaque envelopes such as those used in building construction have been used for plant factories (to cut out sunlight and minimize heat transfer) and cannabis grow-ops (for security purposes). Opaque insulated wall constructions may be beneficial for certain greenhouses, particularly at higher latitudes where long winters can result in unfavorable heat loss to daylight transmission ratios. Thomas (1978) has demonstrated that an opaque reflective material on the north wall can significantly increase the light reaching the greenhouse floor. The

use of opaque wall constructions also offers the opportunity to insulate (reduces heating energy use) or use heat storage materials such as PCM (Berroug et al. 2011) or thermally massive constructions such as sand wall (Beshada and Zhang, 2006). In plant factories, conventional building construction such as insulated stud walls, structurally insulated panels or insulated concrete forms may be employed. Opaque walls may also be achieved by adding permanent or movable insulation on the interior side of conventional glazing. There have not been any prior studies that compare the cost-effectiveness of opaque cladding to transparent/translucent options.

Coatings: Several types of coatings have been developed and applied to glazing materials to increase shortwave radiation transmittance by reducing the reflected light (anti-reflective coating), to reduce longwave radiation transfer (low emissivity coatings) and to increase resistance to UV degradation. Tianhua et al. (2012) have investigated the use of electrochromic film glass in greenhouses to change the optical and thermal properties (opacity and emissivity) in response to changes in voltage. A seasonal white wash (paint) may be used to control light penetration in the summer months.

Spectrally selective glazing: These coatings have been developed to reflect the NIR fraction of sunlight. They are more suitable for hot climates because NIR can help to reduce heating energy use in mid-to-high latitude locations.

Light diffusion: A cover that diffuses the sunlight (high haze) can improve crop yield because the crop temperatures are lower in comparison to a non-haze cover. This is because no direct light falls on the leaves and scattered light is favorable for crop production because more light reaches the lower leaves of the crop (Dueck et al. 2009). Hemming et al. (2006b) performed simulations that indicate that sweet pepper production can potentially be increased by 5-6% during summer months due to the use of diffuse greenhouse covering materials.

Energy generating glazing: These glazings convert a fraction of the sunlight into electricity using the photovoltaic effect. They are covered in detail in section 2.10.1.

Screen systems: Movable screens may be employed to reduce nighttime heat loss while enabling high light transmission during the day (thermal screen), to provide shading from high intensity direct radiation during peak insolation (shading screen) and to completely block out the daylight to control the photoperiod for flowering crops (black-out screens). Shading screen

systems may be located on the interior or exterior side of the envelope. For economic reasons, a single thermal shading screen (TSS) is employed to serve as both a solar shade and thermal screen. When a shading screen and black-out screen are needed, both may be deployed at night to minimize heat loss. There is ongoing research into the benefits of a separate blinds for shading and thermal purposes (Bastien, 2015; Tantau et al., 2011). Shading screens are typically activated when the outside temperature and/or solar radiation exceeds a certain value, or the relative humidity is below a given value, whereas thermal screens are activated when the exterior air temperature drops below a certain temperature (Svensson, 2017; Lorenzo et al., 2004).

2.6.2 Ground envelope design

Thermal insulation may be used to reduce ground heat transfer and plastic films can help reduce moisture transfer from the ground due to evaporation. Heat transfer to the ground can be reduced with a combination of vertical insulation around the perimeter, slanted wing insulation and horizontal insulation beneath the layer of arable soil or finished floor surface. For economic reasons, crops are often planted directly in the soil. This makes it more difficult to install horizontal insulation because the soil must be removed and reinstalled. Historically, the decision to insulate the floor has been based on concerns such as frost protection, condensation control, or improved root zone temperatures rather than for its energy savings potential. The installation of insulation in the ground may be beneficial or not depending on the season and climate. For instance, in lower latitude locations, the relatively cool ground can reduce cooling costs (insulation would not be desired) whereas in mid-to-high latitude locations, long winters entail cooler ground temperatures which can increase heating (insulation may be favorable). In addition, the thermally massive floor can store solar gains during the day and reduce heating when it's released at night. Therefore, the use of perimeter insulation is generally an effective solution as it reduces heat transfer from the relatively cold ground (along the perimeter) while enabling passive solar energy storage.

2.7 Climate Modeling and Simulation

Greenhouse climate models are needed for sizing equipment, to predict the indoor microclimate and to determine the energy consumption, the amount of water transpired by the crop, the amount of CO_2 applied and the dry matter production of the crop for different

scenarios. Depending on the desired outputs, the climate modeling can consist of simplified or detailed analysis. This section is divided into two sub-sections which describe various modeling considerations and the simulation tools that can be used to predict indoor microclimate.

2.7.1 Climate modeling

The dynamic behaviour of the greenhouse microclimate is a combination of physical (energy and mass transfer) and bio-chemical (photosynthesis) processes. The energy transfer considers both sensible and latent heat, whereas mass transfer is for water (moisture) and CO_2. The major energy and mass transfer mechanisms in a greenhouse are discussed next.

Shortwave radiation: The interaction of the greenhouse cover with both direct and diffuse solar radiation determines how much radiation is transmitted and available for crop growth. This can be determined by the optical laws of reflection, absorption and transmission of the greenhouse cover material. For this purpose, the optical properties of the cover and construction, the angle of incoming radiation and the geometry of the construction must be known. The solar radiation that passes through the greenhouse cover can be absorbed/converted by greenhouse indoor components and the remaining portion is lost to the outside. Advanced models will perform separate calculations for determining the transmission of direct and diffuse radiation on each surface, where direct radiation is a function of the incidence angle of the sun. The transmitted shortwave radiation must be distributed on the inside surfaces and the portions that are reflected and re-transmitted back outside can be determined using advanced software. As a rough rule, one-half of the available insolation in the greenhouse is converted immediately to sensible heat added to the air, one-quarter is added as latent heat to the greenhouse air, and the last quarter is usually lost (Albright, 1990; Al-Helal et al., 2011)

Longwave radiation: Heat is transferred between the inside surface of the greenhouse and to the exterior environment via longwave radiation. This heat transfer mechanism is mainly dictated by the material's emissivity and longwave radiation transmittance, and the view factor and temperature difference that exists between the surfaces, the sky and the ground. A simulation study by Lee et al. (2012) found that a model that calculates longwave radiation to the sky with and without a cloudiness factor can lead to deviation up to 5.5% in the greenhouse energy consumption.

Ventilation: Several methods exist for controlling the ventilation rate. A simplified approach is to use a constant minimum ventilation rate and only vary it during the day to avoid overheating. Advanced models can control the ventilation rate based on inside humidity and CO_2 levels. Hellickson and Walker (1983) developed a simple equation can be used to roughly estimate the ventilation rate needed to maintain a specific air temperature inside a greenhouse. Jackson and Darby (2006) provide typical values for summer and winter ventilation rates. Sapounas et al. (2008) and Hemming et al. (2010) used computational fluid dynamic (CFD) simulation software (ANSYS, 2018) to visualize the ventilation efficiency for various design strategies.

Infiltration: The amount of air that infiltrates through the envelope depends on the air tightness of the construction, the difference in inside-outside air temperature, and the wind pressure and direction (Handbook, 2009). Old greenhouse constructions have infiltrations rates of 1-4 ACH whereas for newer constructions it can be as low as 0.5 ACH (ASAE, 2003).

Conduction: The heat is transferred through the walls, roof and ground by conduction. Heat storage in considered for thermally massive constructions elements (e.g. concrete slab, soil) whereas it is usually ignored for the cover materials.

Convection: The thermal resistance of the glazing is relatively low and therefore heat transfer by convection becomes dominant. Many empirical and analytical correlations exist for calculating convective heat transfer coefficient (CHTC). They are typically determined based on the airflow regime (natural, mixed or forced), the direction of heat flow (parallel, upwards or downwards) and the surface geometry (Cengal, 2007). The heat transfer through screens depend on whether to cavity is sealed or ventilated and methods for calculating them can be found in Athienitis (1998) and Bastien (2015). Businger (1963) found the glazing inside CHTC for a greenhouse to be between 1.2 and 4.6 W m^{-2} $°C^{-1}$. A review of CHTC correlations for greenhouse applications was performed by Roy et al. (2002).

Condensation: When water condenses on cold inside surface, some heat is transferred to the surface and moisture is removed from the air. In addition, some of the condensed water evaporates and is transferred back to the air as moisture. This phenomenon is important to consider when the model controls the ventilation rate based on inside humidity levels. Moreover, condensation can increase or decrease the glazing transmittance (Pieters and Deltour, 1997).

The amount of water condensing is a function of the surface-inside air temperature difference, vapor pressure deficit and air movement. Models for calculating condensation have been proposed by Jolliet (1994), Stanghellini and de Jong (1995). Piscia et al. (2012) conducted CFD simulations to calculate condensation.

Crop modeling: Crop modeling typically employs simplified approaches although detailed crop modeling is possible when sufficient growth parameters are known. A rule of thumb states that a 1% reduction in light will decrease crop yield by 1% (Dorais, 2003). Vanthoor (2011) developed a detailed crop model for tomatoes. Simpler models estimate crop production by calculating the net photosynthesis rate of the crop (amount of dry matter produced by the plant). They can be composed of two basic parts: photosynthesis/respiration model and transpiration model, as described in the two heading below.

Photosynthesis and respiration: Photosynthesis models quantify the photosynthesis rate of the crop, the energy spent to keep the crop alive, and the difference between these two values (i.e. the net photosynthesis rate or the dry matter production which includes flowers, fruits, leaves, stems, roots). The maximum conversion efficiency of natural photosynthesis (i.e. solar energy to biomass) in green plants has been estimated to be 4.6–6%. If secondary processing such as growth is also considered, the efficiency will typically not exceed 1–2% under sunlight (Zhu et al., 2008). For this reason, most models ignore the effect of crop growth on the thermal energy balance. The photosynthesis process consumes CO_2 and water whereas they are produced by respiration. The effect of photosynthesis and respiration on the airnode water mass balance is considered by the ET model. When needed, models would also consider the effect of photosynthesis and respiration on the airnode CO_2 mass balance.

Evapotranspiration (ET): This is the combined effect of evaporation (loss of water from the growing medium) and transpiration (loss of water from plants in the form of vapour). They occur simultaneously and there is no easy way of distinguishing between them. Almost all of ET is form evaporation from the sowing stage (when the crop is small) where for full crop cover more than 90% of ET comes from transpiration (Allen, 1998). There is a lot of literature on methods to estimate ET in greenhouses. ET can be measured or estimated by direct or indirect methods. An overview of the evapotranspiration models in greenhouse is described by Fazlil-Ilahil (2009). A simple linear model uses a constant ET rate (to account for respiration) plus another component

that is proportional to the incident shortwave radiation (to account for transpiration during photosynthesis) whereas advanced ET models incorporate the difference in leaf-inside air temperature, leaf area index, vapor pressure deficit, and the aerodynamic and stomatal resistances (Katsoulas and Kittas, 2011).

CO_2 fertilization: CO_2 can be obtained directly from tanks of pure CO_2, by promoting microbial activity inside the greenhouse (e.g. composting as studied by Jin et al., 2009), by extracting it from the exhaust of CHP engines (Modak, 2011) or by burning carbon-based fuels such as natural gas. The latter affects the energy and water mass balance due to the release heat and water in the process.

Humidification: The humidity can be increased by evaporating water (e.g. fan and pad units, mist/fog system) and this process absorbs sensible energy from the airnode. To reduce costs, humidification and absorption cooling can be combined into one system using mist/fog systems (Zwart systems, 2018).

Dehumidification: Dehumidification can be achieved via condensation on a cold surface, ventilation or using a heat exchanger with solid or liquid desiccants. In this case, moisture contained in the air is absorbed/adsorbed by the desiccant, which then must be regenerated with a source of heat to evacuate moisture. Lychnos and Davies (2008) studied the potential of a solar powered liquid desiccant system for greenhouses. Studies using solid absorbing hygroscopic material (Campen et al., 2003) and carbon-based adsorbents (Sultan et al., 2014) for greenhouse dehumidification have also been conducted. Chou et al. (2004) studied the performance of heat pump to meet the heating, cooling and dehumidification requirements in a greenhouse.

Heating: Boilers or unit heaters with exhaust can be used to add sensible heat to the airnode. When unit heaters burn a fuel such as natural gas inside the greenhouse, the produced moisture and CO_2 affect the mass balances.

Cooling: Evaporative cooling is commonly achieved using fan and pad or mist/fog systems (Zwart systems, 2018; Kubo, 2018). This process converts sensible heat (heat removed from the airnode) into latent heat (moisture added to the airnode). Mechanical cooling removes heat and often moisture from the airnode but is rarely used due to its high cost.

Internal heat gains: These result from the use of equipment for HVAC, lighting, air circulation, irrigation, CO_2 fertilization by burning natural gas, etc. Methods for estimating them can be found in Ahamed et al. (2018) and Ganguly et al. (2010).

2.7.2 Climate simulation

Climate models may be used in steady state analysis (e.g. for HVAC equipment sizing) or in transient analysis where simulations using climatic data (usually hourly data from typical meteorological year files) are performed (e.g. to obtain annual energy, water, CO_2 consumption and plant dry matter accumulation). The total set of differential equations used to describe the energy and mass balances may be solved numerically using engineering software (e.g. MATLAB, 2018), BES software (e.g. TRNSYS, EnergyPlus), and greenhouse energy simulation (GES) decision support programs such as KASPRO (de Zwart, 1996), SERRISTE in France (Tchamitchian et al., 2006), HORTEX (Rath, 1992), GREENHEAT (Ahamed et al., 2018).

Many custom models have been developed with varying levels of modeling detail to simulating the climate in greenhouses (Bot, 1983; De Zwart, 1996; Zhang et al., 1997; Hill, 2006). Vanthoor (2011) implemented model-based greenhouse design for different climatic regions with the annual net financial result as an optimisation criterion. Custom modeling enables a high degree of flexibility regarding the interaction between the numerous energy and mass transfer mechanisms. However, developing a model from scratch is a tedious process and is more difficult for others to build upon and modify. Furthermore, it may be difficult to obtain the level of model resolution that is imbedded in BES software (e.g. for complex energy transfer mechanisms such as view factor, shading and insolation matrices).

Energy simulation software including TRNSYS, EnergyPlus, and ESP-r (ESP-r, 2018) is available for simulation of energy requirements in different types of buildings (Crawley et al., 2008). Carlini and Castellucci (2010) discuss how the multizone building model known as Type 56 may be used within TRNSYS to perform a parametric study of a greenhouse. Vadiee (2011) experimentally validated a TRNSYS Type 56 greenhouse model and compared the potential for excess solar heat collection between a ventilated and closed greenhouse. Attar et al. (2013) used TRNSYS to perform a parametric and numerical study of a solar water collector system for heating a greenhouse equipped with a buried heat exchanger. Bastien and Athienitis (2011) used

EnergyPlus to determine the excess solar heat that can be collected from a rooftop greenhouse for use within the building below. Nawalany et al. (2014) adopted the WUFI Plus software (WUFI, 2018) for simulating the thermal performance of various floor designs for a greenhouse using 3-dimensional (3D) transient heat flow.

BES software has several limitations for greenhouse climate modeling such as not accounting for the dynamic heat and mass transfer process caused by ET and condensation in greenhouses. Therefore, some adaptations and additional models need to be included to increase the accuracy of the predicted microclimate. Lee et al. (2012) compared simulation results obtained from KASPRO and ESP-r and listed the additional heat and mass transfer mechanisms that are required for greenhouse modeling using BES software. They concluded that KASPRO is not the most suitable tool for the simulation of innovative greenhouses because it lacks connectivity with other simulation programs for control, extensive HVAC capabilities and airflow modeling.

GES has been carried out using programs specifically designed to calculate the energy and mass transfer between the greenhouse and outdoor environment. De Zwart (1996) developed a greenhouse simulation program to analyse energy performance and crop productivity in Venlo-type greenhouse in the Netherlands, named KASPRO. Hemming et al (2010) and Speetjens et al. (2012) used the KASPRO program to simulate the greenhouse climate for every hour of the year and obtain the energy consumption, the amount of water transpired by the crop, the amount of CO_2 applied and the dry matter production of the crop for different scenarios. The program INKTAM (Elings and Marcelis, 2010) employs light-growth and temperature-growth response curves to calculate the increase in yield that can be obtained with supplemental lighting. Simulations showed that 5% and 30% increase in yield was possible in Taiwan and Netherlands, respectively (Speetjens et al., 2012). These results were then used to feed the economical model to compare design alternatives. “Greenhouse Simulation” is a simplified greenhouse energy model that allows preliminary evaluation of design options under different weather conditions and operational strategies (Fitz-Rodríguez et al., 2010). GREENHEAT was developed by Ahamed et al. (2018) to simulate the heating requirement in conventional greenhouses in cold regions.

2.8 Economic Modeling

Although mass and energy balances provide useful information, they are not sufficient for making investment decisions until they are combined with economic analysis. To assess the viability for operating a greenhouse and to compare various design alternatives, economic analysis may consist of at the analyses described below.

Net financial result (NFR): This measure estimates the potential net profit that can be obtained by investing in a greenhouse operation, typically expressed in \$ m^{-2} yr^{-1}. It accounts for initial construction costs, interest on capital, revenues, depreciation, operation and maintenance costs, etc. Several studies have used the NFR method to identify the most economically viable greenhouse design (Hemming et al., 2010; Speetjens et al., 2012; Vanthoor et al., 2012a,b). The annual NFR (*NFR* in \$ m^{-2} yr^{-1}) can be expressed as (Vanthoor, 2011; Laate, 2013):

$$NFR = C_{crop} - \left[\left(\eta_{int} + \eta_{dep,i} + \eta_{maint,i}\right)/A\right] \cdot \sum_{i=1}^{M} C_{inv,i} - C_{var} - C_{tax} \quad (2.2)$$

where

C_{crop} is the revenues from crop/products sold (\$ m^{-2} yr^{-1})
η_{int} is the interest rate for capital investment costs (% yr^{-1})
$\eta_{dep,i}$ is the depreciation rate for element i (% yr^{-1})
$\eta_{maint,i}$ is the maintenance rate for element i (% yr^{-1})
A is the greenhouse footprint (m^2)
M is the total number of greenhouse elements
C_{inv} is the initial investment cost for element i (includes purchase land, materials, equipment, vehicles) (\$ m^{-2} yr^{-1})
C_{var} is the variable cost (\$ m^{-2} yr^{-1})
C_{tax} is the tax expenses (\$ m^{-2} yr^{-1}).

Payback period: The payback period is the number of months or years it takes to return the initial investment. Simple payback or discounted payback can serve to inform an investor on how fast a greenhouse investment can be recovered. Discounted payback is the preferred method because it requires that cash flows occurring each year be discounted to present value before accumulating them as savings and costs. The payback period can be useful as part of the process for comparing greenhouse design alternatives. However, payback ignores the cash flows beyond

the payback period, thereby ignoring the profitability of the project over the greenhouse's lifespan. Thus, one project may be more valuable than another based on future cash flows, but the payback method does not capture this. Several studies have used the payback period to assess the financial viable of greenhouse design alternatives (Vadiee, 2011; Hussain et al., 2015; Barbera et al., 2017). The payback period is the minimum number of years (y), for which (Fuller and Petersen, 1996):

$$\sum_{t=1}^{y}[(S_t - \Delta I_t)/(1+d)^t] \geq \Delta I_0 \quad (2.3)$$

where

y is the minimum length of time over which future net cash flows have to be accumulated in order to offset initial investment costs
S_t is the savings in operational costs in year t associated with a given alternative ($)
ΔI_t is the additional investment costs in year t, other than initial investment costs ($)
ΔI_0 is the initial investment costs associated with the project alternative ($)
d is the discount rate used to adjust cash flows to present value (%).

Net present value (NPV): This is a measurement of profit calculated by subtracting the present-day values of cash outflows (including initial cost) from the present values of cash inflows over a period of time. After the cash flow for each period is calculated, the present value of each one is achieved by discounting its future value at a periodic rate of return. NPV is the sum of all the discounted future cash flows. Because of its simplicity, NPV is a useful tool to determine whether a project or investment will result in a net profit or a loss. A positive NPV results in profit, while a negative NPV results in a loss. A yearly cash flow diagram allows the investor to visualize the flow of cash and the cumulative cash flow over the project life. Barbera et al. (2017) conducted energy simulations combined with cost benefit analysis to determine the potential for using PV cladding on a greenhouse dedicated to growing algae. Emmott et al. (2015) computed the NPV for greenhouses equipped with organic PV cladding of different efficiencies. If there is a choice between two mutually exclusive alternatives, the one yielding the higher NPV should be selected. NPV does not provide an overall picture of the gain or loss of executing a certain project. To see a percentage gain relative to the investments for the project, usually internal rate of return or other performance measures are used as a complement to NPV.

Sensitivity analysis is often included in NPV analysis to evaluate the risk associated with varying economic conditions.

Life cycle cost analysis (LCCA): LCCA is a tool to determine the most cost-effective option among different competing alternatives to purchase, own, operate, maintain and, finally, dispose of an object or process, when each is equally appropriate to be implemented on technical grounds. All the costs are usually discounted to their present-day value and summed to obtain the NPV. When energy conservation efforts increase the initial capital cost of a new greenhouse, LCCA can determine whether these alternative designs are economically justified from the investor's viewpoint, based on reduced energy costs and other cost implications over the project life or the investor's time horizon. Many design alternatives may be found to be cost effective, but only one can be used in a given application. In such cases, LCCA can be used to identify the most cost-effective alternative for the application. This is generally the alternative with the lowest life cycle cost (LCC). The process of scoping is critical in LCCA, whereby certain aspects of the cost analysis may be omitted if they are the same for the base case and alternative designs. The net savings measure of economic performance is particularly useful for reducing time and effort required for comparing design alternatives. Usually the LCCA term implies that environmental costs are not included whereas the similar life cycle analysis generally has a broader scope that includes environmental costs. Despite its potential for providing detailed financial comparisons, the authors were not able to find any prior work that applied LCCA to greenhouse design. However, LCCA has been applied to study energy efficiency and generation technologies for buildings (Leckner and Zmeureanu, 2011; Marszal et al., 2012). The following is the general formula for the LCC present-value model (Fuller and Petersen, 1996):

$$LCC = \sum_{t=1}^{N} [C_t/(1+d)^t] \quad (2.4)$$

where

LCC is the total LCC in present-value dollars of a given alternative (in $)
C_t is the sum of all relevant costs, including initial and future costs, less any positive cash flows, occurring in year t ($)
N is the number of years in the study period
d is the discount rate (%).

2.9 Integrated Energy Systems

Once the aforementioned energy efficiency measures have been applied to the greenhouse, the next step of low-energy design consists of implementing integrated energy systems to produce renewable energy on-site. This can be achieved most effectively by integrating these systems as part of the building (i.e. building-integrated renewable energy systems). They can come from solar, wind, and biomass sources. Solar greenhouses are designed to maximize the collection of solar energy while providing an environment that is suitable for crop production. Solar energy can be harnessed from the surplus air thermal energy resulting from solar gains and the use of PV cladding. Moreover, a greenhouse produces significant quantities of organic waste which can be ideally co-digested on-site to produce energy and fertilizer. A review of renewable and sustainable energy saving strategies for greenhouse systems is provided by Cuce et al. (2016).

2.10.1 PV greenhouses

Building façades and roofs receive significant amounts of solar radiation, which can be used to generate useful energy on-site. One such solution is the PV greenhouse in which both crop and solar electricity are produced by the same building. By covering the lower perimeter wall of the structure, PV cladding can be integrated onto greenhouses without affecting the sunlight received by the crop. In the past, opaque PV cladding has been employed to cover the south-facing roofs of commercial greenhouses following an east–west orientation (Cossu et al., 2014). A 2.3 MW PV system by Sentinel covers the entire south-facing roof of a six-acre greenhouse and is the largest rooftop installation under the Ontario feed-in tariff program (Fig. 2.9a). Alternatively, STPV can be employed as a greenhouse cladding material to transmit a fraction of sunlight while providing both shading and solar electricity production (Fig. 2.9b). A major drawback of STPV is that they cannot be withdrawn during cloudy days or in winter, when light is limited. However, this could eventually be achieved by incorporating PV material into movable screens.

(a) **(b)**

Figure 2.9: (a) Opaque PV module employed on the south-facing greenhouse roof (Enphase, 2015); (b) STPV modules integrated into a greenhouse roof (Agrithermic, 2018).

Use of generated electricity: During the day, greenhouse electricity demand is relativity small and the solar electricity production can exceed its energy needs. This surplus electricity can either be used by adjacent/neighboring buildings, exported to the grid, or stored for later use on-site. To accelerate the deployment of renewable energy technologies, certain countries or states/provinces have established feed-in-tariff schemes to purchase the generated electricity at a higher rate than grid electricity. PV also has the advantage of generating energy when it is needed most, during periods of peak demand due to air conditioning. Exporting solar electricity to the grid during peak periods can provide higher revenues in locations where time-of-use (TOU) electricity pricing exists. The excess electricity can also be stored in batteries, converted to hydrogen fuel or to natural gas via microbial methanation (Bailera et al., 2017). For instance, a polymer electrolyte membrane electrolyser was employed to convert excess electricity from a PV greenhouse into hydrogen, which is then stored and used in a fuel cell to generate electricity upon demand (Ganguly and Ghosh, 2011).

Types of PV cladding: Various studies on PV greenhouse design have been conducted. Yano et al. (2009) installed amorphous PV modules on the inside of an existing greenhouse structure. However, building-integration of PV materials is a more efficient practice because it replaces the need for conventional glazing. In addition, there is a need to reduce shaded patches inside to greenhouse (which results from using relatively large opaque PV modules) to achieve near uniform crop growth. As shown in Fig 2.10, the most promising designs for generating

electricity from the greenhouse envelope consist of STPV claddings and concentrating PV reflectors. STPV technology can be divided into two categories: shading (Fig. 2.10a) and spectrally selective (Fig. 2.10b). Shading STPV blocks a fraction of the sunlight by using uniformly distributed opaque PV cells (Fig. 2.11a, b) or using thin film technology that provides homogenous transparency (Fig. 2.11c, d). Commercially available shading crystalline silicon STPV modules are comprised of PV cells that are encapsulated between two layers of glass or plastic. Solar electricity can also be generated from the portion of transmitted solar radiation that is reflected by the interior surfaces using bifacial PV cells that are flat (Guerrero-Lemus et al., 2016) or spherical (Cossu et al., 2016).

Second generation solar cells are thin-film technology that are made by depositing one or more thin layers, or thin film of photovoltaic material on a substrate, such as glass or plastic. Thin-film PV cells are commercially used in several technologies, including cadmium telluride, copper indium gallium diselenide, and amorphous thin-film silicon.

Third generation PV technology includes organic STPV cladding that can be designed to be spectrally selective by using semi-conducting polymer materials (with tunable finite bandwidth absorption) capable of harnessing light not required for plant growth. Recently, thin-film and organic STPV technologies have been considered for greenhouse applications due to their transparency, flexibility, lightweight properties and potentially low cost in the future (Emmott et al., 2015). However, organic PV products currently suffer from environmental degradation, lacking effective protective coatings.

Moreover, concentrating PV and PV/thermal systems (Fig. 2.10c) have been proposed for integration with the greenhouse envelope (Sonneveld et al., 2011; Hussain et al., 2015), one of which attaches a NIR reflecting and PAR transmitting material to a concentrator which is the circular curved glass in the south-facing greenhouse cover (Sonneveld et al., 2010). Hussain et al. (2015) found that linear and spot Fresnel lenses concentrating PV systems could have a 70% efficiency and a payback period of approximately 10 years. Aroca-Delgado et al. (2018) provided a review of prior work regarding shading systems, including PV claddings in greenhouses.

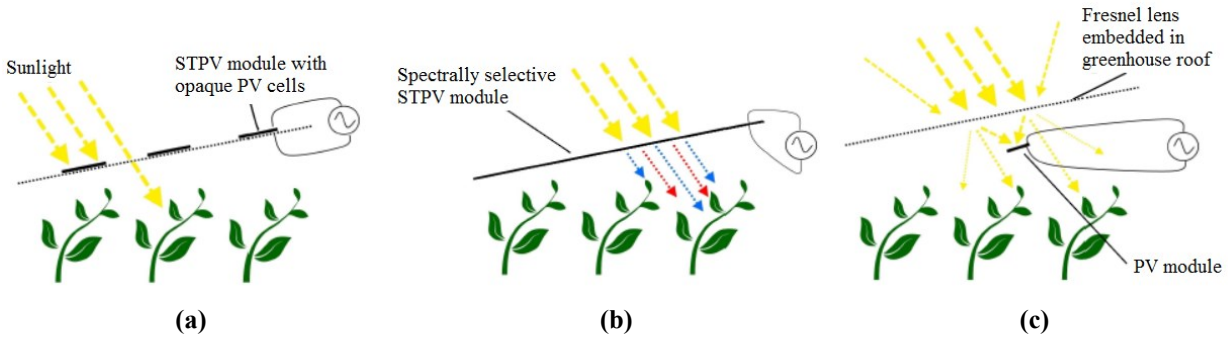

Figure 2.10: Schematics of the various approaches to PV greenhouses (adapted from Emmott et al., 2015): (a) partial shading using STPV modules with uniformly distributed opaque PV cells or opaque modules; (b) spectrally selective organic STPV modules; (c) concentrating of direct light onto PV.

Design considerations for PV cladding: A key design parameter for shading STPV glazing is the amount of light that they transmit. For thin-film STPV this is typically referred to as transparency whereas for crystalline silicon STPV it is the PV area ratio (portion of the glazed area that is covered by PV cells). Commercially available STPV modules vary in efficiency and the available transparency. Crystalline silicon STPV that uses conventional size PV cells can be custom manufactured to provide any transparency, and the efficiency of opaque mono-crystalline PV modules is currently approximately 17% (Canadian Solar, 2017). Bambara and Athienitis (2016) tested an experimental greenhouse concept with faced-integrated mono-crystalline silicon STPV of 48% PV area ratio and obtained an electrical efficiency of 2.9% (11.1% efficiency for the PV cell area) (Fig. 2.11a; Appendix C). Cossu et al. (2016) tested spherical mono-crystalline silicon micro-cells (1.2 mm diameter) sandwiched between glass plates and integrated on a greenhouse roof with 26.5° slope and obtained an efficiency of 0.2% with a 27% PV area ratio (Fig. 2.11b). Cadmium telluride (Fig. 2.11c) thin-film STPV modules of 10% and 50% transparency can convert sunlight into electricity at efficiencies of 10% and 5.6%, respectively (Polysolar, 2018). Sun Well (2018) reports a 6.3% efficiency for their 13.5% and 20% transparency thin-film modules that consist of semi-transparent amorphous silicon and transparent conductive oxide films (Fig. 2.11d). Spectrally selective organic STPV modules have an efficiency of 1.75% (Emmott et al., 2015). The electrical efficiency of PV cells varies with temperature. Due to the PV cell spacing or partial light transmission, shading STPV may have lower temperatures compared to their opaque counterparts, resulting in higher efficiencies.

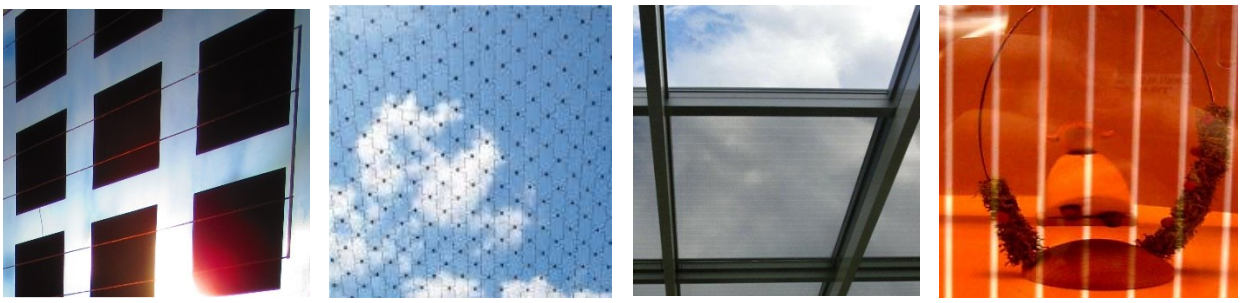

(a) (b) (c) (d)

Figure 2.11: Photographs of various partial shading STPV modules: (a) conventional crystalline silicon PV cells; (b) spherical crystalline silicon micro-cells (Cossu et al., 2016); (c) cadmium telluride thin-film (Polysolar, 2018); (d) amorphous silicon and transparent conductive films (Sun Well, 2018).

Effect of PV cladding on crop growth: Several experimental studies have been carried out to compare crop growth in PV greenhouses compared to a control greenhouse without PV. Ureña-Sánchez et al. (2012) have found that there was no yield reduction for tomato crops (despite negative effects observed on the fruit size and color) grown inside a greenhouse in Almería Spain, when 9.8% of the roof area was covered by amorphous silicon PV modules. Kadowaki et al. (2012) have reported a crop yield loss of 25% for Welsh onions when amorphous silicon PV modules were applied on 13% of the roof area of a greenhouse in Matsue, Japan. Minuto et al. (2009) have reported that the yield of basil and zucchini crops were not significantly affected when 19% of the roof area of a greenhouse located in Sanremo Italy was covered by multilayered copper indium diselenide PV modules.

Effect of PV cladding on shading: STPV cladding can be employed as the roof and/or wall glazing material, though it is more likely to be applied on roof surfaces because they can capture more solar energy. Depending on the greenhouse geometry, the plants will be more or less shaded by the PV surface. In smaller footprint greenhouses, significant light enters from the sides (compared to the roof) and therefore, when some surfaces are covered with PV cladding, undesirable variations in daylight levels can occur within the greenhouse. Large footprint greenhouses with STPV cladding on the roof provides a more uniform light distribution over the crop surface because the effect of transparent side walls is comparatively less. Several daylighting studies have been carried out to study the distribution of light within PV greenhouses. Yano et al. (2010) have performed an experimental and numerical study to

compare the distribution of sunlight inside a greenhouse equipped with a PV array having a straight-line and a checkerboard installation pattern. Fatnassi et al. (2015) have employed CFD software to compare the radiation distribution uniformity for Venlo and asymmetric greenhouse roofs geometries. Castellano (2014) and Castellano et al. (2016) have performed a daylighting analysis by means of the software Autodesk Ecotect Analysis on a greenhouse model with different coverage ratios of polycrystalline PV modules on the roof. Cossu et al. (2017) have developed an algorithm for calculating the direct and diffuse radiation distribution on different canopy heights inside a PV greenhouse. In another study, Cossu et al. (2014) covered the south-facing roof surfaces of a two-span greenhouse located in Sardinia Italy with mono-crystalline silicon PV modules and measured a yearly solar light reduction of 64% compared to the situation without a PV system. This condition decreased the yield of tomato compared to the conventional greenhouses but generated a significant income from PV energy because of European government remuneration policies.

Effect of PV cladding on energy consumption: Detailed energy models are needed to evaluate the effect of STPV cladding design on the overall greenhouse energy performance. Several approaches have been proposed for modeling PV cladding using custom models (Robinson, 2009), BES software such as TRNSYS (Carlini et al., 2012), EnergyPlus (Peng et al., 2016), and CFD (Fatnassi et al., 2015). Carlini et al. (2012) have used the TRNSYS simulation software to create a greenhouse thermal energy model, and annual simulations for three locations in Italy were conducted to compare the energy consumption of a greenhouse with and without opaque PV modules. It was found that the PV cladding can reduce heating and cooling by approximately 10% and 30%, respectively.

PV studies that incorporate economic analysis: Only a couple of studies have been conducted regarding the economics of PV greenhouses. Barbera et al. (2017) performed a cost benefit analysis for a greenhouse dedicated to microalgae production (including the effects of energy and yield) and determined the payback to be approximately 13 years. Emmott et al. (2015) performed economic analysis of an organic STPV greenhouse showing cell efficiencies required to achieve a NPV of zero over a ten-year period.

2.10.2 Thermal Energy Collection and Storage

In addition to generating solar electricity, greenhouses can also be used to collect solar thermal energy. Even when the exterior air temperature is below freezing, the sunlight can cause the greenhouse air temperature to rise above the heating setpoint. This excess solar heat is termed surplus air thermal energy (SATE), which can be collected and stored for later use such as heating at night or delivered to neighbouring/attached buildings (Fig. 2.12a). The heat can be stored for active (e.g. thermal storage and heat exchangers) or passive (e.g. rockbed or tubes buried beneath the soil) release. However, the capacity of heat storage is limited and the efficiencies of heat recovery and supply are low. Another option is to upgrade and store the SATE using a heat pump, heat exchangers, and a thermal storage tank (Fig. 2.12b). Yang et al. (2012) presented the control logic for SATE extraction, which was followed by an experimental study by Yang and Rhee (2013) that found that up to 76.4% of the monthly heating needs of the greenhouse could be supplied using this concept. The SATE was extracted using fan coil units located inside the greenhouse (evaporator), which also served to cool and dehumidify the inside air. A high payback period of 15 years was calculated due to the many heat exchangers and thermal storage tanks required. When thermal energy is also extracted from a PV greenhouse, the system becomes a PV/thermal system. Nayak and Tiwari (2008) experimentally validated a thermal model of a greenhouse equipped with a low-cost PV/thermal system. Sonneveld et al. (2011) used static linear Fresnel concentrators within the greenhouse envelope to produce both hot water and electricity.

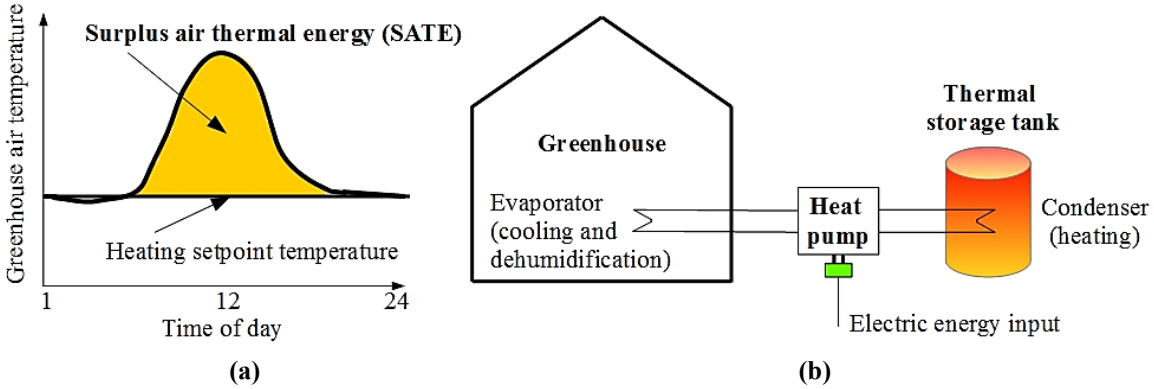

Figure 2.12: (a) Greenhouse air temperature showing SATE; (b) Greenhouse with heat pump for extraction and upgrading of SATE.

2.10.3 Building-integrated wind turbines

Greenhouses can also be equipped with wind turbines to generate renewable electricity. Some views on the potential and challenges for building-integrated wind turbine technology is described by Stathopoulos et al. (2018). Design examples include the roof-mounted ducted wind turbine by Grant et al. (2008), the modern adaptation to the Sistan wind energy mill by Müller et al. (2009), the Crossflex design by Sharpe and Proven (2010), and the three-in-one wind, solar and rain water harvester with a power augmentation guide vane for a vertical axis wind turbine by Chong et al. (2011).

2.10.4 Biomass-to-energy

A strong symbiotic relationship exists between greenhouses and anaerobic digesters (AD). AD can also be combined with greenhouses to make effective use of its outputs, while the greenhouse in turn provide solar energy and organic residues for AD operation. Egigian-Nichols (2013) explains how combining greenhouses with AD would increase the overall economic viability of the project. A Swiss company built a dry anaerobic co-digestion and composting facility in Otelfingen, Switzerland and an adjacent demonstration greenhouse, in which vegetables are grown direct from lumps of digestate and effluent water (Kompogas, 2007). Sturm et al. (2014) studied the potential for using digester biogas in a CHP engine and absorption chiller system to produce electricity, heat, and cooling for a commercial ornamental plant nursery in Germany. In Charlevoix, Quebec, a hydroponic greenhouse operates using energy and effluent water from a dairy farm (De Cotret, 2011). A study by Bambara and Athienitis (2015b) showed how the 9.1 million wet tonnes yr^{-1} of organic waste that is generated in Canada could be used to operate 1.12 million m^2 of new greenhouse agriculture area while producing 1,072 GWh yr^{-1} and 2,070 GWh yr^{-1} of exportable electrical and thermal energy, respectively (Appendix M). The lignocellulosic fraction of greenhouse residues may be more suitable for slow pyrolysis to generate energy and biochar (McHenry, 2009) or gasification to create energy and ash (Manzano, 2007).

Solar energy can be substituted as the prime energy source for AD, allowing the produced biogas to be freed up and directed to higher grade energy requirements elsewhere, such as fuel for waste collection vehicles, or stored for later use. The digester could be placed inside

the greenhouse and undergo passive heating, or the SATE could be collected and used directly. Usmani et al. (1995) found that the erection of a canopy greenhouse around the digester raised the temperature from 20°C (in the conventional system) to nearly 35°C, the optimal temperature for mesophilic AD. However, the direct use of SATE through passive and active approaches does not guarantee that the AD will be heated to the optimal mesophilic setpoint temperature, especially for cold climates. By upgrading SATE using a heat pump, temperatures that are suitable for mesophilic heating can be obtained even on a cold sunny day, where the greenhouse temperature could be as low as 5°C. Curry and Pillay (2015) performed a case study where a heat pump is used to extract and upgrade greenhouse SATE for heating an adjacent digester.

Fig. 2.13 illustrates an integrated anaerobic digester - greenhouse concept, where the greenhouse SATE is collected and stored inside the AD during the day and used to heat the greenhouse at a later point, such as at night. There are several benefits that can result from their combination: 1) the AD biogas can be stored and used as a dispatchable energy source for operating the greenhouse; 2) electricity can be generated from a PV envelope on the greenhouse and AD and SATE can be stored in the thermally massive AD for later use; 3) building integration reduces the energy consumption from heating as compared to building separate systems; 4) the compost and CO_2 fertilizer produced by the AD system can be used to grow plants inside the greenhouse; 5) water can be collected from biogas dehumidification and the CHP engine exhaust; and 6) organic waste and wastewater produced by the greenhouse can be treated on-site, resulting in increased biogas production.

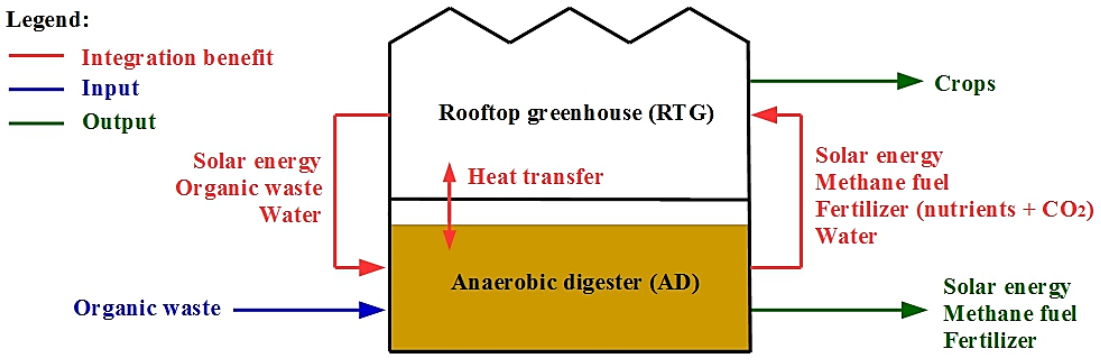

Figure 2.13: Schematic showing the integration benefits of an anerobic digester – rooftop greenhouse system.

2.10 Research Opportunities

Through an extensive literature and technology review, the following major research needs were identified and tackled through this thesis:

- **Integrated thermal-daylight analysis of greenhouses with artificial lighting:** There is a need to describe how an alternative envelope design impacts the interaction between the domains of daylighting, lighting, and thermal energy and to develop a method for obtaining the annual energy performance of a greenhouse using BES software. The combination of daylighting and artificial lighting for crop growth requires the use of PPFD (moles of PAR photons m^{-2} s^{-1}) that is incident on the canopy, as opposed to irradiance (W m^{-2}).
- **Development of a general envelope design methodology for greenhouses with artificial lighting:** There is a need of a method for comparing design alternatives from an investor's perspective. A combined energy and economic analysis is required to identify the most suitable design. Based on the obtained energy performance, a LCCA would be ideal for identifying the most cost-effective design. The net savings method of economic comparison may be used to save time and effort by minimizing the number of required inputs for the comparison.
- **Development of a modeling methodology for STPV cladding:** When STPV cladding is employed, it impacts the daylight availability, artificial lighting control, and the thermal energy aspects. A method that presents how to model single-sided and bifacial STPV of different PV area ratios using BES software is needed. The model must be able to dynamically link the PV electricity generation with the cladding temperature and greenhouse thermal energy consumption.
- **Detailed model for ground heat transfer:** 3D heat transfer analysis is the most suitable method for evaluating the benefits of vertical perimeter and horizontal ground insulation.
- **Demonstrate the use of the design methodology:** Case studies for mid-latitude and high-latitude locations are needed to demonstrate how the design methodology may be used to identify the most suitable envelope alternatives. The cladding options should include conventional and innovative materials that can be applied to the roof, wall and ground surfaces.

CHAPTER 3: DEVELOPMENT OF A METHODOLOGY FOR THE ENVELOPE DESIGN OF GREENHOUSES WITH ARTIFICIAL LIGHTING

The following methodology is intended to assist with the envelope design of greenhouses that control light to a consistent daily integral. In mid-to-high latitude locations, this strategy involves carefully controlling the DLI by activating supplemental lighting when there is insufficient daylight and using movable screens when excess insolation exists. However, as the greenhouse is located at lower latitudes, the need for artificial lights diminishes. This design methodology is intended for greenhouses located in geographic areas where winter daylight levels are not compatible with consistent annual crop production and thus horticultural lighting is required. The analysis of whether artificial lighting should be used in the first place and which type of horticultural lighting technology is most suitable is beyond the scope of this analysis.

The design methodology can be applied to any greenhouse geometry, orientation, glazing and screen types. In particular, it was developed to evaluate the potential for energy generating PV cladding. The analysis consists of comparing the energy and economic performance for a set of discrete envelope design alternative that are applied to one surface of the greenhouse at a time. Typically, the base case greenhouse (BCGH) design would employ the same envelope design on all its surfaces and each of the alternative envelope designs would either provide a higher or lower transmittance to sunlight than the BCGH. When the alternative cladding decreases the transmittance, the surfaces should be evaluated in order of increased solar potential (i.e. the surface receiving the least amount of solar insolation is evaluated first) and vice versa. For instance, if the BCGH consists of a single layer of glass, the alternative envelope materials will decrease the amount of light and so the analysis should proceed by applying alternative designs to the north wall first and the roof last. The methodology can also be used to compare light fixture that provide approximately the same spectrum. For instance, to compare single and double-ended HPS or the latest LED fixtures to older models that have been on the market for a few years.

Furthermore, judgement is needed when alternative envelope materials have significantly different transmittance than the BCGH (e.g. STPV with high PV area ratio/low transparency versus glass) because the shading that is incurred may not be uniform and could lead to unequal

crop growth. The use of advanced daylighting software (e.g. Daysim (Reinhart and Walkenhorst, 2001), AGi32 (2018), CFD (ANSYS, 2018)) could complement the analysis to help visualize internal shading and ensure that uniformity requirements are met or that planting configurations are compatible with local daylight levels. The use of diffusing envelope materials or dimmable LED lighting that is controlled using measurements from distributed light sensors can help to achieve a more even light distribution within the space.

3.1 Integrated Thermal-Daylight Analysis

The climate model consists of the lighting and HVAC energy domains, which are dynamically linked. For these greenhouses, if an alternative envelope design produces a higher internal shading compared to the base case, then the amount of artificial light is increased to counteract this effect. For instance, replacing glass with twin-wall polycarbonate would result in higher lighting electricity consumption (due to the lower light transmission of polycarbonate) but lower energy use for heating (due to the higher thermal resistance of polycarbonate). Therefore, the thermal and lighting domains are interconnected and must be considered together for the holistic envelope design of greenhouses that control light to a consistent daily integral. The climate model must be able to control the artificial light based on daylight availability and transfer their effect on the thermal energy consumption. Consequently, the simulation methodology for these greenhouses should be able to consider both daylighting and thermal parameters, link them in an integrated way, and provide a method for the evaluation of design options based on the obtained performance indices and economic analysis.

The key issue for coupling the two domains is to determine a set of linking parameters that have an impact on both the thermal and lighting performance of the space. Direct links have an immediate impact both on daylighting and thermal performance (e.g. type of glazing). The secondary dynamic link is the artificial lighting control. It is considered a secondary link because, for a given set of direct links, it operates by reading data from the daylighting module and dynamically transfers the effect to the thermal module in the form of resulting internal gains. Fig. 3.1 summarizes the process of coupling and the interactions between linking parameters in the simulation methodology.

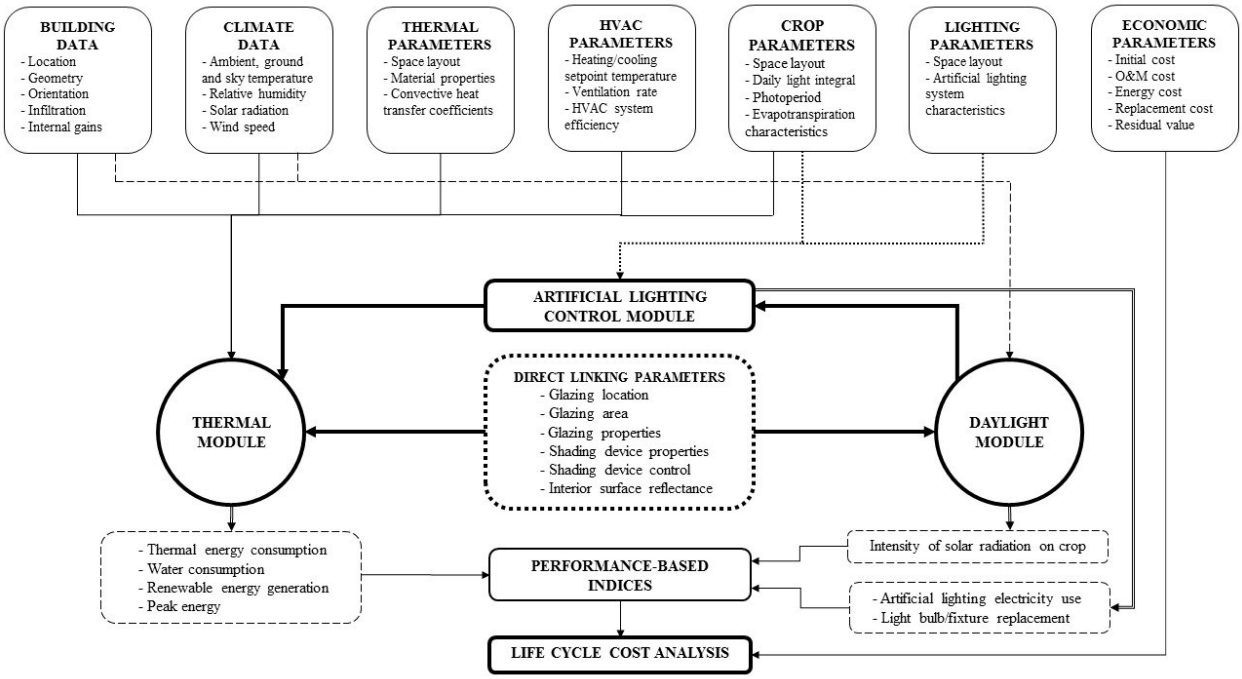

Figure 3.1: Process of coupled thermal-daylighting and life cycle cost analysis.

Modifying the envelope design for these greenhouses should not affect crop growth because the supplemental lighting system adjusts and compensates for any changes in daylight that is produced by the alternative design. In other words, the combination of daylight and artificial lighting should provide an equivalent amount of PAR photons over the canopy each day regardless of the envelope design. Any permutation in the envelope design would affect the daylighting and thermal performance but the crop yield should theoretically remain the same. Therefore, the analysis of these types of greenhouses may be carried out by omitting biological aspects and focusing on the climate and economic models. However, further experimental research is needed to verify that modifying the envelope design would not significantly affect crop yield inside these greenhouses. It is possible to account for any differences in yield by incorporating the appropriate crop model into the current methodology, similarly to the procedure presented by Vanthoor et al. (2011).

3.2 Combining Energy and Economic Analysis

The decision-making process for selecting the most suitable envelope design requires a combined energy and economic analysis. The performance-based indices obtained through energy simulation are not sufficient for selecting the cost-optimal design. From an investor's

perspective, the incremental cost of alternative claddings should be outweighed by operational savings. Several methods of economic evaluation may be employed for comparing greenhouse designs. The proposed methodology uses life cycle cost analysis (LCCA) because of its scoping capabilities which are valuable for minimizing the number of inputs needed to compare envelope design alternatives. The net savings method is a LCCA economic comparison measure that is particularly useful as it minimizes time and effort required for comparing design alternatives to a BCGH whose operations have already been proven to be economically viable. For instance, LCCA can serve to evaluate the potential for STPV cladding without considering the revenue from crop sales or the total construction cost of the greenhouse. Only the incremental cost for the PV cladding, and its impact on future costs need to be considered.

The modeling requirements for comparative analysis may provide the opportunity to save time and effort (e.g. reduced model resolution) because absolute quantities (e.g. for energy consumption) are less important than the relative change of its value. Certain mass and energy transfer mechanisms can have a greater impact on the energy use and deserve more attention. For instance, if heating is the only thermal energy input, then it is important to select inside CHTCs that reflect those conditions (i.e. spending additional effort for determining correlations for the summer conditions would not improve the heating energy predictions). Moreover, if a simplified constant ventilation rate is used, implementing detailed calculations for water mass transfer (e.g. ET and condensation) becomes less important because the humidity is not controlled by the indoor relative humidity. Time can also be saved by neglecting certain aspects in the climate model that are equal for the BCGH and alternative designs such as internal gains from workers.

3.3 Performance-Based Indices

The following performance-based indices are obtained from the integrated energy simulation process:

1) **Electricity consumption for artificial lighting:** The results from the artificial lighting control module indicates the amount of supplemental lighting that is provided at each timestep. Based on this, the annual electricity consumption is calculated.
2) **Light bulb and/or fixture replacement frequency:** Knowledge of the lighting control also enables the annual operating hours and associated light bulb/fixture replacement

frequency to be quantified. For HID fixtures, the bulb and ballast need periodic replacement whereas most horticultural LED fixtures presently require that the entire fixture be replaced.

3) **Thermal energy consumption:** The outputs of the thermal module simulation are used to determine the annual energy consumption for heating and/or cooling. Based on this, the annual fuel/biomass (unit heater, boilers) and/or electricity (heat pumps) that is consumed for heating can be computed. For greenhouses with cooling, the electricity consumed by the water pump (for evaporative cooling) or electricity consumption for mechanical cooling equipment should be estimated.
4) **Peak thermal loads:** The thermal module may be simulated during a summer or winter design day to calculate the peak thermal energy demand which is required for determining the size of the HVAC equipment.
5) **Water consumption:** Evaporative cooling and humidification can consume a significant amount of water. The thermal module can be used to determine the annual water consumption. In some cases, crop models can be used to verify if alternative designs affect irrigation requirements.
6) **Intensity of transmitted solar radiation:** Crop growth may be negatively affected by high light levels and/or the overheating that can result. Moreover, photosynthesis may not be improved or hindered above a certain PPFD threshold. In such cases, transmitted solar radiation should be monitored and adjusted by selecting glazing and/or screen characteristics that improve the greenhouse microclimate and energy performance.
7) **Crop yield:** Modifying the envelope design of greenhouses that control light to a consistent daily integral should not affect the crop yield. In cases where it does (e.g. allowing the DLI to float and significantly rise above the target DLI for fruiting crops), the change in crop yield may be quantified (e.g. with a crop model) and the associated revenue from crops/products sold must be assessed in the economic analysis.
8) **Renewable energy generation:** Building-integrated solar energy technologies, wind turbines and organic waste-to-energy conversion systems may be implemented to generate renewable energy on-site. The energy generation must be quantified and considered in the economic model and, when applicable, the thermal module (e.g. impact of PV cladding on thermal energy use).

3.4 Direct Links

The following parameters were identified as having a direct link between the daylighting and thermal simulations:

1) **Glazing location and area:** Typically, greenhouse wall and roof surfaces are fully covered by transparent/translucent, semi-transparent or opaque materials.
2) **Glazing type and properties:** The glazing material is characterized by its thermal, electrical, and optical properties that may change depending on the direction, wavelength and incidence angle of shortwave radiation.
3) **Shading device type and properties:** The thermal and optical properties (e.g. transmittance) are generally selected based on the crop lighting and/or overheating and/or energy conservation considerations.
4) **Shading device control:** The screens in modern greenhouses are mechanically operated based on sensor readings of sunlight and air temperatures. Their control can range from simple where all the screens open and close at the same time to advanced control algorithms where each surface is individually controlled based on sensor readings.
5) **Interior surface reflectance:** The light reflected by the interior surfaces is a design parameter which affects both the daylight and thermal performance.

3.5 Implementation in Software

BES software was used to obtain the performance-based indices (e.g. energy consumption/generation) over a one-year period so that the economic analysis can be performed. BES software provides a flexible energy simulation platform which builds upon significant previous work that has enabled detailed energy computations for building enclosures (e.g. creation of custom multilayer glazing, incidence angle dependent light transmission, shortwave radiation distribution based on geometrical properties and view factor matrices, reflection and transmission of sunlight back outside, transient 3D heat transfer with the ground) and the adoption of advanced models for HVAC components, amongst others. BES that have the following properties are most likely to be adopted by scientists and engineers for greenhouse design: 1) modular structure with graphical interfaces (e.g. TRNSYS, EnergyPlus); 2) multizone building model with geometry definition using 3D drawing software; 3) enable co-simulation with other programs; and 4) allow the user to choose from pre-existing sub-models or create their

own. However, currently BES are lacking several essential components for climate modeling of greenhouses. For this study, the existing multi-zone building model in TRNSYS (Type 56) was modified to provide adequate model resolution for estimating the greenhouse energy consumption. In the future, the multi-zone building model can be upgraded to include model adaptations (e.g. for modeling photosynthesis (CO_2), ET, and condensation) required for greenhouses (e.g. by connecting to new sub-models or other programs through interactive calls during the simulation). In addition, updates to the Type 56 model may include several key features such as a new type of surface can be created to model ET or condensation and would be dynamically linked to the respective surface energy balance and the airnode mass and energy balances.

A simplified approach for simulating the control of the artificial lighting system may be considered by assuming that supplemental lighting is activated after sunset. This assumption enables the daylight, artificial lighting control and thermal modules to be calculated sequentially, with outputs of one module serving as inputs to another (Fig. 3.1). Other light control strategies such as dimmable LED control could also follow this procedure. However, to consider screen control based on inside environmental parameters (e.g. PPFD or inside air temperature sensors), the modeling procedure would need to simulate the three modules simultaneously and could implement more complex control algorithms. The sequence of energy simulations that may be performed to obtain the desired performance-based indices are as follows:

1) Create the daylight model and perform an annual energy simulation to obtain the amount of natural light that is incident on the crop surface (PPFD in μmol m^{-2} s^{-1}) at each simulation timestep.
2) Based on these results, determine the artificial lighting control that is required to achieve the target DLI (in mol m^{-2} day^{-1}) and the associated electricity consumption, and calculate the resulting internal latent and sensible heat gains at each simulation timestep.
3) Create the greenhouse thermal model and perform the annual energy simulation (which uses the internal gains calculated in step 2 as dynamic inputs) to obtain the thermal energy/water consumption and electricity generation at each simulation timestep.
4) Perform the design day energy simulations of the thermal model to obtain the peak thermal loads.

Currently, a limitation of TRNSYS include its inability to model covers and screens that transmit thermal radiation (e.g. to model longwave radiation heat transfer between a crop surface and the sky, passing through a PE cover). The method for modeling a crop surface is another limitation of BES. The crop surface is typically at the ground level. However, a crop that is grown on tables and dense canopy extending above the ground (e.g. tomatoes) is difficult to model. For these cases, most of the incident solar radiation does not actually strike the ground but is absorbed/reflected by the canopy and a portion is converted to latent heat (ET). A possible solution is to adjust the correlation for calculating the CHTC so that it dissipates the absorbed sunlight and thus the canopy surface temperature becomes close to that of the inside air. Another approach could be to model the canopy as a separate surface above the ground level, with an airspace between. However, this would likely necessitate the creation of a separate thermal zone above the ground because BES programs can only model surfaces enclosed by an airnode.

3.6 Daylight Module

The purpose of the daylight module is to obtain the amount of PAR that is incident on the crop surface. The model consists of three parts: 1) determine the solar radiation that is incident on the building surfaces; 2) calculation of transmitted solar radiation into the space; and 3) distribution of transmitted solar radiation on inside surfaces and conversion to PAR received by the crop surface.

TRNSYS 17.2, a building energy simulation software which has a modular structure, was selected for the transient simulation of the greenhouse daylight module (Klein et al., 2014). A TRNSYS project is typically set up by connecting components graphically in the simulation studio. TRNSYS components are often referred to as “Types,” which are described by a mathematical model in the TRNSYS simulation engine (Klein et al., 2014). Type 56 was originally developed to model multizone buildings and is used here with certain assumptions to create the greenhouse energy model (TRANSSOLAR, 2005). The visual interface for Type 56 is called TRNBuild. The greenhouse geometry is first created using the Sketchup Trnsys3d plugin (Sketchup, 2015; TRANSSOLAR, 2005) and then imported into TRNBuild so that detailed shortwave and longwave radiation calculations may be performed. The set of equations for energy and mass transfer from and within the zone are formulated in a matrix in Type 56 and solved using the modified Euler method with successive substitution at each simulation timestep.

The greenhouse daylight model requires as inputs the building data (geometry, orientation) and direct links (glazing location, area and optical properties, blind optical properties and control, and surface solar reflectances).

Incident solar radiation on building surfaces: TRNSYS uses a weather data processor to calculate the solar radiation (beam, diffuse and reflected components) that is incident on each building surface using as inputs standardized weather data and the surface slope and azimuth angle. Type 15 is a weather data processor that reads and interprets weather data available in a series of standardized formats (Klein et al., 2014). This study uses typical meteorological year weather files which include hourly values of global horizontal irradiation, sun tracking beam irradiation, ambient air temperature, wind speed, wet bulb temperature, wind direction and cloud cover. The diffuse solar radiation component is calculated using the anisotropic diffuse model by Perez et al. (1988). The ground-reflected component is considered to be diffuse and is calculated using the total horizontal solar radiation, the view factor between the ground and surface, and the ground reflectance.

Calculation of transmitted solar radiation: Each glazing system reflects (ρ), transmits (τ) and absorbs (α) a part of the incident solar radiation, depending on the glazing material, the solar incidence angle (θ) and wavelength (λ), which is expressed by:

$$\rho(\theta,\lambda) + \tau(\theta,\lambda) + \alpha(\theta,\lambda) = 1 \tag{3.1}$$

The amount of transmitted solar radiation (Q_t in W m^{-2}) is equal to the incident irradiance (I in W m^{-2}) multiplied by the glazing transmittance (τ):

$$Q_t = I \cdot \tau \tag{3.2}$$

The amount of transmitted irradiance is also affected by the presence of an external or internal shading device, which may be defined for each external window of the building. External shading devices reduce the incoming solar radiation on the glazing area of the external window by a factor given in the building description. An internal shading device is specified giving the reduction of the transmitted solar radiation and a reflection coefficient for solar radiation for both faces of the shading device. The Type 56 model takes into account multiple

reflections between the internal shading device and the window panes and calculates the absorption of reflected solar radiation from the internal shading on the different window panes.

WINDOW 7.4 (DOE, 2015) or similar programs can be used to generate detailed thermal and optical properties for custom window assemblies, comprised of glazing(s) and framing. The glazing optical properties (solar and visible) at normal incidence angle are input into WINDOW 7.4, which then computes the reflectance and transmittance hemispherically for diffuse radiation and in incidence angle steps of 10° for direct solar radiation. These values are copied to a text file and read/interpolated by Type 56 during the TRNSYS simulation.

Transmitted beam and diffuse (sky and reflected) solar radiation are considered separately, whereby the diffuse optical properties are equal to the beam values when the incidence angle is 60°. Type 56 employs 2-band models solar radiation transmission, which splits the external solar radiation into a visible part (46.6%) and a non-visible part (53.4%). The model calculates the reflected and transmitted shortwave radiation separately based on the optical properties that are specified for each waveband. Since wavebands for PAR (400-700 nm) and visible light (380-780 nm) are close, they can be used interchangeably. It should be noted that only the total solar radiation values are used for all energy and temperature calculations in the thermal module.

For a glazing comprised of multiple layers, the total optical properties (reflectance for light direct on the outside surface (*so*) and inside surface (*si*)) can be calculated by solving the recursion equations between layers (*i*) and (*j*), including inter-reflections, from:

$$\tau_{i,j} = \left(\tau_{i,j-1} \cdot \tau_{j,j}\right)/\left(1 - \rho_{j,j}^{so} \cdot \rho_{j-1,i}^{si}\right) \tag{3.3}$$

$$\rho_{i,j}^{so} = \rho_{i,j-1}^{so} + \left(\tau_{i,j-1}^{2} \cdot \rho_{j,j}^{so}\right)/\left(1 - \rho_{j,j}^{so} \cdot \rho_{j-1,i}^{si}\right) \tag{3.4}$$

$$\rho_{j,i}^{si} = \rho_{j,j}^{si} + \left(\tau_{j,j}^{2} \cdot \rho_{j-1,i}^{si}\right)/\left(1 - \rho_{j-1,i}^{si} \cdot \rho_{j,j}^{so}\right) \tag{3.5}$$

$$\alpha_j = \left[\tau_{1,j-1}\left(1 - \tau_{j,j} - \rho_{j,j}^{so}\right) + \tau_{1,j} \cdot \rho_{j+1,N}^{so}\left(1 - \tau_{j,j} - \rho_{j,j}^{si}\right)\right]/\left(1 - \rho_{j,N}^{so} \cdot \rho_{j-1,1}^{si}\right) \tag{3.6}$$

A detailed explanation of the above can be found in ASHRAE (Handbook, 2009). It should be noted that each property is a function of the solar incidence angle and wavelength.

Typically, greenhouse windows (comprised of glazing and frame sections) cover the entire surface of the walls and roof. However, Type 56 requires that an opaque wall be defined around any given window. Therefore, a wall of negligible area (1 mm offset) can be created around each window.

Distribution of transmitted solar radiation: The final step is to determine the distribution of transmitted solar radiation on the inside surfaces and convert it to PAR received on the surface of the crop surface. In greenhouses, a significant portion of the transmitted light is retransmitted back to the outside. For highly glazed spaces, Wall (1995) has shown that only 30-90% of radiation transmitted through the glazing is retained in the space. Therefore, detailed radiation models are needed to adequately model the radiation transfer. TRNSYS 17.2 enables detailed computations for radiation distribution, including multi-reflection and solar radiation leaving the zone through the windows, whereby beam and diffuse components are considered separately.

For a detailed treatment of shortwave diffuse radiation, the TRNSYS radiation model applies so-called Gebhart factors (Gebhart, 1961, 1971). The key factor of this method is the view factor matrix. For generating the matrix, TRNBuild calls an auxiliary program called TRNVFM which uses a combination of an algorithm of Schröder and Hanrahan (1993) and view factor relationships (symmetry, reciprocity). In addition, longwave radiation heat transfer is significant in highly glazed structures and a detailed model that also employs these view factor matrixes is the preferred method. However, detailed diffuse shortwave and longwave radiation calculations using view factor matrices require that the radiative zone be a convex polyhedron. As a consequence, it is not possible to model a multispan greenhouse using detailed radiation calculations, unless each span is modeled as a distinct thermal zone with virtual surfaces as separation walls, which is a tedious process. A solution that may be adopted is to assume that the roof is flat. This assumption does entail some loss of information regarding the total area for heat transfer, the incidence angle for sunlight transmission, and electricity generation in the case of PV cladding materials. However, the advantages of increased accuracy of radiation calculations are expected to be of greater importance that these drawbacks.

A detailed calculation for distributing the primary solar direct radiation entering the zone is achieved using geometric distribution, as opposed to user defined distribution factors. Type 56 calls an auxiliary program called TRNSHD to calculate the shading and insolation matrices based on the 3D geometric surface information generated by Sketchup. The integrated tool for calculating solar sunlit and distribution factors is based on Hiller et al. (2000).

The absorbed shortwave radiation (Q_{swr} in W m^{-2}) on a given surface is defined by the amount of transmitted incident solar radiation (Q_t in W m^{-2}) multiplied by the surface absorptance (α):

$$Q_{swr} = Q_t \cdot \alpha \tag{3.7}$$

For an opaque surface, the absorptance is given by:

$$\alpha = 1 - \rho \tag{3.8}$$

The purpose of the daylight module is to obtain the amount of photosynthetically active radiation (PAR) that is incident on the crop surface. The only available output from the Type 56 model is the total solar radiation absorbed by the crop surface (Q_{swr_c} in kJ hr^{-1}). Based on this, the average incident solar radiation on the crop surface (I_c in W m^{-2}) is calculated from:

$$I_c = Q_{swr\_c}/3.6 \cdot A \cdot F_c \cdot \alpha_{c\_sol} \tag{3.9}$$

where

Q_{swr_c} is the absorbed shortwave radiation on the crop surface (kJ hr^{-1})

A is the greenhouse surface area (m)

F_c is the fraction of the greenhouse footprint that is occupied by crops (dimensionless)

α_{c_sol} is the solar absorptance of the crop surface (dimensionless)

the factor 3.6 serves to convert units kJ hr^{-1} to W.

The solar radiation consists of UV (350-400 nm), PAR (400-700 nm) and NIR (700-2500 nm) portions. Assuming the relatively small UV portion is neglected, the crop solar absorptance (α_{c_sol}) is expressed by:

$$\alpha_{c\_sol} = F_{PAR} \cdot \alpha_{c\_PAR} + F_{NIR} \cdot \alpha_{c\_NIR} \tag{3.10}$$

where

F_{PAR} is the fraction of PAR radiation in sunlight (dimensionless)

α_{c_PAR} is the crop surface PAR radiation absorptance (dimensionless)

F_{NIR} is the fraction of NIR radiation in sunlight (dimensionless)

α_{c_NIR} is the crop surface NIR radiation absorptance (dimensionless).

It is assumed that all the incident solar radiation is intercepted by the crop canopy. Finally, the absorbed solar radiation is converted to photosynthetic photon flux density incident on the crop surface ($PPFD_{c\_sol}$ in μmol m^{-2} s^{-1}) using the formula:

$$PPFD_{c\_sol} = I_c \cdot PE_{sol} \cdot F_{PAR} \tag{3.11}$$

where

I_c is solar radiation incident on the crop surface (W m^{-2})

PE_{sol} is photon efficiency of sunlight (μmol J^{-1}).

where the photosynthetic photon efficiency of the sunlight is defined by:

$$PE_{sol} = \sum_{\lambda=400}^{700} \left(\frac{\lambda \cdot 10^{-9} \cdot 10^{6}}{300 \cdot N \cdot h_p \cdot c} \right) \tag{3.12}$$

where

λ is the wavelength (nm)

N is Avogadro's constant (photons $mole^{-1}$)

h_p is Planck's constant (J s)

c is the speed of light (m s^{-1})

the factor 10^{-9} serves to convert units nm to m

the factor 10^{6} is used to convert moles of photons to μmols

300 is the number of wavelengths in the PAR range.

It should be noted that the approach described above is only valid for cover materials that have similar optical properties for solar and visible light. When the optical properties are significantly different (e.g. more than about 5% difference), a more advanced treatment of the shortwave radiation spectrum should be implemented. The latest version of TRNSYS 18.0

(TRANSSOLAR, 2018) has a valuable update that enables dynamic daylight simulation based on DaySIM into the TRNSYS multizone building model Type 56. The 3D geometries of the existing building model are used to calculate illuminance levels for user specified sensor points. These illuminance values (lux) can be converted to PPFD by implementing conversion factors for daylight and artificial light fixtures. A specific conversion factor can be determined from the spectral power distribution of the light bulb. However, a detailed conversion for sunlight should consider the time of day (e.g the color temperature of sunlight is 4500 K in the mid-morning and mid-afternoon, 7500 K from skylight only on a clear day, and 6000 K on an overcast day (ePHOTOzine, 2018)). AGi 32 (2018) uses an average value of 18.3 to convert illuminance (in kilolux) to PPFD (in μmol m^{-2} s^{-1}) for greenhouse applications. The new capabilities of TRNSYS 18.0 would enable detailed modeling of organic STPV where optical properties for solar and visible (PAR) portions can be considered separately. It may also be useful for determining the PPFD on a canopy that is located above ground level (e.g. fruiting crops).

3.7 Artificial Lighting Control Module

The secondary link is the artificial lighting control, which uses the daylight module output (PPFD on crop surface from daylight) to calculate the activation period for supplemental lighting. Once the lighting schedule is known, two key performance-based indices can be determined: the artificial lighting electricity use and the light bulb/fixture replacement frequency. The output of the artificial lighting control is then used to calculate the resulting internal sensible and latent heat gains in the thermal module. The calculations for artificial lighting depend on the surface area that is lite. This methodology assumes that lighting is only provided over the crop area and that the floor zones, which are representative of service areas at each end of the greenhouse (e.g. raft hydroponic systems), are not lite. Alternatively, the floor surface may be a narrow path between rows of crops in which case the entire footprint may be lite.

Various strategies can be employed for controlling the supplemental lighting. The simplest is to activate the lights after sunset until the target DLI has been reached. Other strategies may consist of supplementing lighting during the day according to control algorithms of varying complexity using on/off control (Albright et al., 2000) or dimmable control of horticultural LED lighting (Pinho et al., 2013). In the future, model-based predictive control using weather forecasts may serve to determine optimal light and screen control strategies in

greenhouses. Nevertheless, it is presumed that increasing the complexity of the lighting control would not significantly impact on the LCC outcome because the investigation consists of a comparative analysis between a base case and a design alternative.

When a simple lighting control strategy is employed (whereby supplemental lighting, when needed, is provided after sunset), the PPFD on the crop surface that was obtained from the daylight module is summed and compared to the target DLI. If supplemental lighting is needed, the lights are activated until the target DLI has been reached. The calculations may be further simplified by assuming that all the supplemental lighting requirements are provided before sunrise. However, this assumption is valid for plants that prefer longer photoperiods such as leafy greens. Assuming the worst-case scenario where daylight is negligible, the PPFD level to be supplied by the artificial lights ($PPFD_{c\_AL}$ in μmol m^{-2} s^{-1}) is determined from:

$$PPFD_{c\_AL} = 10^4 \cdot DLI/(36 \cdot PP_{AL}) \tag{3.13}$$

where

DLI is the daily light integral (mol m^{-2} day^{-1})

PP_{AL} is the photoperiod for supplemental lighting (hr day^{-1})

the factor $10^4/36$ serves to convert units mol m^{-2} hr^{-1} to μmol m^{-2} s^{-1}.

The amount of artificial light supplemented at each simulation timestep (TLI_{AL} in mol m^{-2}) is determined by:

$$TLI_{AL} = 36 \cdot 10^{-4} \cdot PPFD_{c\_AL} \cdot \Delta t \tag{3.14}$$

where

Δt is the simulation timestep (s)

the factor $36 \cdot 10^{-4}$ serves to convert units μmol $m^{-2} \cdot s^{-1}$ to mol m^{-2} hr^{-1}.

Horticultural lighting fixture specifications provide the fixture power rating and light bulb/fixture photosynthetic photon flux (PPF). The fixture photon efficiency (PE_{AL} in μmol J^{-1}) is equal to the photosynthetic photon flux of the light fixture (PPF_{AL} in μmol s^{-1}) divided by the electric power rating of light fixture (E_{AL_r} in W):

$$PE_{AL} = PPF_{AL}/E_{AL\_r} \tag{3.15}$$

The electricity consumption for artificial lighting per unit area (E_{AL} in W m^{-2}) is defined as the PPFD level to be supplied by the artificial lights ($PPFD_{c\_AL}$ in μmol m^{-2} s^{-1}) divided by its photon efficiency (PE_{AL} in μmol J^{-1}):

$$E_{AL} = PPFD_{c\_AL}/PE_{AL} \tag{3.16}$$

The annual electric energy consumption for artificial lighting (E_{AL_yr} in kWh yr^{-1}) is computed as:

$$E_{AL\_yr} = \sum_{\Delta t=0}^{365\cdot 24/\Delta t}(A \cdot F_c \cdot E_{AL} \cdot \Delta t/10^3) \tag{3.17}$$

where the factor 10^3 serves to convert units W to kW.

The number of hours that the light fixtures operate each year is computed based on the simulation results of the artificial lighting control module. Then, the replacement frequency of the artificial light bulbs/fixtures (P_{AL_repl} in yr) is found by dividing the artificial light lifespan (P_{AL} in hr) by the number of hours that the light fixtures operate each year (P_{op} in hr yr^{-1}):

$$P_{AL\_repl} = P_{AL}/P_{op} \tag{3.18}$$

The loss of light output over time can be neglected by assuming that the lights would compensate by operating for longer periods of time.

To estimate the number of fixtures that need to be replaced, the area covered by each fixture (A_{AL} in m^2) must first be determined by dividing the electric power rating of the light fixture (E_{AL_r} in W) by the electricity consumption for artificial lighting per unit area (E_{AL} in W m^{-2}):

$$A_{AL} = E_{AL\_r}/E_{AL} \tag{3.19}$$

Then, the number of fixtures required to illuminate the crop surface area (Nb_{AL}) is approximated by:

$$Nb_{AL} = A \cdot F_c/A_{AL} \tag{3.20}$$

where A is the greenhouse footprint (m^2).

This approach slightly underestimates the required number of fixtures because it assumes the lighting uniformity is equal and thus does not account for the reduced PPFD levels around the perimeter of the lite area. In reality, the fixtures may be positioned closer together so that a certain amount of lighting overlap exists near the perimeter. A correction factor may be applied to account for this effect. However, this is expected to have a small impact on the results because of the comparative nature of the design methodology. The analysis should be supplemented with lighting software (e.g. Calculux by Philips, 2018) to optimize the distance between lights and their height above the canopy.

3.8 Thermal Energy Module

A greenhouse energy model is created to predict the indoor climate and determine the key performance-based indices that are required for the economic analysis. Fig. 3.2 illustrates the major mass and energy fluxes that could be considered in the general greenhouse model. The model divides the greenhouse into two thermal zones, one for the greenhouse air below *(l)* and above *(u)* the TSS, as proposed by De Zwart (1996). The model reflects the case where leafy green vegetables are grown on the same level as the floor and may apply to ventilated, semi-closed and closed (no ventilation, carbon dioxide fertilization) greenhouses.

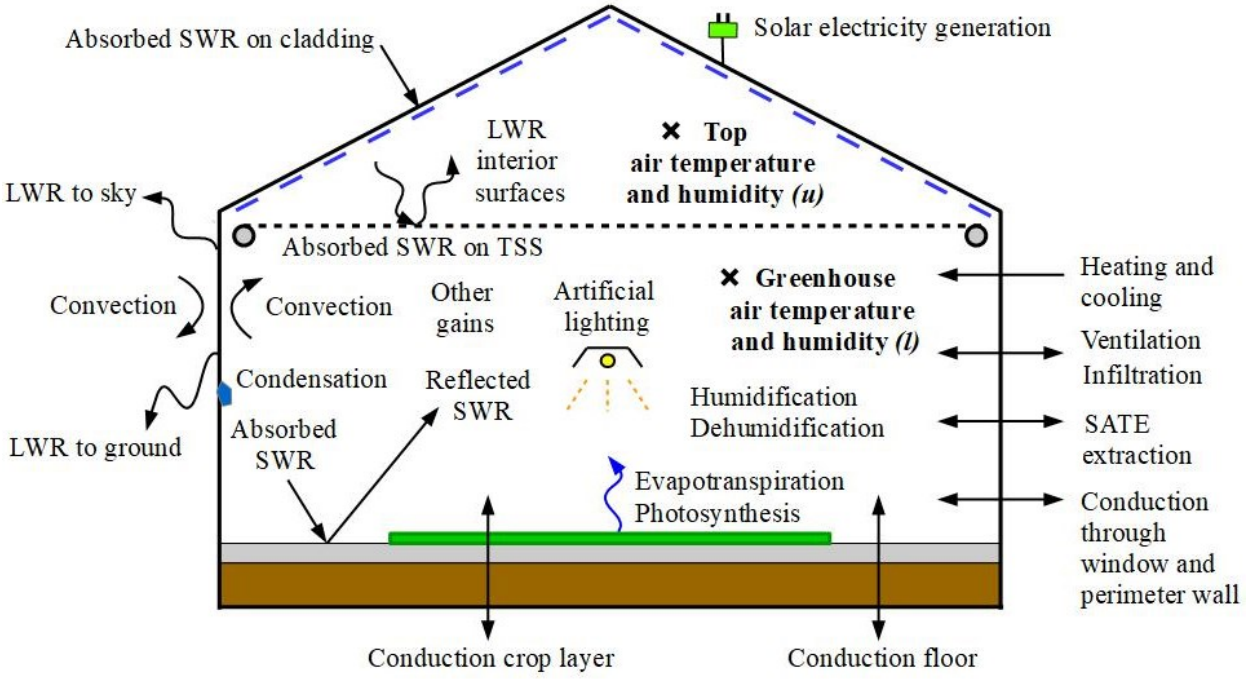

Figure 3.2: Schematic showing the mass and energy fluxes considered in the general model.

When a greenhouse that controls light to a consistent daily integral employs PV cladding, it causes an internal shading (daylight module) that is counteracted by increasing the amount of supplemental lighting (artificial light control module). This will presumably reduce heating energy consumption (thermal energy module) because the lighting is an internal heat gain. There are several modeling approaches for PV cladding. A detailed model would consider the impact of electricity that is generated by the surface on the thermal energy balance (reduces cladding surface temperature and this effect is transferred to the airnode). Furthermore, the accuracy for predicting electricity generation is improved by considering the effect of the solar incidence angle and temperature-dependent efficiency. The approach that was adopted for modeling shading STPV cladding is described in Appendix C.

An energy balance is required to predict the indoor air temperature and the associated auxiliary energy needs (heating and cooling) for controlling it to the desired setpoint. The energy balance equation for the airnode below (*l*) the TSS can be written as:

$$Q_{stor\_l} = Q_{aux} + Q_{sol} + Q_{gains} + Q_{vent\_l} + Q_{\mathrm{inf}\_l} + Q_{conv\_si\_l} + Q_{dehu} + Q_{cpl} - Q_{hum} - Q_{SATE} \quad (3.21)$$

where

Q_{stor_l} is the energy storage (W)

Q_{aux} is the auxiliary heating/cooling energy (W)

Q_{sol} is the fraction of solar radiation that is absorbed by internal elements and transferred to the airnode by convection (W)

Q_{gains} is the internal heat gains (W)

Q_{vent_l} is the heat transfer due to ventilation (W)

Q_{inf_l} is the heat transfer due to air infiltration (W)

$Q_{conv\_si\_l}$ is the heat transfer by convection with interior surfaces (W)

Q_{dehu} is the potential heat recovered mechanical dehumidification (W)

Q_{cpl} is the heat transfer due to air movement between the two airnodes (W)

Q_{hum} is the heat removed by humidification (W)

Q_{SATE} is the surplus air thermal energy (collected and stored for later use) (W).

The energy balance equation for the airnode above the TSS (u) can be defined as:

$$Q_{stor\_u} = Q_{vent\_u} + Q_{inf\_u} + Q_{conv\_si\_u} + Q_{cpl} \tag{3.22}$$

where

Q_{stor_u} is the energy storage (W)
Q_{vent_u} is the heat transfer due to ventilation (W)
Q_{inf_u} is the heat transfer due to air infiltration (W)
$Q_{conv\_si\_u}$ is the heat transfer by convection with interior surfaces (W)
Q_{cpl} is the heat transfer due to air movement between the two airnodes (W).

The mass balance is required to predict the indoor humidity and methods required to the control it to the desired setpoint. The water balance equation for the airnode below the TSS may be described by:

$$m_{stor\_l} = m_{ET} + m_{vent\_l} + m_{\mathrm{inf}\_l} + m_{hum} + m_{cool} + m_{cpl} - m_{dehum} - m_{cds\_l} \tag{3.23}$$

where

m_{stor_l} is the water storage (kg)
m_{ET} is the water transfer due to evaporation and transpiration (kg)
m_{vent_l} is the water transfer due to ventilation (kg)
m_{inf_l} is the water transfer by infiltration (kg)
m_{hum} is the water added from humidification (kg)
m_{cool} is the water added from evaporative cooling or removed from mechanical cooling (kg)
m_{cpl} is the water transfer due to air movement between the two airnodes (kg)
m_{dehum} is the water removed by dehumidification (kg)
m_{cds_l} is the water removed by condensation (kg).

The water balance equation for the airnode above the TSS may be expressed by:

$$m_{stor\_u} = m_{vent\_u} + m_{inf\_u} + m_{cpl} - m_{cds\_u} \tag{3.24}$$

where

m_{stor_u} is the water storage (kg)

m_{vent_u} is the water transfer due to ventilation (kg)

m_{inf_u} is the water transfer by infiltration (kg)

m_{cpl} is the water transfer due to air movement between the two airnodes (kg)

m_{cds_u} is the water removed by condensation (kg).

Another mass balance may be needed to predict the indoor CO_2 concentration and methods required to the control it to the desired setpoint. The CO_2 balance equation for the airnode below the TSS may be given by:

$$CO2_{stor\_l} = CO2_{fert} + CO2_{vent\_l} + CO2_{inf\_l} + CO2_{cpl} - CO2_{crop} \quad (3.25)$$

where

$CO2_{stor\_l}$ is the CO_2 storage (kg)

$CO2_{fert}$ is the CO_2 fertilization (kg)

$CO2_{vent\_l}$ is the CO_2 transfer due to ventilation (kg)

$CO2_{inf\_l}$ is the CO_2 transfer due to infiltration (kg)

$CO2_{cpl}$ is the CO_2 transfer due to air movement between the two airnodes (kg)

$CO2_{photo}$ is the net CO_2 transfer due to photosynthesis and respiration (kg).

The CO_2 balance equation for the airnode above the TSS may be written as:

$$CO2_{stor\_u} = CO2_{vent\_u} + CO2_{inf\_u} + CO2_{cpl} \quad (3.26)$$

where

$CO2_{stor\_u}$ is the CO_2 storage (kg)

$CO2_{vent\_u}$ is the CO_2 transfer due to ventilation (kg)

$CO2_{inf\_u}$ is the CO_2 transfer due to infiltration (kg)

$CO2_{cpl}$ is the CO_2 transfer due to air movement between the two airnodes (kg).

The energy balance for an inside surface (*si*) of the cover or an opaque surface per unit area is expressed as:

$$0 = Q_{cond} + Q_{conv\_si} + Q_{swr\_si} + Q_{lwr\_si} + Q_{cds} - E_{pv\_si} \quad (3.27)$$

where

Q_{cond} is the heat transfer by conduction (W m^{-2})

Q_{conv_si} is the heat transfer by convection (W m^{-2})

Q_{swr_si} is the absorbed shortwave radiation (W m^{-2})

Q_{lwr_si} is the heat transfer by longwave radiation between interior surfaces, to the sky and the ground (W m^{-2})

Q_{cds} is the heat transfer to the surface due to condensation (W m^{-2})

E_{pv_si} is the electricity generated by the PV cladding (W m^{-2}).

The energy balance for the outside surface of the cover or an opaque surface per unit area is described by:

$$0 = Q_{cond} + Q_{conv\_so} + Q_{swr\_so} + Q_{lwr\_sky} + Q_{lwr\_gnd} - E_{pv\_so} \quad (3.28)$$

where

Q_{cond} is the heat transfer by conduction (W m^{-2})

Q_{conv_so} is the heat transfer by convection (W m^{-2})

Q_{swr_so} is the absorbed shortwave radiation (W m^{-2})

Q_{lwr_sky} is the heat transfer by longwave radiation to the sky (W m^{-2})

Q_{lwr_gnd} is the heat transfer by longwave radiation to the ground (W m^{-2})

E_{pv_so} is the electricity generated by the PV cladding (W m^{-2}).

The energy balance for the top and bottom surface of the TSS per unit area is defined as:

$$0 = Q_{cond} + Q_{conv\_si} + Q_{swr\_si} + Q_{lwr\_si} + Q_{cds} \quad (3.29)$$

The energy balance for the floor inside surface per unit area is expressed as:

$$0 = Q_{cond} + Q_{conv\_si} + Q_{swr\_si} + Q_{lwr\_si} + Q_{cds} \quad (3.30)$$

The energy balance for the crop interior surface per unit area is defined as:

$$0 = Q_{cond} + Q_{conv\_si} + Q_{swr\_si} + Q_{lwr\_si} + Q_{cds} - Q_{ET} - Q_{crop} \quad (3.31)$$

where

Q_{ET} is the heat transfer due to evaporation and transpiration (W m^{-2})

Q_{crop} is the chemical energy conversion due to photosynthesis (W).

There are numerous methods, with varying levels of detail, for calculating each of the variables in the above energy and mass balance equations. Once the variables have been defined using a suitable model resolution, the inside air temperature, humidity and CO_2 concentration may be determined by solving the system of equations at each timestep using specified weather data as boundary condition inputs. Simulations of the energy model over a one-year period using standardized weather files provides the key performance-based indices that are required for conducting the economic analysis. In addition, simulations of the model for design day conditions will provide the performance-based indices related to peak energy demand/generation that is useful for sizing HVAC and solar energy capture equipment.

3.9 Life Cycle Cost Analysis

LCCA is conducted to determine the cost-optimal solution out of a set of discrete envelope design alternatives that can applied to each wall sequentially or to all the greenhouse surfaces at once. The design permutations are comparable only with the same economics assumptions, the same study period and service date. The LCCA conducted in this research is built upon the approach developed by Fuller and Petersen (1996).

Since economic analysis itself requires resources – time and money – the effort should be tailored to the needs of the project. When two or more envelope materials are compared, there is mainly a desire to know whether the incremental initial investment cost can be recovered through operations related savings over the lifespan of the building. The net savings (NS) measure of economic comparison enables this type of analysis with the least amount of economic input information and is therefore an efficient method for comparing designs on a relative basis. The NS computes operational savings less the difference in capital investment costs for an alternative (AGH) relative to a base case (BCGH). The net savings (*NS* achieved by the AGH compared to the BCGH, in $) formula for the LCCA is given by:

$$NS_{AGH:BCGH} = (\Delta E + \Delta W + \Delta OM\&R + \Delta Y) - (\Delta Inv + \Delta Repl - \Delta Res) \quad (3.32)$$

where

ΔE is the change in energy cost ($)

ΔW is the change in water cost ($)

ΔOM&R is the change in operation, maintenance and replacement cost ($)

ΔY is the change in revenue from crop/product sales ($)

ΔInv is the change in initial investment cost ($)

ΔRepl is the change in capital replacement cost ($)

ΔRes is the change in residual value ($).

This method requires that all future costs are discounted to their present value equivalent and uses constant dollars. Although the net savings measure of economic comparison provides the dollar savings, it may be convenient to express this amount as a percentage change in life cycle cost. To obtain this value, the total cost of the greenhouse (structure, envelope, and HVAC system) must be estimated. The change in LCC (*ΔLCC* achieved by the AGH compared to the BCGH, in %) is computed as:

$$\Delta LCC_{AGH:BCGH} = 100 \cdot (-NS_{AGH:BCGH}/LCC_{BCGH}) \quad (3.33)$$

where the life cycle cost (*LCC*, in $) may be estimated as:

$$LCC = Inv + Repl + E + W + OM\&R - Res \quad (3.34)$$

where

Inv is the initial investment cost ($)

Repl is the life cycle capital replacement cost ($)

E is the life cycle energy cost ($)

W is the life cycle water cost ($)

OM&R is the life cycle operation, maintenance and replacement cost ($)

Res is the residual value ($).

A detailed explanation of the terms in Eq. (3.32) follows.

Change in energy cost (ΔE): Improvements in the building envelope design will alter the overall energy costs. A change in energy cost may be in the form of lighting electricity consumption, ventilation fan electricity consumption, heating related energy used in the form of electricity (heat pump), fuel (e.g. natural gas) or biomass (digestion/gasification/pyrolysis), cooling related energy used in the form of electricity (electric chiller, pumps for evaporative cooling) or fuel (gas chiller), solar thermal energy capture and renewable electricity generation. Theses annually recurring energy related cash flows are subject to price escalation and must be discounted to their present value as of the base date before they can be combined in the LCC estimate. The real discount rate is needed to discount constant dollar amounts to present value to reflect the real earning power of money. The real discount rate (d in %) can be derived from:

$$d = [(1 + D)/(1 + I)] - 1 \tag{3.35}$$

where

D is the nominal discount rate (%)

I is the inflation rate (%).

Annually recurring costs that change from year-to-year at a constant cost escalation rate (ARNU, annually recurring non-uniform) are converted to present value (PV_{ARNU} in $) using the formula:

$$PV_{ARNU} = AR \cdot [(1 + e)/(d - e)] \cdot \{1 - [(1 + e)/(1 + d)]^n\} \tag{3.36}$$

where

AR is the annually recurring costs ($ yr^{-1})

e is the escalation rate (%)

n is the study period (yr).

The savings in energy costs (ΔE in $) is the difference between the present value energy costs (PV_{energy} in $) for the AGH and BCGH expressed as:

$$\Delta E = \left[\sum PV_{energy}\right]_{BCGH} - \left[\sum PV_{energy}\right]_{AGH} \tag{3.37}$$

Change in water cost (ΔW): Alternative envelope designs may impact the water that is utilized for humidification, evaporative cooling and/or irrigation. Typically, the cost of water is subject to price escalation, in which case Eq. (3.36) can be used to determine present value of the annually recurring water expenses.

The savings in water costs (ΔW in \$) is the difference between present value water costs (PV_{water} in \$) for the AGH and BCGH calculated as:

$$\Delta W = [PV_{water}]_{BCGH} - [PV_{water}]_{AGH} \tag{3.38}$$

Change in operation, maintenance and replacement cost (ΔOM&R): The OM&R costs occur annually and may or may not be subject to price escalation. Eq. (3.36) is used when the annually recurring amounts are subject to price escalation. Annually recurring amounts that vary solely with the discount rate (ARU, annually recurring uniform) are converted to present value (PV_{ARU} in \$) using the formula:

$$PV_{ARU} = AR \cdot [(1+d)^n - 1]/[d \cdot (1+d)^n] \tag{3.39}$$

The change in OM&R cost ($\Delta OM\&R$ in \$) is the difference between the present value OM&R costs ($PV_{OM\&R}$ in \$) for the AGH and BCGH defined as:

$$\Delta OM\&R = [\sum PV_{OM\&R}]_{BCGH} - [\sum PV_{OM\&R}]_{AGH} \tag{3.40}$$

Change in revenue from crop/product sales (ΔY): For greenhouses that control light to a consistent daily integral, envelope design permutations should not affect the crop yield because the interior environmental conditions, including DLI, are controlled to a target value. However, differences in crop yield may occur if the screens are controlled to allow more sunlight than the target DLI. The cost of produce may or may not be subject to price escalation. In either case, it is required to determine the annually recurring revenue from crop/product sales and discount it to present value using Eq. (3.36) or Eq. (3.39). The change in revenue from crop/product sales (ΔY in \$) is the difference between their present value costs (PV_Y in \$) for the AGH and BCGH expressed as:

$$\Delta Y = [PV_Y]_{BCGH} - [PV_Y]_{AGH} \tag{3.41}$$

Change in investment cost (ΔI): Since this analysis uses the NS method, only the difference in costs that is incurred by implementing the AGH design need to be considered. More specifically, these may include the change in cost (material, equipment and labor) for installing the alternative envelope, HVAC and lighting system. The change in investment cost (*ΔInv* in $) is the difference of investment cost (*Inv* in $) between the AGH and the BCGH computed as:

$$\Delta Inv = Inv_{AGH} - Inv_{BCGH} \tag{3.42}$$

Change in capital replacement cost (ΔRepl): These costs are associated with the replacement of material and equipment (C_{repl} in $) that occurs at some point in the future (*P* in yr). When the value of the replaced item varies solely with the discount rate, the present value replacement cost (PV_{repl} in $) is calculated as:

$$PV_{repl} = C_{repl}/(1+d)^P \tag{3.43}$$

When the value of the replaced item is subject to constant price escalation, the present value replacement cost is defined as:

$$PV_{repl} = C_{repl} \cdot [(1+e)/(1+d)]^P \tag{3.44}$$

The change in capital replacement cost (*ΔRepl* in $) is the difference between the replacement cost (*Repl* in $) of the AGH and BCGH is computed as:

$$\Delta Repl = Repl_{AGH} - Repl_{BCGH} \tag{3.45}$$

Change in residual value (ΔRes): This quantity is determined so that the value of the replaced items can be assessed at the end of the study period. The residual value (*Res* in $) of a given item is estimated by linearly prorating the difference in its initial cost (*ΔC* in $) and may be expressed as:

$$Res = \Delta C \cdot [roundup(n/P, 0) - n/P]/(1+d)^n \tag{3.46}$$

The change in residual value (*ΔRes* in $) is the difference between the residual value (*Res* in $) of the AGH and BCGH is given by:

$$\Delta Res = Res_{AGH} - Res_{BCGH} \tag{3.47}$$

3.10 Application of the Design Methodology to Relevant Case Studies

It should be noted that this chapter presents a general model that covers most of the energy and economic factors that may occur in a greenhouse. Depending of the specific design problem and the desired level of modeling detail, several of these mechanisms can be omitted from the analysis. The subsequent chapters serve to demonstrate how the developed methodology can be applied to determine the most cost-effective envelope design between several conventional and new building materials that may be applied to the walls, roof and ground. In Chapter 4, the methodology is employed to design innovative semi-transparent photovoltaic cladding applied to the rooftop of a greenhouse. Chapter 5 serves to determine the most suitable envelope design for each of the walls and the roof, with construction options comprised of either glass, twin-wall polycarbonate, or opaque reflective insulation that is applied to the interior surface of the glass. Chapter 6 presents the third case study that covers the ground envelope design, whereby the economic viability for employing various configurations of vertical perimeter and horizontal ground insulation is assessed.

CHAPTER 4: DESIGN OF SEMI-TRANSPARENT PHOTOVOLTAIC CLADDING[1]

4.1 Abstract

PV greenhouses generate solar electricity while providing a suitable environment for crop production. Energy and life cycle cost (LCC) analysis were employed to study the potential for installing semi-transparent photovoltaic (STPV) cladding on the roof of a greenhouse that employs supplemental lighting located in Ottawa, Ontario, Canada (45.4°N). The study was conducted using current and future projected (future projection study) values for the efficiency of PV and horticultural lighting technology. The STPV cladding generated solar electricity but also caused internal shading that was counteracted by augmenting supplemental lighting by as much as 84%, which in turn reduced heating energy use by up to 12%. Although STPV cladding increased lighting electricity use, it generated 43.7% of the electricity that was consumed for supplemental lighting in the present study and 107.2% in the future projection study. Therefore, in the future, a STPV roof could potentially displace all the greenhouse's electricity needs for supplemental lighting. Currently, STPV cladding would not an economically attractive investment. However, a nearly 23% reduction in LCC was achieved in the future projection study. STPV will increasingly become a promising cladding alternative for improving energy efficiency and economics of greenhouse operations.

4.2 Introduction

Photovoltaic (PV) greenhouses combine crop production and solar electricity generation within the same building. However, replacing the existing glazing surface with a PV cladding leads to higher initial costs and produces internal shading that may affect crop yield and/or energy use. Therefore, optimal designs that consider energy, crop yield and economic aspects are required. Strategic greenhouse envelope design should follow a systematic approach which integrates physical, biological and economic models. Vanthoor (2011) provided a methodology for greenhouse design based on climatic, crop yield and economic models. The methodology was

[1] Bambara, J. & Athienitis, A. K. (2019). Energy and economic analysis for the design of greenhouses with semi-transparent photovoltaic cladding. Renewable Energy, 131, 1274-1287.

applied to design tomato greenhouses in Spain and Netherlands using the annual net financial result as a method for economic assessment.

Most prior work on PV greenhouses focuses on the development of novel semi-transparent photovoltaic (STPV) claddings. Various STPV technologies exist or are being developed. The STPV cladding can provide partial shading by encapsulating uniformly distributed crystalline silicon PV cells between glazing materials or using thin-film PV modules (Emmott et al., 2015). Another promising approach is to use spectrally selective STPV cladding, whereby the sunlight wavelengths that are less useful for crop growth serve to generate electricity (Cossu et al., 2016). Other studies have focused on the impact of STPV on internal shading (Yano et al., 2010; Fatnassi et al., 2015; Cossu et al., 2017), the impact of shading on crop growth/yield (Minuto et al., 2009; Kadowaki et al., 2012; Ureña-Sánchez et al., 2012) and their effect on energy generation/consumption (Carlini et al., 2010; Barbera et al., 2017), whereby economic considerations were not considered in the analysis. There was only one study that analyzed the effect of PV cladding on energy, microalgae yield and economics using a cost benefit analysis (Barbera et al., 2017).

Greenhouses that employ supplemental lighting contribute to food security by enabling crop production near the consumer regardless of their location in the world. In mid-to-high latitude locations, horticultural lighting fixtures are used to maintain crop yield and shading devices are employed to control excess solar radiation. To assess the overall viability of a PV envelope for these types of greenhouses, the analysis must simultaneously quantify the solar electricity generation, the impact of shading on electricity consumed for artificial lighting/thermal energy used for heating, and economic performance over the lifespan of the greenhouse. A methodology for the envelope design of these greenhouses is currently unavailable. The methodology proposed by Vanthoor does not cover greenhouses that use artificial lighting and the required method for modeling the interaction between the daylighting, lighting, electric and thermal domains for PV greenhouses. Moreover, life cycle cost analysis provides a better assessment of the long-term cost effectiveness of a project, in contrast to alternative economic methods that solely focus on first costs or on operating-related costs in the short run (e.g. annual net financial result, payback period) (Fuller and Petersen, 1996).

The aim of this paper is to demonstrate how integrated thermal-daylight energy analysis and life cycle cost analysis (LCCA) can be employed to assess the economic viability of PV cladding for a greenhouse that controls light to a consistent daily integral located in Ottawa, Ontario, Canada (45.4°N, mid-latitude, 4,560 heating degree-days).

4.3 Energy and Economic Analysis

For greenhouses that supplement daylight with horticultural lighting, the choice of cover materials may alter the daylight availability and lighting electricity use. The effect of such alterations must be transferred to the module which calculates the thermal energy consumption. In theory, modifying the envelope design for greenhouses that control light to a consistent daily integral (e.g. for producing leafy green vegetables year-round near the consumer) should not affect crop growth as the supplemental lighting, shading screen and HVAC systems control will adjust and compensate for any changes in the indoor climate. Consequently, the analysis of this type of greenhouse will be carried out by omitting biological aspects.

The decision-making process for envelope design requires both energy and economic analysis. The performance obtained through energy simulation is not sufficient for determining a cost-optimal design. From an investor's perspective, the incremental cost of alternative claddings should be outweighed by operational savings. This study employs LCCA and the net savings method was selected for comparing envelope design alternatives. The net savings method can provide detailed economic analysis in a time efficient manner (it only requires economic aspects that are impacted by a design variation to be quantified).

4.4 Greenhouse Characteristics

A schematic of the 929.03 m^2 (10,000 sqft) greenhouse considered for this study is provided in Fig. 4.1. It has an equal length and width of 30.48 m, and a height of 3.66 m. The floor surface consists of a crop zone located between two identical floor areas. Heating and ventilation is used to control inside humidity and temperature. The greenhouse does not utilize humidification, cooling is provided by mechanical ventilation only, and condensation is ignored in this study. The artificial lights (AL) are the only internal gain considered in the model.

The base case greenhouse (BCGH) is clad with a single layer of glass. The alternative envelope design consists of replacing the roof glazing with crystalline silicon STPV glazing of various PV area ratios (photovoltaic greenhouse, PVGH).

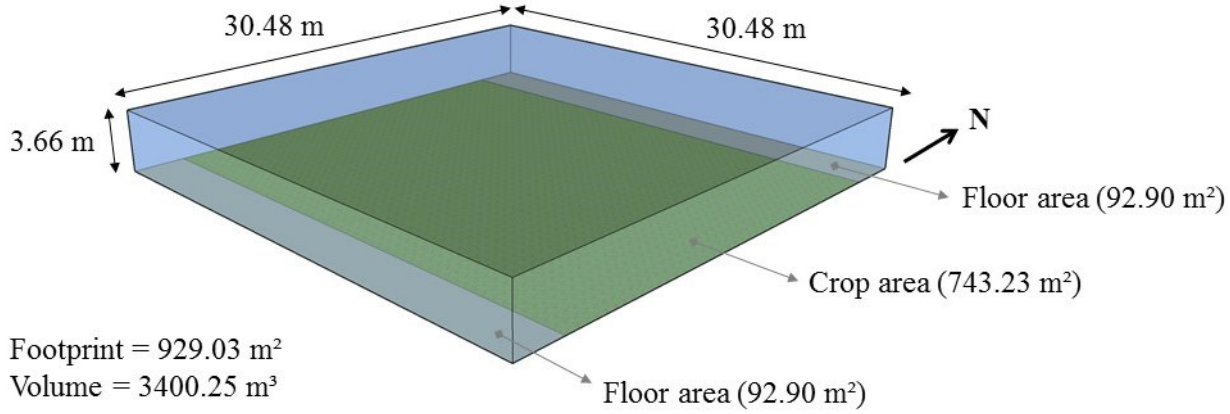

Figure 4.1: Schematic showing the modeled greenhouse.

4.5 Energy Analysis

TRNSYS 17.2 was selected for the transient simulation of the greenhouse climate (Klein et al., 2014). Type 56 multizone building model was used to create the greenhouse energy model (TRANSSOLAR, 2005). Annual and design day energy simulations of the model are performed to obtain the energy-related inputs that are needed for conducting the LCCA. The energy analysis is separated into daylight, artificial light and thermal modules.

4.5.1 Daylight module

The methodology for the daylight module is described in section 3.6.

4.5.2 Artificial lighting control module

The methodology for the artificial light control module is described in section 3.7.

4.5.3 Thermal module

The purpose of the thermal module is to determine the heating energy consumption and peak demand, with artificial lighting as a dynamic input. Fig. 4.2 illustrates the major mass and energy fluxes that are considered in the greenhouse model.

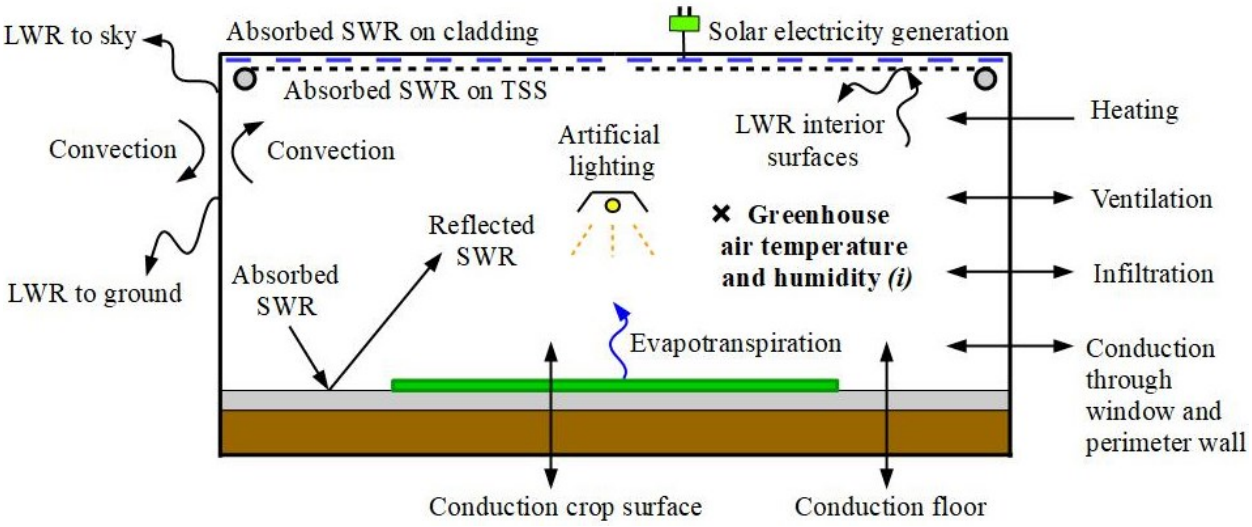

Figure 4.2: Schematic showing the mass and energy fluxes considered in the PV greenhouse model.

The mass balance for the greenhouse airnode (*i*) is given by:

$$X_m \cdot \rho_a \cdot V \cdot (\partial \omega_i / \partial t) = m_{vent} + m_{inf} + m_{ET} \quad (4.1)$$

where

X_m is the moisture capacitance multiplier (dimensionless)

ρ_a is the density of air (kg m^{-3})

V is the greenhouse volume (m^3)

$\partial \omega_i$ is the rate of change of the inside air humidity ratio (kg_{water} $kg_{dry\_air}^{-1}$)

∂t_i is the rate of change of time (s)

m_{vent} is the mass transfer rate of water due to ventilation (kg hr^{-1})

m_{inf} is the mass transfer rate of water due to infiltration (kg hr^{-1})

m_{ET} is the mass transfer rate of water due to evapotranspiration (kg hr^{-1}).

The energy balance for the greenhouse airnode is written as:

$$X_{th} \cdot \rho_a \cdot c_{p\_a} \cdot V \cdot (\partial T_i / \partial t) = Q_{conv\_si} + Q_{vent} + Q_{inf} + Q_{TSS} + Q_{AL} + Q_{heat} \quad (4.2)$$

where

X_{th} is the thermal capacitance multiplier (dimensionless)

c_{p_a} is specific heat of air at constant pressure (kJ kg^{-1} $°C^{-1}$)

∂T_i is the rate of change of the inside air temperature (°C)

Q_{conv_si} is the energy flux due to convection (W)

Q_{vent} is the energy flux due to ventilation (W)

Q_{inf} is the energy flux due to infiltration (W)

Q_{TSS} is the energy flux from the thermal shading screen (W)

Q_{AL} is the energy flux from artificial lighting (W)

Q_{heat} is the energy flux from auxiliary heating (W).

The energy balance for the inside surface (*si*) of the cover and an opaque surface is expressed as:

$$0 = Q_{cond} + Q_{conv\_si} + Q_{swr\_si} + Q_{lwr\_si} \tag{4.3}$$

where

Q_{cond} is the energy flux due to conduction (W)

Q_{swr_si} is the energy flux due to absorbed shortwave radiation (W)

Q_{lwr_si} is the energy flux due to longwave radiation (W).

The energy balance for the outside surface (*so*) of the cover and an opaque surface is described by:

$$0 = Q_{cond} + Q_{conv\_so} + Q_{swr\_so} + Q_{lwr\_sky} + Q_{lwr\_gnd} - E_{pv\_so} \tag{4.4}$$

where

Q_{conv_so} is the energy flux due to convection (W)

Q_{swr_so} is the energy flux due to absorbed shortwave radiation (W)

Q_{lwr_sky} is the longwave radiation energy flux to the sky (W)

Q_{lwr_gnd} is the longwave radiation energy flux to the ground (W)

E_{pv_so} is the electricity generated by the STPV cladding (W).

The energy balance for the floor inside surface is expressed as:

$$0 = Q_{cond} + Q_{swr\_si} + Q_{conv\_si} + Q_{lwr\_si} \tag{4.5}$$

Neglecting chemical energy conversion by photosynthesis, the energy balance for the crop interior surface is defined as:

$$0 = Q_{cond} + Q_{swr\_c} + Q_{swr\_c\_AL} + Q_{conv\_si} + Q_{lwr\_si} - Q_{ET} \quad (4.6)$$

where

$Q_{swr\_c\_AL}$ is the energy flux due to absorbed shortwave radiation on the crop surface (W)

Q_{ET} is the energy flux due to evapotranspiration (W).

4.5.4 Energy modeling key assumptions

The details and assumptions for calculating the variables in the above energy and mass balance equations are presented below.

Weather data: A typical meteorological year (TMY) weather file for Ottawa, Ontario, Canada (45.4°N, which represents mid-latitude climatic conditions) was used to run the simulations and obtain the energy performance over a one-year period. The ground temperature was defined as an annual sinusoidal function of 10±2°C (minimum temperature occurring on the 90th day of the year). Type 15 calculates the sky temperature for longwave radiation calculations (Klein et al., 2014). A simulation timestep of 15 minutes (Δt = 0.25 hr) was selected. The energy model was simulated for 396 days, with the first month of results discarded to eliminate the initial transient effects. For an analysis at peak heating design conditions, no solar radiation, a wind speed of 10 m s^{-1}, exterior air relative humidity of 20%, exterior air temperature of -21.8°C, sky temperature of -52°C, and ground temperature of 8°C were selected (RETScreen, 2013).

Conduction: Type 56 uses the ASHRAE transfer function method to solve the transient conduction heat transfer through opaque envelope components (Mitalas and Arseneault, 1970; Stephenson and Mitalas, 1971). Thermal energy storage is neglected for heat conduction through windows, the thermal shading screen (TSS), and one-dimensional steady state heat conduction (Q_{cond} in W) is modeled by:

$$Q_{cond} = C \cdot A_{si} \cdot (T_{si} - T_i) \quad (4.7)$$

where

C is the thermal conductance (W m^{-2} °C^{-1})

A_{si} is area of the inside surface (m)

T_{si} is inside surface temperature (°C)

T_i is greenhouse air temperature (°C).

Convection: The convection heat flux between an inside surface and the air (Q_{conv_si} in W) is calculated by:

$$Q_{conv\_si} = h_{si} \cdot A_{si} \cdot (T_{si} - T_i) \tag{4.8}$$

Type 56 provides internal calculation of natural convective heat transfer coefficients (CHTC) (h_{si} in W m^{-2} °C^{-1}) using the following empirical correlation that is a function of the temperature difference between the inside surface and the air:

$$h_{si} = a \cdot (T_{si} - T_i)^b \tag{4.9}$$

Since the main purpose of the thermal module is to quantify heating energy consumption, turbulent natural CHTC correlations developed by McAdams (1959) are selected. For heat flow downwards, the coefficient b is 0.25 and a is calculated from:

$$a = 0.59/(A/P)^{0.25} \tag{4.10}$$

where P is the greenhouse perimeter (m).

For heat flow upwards, the coefficient b is 0.33 and a is 1.52. For vertical surfaces, the coefficient b is 0.33 and a is 1.31.

Similarly, the convection heat flux between an outside surface and the air (Q_{conv_so} in W) is calculated by:

$$Q_{conv\_so} = h_{so} \cdot A_{so} \cdot (T_{so} - T_o) \tag{4.11}$$

where

h_{so} is the outside surface convective heat transfer coefficient (W m^{-2} °C^{-1})

A_{so} is area of the outside surface (m)

T_{so} is outside surface temperature (°C)

T_o is outside air temperature (°C).

The exterior CHTC (h_{so} in W m^{-2} °C^{-1}) is mainly a function of wind speed (V_{wind} in m s^{-1}), and the following empirical correlation by McAdams (1959) was selected in the model:

$$h_{so} = 5.7 + 3.8 \cdot V_{wind} \tag{4.12}$$

Moreover, the model assumes that the air is well-mixed inside the greenhouse.

Shortwave radiation: Type 56 enables detailed computations for radiation distribution, including multi-reflection and solar radiation leaving the zone through the windows, whereby beam and diffuse components are considered separately. A detailed calculation for distributing the primary solar direct radiation entering the zone is achieved using geometric distribution (TRANSSOLAR, 2005). For a detailed treatment of shortwave diffuse radiation, the TRNSYS radiation model applies Gebhart factors (Gebhart 1961, 1971).

Longwave radiation: Longwave radiation heat flux (Q_{lwr} in W) between two inside surfaces (*si* and *sj*) is given by:

$$Q_{lwr} = F_{si,sj} \cdot \varepsilon_{si} \cdot \sigma \cdot A_{si} \cdot \left[\left(T_{sj} + 273.15\right)^4 - (T_{si} + 273.15)^4\right] \tag{4.13}$$

where

$F_{si,sj}$ is the view factor between surfaces si and sj (dimensionless)

ε_{si} is surface area of the outside surface (dimensionless)

σ is the Stefan-Boltzmann constant (W m^{-2} K^{-4}).

For longwave radiation exchange on exterior surfaces, the viewing surfaces include the sky and ground. The procedure for longwave radiation heat transfer between interior surfaces follows that of diffuse shortwave radiation.

Ventilation: A constant minimum ventilation is used at nighttime and variable temperature-dependent ventilation controls overheating. The temperature-dependent ventilation rate (ACH_{vent} in hr^{-1}) is calculated using the following second order polynomial curve fit to several user-specified data points:

$$ACH_{vent} = \max\left(ACH_{min}, 0.5403 \cdot {T_i}^2 - 22.182 \cdot T_i + 228.5\right) \tag{4.14}$$

where ACH_{min} is the minimum ventilation rate (hr^{-1}).

The thermal (Q_{vent} in W) and moisture gains (m_{vent} in kg hr^{-1}) due to ventilation are calculated from:

$$Q_{vent} = ACH_{vent} \cdot \rho_a \cdot c_{p\_a} \cdot V \cdot (T_o - T_i) \quad (4.15)$$

$$m_{vent} = ACH_{vent} \cdot \rho_a \cdot V \cdot (\omega_o - \omega_i) \quad (4.16)$$

where ω_o *and* ω_i (in $kg_{water}\ kg_{dry\_air}^{-1}$) is the humidity ratios of the air outside and inside air, respectively.

Infiltration: Dynamic infiltration (Q_{inf} in W) is estimated using Type 571 and determined from (Klein et al., 2014):

$$Q_{inf} = ACH_{inf} \cdot \rho_a \cdot c_{p\_a} \cdot V_{wind} \cdot (T_o - T_i) \quad (4.17)$$

where ACH_{inf} (hr^{-1}) is calculated from ASHRAE (Handbook, 2009) for medium constructions.

The mass flow rate of water due to infiltration (m_{inf} in kg hr^{-1}) is given by:

$$m_{inf} = ACH_{inf} \cdot \rho_a \cdot V_{wind} \cdot (\omega_o - \omega_i) \quad (4.18)$$

Artificial lighting: This case study considers the use of high intensity light emitting diode (LED) horticulture fixtures. Thermal energy dissipated from the fixture's heat sink and convected to the airnode (Q_{AL_sink} in W) is defined as:

$$Q_{AL\_sink} = E_{AL} \cdot A \cdot F_c \cdot (1 - \eta_{AL}) \quad (4.19)$$

where η_{AL} is the electrical efficiency of light fixtures (dimensionless).

The portion that is reflected from the crop surface (Q_{AL_refl} in W), which is assumed to be fully convected to the airnode, is expressed as:

$$Q_{AL\_refl} = E_{AL} \cdot A \cdot F_c \cdot \eta_{AL} \cdot \left(1 - \alpha_{c\_PAR}\right) \quad (4.20)$$

Assuming that all the light emitted by the fixtures is received by the crop surface, the absorbed portion ($Q_{swr\_c\_AL}$ in W) is computed as:

$$Q_{swr\_c\_AL} = E_{AL} \cdot A \cdot F_c \cdot \eta_{AL} \cdot \alpha_{c\_PAR} \quad (4.21)$$

The total sensible heat gain to the airnode (Q_{AL} in W) is written as:

$$Q_{AL} = Q_{AL\_sink} + Q_{AL\_refl} \quad (4.22)$$

Evapotranspiration: A simplified evapotranspiration model was employed, where the latent heat flux at the crop surface (Q_{ET} in W) is approximated by:

$$Q_{ET} = A \cdot F_c \cdot [F_{ET} \cdot (I_c + E_{AL} \cdot \eta_{AL}) + ET_{cst}] \quad (4.23)$$

where

F_{ET} is the fraction of shortwave radiation that is converted to latent energy (dimensionless)
ET_{cst} is constant evapotranspiration rate (W m^{-2}).

The moisture gain to the airnode due to evapotranspiration (m_{ET} in kg hr^{-1}) is equal to:

$$m_{ET} = 3.6 \cdot Q_{ET}/h_v \quad (4.24)$$

where

h_v is the latent heat of vaporization of water (kJ kg^{-1})
is the factor 3.6 serves to convert units kJ^{-1} s^{-1} to J^{-1} hr^{-1}.

Ground heat transfer: The ground surface is divided in two floor zones and one crop zone (80% of footprint). The entire footprint is covered by a standard concrete slab and a layer of soil beneath. Insulation is installed beneath the concrete slab on the north and south floor areas. The model considers heat storage in the concrete and soil. The moisture effects are not accounted for in the model. The thermal capacitance of the ground insulation is ignored. The type of crop produced is a leafy green vegetable (e.g. lettuce, spinach, kale). The crop layer is approximated as a smooth and uniform surface located directly above the concrete slab and its thermal resistance and capacitance are ignored. In addition, the impact of the stage of crop growth on the energy and mass transfer is ignored.

Windows: The windows consist of a glazed portion and a frame portion. The frame properties are the same for the BCGH and PVGH. The edge heat transfer effects are ignored, and the thermal resistance of the metal frame is negligible and assumed to be equal to that of the glazing

itself. Energy storage in glazing materials and framing is neglected. Five custom STPV windows that provide partial shading have been created for this investigation. The multi-layered STPV glazing is constructed by encapsulating uniformly distributed monocrystalline silicon PV cells between a layer of polyvinyl butyral (PVB) and low-iron glass, on each side (Canadian Solar, 2016). The evenly spaced PV cells help to transmit sunlight in a uniform manner over the crop surface (avoiding shading patches). The PV cells have a white backsheet on the inside surface. Table 4.1 provides the thermal and optical properties of the float glass (BCGH), the individual layers that make up the STPV glazing, and the multi-layered clear glazed and opaque portions of the STPV glazing. The longwave radiation transmittance of the STPV glazing is equal to zero. Window 7.3 (DOE, 2015) was used to determine transmission, reflection and absorption of beam solar radiation within the multi-layered clear glazed and opaque portions of the STPV glazing.

Table 4.1: Thermal and optical properties of the individual and multi-layered glazings.

Layer	Thickness (mm)	Thermal conductivity (W m^{-1} K^{-1})	Outside solar transmittance	Outside solar reflectance	Inside solar transmittance	Inside solar reflectance
Float glass (Guardian, 2017)	4	1	0.84 (0.9)*	0.08	0.84 (0.9)	0.08
Low-iron glass (Wuhu, 2017)	2.5	1	0.92	0.06	0.92	0.06
PVB encapsulant (Dupont, 2014; Solutia, 2010)	0.4	0.19	0.934	0.033	0.934	0.033
PV cells (Armstrong and Hurley, 2010; Kapsis, 2016)	0.2	148	0	0.01	0	0.8
Clear portion of STPV glazing	5.8	0.63	0.746	0.152	0.746	0.152
PV cell portion of STPV glazing	5.8	0.63	0	0.089	0	0.722

*visible optical properties are in parenthesis when different from solar counterparts

Crystalline silicon STPV modules consist of a frame, clear-glazed and PV cell portions. This study uses the "effective" method described in (Bambara and Athienitis, 2016; Appendix C) to model the STPV glazing. This effective STPV glazing is specified as a custom window in Type 56, where the glazed portion (comprised of a clear glazing and PV cell portion) is modeled as an effective layer which optical properties depend on the PV area ratio (F_{pv}). The effective (e)

transmittance (τ) and reflectance (ρ) of the effective STPV glazing, for shortwave radiation directed from outside (so) to inside (si) and vice versa, are calculated from:

$$\tau_{e\_so} = \tau_{g\_so} \cdot \left(1 - F_{pv}\right) \tag{4.25}$$

$$\tau_{e\_si} = \tau_{g\_si} \cdot \left(1 - F_{pv}\right) \tag{4.26}$$

$$\rho_{e\_so} = \rho_{pv\_so} \cdot F_{pv} + \rho_{g\_so} \cdot \left(1 - F_{pv}\right) \tag{4.27}$$

$$\rho_{e\_si} = \rho_{pv\_si} \cdot F_{pv} + \rho_{g\_si} \cdot \left(1 - F_{pv}\right) \tag{4.28}$$

The effective absorptance (α) for each side of the glazing is given by:

$$\alpha_e = 1 - \tau_e - \rho_e \tag{4.29}$$

Table 4.2 provides the area-weighted effective solar optical properties for the STPV glazing that were calculated using Eq. (4.25-4.29). A maximum PV area ratio of 50% is selected in accordance with European regulations (Castellano, 2014) and because the greenhouse is designed for mid-to-high latitude locations where winter daylight is limited.

Table 4.2: Area-weighted effective solar optical properties for the STPV glazing.

Optical property	Effective STPV glazing				
	STPV 10%	STPV 20%	STPV 30%	STPV 40%	STPV 50%
$\tau_{e,so}$	0.671	0.597	0.522	0.448	0.373
$\tau_{e,si}$	0.671	0.597	0.522	0.448	0.373
$\rho_{e,so}$	0.146	0.139	0.133	0.127	0.121
$\rho_{e,si}$	0.209	0.266	0.323	0.380	0.437

Solar electricity generation: The rate of electricity generation (E_{pv_so} in W) from the outside surface of the STPV roof is estimated using (Skoplaki and Palyvos, 2009):

$$E_{pv\_so} = I_{pv\_so} \cdot F_{pv} \cdot \left(A - F_{fr} \cdot A\right) \cdot \eta_{STC} \cdot \left(1 - \beta_{pv} \cdot \left[T_{pv\_so} - T_{STC}\right]\right) \cdot (1 - L_w) \cdot \eta_{inv} \tag{4.30}$$

where

I_{pv_so} is solar radiation incident on the outside PV surface (W m^{-2})

A is the STPV area on the roof equal to the greenhouse footprint (m^2)

F_{fr} is the window frame fraction (dimensionless)

η_{STC} is the electrical efficiency of the PV module at STC (dimensionless)

β_{PV} is the PV module temperature coefficient (% °C^{-1})

T_{pv_so} is the temperature of outside surface temperature of the PV cells (°C)

T_{STC} is the PV cells temperature at STC (°C)

L_w is the wiring losses (dimensionless)

η_{inv} is the inverter efficiency (dimensionless).

The effect of solar incidence angle was neglected and may be included for a more detailed analysis. The effect of solar incidence angle on electricity generation is not considered. The annual electric energy (E_{pv_yr} in kWh yr^{-1}) generated by the STPV cladding is determined from:

$$E_{pv\_yr} = \sum_{\Delta t=0}^{365\cdot 24/\Delta t}\left[\Delta t \cdot \left(E_{pv\_so}\right)/10^3\right] \quad (4.31)$$

where the factor 10^3 serves to convert units W to kW.

Walls: A 1 mm thick wall is specified around the windows and has the same thermal and optical properties as the frame for the walls. For the roof, it has the same thermal and optical properties as the PV cell portion of STPV glazing so that it can be used as a reference temperature for calculating PV power output (Bambara and Athienitis, 2016; Appendix C).

Roof: The roof is assumed to be flat so that detailed diffuse shortwave and longwave radiation calculations using view factor matrices can be performed.

Thermal shading screen: A single motorized TSS is installed on the inside surface of the all windows to act as both a thermal screen and a solar blind. A simplified TSS control strategy was used, whereby the devices close at the same time based on a user-specified upper limit value of the global horizontal irradiance and exterior air temperature and when the target DLI target has been reached. More advanced control algorithms (e.g. based on predictive models and weather forecasts) may be implemented to improve the control of daylight and minimize the cases where DLI is exceeded. By using the simplified approach, the heating energy consumption for the BCGH (design that transmits the most sunlight) will be underestimated for days when the natural DLI exceeds the target value because more solar radiation enters the greenhouse than should be allowed. In reality, the TSS would be closed sufficiently in advance to avoid this issue.

Therefore, the results of this study provide a conservative energy savings estimate since the actual reduction in heating energy use would be greater if the TSS was controlled to avoid exceeding the target DLI. The longwave radiation transmittance of the TSS is neglected and assumed to be zero. The solar radiation that is absorbed on the TSS and convected to the greenhouse airnode (Q_{TSS} in W) is given by:

$$Q_{TSS} = I_{TSS} \cdot (1 - \rho_{TSS}) \cdot F_{conv\_TSS} \tag{4.32}$$

where

I_{TSS} is solar radiation incident on the TSS (W m^{-2})

ρ_{TSS} is solar reflectance of the TSS (dimensionless)

F_{conv_TSS} is the fraction of absorbed solar radiation convected to the air (dimensionless).

Capacitance multiplier: A thermal capacitance multiplier of ten was specified so that the temperature-dependent ventilation control can occur without producing rapid air temperature fluctuations that can trigger numerical instability.

Thermal energy consumption: The output of the TRNSYS simulation provides the heating power at each timestep (Q_{heat} in kJ hr^{-1}) that is required to maintain the desired setpoint temperature. The annual thermal energy consumption for heating (Q_{heat_yr} in GJ yr^{-1}) is expressed as:

$$Q_{heat\_yr} = \sum_{\Delta t=0}^{365 \cdot 24/\Delta t} (Q_{heat} \cdot \Delta t / 10^6) \tag{4.33}$$

where the factor 10^6 serves to convert units kJ to GJ.

A natural gas fired condensing boiler is used for heating and the annual gas consumption (m_{gas_yr} in m^3 yr^{-1}) is computed as:

$$m_{gas\_yr} = 10^3 \cdot Q_{heat\_yr} / (EV_{gas} \cdot \eta_{boil}) \tag{4.34}$$

where

EV_{gas} is the energy value of natural gas (MJ m^{-3})

η_{boil} is efficiency of the boiler (dimensionless).

The peak thermal energy demand is obtained for heating design day conditions. A simulation was performed for ten identical days and the peak demand was taken from the last day.

4.5.5 Values of greenhouse design parameters and their variation

Technological advances and economies of scale are expected to increase the efficiency and decrease the cost of PV and horticultural lighting technology in the future. Consequently, economic analysis using current efficiency and cost data could lead an investor to conclude that it is not economically viable to install a PV greenhouse today, but this will certainly change in the future. Therefore, a future projection study which uses the forecasted efficiencies for PV and LED lighting technology is conducted to assess the impact of such improvements on the economic viability of STPV greenhouses. The variation of the efficiency parameter for both the present and future projection studies are given in Table 4.3.

Table 4.3: Parameter values and their variation for the present and future projection studies.

Parameter	Present study value (2017)	Future projection study value (2027)	Reference
PV electrical efficiency at STC (η_{pv})	17%	23%	Canadian Solar (2016); Green et al. (2015)
Artificial light electrical efficiency (η_{AL})	40%	60%	Pinho et al. (2012)
Artificial light photon efficiency (PE_{AL})	1.77 µmol J^{-1}	3.2 µmol J^{-1}	

It is not possible to determine exactly when the efficiency of PV modules and LED horticultural fixtures will achieve these values. However, it is estimated that products with this performance will reach the market within the next 10 years (approximate year 2027). To simplify the economic analysis in the future projection study, all other parameters (the price of energy, energy cost escalation rate, and initial cost of PV and LED horticulture lighting technology) are assumed to remain unchanged from their present-day value.

Appendix A provides the values of properties for different materials and components used in the greenhouse energy model.

4.6 Economic Analysis

The net savings (*NS* achieved by the AGH compared to the BCGH, in $) formula for the LCCA is given by:

$$NS_{AGH:BCGH} = (\Delta E + \Delta W + \Delta OM\&R) - (\Delta Inv + \Delta Repl - \Delta Res) \quad (4.35)$$

where

ΔE is the change in energy cost ($)

ΔW is the change in water cost ($)

ΔOM&R is the change in operation, maintenance and replacement cost ($)

ΔInv is the change in initial investment cost ($)

ΔRepl is the change in capital replacement cost ($)

ΔRes is the change in residual value ($).

This method requires that all future costs are discounted to their present value equivalent and uses constant dollars.

The change in LCC (*ΔLCC* achieved by the AGH compared to the BCGH, in %) may be estimated as:

$$\Delta LCC_{AGH:BCGH} = 100 \cdot (-NS_{AGH:BCGH}/LCC_{BCGH}) \quad (4.36)$$

where

$$LCC = Inv + Repl + E + W + OM\&R - Res \quad (4.37)$$

where

Inv is the initial investment cost ($)

Repl is the life cycle capital replacement cost ($)

E is the life cycle energy cost ($)

W is the life cycle water cost ($)

OM&R is the life cycle operation, maintenance and replacement cost ($)

Res is the residual value ($).

4.6.1 Economic analysis key assumptions

A detailed explanation of the terms in Eq. (4.35), as it applies to the case study, follows. The analysis assumes that the cost of materials, equipment (except for the cost escalation of LED fixtures) and labor varies solely with the discount rate.

Change in energy cost (ΔE): The present value of the annually recurring costs (*PV* in $) for lighting electricity (*AL*) and natural gas for heating (*gas*) and revenue from solar electricity generation (*pv*) are calculated by Eq. (4.38), Eq. (4.39) and Eq. (4.40), respectively:

$$PV_{E\_AL} = C_{el} \cdot E_{AL\_yr} \cdot (1 + e_{el})/(d - e_{el}) \cdot [1 - [(1 + e_{el})/(1 + d)]^n] \quad (4.38)$$

$$PV_{E\_gas} = C_{gas} \cdot m_{gas\_yr} \cdot \left(1 + e_{gas}\right)/\left(d - e_{gas}\right) \cdot \left[1 - \left[\left(1 + e_{gas}\right)/(1 + d)\right]^n\right] \quad (4.39)$$

$$PV_{E\_pv} = C_{el} \cdot E_{pv\_yr} \cdot (1 + e_{el})/(d - e_{el}) \cdot [1 - [(1 + e_{el})/(1 + d)]^n] \quad (4.40)$$

where

C_{el} is the average electricity price including consumption and power demand ($ kWh^{-1})
e_{el} is the electricity cost escalation rate (%)
n is the study period (yr)
C_{gas} is the natural gas price ($ m^{-3})
e_{gas} is the electricity cost escalation rate (%).

The savings in energy costs (ΔE in $) are the difference between that of the PVGH and BCGH expressed as:

$$\Delta E = \left[PV_{E\_AL} + PV_{E\_gas}\right]_{BCGH} - \left[PV_{E\_AL} + PV_{E\_gas} - PV_{E\_pv}\right]_{PVGH} \quad (4.41)$$

Change in water cost (ΔW): It is assumed that no difference in water consumption occurs between the PVGH and BCGH.

Change in operation, maintenance and replacement cost (ΔOM&R): The implementation of the PVGH is assumed to not impact this annual recurring cost.

Change in initial investment cost (ΔInv): The incremental cost for STPV glazing compared to single glass is assumed to be equal to the price per Watt of PV modules. The incremental price per Watt for the installation of the STPV glazing and inverters are 0.2 \$ W^{-1} (Fu et al., 2017). It is assumed that the inverter portion represents 25% of this cost or 0.05 \$ W^{-1} and therefore PV installation costs are 0.15 \$ W^{-1} (Appendix B). The power rating of the PV system (E_{pv_r} in W) is defined by:

$$E_{pv\_r} = I_{STC} \cdot F_{pv} \cdot \left(A - F_{fr} \cdot A\right) \cdot \eta_{STC} \tag{4.42}$$

The total additional initial investment cost for the STPV glazing and inverter (ΔInv in \$) is obtained by multiplying the price per Watt value by the power rating of the PV system as follows:

$$\Delta Inv = E_{pv\_r} \cdot \left(\Delta C_{PV\_mat} + \Delta C_{PV\_inst} + C_{inv\_mat} + C_{inv\_inst}\right) \tag{4.43}$$

where

ΔC_{pv_mat} is the incremental material cost for STPV cladding (\$ W^{-1})

ΔC_{pv_inst} is the incremental installation cost for STPV cladding (\$ W^{-1})

C_{inv_mat} is the inverter material cost (\$ W^{-1}).

C_{inv_inst} is the inverter installation cost (\$ W^{-1}).

The thermal resistance of the STPV cladding is close to that of the glass used in the BCGH. Therefore, it is assumed that the boiler cost will not change.

Change in capital replacement cost (ΔRepl): By the end of the study period, the cost of LED fixtures is assumed to decrease to the current cost of double-ended HPS lights. The current price per Watt of the LED fixture is 1.61 \$ W^{-1} (Illumitex, 2018) and will decrease to a forecasted future value price per Watt of 0.28 \$ W^{-1} (Gravita, 2016). The annual linear cost escalation rate for the light fixtures (e_{AL}) is given by:

$$e_{AL} = \left(C_{AL\_FF}/C_{AL}\right)^{1/n} - 1 \tag{4.44}$$

where

C_{AL_FF} is forecasted future artificial light fixture price (\$ W^{-1})

C_{AL} is artificial light fixture price ($ W^{-1}).

The present value of the artificial light fixture replacement cost ($\Delta Repl_{AL\_mat}$ in $) is determined as follows:

$$Repl_{AL\_mat} = C_{AL} \cdot Nb_{AL} \cdot E_{AL\_r} \cdot [(1 + e_{AL})/(1 + d)]^{P_{AL\_repl}} \quad (4.45)$$

If the period before the fixtures need replacement (P_{AL_repl} in yr) exceeds the maximum fixture lifespan, the replacement frequency is set to the maximum fixture lifespan (P_{AL_repl}=P_{AL_max}).

The labor cost for replacing the light fixtures ($Repl_{AL\_lab}$ in $) is calculated using the single present value formula as follows:

$$Repl_{AL\_lab} = HW \cdot p \cdot Nb_{AL}/(1 + d)^{P_{AL\_repl}} \quad (4.46)$$

where

HW is hourly wage for an electrician ($ hr^{-1})

p is the labor time per fixture replaced (hr fixture^{-1}).

The total present value of the artificial light fixture replacement cost ($Repl_{AL}$ in $) is computed as:

$$Repl_{AL} = PV_{AL\_mat} + PV_{AL\_lab} \quad (4.47)$$

The one-time replacement cost of the inverters ($Repl_{inv}$ in $) is equal to:

$$Repl_{inv} = E_{pv\_r} \cdot \left(C_{inv\_mat} + C_{inv\_inst}\right)/(1 + d)^{P_{inv}} \quad (4.48)$$

where P_{inv} is the inverter lifespan (yr).

The replacement cost of the glass and STPV glazing are not considered because it is assumed that their lifespan is equal to that of the study period.

The total additional capital replacement cost ($\Delta Repl$ in $) is the difference between that of the PVGH and BCGH expressed as:

$$\Delta Repl = [Repl_{AL} + Repl_{inv}]_{PVGH} - [Repl_{AL}]_{BCGH} \quad (4.49)$$

Change in residual value (ΔRes): The residual value of the light fixtures (Res_{AL} in $) is estimated by linearly prorating its initial costs and it is estimated from:

$$Res_{AL} = C_{AL} \cdot Nb_{AL} \cdot E_{AL\_yr} \cdot (1 + e_{AL})^{P_{AL\_repl}} \cdot \left[roundup\left(n/P_{AL\_repl}, 0\right) - n/P_{AL\_repl}\right]/(1 + d)^n \quad (4.50)$$

Similarly, the residual value of the inverters (Res_{inv} in $) is approximated by:

$$Res_{inv} = E_{pv\_r} \cdot C_{inv\_mat} \cdot [roundup(n/P_{inv}, 0) - n/P_{inv}]/(1 + d)^n \quad (4.51)$$

The total residual value (ΔRes in $) is the difference between that of the PVGH and BCGH given by:

$$\Delta Res = [Res_{AL} + Res_{inv}]_{PVGH} - [Res_{AL}]_{BCGH} \quad (4.52)$$

Initial investment cost (Inv): The initial investment cost of the greenhouse (Inv in $) is taken as the sum of the structure (framing, foundation, floor, covering and TSS), HVAC (ventilation and heating system) and AL components.

$$Inv = A \cdot \left(C_{stru\_tot} + C_{HVAC\_tot} + C_{AL\_tot}\right) \quad (4.53)$$

where

C_{stru_tot} is the installed cost of the greenhouse structure per unit area ($ m^{-2})

C_{HVAC_tot} is the installed cost of the HVAC system per unit area ($ m^{-2})

C_{AL_tot} is the installed cost of the AL system per unit area ($ m^{-2}).

4.6.2 Values of greenhouse LCCA parameters

Appendix B provides the values of the cost data (in $CAD 2017) used in the LCCA. A conversion rate of 1.30 in 2017 was used to convert USD to CAD (BOC, 2018).

4.7 Results and Discussion

This section presents the results for single-sided STPV of 10-50% PV area ratio using constant electricity pricing for Ottawa, Canada. Appendix D presents the results for bifacial

STPV of 10-50% PV area ratio and the effect of TOU electricity pricing for Ottawa. Appendix E presents the results for single-sided STPV of 10-50% PV area ratio using constant electricity pricing for Whitehorse, Canada. Appendix F reveals the sensitivity of net savings to economic parameter values for both locations.

4.7.1 Electricity consumption for artificial lighting

The simulation results for energy consumption/generation of the BCGH and PVGH are given in Table 4.4. Fig. 4.3 shows the lighting electricity consumption for the BCGH and PVGH designs. Higher PV area ratios increased the lighting electricity consumption compared to the BCGH by 21.2% for 10% PV area ratio and 83.7% for 50% PV area ratio for both studies. Lighting electricity consumption decreased by 44.7% (in all cases) due to more efficient lighting technology in the future projection study.

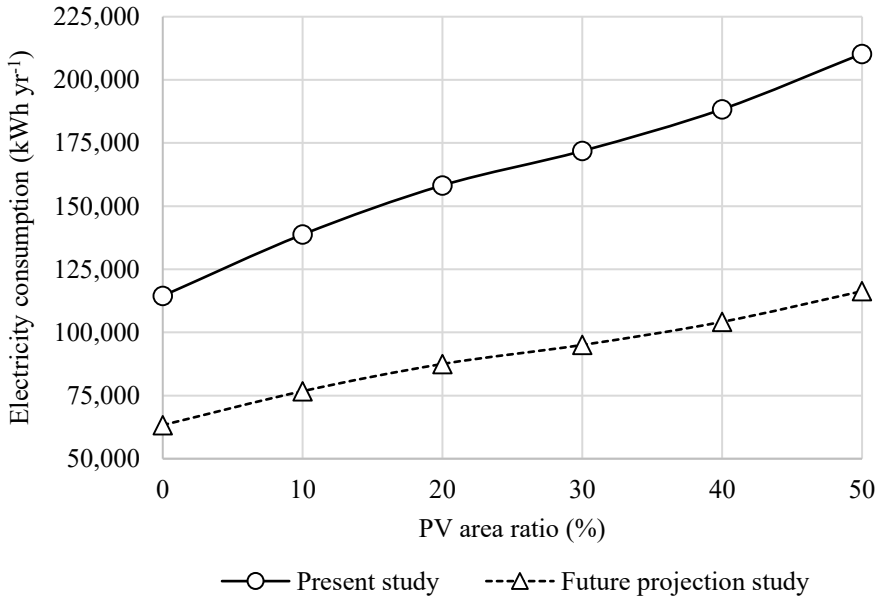

Figure 4.3: Annual electricity consumption for artificial lighting.

4.7.2 Electricity generation from STPV cladding

Fig. 4.4 illustrates how solar electricity generation increased linearly with the PV area ratio. The PV roof surface generated between 19.8-98.9 kWh m^{-2} yr^{-1} of solar electricity in the present study. Improving the PV electrical efficiency from 17% (present study) to 23% (future projection study) increased electricity production by approximately 36% in all cases. The

difference in electricity generation between both studies increased with the PV area ratio. This is explained by the higher electricity generated by improved PV technology and is directly proportional to the PV area ratio.

Table 4.4: Greenhouse energy consumption/generation in the present study.

Study	Roof envelope design	AL electricity consumption (kWh yr^{-1})	PV electricity generation (kWh yr^{-1})	Net electricity consumption (kWh yr^{-1})*	Difference in electricity consumption (kWh yr^{-1})**	Natural gas consumption (m^3 yr^{-1})
Present	BCGH	114,475	-	114,475	-	62,783
	STPV 10%	138,766	18,354	120,412	5938	60,328
	STPV 20%	158,224	36,717	121,507	7032	58,733
	STPV 30%	171,857	55,088	116,769	2294	57,811
	STPV 40%	188,381	73,467	114,914	439	56,812
	STPV 50%	210,318	91,850	118,468	3993	55,260
Future projection	BCGH	63,316	-	63,316	-	66,372
	STPV 10%	76,751	24,924	51,827	-11489	65,014
	STPV 20%	87,513	49,863	37,651	-25665	64,007
	STPV 30%	95,054	74,812	20,242	-43074	63,521
	STPV 40%	104,193	99,774	4,419	-58896	62,986
	STPV 50%	116,326	124,742	-8,415	-71731	61,987

*calculated as the AL electricity consumption minus the PV electricity generation
**between the PVGH and BCGH (calculated using Eq. (4.54))

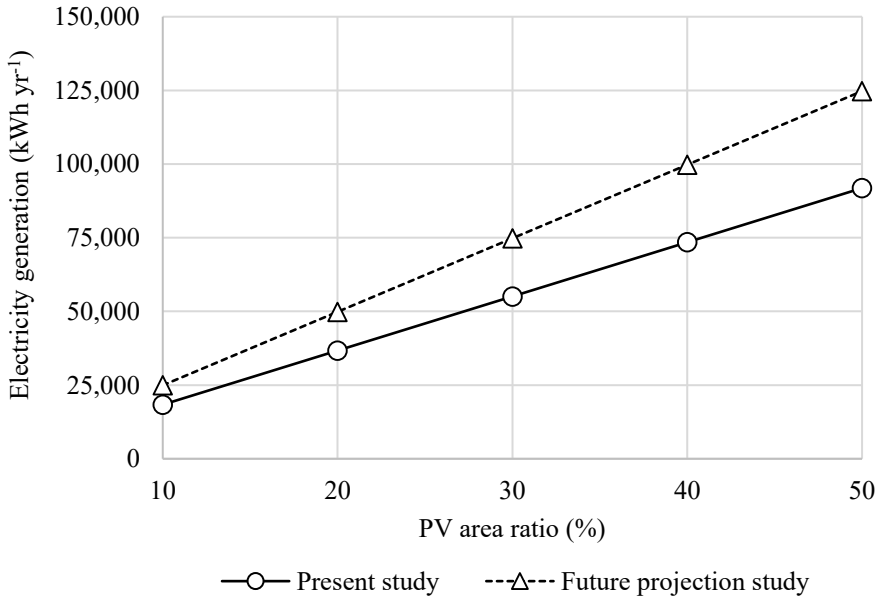

Figure 4.4: Electricity generation from STPV cladding.

4.7.3 Net electricity consumption/generation

The PVGH produced internal shading which increased electricity consumption for artificial lighting. For a PVGH to be viable in terms of energy costs, the increase in lighting electricity costs must be counteracted by a reduction in heating fuel costs and/or revenues from the sale of solar electricity. In summer, little artificial lighting is consumed compared to the solar electricity that is generated, in winter, it is the contrary. Therefore, over an average year, it may be desirable that the solar electricity generation exceeds the incremental electricity consumption for lighting. Table 4.4 and Fig. 4.5 give the difference in the electricity consumption (lighting and PV electricity) between the PVGH and BCGH ($\Delta E_{PVGH:BCGH}$ in kWh yr^{-1}) which is calculated from:

$$\Delta E_{PVGH:BCGH} = E_{AL\_yr\_PVGH} - E_{AL\_yr\_BGGH} - E_{pv\_yr} \quad (4.54)$$

where

$E_{AL\_yr\_PVGH}$ is electricity consumption for artificial lighting for the PVGH (kWh yr^{-1})
$E_{AL\_yr\_BCGH}$ is electricity consumption for artificial lighting for the BCGH (kWh yr^{-1})
E_{pv_yr} is electricity generated by the STPV cladding (kWh yr^{-1}).

The results for the present study indicated that the PVGH did not produce enough solar electricity to compensate for the increased use of lighting electricity that is provoked by the STPV shading. At best, the greenhouse with 40% PV area ratio consumed 440 kWh yr^{-1} more than the BCGH. This is because the net electricity consumption for the PVGH was minimal at 40% PV area ratio. However, in the future projection study, the net electricity consumption for the PVGH was always less than the BCGH (reduction of between 11,500-71,700 kWh yr^{-1}). The difference in electricity use between the PVGH and BCGH evolved in a linear manner as the net electricity consumption decreased linearly with the PV area ratio. Above 40% PV area ratio, the PVGH generates more electricity than it consumes for artificial lighting. Therefore, the energy balance is sensitive to the efficiency of PV and lighting technology. The difference in electricity consumption between both studies increased with the PV area ratio as it remained nearly constant for the present study and increased linearly for the future projection study.

Fig. 4.6 gives the fraction of consumed lighting electricity that was offset by electricity generated from the STPV roof. For the present study, the STPV roof generated between 13.2-43.7% of the electricity that was consumed for supplemental lighting, whereas 32.5-107.2% of the electricity needs were produced in the future projection study. Therefore, in the future, a PV roof could potentially displace all the greenhouse's electricity needs for supplemental lighting.

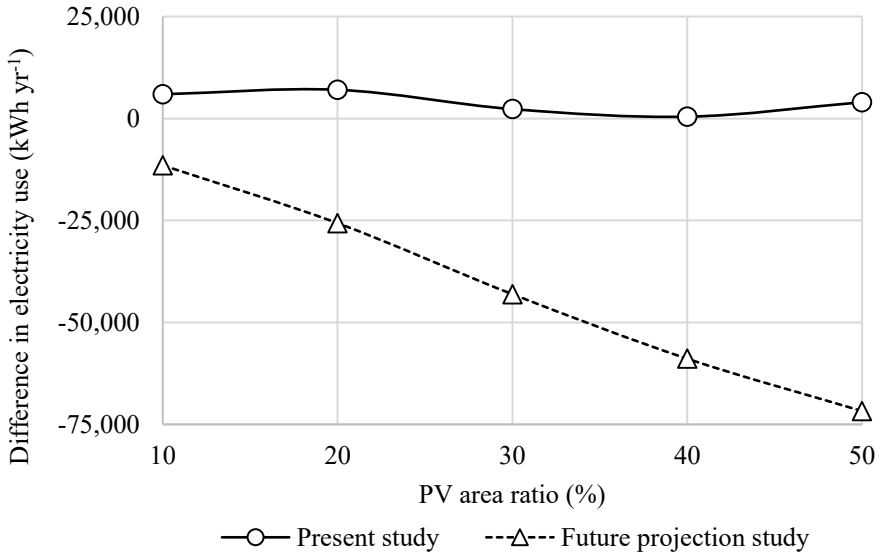

Figure 4.5: Difference in electricity consumption (for lighting minus PV generation) between the PVGH and BCGH (negative indicates PVGH consumes less electricity than BCGH).

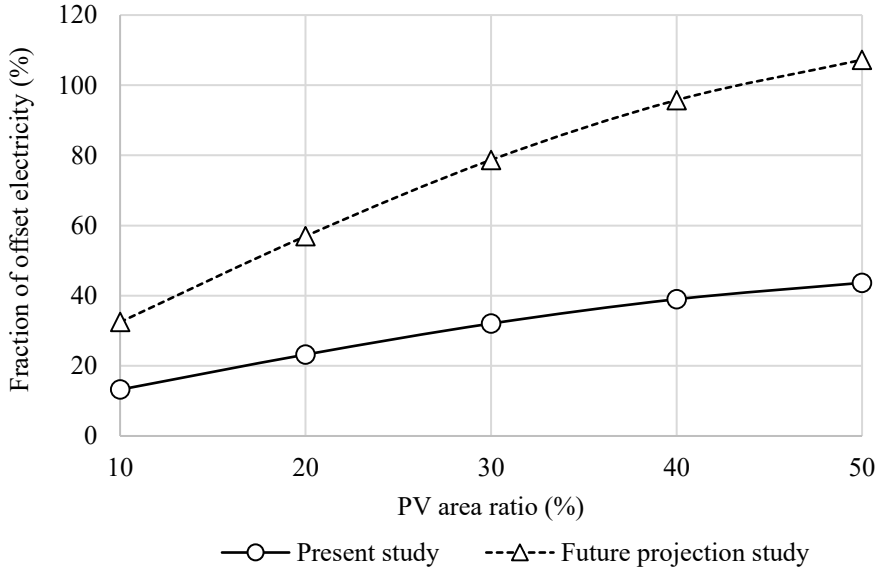

Figure 4.6: Fraction of electricity consumed for artificial lighting that is offset by electricity generated from STPV.

4.7.4 Natural gas consumption

Fig. 4.7 presents the natural gas consumed for heating for the various STPV designs. The heating energy consumption decreased in a nearly linear manner with increasing PV area ratios by a minimum of 2.0% for 10% PV area ratio in the future projection study and by a maximum of 12.0% for 50% PV area ratio in the present study. This may be explained in part by the following reasons: 1) as the PV area ratio increases, so does the operation of the artificial lights which gives off heat and thus reduces the amount of energy consumed for heating; 2) the STPV roof absorbs more solar energy which results in a higher surface temperature and thus less heat loss compared to glass; and 3) due to the opaque PV cells, less of the sunlight that is reflected by the interior surfaces of the PV greenhouse is transmitted back outside. More efficient light fixtures caused heating energy consumption to increase by 5.7-12.2% in the future projection study.

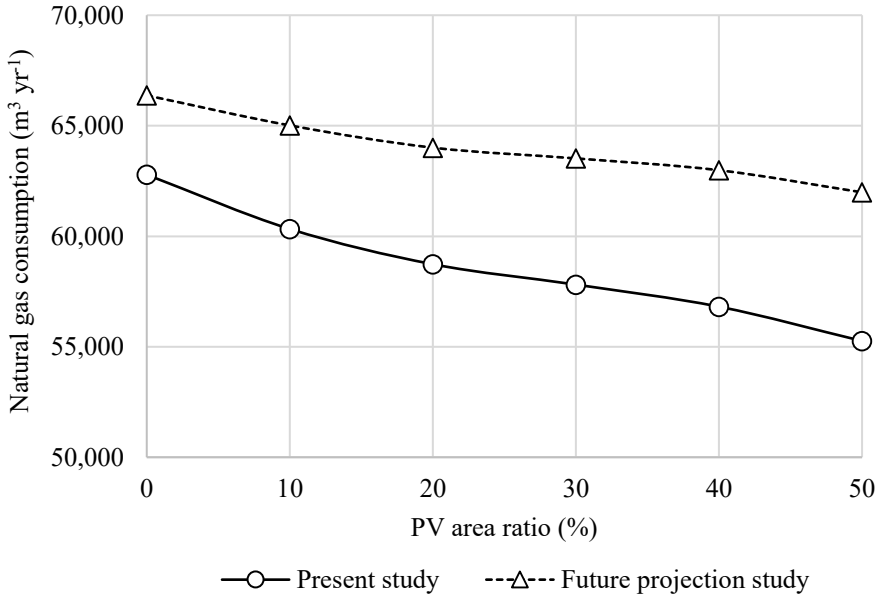

Figure 4.7: Natural gas consumption for heating.

4.7.5 Life cycle cost analysis

Table 4.5 provides the present-value costs, residual value, NS (in $CAD 2017), and change in LCC and Fig. 4.8 depicts the NS that was achieved for the various PVGH designs. For the present study, installing STPV cladding would produce a financial loss of between $12,450 and $44,811 over its lifespan (0.5-1.9% increase in LCC). The incurred loss was minimal ($12,450) at a PV area ratio of 40% and increases at the higher and lower PV area ratios. This is explained by the fact that the life cycle energy costs are minimal at a PV area ratio of 40%, whereas all other present-value costs and the residual value increase with the PV area ratio. As a result, STPV cladding is not yet an economically attractive investment. In the future projection study, a reduction in LCC was achieved for all the PVGH designs. The reduction was lowest for 10% PV area ratio (3.8% reduction in LCC, NS of $75,186) and greatest for 50% PV area ratio (22.8% reduction in LCC, NS of $454,893). The net savings follows a linear trend in the future projection study as the life cycle energy costs also decrease in a linear manner with the PV area ratio. The difference in net savings between both studies increased with the PV area ratio as the net savings remained nearly constant for the present study and increased linearly for the future projection study. Therefore, the economic situation is evolving towards increased viability of STPV claddings and there may be significant potential for reducing energy use and overall costs in the future.

It should be noted that LED horticultural lighting was selected for use in the BCGH and PVGH without considering whether it is the most cost-effective lighting solution. Since both greenhouses were equipped with the same lighting installation at the base date, their initial cost did not impact the net savings measure. However, the change in LCC would be higher if HPS lights would have been selected for the analysis because their initial investment cost is, at present, significantly lower. A separate energy and economic study should be performed to validate the economic viability of LED lighting over competing technology such as double-ended HPS fixtures.

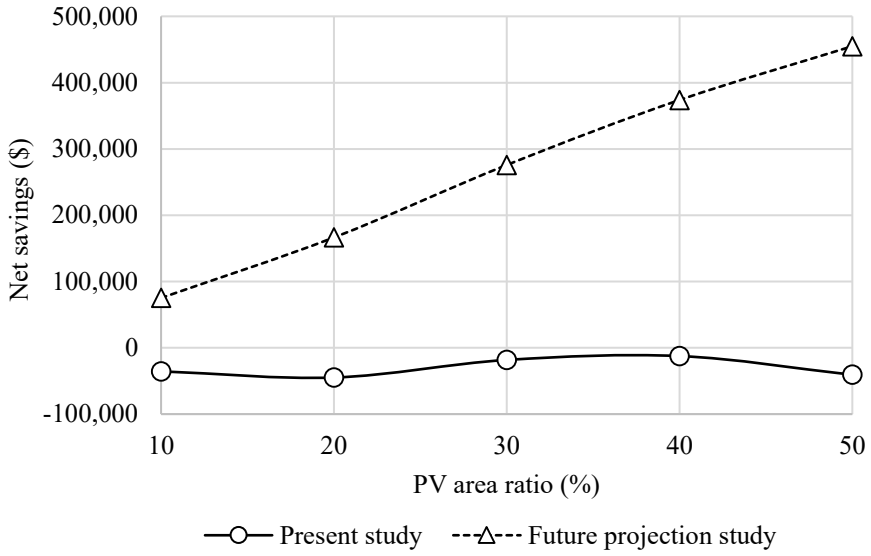

Figure 4.8: NS achieved by integrating STPV cladding on the greenhouse roof.

Table 4.5: Present-value costs, residual value, NS, and change in LCC.

Study	Roof envelope design	Energy cost	Initial investment cost	Capital replacement cost	Residual value	NS	Change in LCC
Present	BCGH	$1,588,749	$0	$84,949	$25,586	-	-
	STPV 10%	$1,604,584	$17,483	$87,856	$26,287	-$35,525	1.5%
	STPV 20%	$1,594,180	$34,967	$90,764	$26,989	-$44,811	1.9%
	STPV 30%	$1,547,967	$52,450	$93,672	$27,690	-$18,287	0.8%
	STPV 40%	$1,522,440	$69,934	$96,580	$28,392	-$12,450	0.5%
	STPV 50%	$1,530,954	$87,417	$99,487	$29,093	-$40,654	1.7%
Future projection	BCGH	$1,247,596	$0	$46,968	$14,146	-	-
	STPV 10%	$1,145,772	$23,654	$50,902	$15,095	$75,186	-3.8%
	STPV 20%	$1,027,912	$47,308	$54,836	$16,045	$166,406	-8.3%
	STPV 30%	$891,914	$70,962	$58,770	$16,994	$275,766	-13.8%
	STPV 40%	$767,240	$94,616	$62,704	$17,943	$373,801	-18.7%
	STPV 50%	$659,509	$118,270	$66,638	$18,892	$454,893	-22.8%

4.8 Conclusion

This chapter demonstrates how the combination of integrated thermal-daylight energy analysis and life cycle cost analysis can be employed to compare innovative cladding designs for greenhouses. To the best of the author's knowledge, it is the first time that PV envelope design alternatives for a greenhouse that controls light to a consistent daily integral were compared based on local climatic and economic conditions. The methodology was applied to assess the economic viability of STPV cladding employed on a greenhouse located in Ottawa, Ontario, Canada. The study was conducted using current (present study) and future projected (future projection study) values for the efficiency of PV and horticultural lighting technology.

The STPV cladding generated solar electricity but also caused internal shading that was counteracted by increasing supplemental lighting by as much as 84%, which in turn reduced heating energy consumption by up to 12%. Although STPV cladding would not be an economically attractive investment today, a nearly 30% reduction in LCC was achieved in the future projection study. When the efficiency of PV and lighting technology reaches the future projection values, a STPV roof has the potential to displace all the greenhouse's electricity needs for supplemental lighting. Therefore, STPV will increasingly become a promising cladding alternative that can improve energy efficiency and the economics of greenhouse operations.

An important factor to consider is the internal shading pattern and uniformity that occurs when employing STPV cladding. Ideally, the greenhouse side walls and STPV glazing would diffuse the transmitted daylight so that it is distributed as uniformly as possible over the crop canopy. Moreover, additional experimental research, whereby PV and conventional greenhouses operate side-by-side, is needed to validate theoretical findings, evaluate the performance of new technologies, and develop optimal control strategies. PV greenhouses can contribute to reducing the human footprint on the environment by enabling renewable energy generation and crop production within the same structure.

CHAPTER 5: COMPARISON OF GLASS, POLYCARBONATE AND OPAQUE CLADDING[2]

5.1 Abstract

The energy consumption of a building is significantly impacted by its envelope design, particularly for greenhouses where coverings typically provide high heat and daylight transmission. Energy and life cycle cost (LCC) analysis were employed to identify the most-cost effective cladding design for a greenhouse that employs supplemental lighting located in Ottawa, Ontario, Canada (45.4°N). The base case envelope design uses single glazing whereas the two alternative designs consist of replacing glass with twin-wall polycarbonate and adding of foil-faced rigid insulation (permanent and movable) on the interior surface of the glass. All the alternative envelope designs increased lighting electricity consumption and decreased heating energy use except when permanent and movable insulation were applied to the north wall and in the case of permanent insulation on the north wall plus polycarbonate on the east wall. This demonstrates how the use of reflective opaque insulation on the north wall can be beneficial for redirecting light onto the crops to achieve simultaneous reductions in electricity and heating energy costs. A maximum reduction in LCC of 5.5% (net savings of approximately $130,000) was achieved when permanent insulation was applied to the north and east walls plus polycarbonate on the west wall. This alternative envelope design increased electricity consumption for horticultural lighting by 4.3%, reduced heating energy use by 15.6% and caused greenhouse gas emissions related to energy consumption to decrease by 14.7%. This analysis demonstrates how energy and economic analysis can be employed to determine the most suitable envelope design based on local climate and economic conditions.

5.2 Introduction

The greenhouse envelope design dictates the daylight transmission and heat transfer that occurs between the outside and inside environment and has a significant impact on the energy required for heating and lighting. Technological advances are providing greenhouse owners with an increasing number of cladding options and methods for determining the most suitable design for a given climate and local economic conditions are required. Greenhouse envelope design is a

[2] Bambara, J. & Athienitis, A. K. (2018). Energy and economic analysis for greenhouses envelope design. Transactions of the American Society of Agricultural and Biological Engineers, 61(6), 1-16.

challenging task because it must simultaneously consider the interaction between many design elements and weight the impact on key decision-making factors (e.g. indoor climate control, crop growth, economics). Strategic greenhouse envelope design should follow a systematic approach which integrates physical, biological and economic models. However, Table 2.4 shows how most prior work focuses on either energy or crop yield, with economic considerations often omitted from the decision-making process. Vanthoor (2011) provided a methodology for greenhouse design based on climatic, crop yield and economic models. The methodology was applied to design tomato greenhouses in Spain and Netherlands using the annual net financial result as a method for economic assessment.

Greenhouses that employ supplemental lighting contribute to food security by enabling crop production near the consumer regardless of their location in the world. In mid-to-high latitude locations, horticultural lighting fixtures are used to maintain crop yield in winter and shading devices are employed to control excess solar radiation in summer. To compare alternative envelope designs for these types of greenhouses, the analysis must simultaneously quantify their impact on electricity consumed for artificial lighting/thermal energy used for heating, and economic performance over the lifespan of the greenhouse. For instance, the use of polycarbonate instead of glass cladding will increase lighting energy use, decrease heating, and will likely have a different initial cost and lifespan. A methodology for the envelope design of these greenhouses is currently unavailable. The methodology proposed by Vanthoor (2011) does not cover greenhouses that use artificial lighting and the required method for modeling the interaction between the daylighting, lighting and thermal domains. Moreover, life cycle cost analysis provides a better assessment of the long-term cost effectiveness of a project, in contrast to alternative economic methods that solely focus on first costs or on operating-related costs in the short run (e.g. annual net financial result, payback period) (Fuller and Petersen, 1996).

The aim of this paper is to demonstrate how integrated thermal-daylight energy analysis and life cycle cost analysis (LCCA) can be employed to identify the most-cost effective cladding design for a greenhouse that controls light to a consistent daily integral located in Ottawa, Ontario, Canada (45.4°N, mid-latitude, 4,560 heating degree-days).

5.3 Energy and Economic Analysis

For greenhouses that supplement daylight with horticultural lighting, the choice of cover materials may alter the daylight availability and lighting electricity use. The effects of such alterations must be transferred to the module which calculates the thermal energy consumption. In theory, modifying the envelope design for greenhouses that control light to a consistent daily integral (e.g. for producing leafy green vegetables year-round near the consumer) should not affect crop growth as the supplemental lighting, shading screen and HVAC systems control will adjust and compensate for any changes in the indoor climate. Consequently, the analysis of this type of greenhouse will be carried out by omitting biological aspects.

The decision-making process for envelope design requires both energy and economic analysis. The performance obtained through energy simulation is not sufficient for determining a cost-optimal design. From an investor's perspective, the incremental cost of alternative claddings should be outweighed by operational savings. This study employs LCCA and the net savings method was selected for comparing envelope design alternatives. The net savings method can provide detailed economic analysis in a time efficient manner (it only requires economic aspects that are impacted by a design variation to be quantified).

5.4 Greenhouse Characteristics

A schematic of the 929.03 m^2 (10,000 sqft) greenhouse considered for this study is provided in Fig. 4.1. It has an equal length and width of 30.48 m, and a height of 3.66 m. The floor surface consists of a crop zone located between two identical floor areas. Heating and ventilation is used to control inside humidity and temperature. The greenhouse does not utilize humidification, cooling is provided by mechanical ventilation only, and condensation is ignored in this study. The AL are the only internal gain considered in the model.

The BCGH is clad with a single layer of glass. Three alternative greenhouse (AGH) envelope designs that will be considered in this study consist of: 1) replacing the glass cladding of the BCGH with twin-wall polycarbonate sheets; 2) adding permanent opaque insulation on the inside surface of the glass cladding of the BCGH; and 3) applying movable opaque insulation on the inside surface of the glass cladding of the BCGH.

5.5 Energy Analysis

TRNSYS 17.2 was selected for the transient simulation of the greenhouse climate (Klein et al., 2014). Type 56 multizone building model was used to create the greenhouse energy model (TRANSSOLAR, 2005). Annual and design day energy simulations of the model are performed to obtain the energy-related inputs that are needed for conducting the LCCA. The energy analysis is separated into daylight, artificial light and thermal modules.

5.5.1 Daylight module

The methodology for the daylight module is described in section 3.6.

5.5.2 Artificial lighting control module

The methodology for the artificial light control module is described in section 3.7.

5.5.3 Thermal module

The methodology for the thermal module is the same as in section 4.5, except that there is no electricity generated by the STPV cladding.

5.5.4 Energy modeling key assumptions

The details and assumptions for calculating the variables in the above energy and mass balance equations are the same as in section 4.5, except for those presented below.

Windows: The windows consist of a glazed portion and a frame portion. The thermal properties for the glass and polycarbonate glazing are given in Table 5.1. The longwave radiation transmittances of both glazing are equal to zero. The frame properties are the same for the BCGH and AGH. The edge heat transfer effects are ignored, and the thermal resistance of the metal frame is negligible and assumed to be equal to that of the glazing itself. Energy storage in glazing materials and framing is neglected.

Table 5.1: Thermal and optical properties of the glass and twin-wall polycarbonate glazing.

Layer	Thickness (mm)	Thermal conductivity (W m^{-1} K^{-1})	Solar transmittance (both directions)	Solar reflectance (both directions)	Emissivity (both directions)	Transmittance to LWR (both directions)
Float glass (Guardian, 2017)	4	1	0.84 (0.9)*	0.08	0.9	0
Polycarbonate (Polygal, 2018)	8	0.026	0.68 (0.79)	0.15 (0.17)	0.9	0

*visible optical properties are in parenthesis when different from solar counterparts.

Walls: A 1 mm thick wall is specified around the windows and has the same thermal and optical properties as the window frames. The TSS shading factor and its thermal and optical properties were modified to model a window this is covered with an opaque alternative envelope option (permanent or movable foil-faced expanded polystyrene (EPS) insulation boards). The thermal capacitance of insulation is ignored.

Movable insulation: The movable insulation has the same properties as the permanent insulation and is installed on November 1st and removed on March 1st.

Thermal shading screen: Same as in section 4.5 but the north wall only has a thermal screen.

Greenhouse gas (GHG) emissions: The GHG emissions produced from electricity generation and fuel combustion for heating can be estimated by multiplying the annual energy consumption (EC in kWh yr^{-1} for electricity and m^3 yr^{-1} for natural gas) and the location-specific emission factor (EF in kg eCO_2 kWh^{-1} for electricity and kg eCO_2 m^{-3} for natural gas):

$$GHG = EC \cdot EF \tag{5.1}$$

5.6 Economic Analysis

The net savings (NS) formula for the LCCA is given by Eq. (4.35). The change in LCC may be estimated using Eq. (4.36):

5.6.1 Economic analysis key assumptions

A detailed explanation of the terms in Eq. (4.35), as it applies to the case study, follows. The analysis assumes that the cost of materials, equipment (except for the cost escalation of LED fixtures) and labor varies solely with the discount rate.

Change in energy cost (ΔE): The present value of the annually recurring cost for lighting electricity and natural gas for heating are calculated by Eq. (4.38) and Eq. (4.39), respectively. The savings in energy costs is the difference between that of the AGH and BCGH expressed as:

$$\Delta E = \left[PV_{E\_AL} + PV_{E\_gas}\right]_{BCGH} - \left[PV_{E\_AL} + PV_{E\_gas}\right]_{AGH} \tag{5.2}$$

Change in water cost: It is assumed that no difference in water consumption occurs between the AGH and BCGH.

Change in operation, maintenance and replacement cost (O&MR): Manual labor is needed to install the movable insulation for the cold season and to remove it for the warm season. The present value of annually recurring cost related to movable insulation ($PV_{OM\&R\_mov}$ in \$) is computed as:

$$PV_{OM\&R\_mov} = A_{mov} \cdot C_{mov\_lab} \cdot [(1+d)^n - 1]/[d \cdot (1+d)^n] \tag{5.3}$$

where

A_{mov} is the area with movable insulation (m^2)

C_{mov_lab} is the labor cost for installing and removing movable insulation (\$ yr^{-1}).

The savings in OM&R cost ($\Delta OM\&R$ in \$) is the difference between that of the AGH and BCGH expressed as:

$$\Delta OM\&R = -\left[PV_{OM\&R\_mov}\right]_{AGH} \tag{5.4}$$

Change in investment cost (ΔInv): The installation cost for glass and polycarbonate cladding are assumed to be identical (Westbrook, 2017) and the additional cost for the polycarbonate cladding (ΔC_{poly} in \$) is calculated as:

$$\Delta C_{poly} = A_{poly} \cdot \left(C_{poly\_mat} - C_{glass\_mat}\right) \tag{5.5}$$

where

A_{poly} is the area with replaced with polycarbonate (m^2)

C_{poly_mat} is the cost of polycarbonate (\$ m^{-2})

C_{glass_mat} is the cost of glass (\$ m^{-2}).

The additional material and installation cost for the added rigid insulation (ΔC_{ins} in \$) is determined as follows:

$$\Delta C_{ins} = A_{ins} \cdot \left(C_{ins\_mat} + C_{ins\_inst}\right) \tag{5.6}$$

where

A_{ins} is the area with replaced with permanent or movable insulation (m^2)
C_{ins_mat} is the material cost of insulation (\$ m^{-2})
C_{ins_inst} is the installation cost of insulation (\$ m^{-2}).

The additional material cost for the movable rigid insulation (ΔC_{mov} in \$) is determined as follows:

$$\Delta C_{mov} = A_{mov} \cdot \left(C_{ins\_mat}\right) \tag{5.7}$$

When permanent rigid insulation is added to the glazing, there is no need for a TSS (cost savings). Therefore, the avoided material and installation cost associated with not using a TSS (ΔC_{TSS} in \$) is given by:

$$\Delta C_{TSS} = A_{ins} \cdot \left(C_{TSS\_mat} + C_{TSS\_inst}\right) \tag{5.8}$$

where

C_{TSS_mat} is the material cost of TSS (\$ m^{-2})
C_{TSS_inst} is the TSS installation cost (\$ m^{-2}).

The AGH envelope designs reduce the peak heating energy demand and this may cause the size and associated cost of the boiler to decrease. The change in material and installation cost for the boiler (ΔC_{boil} in \$) is computed as:

$$\Delta C_{boil} = \left[Q_{p\_heat} \cdot \left(C_{boil\_mat} + C_{boil\_inst}\right)\right]_{AGH} - \left[Q_{p\_heat} \cdot \left(C_{boil\_mat} + C_{boil\_inst}\right)\right]_{BCGH} \tag{5.9}$$

where

Q_{p_heat} is the rated thermal output of the nearest commercially available boiler that can satisfy the simulated peak thermal energy demand (kW)

C_{boil_mat} is the material cost of the boiler (\$ kW^{-1})

C_{boil_inst} is the boiler installation cost (\$ kW^{-1}).

The total additional investment cost (ΔInv in \$) is determined as follows:

$$\Delta Inv = \Delta C_{poly} + \Delta C_{ins} + \Delta C_{mov} - \Delta C_{TSS} + \Delta C_{boil} \quad (5.10)$$

Change in capital replacement cost (ΔRepl): Polycarbonate has a shorter replacement period than glass. The additional one-time material ($\Delta Repl_{poly\_mat}$ in \$) and labor ($\Delta Repl_{poly\_lab\_repl}$ in \$) replacement cost for the polycarbonate is calculated using Eq. (5.11) and Eq. (5.12), respectively:

$$Repl_{poly\_mat} = A_{poly} \cdot C_{poly\_mat}/(1+d)^{P_{poly}} \quad (5.11)$$

$$Repl_{poly\_lab\_repl} = A_{poly} \cdot C_{poly\_lab\_repl}/(1+d)^{P_{poly}} \quad (5.12)$$

where

P_{poly} is the polycarbonate lifespan (yr)

$C_{poly\_lab\_repl}$ is the labor cost for replacing polycarbonate (\$ m^{-2}).

The total polycarbonate replacement cost ($\Delta Repl_{poly}$ in \$) is computed as:

$$Repl_{poly} = Repl_{poly\_mat} + Repl_{poly\_lab\_repl} \quad (5.13)$$

The total present value of the artificial light fixture replacement cost is computed using Eq. (4.44-4.47).

The cost for replacing a boiler ($Repl_{boil}$ in \$) is equal to:

$$Repl_{boil} = Q_{p\_heat} \cdot \left(C_{boil\_mat} + C_{boil\_lab\_repl}\right)/(1+d)^{P_{boil}} \quad (5.14)$$

where P_{boil} is the boiler lifespan (yr).

Since the replacement period for rigid insulation and the glass is the same as the study period, they are ignored in the LCCA.

The total additional capital replacement cost ($\Delta Repl$ in \$) is the difference between that of the AGH and BCGH expressed as:

$$\Delta Repl = \left[Repl_{poly} + Repl_{AL} + Repl_{boil}\right]_{AGH} - \left[Repl_{AL} + Repl_{boil}\right]_{BCGH} \quad (5.15)$$

Change in residual value (ΔRes): The residual value of the polycarbonate (Res_{poly} in \$) is estimated by linearly prorating its initial costs and is computed as:

$$Res_{poly} = \Delta C_{poly} \cdot \left[roundup\left(n/P_{poly}, 0\right) - n/P_{poly}\right]/(1+d)^n \quad (5.16)$$

The residual value of the light fixtures (Res_{AL} in \$) is estimated by linearly prorating its initial costs and it is estimated from:

$$Res_{AL} = C_{AL} \cdot Nb_{AL} \cdot E_{AL\_yr} \cdot (1+e_{AL})^{P_{AL_{repl}}} \cdot \left[roundup\left(n/P_{AL\_repl}, 0\right) - n/P_{AL\_repl}\right]/(1+d)^n \quad (5.17)$$

The residual value for the boilers (Res_{boil} in \$) is approximated by:

$$Res_{boil} = Q_{p\_heat} \cdot \left(C_{boil\_mat}\right) \cdot \left[roundup(n/P_{boil}, 0) - n/P_{boil}\right]/(1+d)^n \quad (5.18)$$

The total residual value (ΔRes in \$) is the difference between that of the AGH and BCGH given by:

$$\Delta Res = \left[Res_{poly} + Res_{AL} + Res_{boil}\right]_{AGH} - \left[Res_{AL} + Res_{boil}\right]_{BCGH} \quad (5.19)$$

Initial investment cost (Inv): The initial investment cost of the greenhouse is calculated using Eq. (4.53).

5.6.2 Values of greenhouse LCCA parameters

Appendix B provides the values of the cost data (in \$CAD 2017) used in the LCCA. A conversion rate of 1.30 in 2017 was used to convert USD to CAD (BOC, 2018).

5.7 Results and Discussion

This section presents the most cost-effective envelope design between glass, polycarbonate and opaque insulation for each surface of a greenhouse located in Ottawa, Canada. The analysis is repeated for Whitehorse, Canada in Appendix G. Appendix H reveals the sensitivity of net savings to energy model input parameters, operation parameters, and economic parameter values for both locations.

To ensure that the energy consumption predictions obtained using TRNSYS are sufficiently realistic, the greenhouse model was run for Calgary, Alberta (without artificial lighting) and compared to energy bills provided by several greenhouse operators in that location. The measured annual heating energy consumption was found to be 2.7 GJ m^{-2} yr^{-1} for cucumbers and 3.2 GJ m^{-2} yr^{-1} for tomatoes (Laate, 2013) and the value obtained using TRNSYS simulations was 3.0 GJ m^{-2} yr^{-1}. Since the simulated value is found to be in approximately in the center of the range that was measured for two common fruiting crops, it can be concluded that annual simulations of the greenhouse energy model are suitable for representing the actual performance.

Table 5.2 provides the incident solar radiation on the greenhouse surfaces. The analysis of the surfaces will be in the order: north, east, west and south walls, and roof.

Table 5.2: Annual incident solar radiation on greenhouse surfaces.

Surface	north wall	east wall	west wall	south wall	roof
Incident solar radiation (GJ m^{-2} yr^{-1})	1.46	2.99	3.05	4.15	4.96

The present-value costs, residual value, NS (in $CAD 2017), and change in LCCA for the AGH and BCGH are provided in Table 5.3. Table 5.4 gives the annual energy consumption (lighting electricity and fuel consumed for heating) and the annual GHG emissions related to energy consumption.

It was found that placing permanent insulation on the north wall reduced the LCC by 2.6% (NS of $61,390). The savings are mainly the result of reduced energy costs produced by the AGH design. Interestingly, in addition to decreasing heating energy consumption by approximately 5.9%, a north wall employing permanent insulation also reduced the lighting electricity consumption by 1.7%. This means that the amount of sunlight that is reflected by the

opaque north wall is greater than what would otherwise be transmitted by the glass wall of the BCGH. Moreover, the initial investment cost is negative because the savings that results from not installing the TSS ($3,191) outweigh the additional expense of the added insulation ($1,731). Next, movable insulation was applied to the north wall. The design alternative did not reduce the LCC as much (0.4%) as for permanent insulation (2.6%). This is mainly due to the annual O&MR costs associated with installing and taking away the movable insulation. Despite this, the movable insulation on the north wall was the design that reduced the lighting electricity consumption the most (112,409 kWh yr^{-1} versus 114,475 kWh yr^{-1} for the BCGH). However, heating energy use was more than the AGH with permanent insulation because there was still heating required before it is installed (November 1st) and after it is removed (March 1st). The third case consists of replacing the glass on the north wall with polycarbonate. This alternative design reduced the LCC by 0.7%, which is less than the case of permanent insulation (2.7%). As expected, polycarbonate on the north wall increased lighting electricity use and decreased heating energy use. Therefore, although each of these three designs produced NS, the case of permanent insulation on the north wall is the most cost-effective design since it produced the highest NS. Consequently, this design will be carried forward in the subsequent analysis.

The next building surface to consider is the east wall because it receives the lowest sunlight after the north wall. When permanent and movable insulation and polycarbonate were applied to the east wall, the LCC decreased by 5.3%, 3.6% and 5.2%, respectively (NS of $126,611, $86,250 and $124,764). Therefore, the most suitable envelope design for the east wall is also when permanent insulation is employed, and this will be carried forward in the subsequent analysis. The economic results for polycarbonate was, however, very similar to that of permanent insulation. Meanwhile, it is interesting to note that polycarbonate was the only east wall AGH design that reduced the lighting electricity consumption (113,814 kWh yr^{-1} versus 114,475 kWh yr^{-1} for the BCGH). Despite this, the GHG emissions related to energy consumption were lowest for the permanent insulation option because of the higher carbon footprint of heating fuel compared to electricity.

When permanent and movable insulation and polycarbonate were applied to the west wall, the LCC decreased by 5.3%, 3.8% and 5.5%%, respectively (NS of $127,364, $91,826 and $131,143). Therefore, the most suitable envelope design for the west wall is when polycarbonate

is employed, and this will be carried forward in the subsequent analysis. Meanwhile, the reduction in GHG emissions related to energy consumption was slightly higher for the west wall AGH design that employs permanent insulation (16.8%) that the most cost-effective AGH design (polycarbonate with 14.7% emission reduction).

When permanent and movable insulation and polycarbonate were applied to the south wall, the LCC decreased by 1.6%, 0.4% and 5.1%%, respectively (NS of $39,115, $9,367 and $121,854). None of these AGH designs will be carried forward in the subsequent analysis because they do not provide a greater economic benefit (nor greater reduction in GHG emissions related to energy consumption) than most cost-effective design that was obtained so far (permanent insulation on north and east walls plus polycarbonate on west wall, which provided NS of $131,143). Therefore, the most suitable option for the south wall remains the glass base case.

Based on the findings that NS decreased for each of the south wall alternative designs, it can be predicted that the other surfaces receiving even higher solar insolation would also decrease the NS. Indeed, when permanent and movable insulation were applied to the roof, the LCC was negatively impacted and increased by 116.6% and 25.0%, respectively (financial loss of $2,785,706 and $596,803, respectively). The significantly higher LCC associated with these opaque cladding options demonstrates the importance of allowing natural light into the greenhouse through critical surfaces such as the roof for this location. Consequently, these two AGH design options are rejected. For polycarbonate applied to the roof, the LCC decreased but by only a small amount (0.9%). Therefore, all three design alternatives did not improve the economic outcome (compared to most cost-effective design that was previously obtained) and the most suitable option for the roof remains the glass base case.

The overall results for the greenhouse envelope design indicate that the most cost-effective design consists of covering the inside surface of the glass with permanent insulation on the north and east walls, employing polycarbonate on the west wall and glass on the south wall and the roof (LCC decreased by 5.5%, NS of $131,143). This AGH design caused the lighting electricity consumption to increase by 4.3% (from 114,475 kWh yr^{-1} to 119,350 kWh yr^{-1}), the amount of natural gas used for heating to decrease by 15.6% (from 65,119 m^3 yr^{-1} to

54,992 m^3 yr^{-1}) and GHG emissions related to energy consumption to decrease by 14.7% (128,798 $kgeCO_2$ yr^{-1} to 109,902 $kgeCO_2$ yr^{-1}).

Table 5.3: Present-value costs, residual value, NS, and change in LCC.

	Energy costs	Initial investment costs	O&MR costs	Capital replacement cost	Residual value	NS	Change in LCC
Base case	$1,615,972	-	-	$84,949	$25,586	-	-
N wall permanent insulation	$1,556,041	-$1,459	-	$84,949	$25,586	$61,390	-2.6%
N wall movable ins.	$1,576,877	$1,089	$29,072	$84,949	$25,586	$8,933	-0.4%
N wall polycarbonate (poly.)	$1,589,793	$1,116	-	$94,176	$25,892	$16,142	-0.7%
NE wall permanent ins.	$1,548,998	-$34,463	-	$56,892	$22,703	$126,611	-5.3%
N wall permanent ins.; E wall movable ins.	$1,557,739	-$31,915	$29,072	$56,892	$22,703	$86,250	-3.6%
N wall permanent ins.; E wall poly.	$1,539,348	-$31,889	-	$66,120	$23,008	$124,764	-5.2%
NEW wall permanent ins.	$1,549,704	-$35,923	-	$56,892	$22,703	$127,364	-5.3%
NE wall permanent ins.; W wall movable ins.	$1,553,621	-$33,375	$29,072	$56,892	$22,703	$91,826	-3.8%
NE wall permanent ins.; W wall poly.	$1,534,429	-$33,348	-	$66,120	$23,008	$131,143	-5.5%
NEWS wall permanent ins.	$1,627,916	-$34,807	-	$66,120	$23,008	$39,115	-1.6%
NE wall permanent ins.; W wall poly.; S wall movable ins.	$1,626,044	-$32,259	$29,072	$66,120	$23,008	$9,367	-0.4%
NE wall permanent ins.; WS wall poly.	$1,533,680	-$32,232	-	$75,347	$23,314	$121,854	-5.1%
NE wall and roof permanent ins.; W wall poly.	$4,476,617	-$56,780	-	$59,449	$18,246	-$2,785,706	116.6%
NE wall permanent ins.; W wall poly.; roof movable ins.	$2,031,484	-$35,560	$242,105	$56,087	$21,977	-$596,803	25.0%
NE wall permanent ins.; W wall and roof poly.	$1,560,888	-$24,058	-	$142,965	$25,556	$21,095	-0.0%

Table 5.4: Energy consumption and associated GHG emissions.

	Lighting electricity consumption (kWh yr^{-1})	Natural gas consumption (m^3 yr^{-1})	Peak thermal energy demand (kW)	Lighting electricity CO_2 emissions (kg eCO_2 yr^{-1})	Natural gas CO_2 emissions (kg eCO_2 yr^{-1})	Total CO_2 emissions (kg eCO_2 yr^{-1})	Change in CO_2 emissions
Base case	114,475	65,119	261	5,724	123,075	128,798	-
N wall permanent insulation	112,492	61,251	253	5,625	115,764	121,388	-5.8%
N wall movable ins.	112,409	63,091	253	5,620	119,243	124,863	-3.1%
N wall polycarbonate	114,599	62,793	253	5,730	118,679	124,409	-3.4%
NE walls permanent ins.	117,738	57,277	244	5,887	108,253	114,140	-11.4%
N walls permanent ins.; E wall movable ins.	116,127	59,061	244	5,806	111,626	117,432	-8.8%
N walls permanent ins.; E wall poly.	113,814	58,969	244	5,691	111,452	117,143	-9.1%
NEW walls permanent ins.	123,853	53,410	235	6,193	100,946	107,138	-16.8%
NE walls permanent ins.; W wall movable ins.	121,787	55,073	235	6,089	104,088	110,178	-14.5%
NE walls permanent ins.; W wall poly.	119,350	54,992	236	5,967	103,935	109,902	-14.7%
NES walls permanent ins.; W wall poly.	138,807	50,516	227	6,940	95,475	102,415	-20.5%
NE walls permanent ins.; W wall poly.; S wall movable ins.	136,329	51,947	227	6,816	98,180	104,996	-18.5%
NE walls permanent ins.; WS walls poly.	123,109	52,513	227	6,155	99,250	105,406	-18.2%
NE walls and roof permanent ins.; W wall poly.	570,184	17,863	166	28,509	33,762	62,271	-51.7%
NE walls permanent ins.; W wall poly.; roof movable ins.	216,763	35,072	166	10,838	66,287	77,125	-40.1%
NE walls permanent ins.; W wall and roof poly.	146,905	39,565	202	7,345	74,777	82,123	-36.2%

5.8 Conclusion

This chapter demonstrates how the combination of integrated thermal-daylight energy analysis and life cycle cost analysis can be employed to compare envelope designs for greenhouses. To the best of the author's knowledge, it is the first time that envelope design alternatives for a greenhouse that controls light to a consistent daily integral were compared based on local climatic and economic conditions. The methodology was applied to determine the most cost-effective envelope design for a greenhouse located in Ottawa, Ontario, Canada. The

base case envelope design consists of glass whereas the three alternative designs consist of adding permanent insulation or movable insulation to interior side of the glazing and replacing glass with twin-wall polycarbonate.

All the AGH designs increased lighting electricity consumption and decreased heating energy use except when permanent and movable insulation were applied to the north wall and in the case of permanent insulation on the north wall plus polycarbonate on the east wall. This demonstrates how the use of reflective opaque insulation on the north wall can be beneficial for redirecting light onto the crops to achieve simultaneous reductions in electricity and heating energy costs. The most cost-effective envelope design consists of covering the inside surface of the glass with permanent insulation on the north and east walls, employing polycarbonate on the west wall and glass on the south wall and the roof (LCC decreased by 5.5%, NS of $131,143). This AGH design caused the lighting electricity consumption to increase by 4.3%, the amount of natural gas used for heating to decrease by 15.6% and GHG emissions related to energy consumption to decrease by 14.7%.

Increasing the model resolution could further improve design solution accuracy. For instance, the ventilation rate could be controlled based on inside humidity levels, and a condensation model, more detailed evapotranspiration models, advanced artificial lighting and TSS control strategies could be implemented. Moreover, the model-based analysis does not provide feedback on the uniformity of shading that results from the envelope permutations. Therefore, the use of daylighting software could complement the analysis to help visualize internal shading and ensure that uniformity requirements are met or that planting configurations are compatible with local daylight levels. The uniformity of transmitted daylight could be improved by choosing translucent claddings that diffuse light. Significant energy (and associated pollution) can be saved, and economic viability improved, when greenhouse envelope design is optimized at the early stages for a given geographic location and design/operation characteristics.

CHAPTER 6: GROUND INSULATION DESIGN[3]

6.1 Abstract

Energy and life cycle cost analysis were employed to identify the most-cost effective ground envelope design for a greenhouse that employs supplemental lighting located in Ottawa, Ontario, Canada (45.4°N). The envelope design alternatives that were investigated consist of installing insulation vertically around the perimeter and horizontally beneath the footprint of a greenhouse with a concrete slab and unfinished soil floor. Detailed thermal interaction between the greenhouse and the ground surface is achieved by considering 3-dimensional conduction heat transfer within the TRNSYS 17.2 simulation software. The portion of total heat loss that occurred through the ground was approximately 4% and permutations in ground insulation design reduced heating energy consumption by up to 1%. For the two floor designs, the highest net savings was achieved when perimeter and floor zone horizontal insulation was installed whereas a financial loss occurred when it was also placed beneath the crop zone. However, in all cases, the improvement in economic performance was small (net savings below $4,000 and reduction in life cycle under 0.2%). Combined energy and life cycle cost analysis is valuable for selecting optimal envelope designs that are capable of lowering energy consumption, improving economics and enhancing greenhouse durability.

6.2 Introduction

Heating is a major operating expense for greenhouses that are located in mid-to-high latitude locations. In addition, heating is commonly achieved by burning fossil fuels, which contribute to greenhouse gas emissions and environmental degradation. Since most of heat loss occurs through the envelope (walls, roof and floor), optimal designs, which reduce energy use while addressing economics concerns, are required.

Much of the prior work regarding ground heat transfer has been performed for buildings (Deru, 2002; Andolsun, 2012; Chen, 2013) whereas only a few studies have been performed for greenhouses. Most of the research for greenhouses ground heat transfer consists of case studies (Al-Kayssi, 2002; Kittas et al., 2005; Nawalany et al., 2014) or the potential for design

[3] Bambara, J. & Athienitis, A. K. (2018). Energy and economic analysis for greenhouses ground insulation design. Energies, 11(11), 3218.

improvements such as ground-source heat exchangers (Ghosal et al., 2004; Hepbasli, A. 2013). Various levels of modeling resolution have been employed for representing the thermally massive ground. Most studies have separated the ground into one or more relatively thin earth layer and energy transfer is solved using 1-dimensonal (1D) heat transfer equations (Pieters and Deltour, 1997; Gupta and Chandra, 2002; Bastien, 2015). The advantage of 2-dimensional (2D) heat transfer is that it enables interaction with the greenhouse edge/perimeter. For instance, a numerical study using computational fluid dynamics enables visualization of the ground temperature profile (Tong et al., 2009). However, the entire footprint (and interaction with the perimeter) can only be studied when 3-dimensional (3D) discretization of the ground is performed, whereby the ground is divided into control volumes so that overall heat transfer can be solved analytically or numerically. The only study that employed 3D analysis of ground heat transfer in greenhouses used the WUFI software to compare thermal energy use for a greenhouse located above, below and at ground level (Nawalany et al., 2014). However, these studies did not consider economic implications of employing ground insulation. To determine the most cost-effective design, a combined energy and economic analysis must be performed. To our best knowledge, there has not been any previously published work regarding the detailed 3D energy analysis and economic analysis for the design of a greenhouse floor envelope.

The aim of this paper is to demonstrate how integrated thermal-daylight energy analysis and life cycle cost analysis (LCCA) can be employed to identify the most-cost effective ground insulation design for a greenhouse that controls light to a consistent daily integral located in Ottawa, Ontario, Canada (45.4°N, mid-latitude, 4,560 heating degree-days).

6.3 Energy and Economic Analysis

For greenhouses that supplement daylight with horticultural lighting, the choice of cover materials may alter the daylight availability and lighting electricity use. The effect of such alterations must be transferred to the module which calculates the thermal energy consumption. In theory, modifying the envelope design for greenhouses that control light to a consistent daily integral (e.g. for producing leafy green vegetables year-round near the consumer) should not affect crop growth as the supplemental lighting, shading screen and HVAC systems control will adjust and compensate for any changes in the indoor climate. Consequently, the analysis of this type of greenhouse will be carried out by omitting biological aspects.

The decision-making process for envelope design requires both energy and economic analysis. The performance obtained through energy simulation is not sufficient for determining a cost-optimal design. From an investor's perspective, the incremental cost of alternative claddings should be outweighed by operational savings. This study employs LCCA and the net savings method was selected for comparing envelope design alternatives. The net savings method can provide detailed economic analysis in a time efficient manner (it only requires economic aspects that are impacted by a design variation to be quantified).

6.4 Greenhouse Characteristics

A schematic of the 929.03 m2 (10,000 sqft) greenhouse considered for this study is provided in Fig. 4.1. It has an equal length and width of 30.48 m, and a height of 3.66 m. The floor surface consists of a crop zone located between two identical floor areas (floor zone). Heating and ventilation are used to control inside humidity and temperature. The greenhouse does not utilize humidification, cooling is provided by mechanical ventilation only, and condensation is ignored in this study. The artificial lights (AL) are the only internal gain considered in the model.

6.5 Energy Analysis

TRNSYS 17.2 was selected for the transient simulation of the greenhouse climate (Klein et al., 2014). Type 56 multizone building model was used to create the greenhouse energy model (TRANSSOLAR, 2005). Fig. 6.1 depicts the three most common locations for ground insulation of greenhouse: vertical along the perimeter, slanted wing, and horizontal beneath the floor. Slanted wing insulation is excluded from the analysis because of modeling limitations of the TRNSYS software.

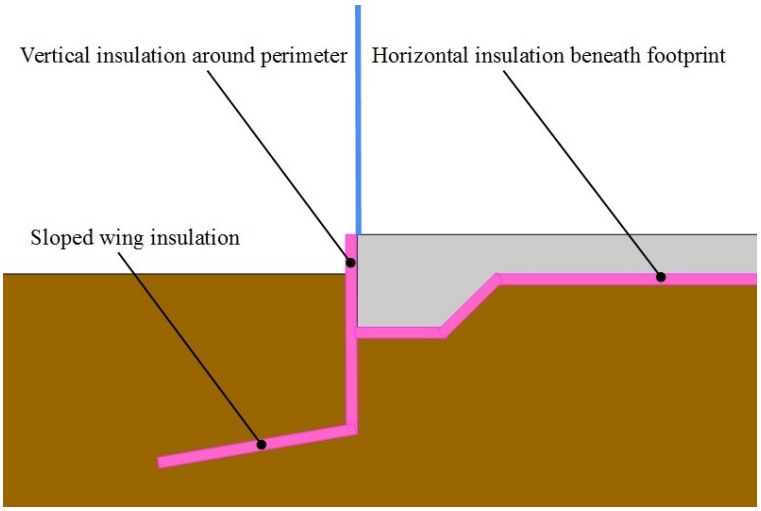

Figure 6.1: Common locations for ground insulation on buildings.

This study compares a base case greenhouse (BCGH) without thermal insulation to alternative designs (AGH) that consist of: 1) perimeter insulation; 2) perimeter insulation and horizontal insulation beneath the both floor zones; 3) perimeter insulation and horizontal insulation beneath both floor zones and the crop zone; and 4) perimeter insulation and horizontal insulation beneath the crop zone. Installing horizontal insulation alone is not considered because it is unlikely that it would be a viable option if perimeter insulation is not. The objective of this study is to determine whether the most cost-effective envelope design for the floor is no insulation, perimeter insulation, or a combination of perimeter and horizontal insulation. The investigation will consider two types of greenhouse floor designs: one with a concrete slab over soil (Fig. 6.2) and another with unfinished soil (Fig. 6.3). For the greenhouse with a ground consisting of unfinished soil, the concrete slab is replaced with a single layer of soil whose thickness is satisfactory for root development. As depicted in Fig. 6.3, when thermal insulation is installed, it is assumed to be located beneath this layer of arable soil.

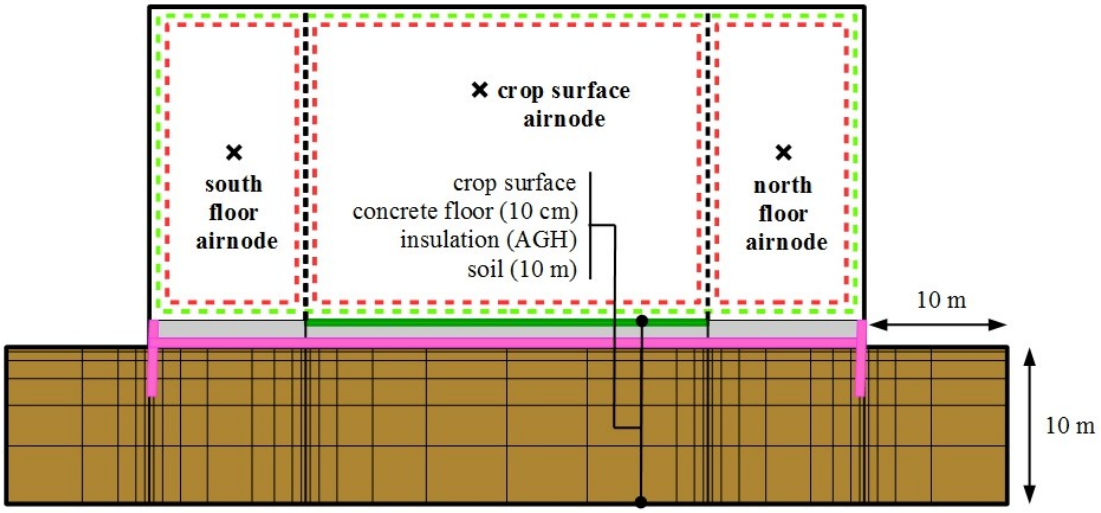

Figure 6.2: Greenhouse model (concrete floor) with three airnodes and discretized ground zones.

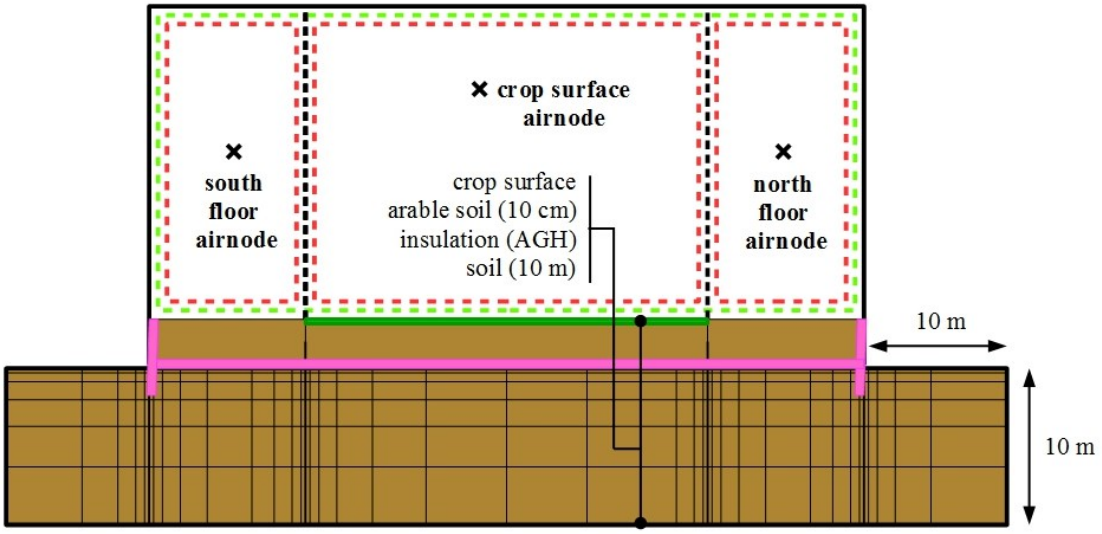

Figure 6.3: Same greenhouse model as Fig. 6.2 but with a floor consisting of unfinished soil.

The two models which enable detailed 3D ground heat transfer in TRNSYS consist of Type 49 (Klein et al., 2014) and Type 1244 (TESS, 2012). When these ground heat transfer models are selected for interaction with Type 56, each floor area must be associated with a dedicated thermal zone or airnode. Therefore, the adopted solution for enabling 3D ground heat transfer with multiple floor areas within a single zone is to separate the greenhouse into multiple airnodes. The volume associated with each airnode is dictated by the ground area which is belongs to.

The modeled greenhouse has three floor surfaces (two for the floor and one for crop zone) and therefore the single greenhouse zone is separated into three airnodes. The surface between the airnodes is defined as a "virtual" surface (shown in Fig. 6.4), which enables unobstructed radiation heat transfer. Meanwhile, mass and energy flow between airnodes is specified by air "coupling" to maintain the well-mixed assumption (that is commonly achieved using horizontal airflow fans in greenhouses). Figs. 6.2 and 6.3 illustrate the three airnode greenhouse models with the discretization of the ground into control volumes. A user defined volume of soil is specified in the model so that 3D heat transfer can be calculated within this "ground zone". Each airnode contains a certain volume of soil beneath the area that is in contact with the ground, with smaller discretization of the layers around the perimeter that are in contact with adjacent airnodes. The same concept is applied for the areas in contact with the exterior environment.

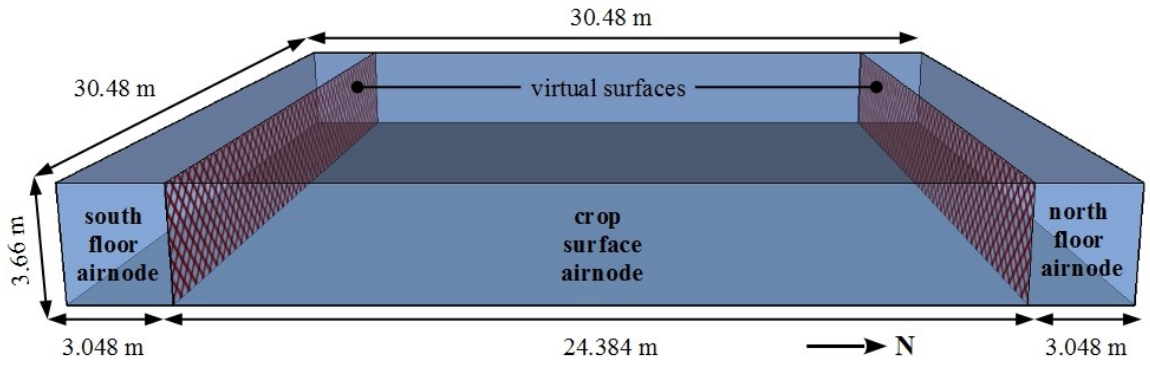

Figure 6.4: Schematic showing the two virtual surfaces that separate the three airnodes.

Annual and design day energy simulations of the model are performed to obtain the energy-related inputs that are needed for conducting the LCCA. The energy analysis is separated into daylight, artificial light and thermal modules.

6.5.1 Daylight module

The methodology for the daylight module is described in section 3.6.

6.5.2 Artificial lighting control module

The methodology for the artificial light control module is described in section 3.7.

6.5.3 Thermal module

The purpose of the thermal module is to determine the heating energy consumption and peak demand, with artificial lighting as a dynamic input. Fig. 6.5 illustrates the major mass and energy fluxes that are considered in the three airnode greenhouse model. The energy balances are presented for the crop surface airnode that is located between the two floor airnodes (north and south sides of the greenhouse).

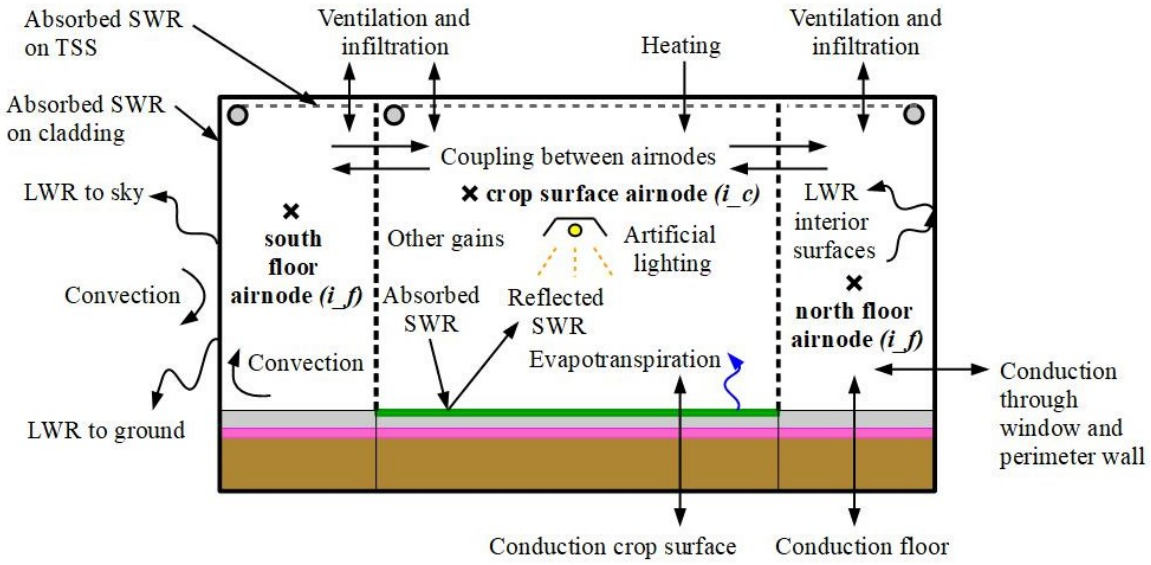

Figure 6.5: Schematic showing the mass and energy fluxes considered in the three airnode greenhouse model.

The mass balance for the crop surface airnode (i_c) is given by:

$$X_m \cdot \rho_a \cdot V_{i\_c} \cdot \left(\partial \omega_{i\_c} / \partial t\right) = m_{vent} + m_{inf} + m_{ET} + m_{m\_cpl} \tag{6.1}$$

where

X_m is the moisture capacitance multiplier (dimensionless)

ρ_a is the density of air (kg m^{-3})

V_{i_c} is the volume of the crop zone airnode (m^3)

$\partial \omega_{i\_c}$ is the rate of change of the inside air humidity ratio (kg_{water} $kg_{dry\_air}^{-1}$)

∂t_i is the rate of change of time (s)

m_{vent} is the mass transfer rate of water due to ventilation (kg hr^{-1})

m_{inf} is the mass transfer rate of water due to infiltration (kg hr^{-1})

m_{ET} is the mass transfer rate of water due to evapotranspiration (kg hr^{-1})

m_{cpl} is the mass transfer rate of water due air movement between the airnodes (kg hr^{-1}).

The energy balance for the crop surface airnode is written as:

$$X_{th} \cdot \rho_a \cdot c_{p\_a} \cdot V_{i\_c} \cdot \left(\partial T_{i\_c}/\partial t\right) = Q_{conv\_si} + Q_{vent} + Q_{inf} + Q_{TSS} + Q_{AL} + Q_{heat} + Q_{cpl} \quad (6.2)$$

where

X_{th} is the thermal capacitance multiplier (dimensionless)

c_{p_a} is specific heat of air at constant pressure (kJ kg^{-1} $°C^{-1}$)

∂T_{i_c} is the rate of change of the inside air temperature (°C)

Q_{conv_si} is the energy flux due to convection (W)

Q_{vent} is the energy flux due to ventilation (W)

Q_{inf} is the energy flux due to infiltration (W)

Q_{TSS} is the energy flux from the thermal shading screen (W)

Q_{AL} is the energy flux from artificial lighting (W)

Q_{heat} is the energy flux from auxiliary heating (W)

Q_{cpl} is the energy flux due air movement between the airnodes (W).

The energy balance for the inside surface of the cover and an opaque surface is given by Eq. (4.3). The energy balance for the outside surface of the cover and an opaque surface is described by Eq. (4.4). The energy balance for the crop interior surface is defined by Eq. (4.6).

The mass balance for each floor airnode (i_f) is given by:

$$X_m \cdot \rho_a \cdot V_{i\_f} \cdot \left(\partial \omega_{i\_f}/\partial t\right) = m_{vent} + m_{inf} + m_{cpl} \quad (6.3)$$

The energy balance for each floor airnode is written as:

$$X_{th} \cdot \rho_a \cdot c_{p_a} \cdot V_{i\_f} \cdot \left(\partial T_{i\_f}/\partial t\right) = Q_{conv\_si} + Q_{vent} + Q_{inf} + Q_{TSS} + Q_{cpl} \quad (6.4)$$

The energy balance for the floor inside surface is given by Eq. (4.5).

6.5.4 Energy modeling key assumptions

The details and assumptions for calculating the variables in the above energy and mass balance equations are the same as in section 4.5, except for those presented below.

Weather data: A typical meteorological year weather file for Ottawa, Ontario, Canada (45.4°N, which represents mid-latitude climatic conditions) was used to run the simulations and obtain the energy performance over a one-year period. The temperature of the far-field soil is set using the Kasuda correlation which estimates the temperature of the soil at a given depth given the time of year, the soil properties, the average annual soil surface temperature, the amplitude of the annual soil surface temperature, and the day of the year at which the minimum annual surface temperature occurs (Kusuda and Achenbach, 1965). Type 15 calculates the sky temperature for longwave radiation calculations (Klein et al., 2014). A simulation timestep (Δt) of 15 minutes was selected. The energy model was simulated for 638 days, with the first nine months of results discarded to eliminate the initial condition transient effects. For an analysis at peak heating design conditions, no solar radiation, a wind speed of 10 m s-1, exterior air relative humidity of 20%, exterior air temperature of -21.8°C, sky temperature of -52°C, and ground temperature of 8°C were selected (RETScreen, 2013).

Ground heat transfer: The ground surface is divided in two floor zones and one crop zone (80% of footprint). The moisture effects are not accounted for in the model. The type of crop produced is a leafy green vegetable (e.g. lettuce, kale). The crop layer is approximated as a smooth and uniform surface located directly above the concrete slab or soil surface and its thermal resistance and capacitance are ignored.

Several models with varying levels of detail exists in TRNSYS for calculating heat transfer with the ground. Type 49 and 1244 are the most detailed models because they enable 3D heat transfer to be calculated between the Type 56 multi-zone building model and the ground surface. A user defined volume of soil is considered for ground heat transfer and divided into control volumes that are assumed to be cubic in shape so there are six unique heat transfers to analyze per control volume. There are several other available methods to solve coupled 3D differential heat transfer equations using iterative methods. Type 49 uses an approximate analytical solution (Klein et al., 2014) whereas Type 1244 uses finite difference (TESS, 2017).

The analytical solution is timestep independent but does require an iterative solution inside the subroutine to solve the coupled differential equations.

Type 49 assumes that the ground surface is flat, that the soil has homogenous thermal properties, and that the temperature of the ground surface is not affected by the presence of the building and is instead set from long term averages. In contrast, Type 1244, does not impose the assumption of a soil surface temperature unaffected by the building and can model cases where the zone is underground. A major limitation of Type 1244 is that is cannot model perimeter insulation when the building ground level is the same as the exterior. Since perimeter insulation is a practical ground insulation technique for greenhouses, Type 49 was selected to calculate 3D heat transfer between the greenhouse and the ground. Nevertheless, simulation results of the BCGH using both models will be presented to assess the importance of the ground surface being affected by the presence of the building.

A "map" of the soil surface was created. This map file indicates to the model whether the surface of the soil control volume is covered by one of the multi-zone building floors or whether the surface is exposed to the exterior environment. This model calculates the average surface temperature of the soil directly underneath each of the floors of the multi-zone building. These average surface temperatures are then passed to Type 56 as boundary temperature inputs for each of the floors. Based on the boundary floor temperatures provided to Type 56 by this model, Type 56 calculates the rate of energy that passes from the floors of each zone into the soil. With the soil heat transfer for each zone provided by Type 56, the thermal history of the soil field and the properties of the soil known, the temperatures of each of the control volumes of the 3D soil field can be calculated by this model. Based on the calculated soil temperatures and the zone heat flows, the average zone surface temperatures can be calculated and passed back to Type 56. This iterative methodology is then solved with the standard TRNSYS convergence algorithms.

The size of the control volumes were multiplied by a factor of two as they expanded away from the perimeter of the greenhouse airnodes. The near field/far field boundary is conductive and the temperature of the far field is set by the Kasuda correlation for the x, y and z axes. The deep ground temperature is assumed to be equal to the yearly average outside air temperature. The amplitude of the annual surface temperature profile of the soil is assumed to be equal to the maximum monthly soil surface temperature minus the average annual soil surface

temperature. The soil temperature was assumed to be unaffected by the building at a distance of 10 m beneath the ground surface (in the vertical direction) and 10 m from the edge of the greenhouse (in the horizontal direction).

Windows: The windows consist of a glazed portion and a frame portion. The thermal properties for the glass glazing are given in Table 5.1. The edge heat transfer effects are ignored, and the thermal resistance of the metal frame is negligible and assumed to be equal to that of the glazing itself. Energy storage in glazing materials and framing is neglected.

Coupling mass and energy transfer: Air movement is specified between the three airnodes of the air thermal zone so that they are all nearly at the same temperature (well-mixed assumption). For airflow from the crop airnode (i_c) to a floor airnode (i_f), the thermal (Q_{cpl} in W) and moisture (m_{m_cpl} in kg hr^{-1}) gains due to coupling are calculated from:

$$Q_{cpl} = m_{cpl} \cdot c_{p\_a} \cdot \left(T_{i\_c} - T_{i\_f}\right)/3.6 \tag{6.5}$$

$$m_{m\_cpl} = m_{cpl} \cdot \left(\omega_{i\_c} - \omega_{i\_f}\right) \tag{6.6}$$

where

m_{cpl} is coupling mass flow of air between the airnodes (kg hr^{-1})
the factor 3.6 serves to convert units kJ hr^{-1} to W.

Similarly, for airflow from a floor airnode to the crop airnode, the thermal gains due to coupling are defined as:

$$Q_{cpl} = m_{cpl} \cdot c_{p_a} \cdot \left(T_{i\_f} - T_{i\_c}\right)/3.6 \tag{6.7}$$

$$m_{m\_cpl} = m_{cpl} \cdot \left(\omega_{i\_f} - \omega_{i\_c}\right) \tag{6.8}$$

where the coupling mass flow rate is selected so that the airnode temperature become nearly identical due to mixing.

Thermal energy consumption: The output of the TRNSYS simulation provides the heating power at each timestep (Q_{heat} in kJ hr^{-1}) that is required to maintain the desired setpoint temperature. The annual thermal energy consumption for heating (Q_{heat_yr} in GJ yr^{-1}) is expressed as:

$$Q_{heat\_yr} = \sum_{\Delta t=0}^{365\cdot 24/\Delta t}(Q_{heat} \cdot \Delta t/10^6) \quad (6.9)$$

where the factor 10^6 serves to convert units kJ to GJ.

A natural gas fired condensing boiler is used for heating and the annual gas consumption (m_{gas_yr} in m^3 yr^{-1}) is computed as:

$$m_{gas\_yr} = 10^3 \cdot Q_{heat\_yr}/\left(EV_{gas} \cdot \eta_{boil}\right) \quad (6.10)$$

where

EV_{gas} is the energy value of natural gas (MJ m^{-3})

η_{boil} is efficiency of the boiler (dimensionless).

The peak thermal energy demand is obtained for heating design day conditions. A simulation was performed for ten identical days and the peak demand was taken from the last day.

6.5.5 Values of greenhouse design parameters

Appendix A provides the values of properties for different materials and components used in the greenhouse energy model.

6.6 Economic Analysis

The net savings (NS) formula for the LCCA is given by Eq. (4.35). The change in LCC may be estimated using Eq. (4.36):

6.6.1 Economic analysis key assumptions

A detailed explanation of the terms in Eq. (4.35), as it applies to the case study, follows. The analysis assumes that the cost of materials, equipment (except for the cost escalation of LED fixtures) and labor varies solely with the discount rate.

Change in energy cost (ΔE): Modifying the ground insulation design does not impact the indoor lighting and its associated cost. The present value of the annually recurring cost for natural gas for heating is calculated by Eq. (4.39). The savings in energy costs is the difference between that of the AGH and BCGH expressed as:

$$\Delta E = \left[PV_{E\_gas}\right]_{BCGH} - \left[PV_{E\_gas}\right]_{AGH} \quad (6.11)$$

Change in water cost: It is assumed that no difference in water consumption occurs between the AGH and BCGH.

Change in operation, maintenance and replacement cost (O&MR): It is assumed that no difference in OM&R cost occurs between the AGH and BCGH.

Change in investment cost (ΔInv): The additional material and installation cost for the added rigid insulation is determined using Eq. (5.6). The change in material and installation cost for the boiler is computed using Eq. (5.9). The total additional investment cost is determined as follows:

$$\Delta Inv = \Delta C_{ins} + \Delta C_{boil} \quad (6.12)$$

Change in capital replacement cost (ΔRepl): The replacement period for rigid insulation is assumed to be the same as the study period and is ignored in the LCCA. Since indoor lighting is not affected by modifying the ground envelope design, the replacement costs for artificial lighting is the same in the AGH and BCGH and can be ignored. The cost for replacing a boiler is calculated using Eq. (5.14). The total additional capital replacement cost is the difference between that of the AGH and BCGH is expressed as:

$$\Delta Repl = [Repl_{boil}]_{AGH} - [Repl_{boil}]_{BCGH} \quad (6.13)$$

Change in residual value (ΔRes): The residual value for the boilers is approximated by Eq. (5.18). The total residual value is the difference between that of the AGH and BCGH given by:

$$\Delta Res = [Res_{boil}]_{AGH} - [Res_{boil}]_{BCGH} \quad (6.14)$$

Initial investment cost (Inv): The initial investment cost of the greenhouse is calculated using Eq. (4.53).

6.6.2 Values of greenhouse LCCA parameters

Appendix B provides the values of the cost data (in $CAD 2017) used in the LCCA. A conversion rate of 1.30 in 2017 was used to convert USD to CAD (BOC, 2018).

6.7 Results and Discussion

This section presents the most cost-effective ground insulation configuration for a greenhouse located in Ottawa, Canada. Appendix I extends the analysis for a raft hydroponic growing system. Appendix J provides the results for Whitehorse, Canada. Appendix K reveals the sensitivity of net savings to energy model input parameters, operation parameters, and economic parameter values for both locations.

6.7.1 Portion of Heat Loss through Ground

The average heat loss pathways for the BCGH with a concrete slab in January, were determined to be: 18.6% for infiltration, 21.9% for ventilation, 37.7% from the roof, 17.8% from the walls and 4.0% from the ground. These results are from sunset to sunrise because the ground becomes a source of heat gain when sunlight exists. The portion of the envelope heat loss (walls, roof and ground) that occurred through the ground was approximately 7%. Consequently, permutations in the ground envelope design will have a small impact on the overall greenhouse energy savings.

6.7.2 Net Savings Achieved by the Ground Insulation Configurations

The present-value costs, residual value, NS (in $CAD 2017), and change in LCC for the AGH and BCGH are provided in Table 6.1. The two main design alternatives for ground insulation consist of adding vertical insulation around the greenhouse perimeter and horizontal insulation beneath the floor and/or crop zones. The perimeter insulation is considered as the first design alternative because it is the most likely to provide NS. It should be noted that perimeter insulation also has the added benefit of foundation frost protection and improved crop root zone temperatures and therefore, there may be incentive to apply it even if it does not result in NS. If NS are obtained for perimeter insulation, then the next design alternatives will be to consider horizontal insulation beneath the floor zone. If perimeter insulation does not provide NS, then subsequent designs would only consider horizontal insulation, although it is unlikely that horizontal insulation would be cost effective if perimeter insulation is not. Based on this economic result, two possibilities for subsequent envelope designs will be considered. If combined perimeter and floor zone insulation provides higher NS crop zone insulation (entire footprint). If not, the case of perimeter and crop zone insulation will be assessed. The use of

ground insulation had a negligible impact on the peak energy demand for heating and therefore changes in the heating system cost are not considered.

For the concrete slab and soil floor greenhouse designs, the economic results were improved when perimeter insulation is applied (NS of $1,575 and $1,483, respectively and the LCC decreased by 0.1% for both). When horizontal floor insulation is added, the NS increased by 20.6% for the greenhouse with a concrete slab and 128.0% for the greenhouse with a soil floor. When horizontal crop zone insulation was added, a financial loss of $7,835 (0.3% increase in LCC) was observed for the greenhouse with a concrete slab and $5,562 (0.2% increase in LCC) for the greenhouse with a soil floor. Therefore, the most cost-effective design for the greenhouses with a concrete slab and soil floor is when perimeter and floor zone horizontal insulation are applied. Although this analysis provided insight into the most cost-effective greenhouse ground insulation design for Ottawa, the NS are negligible compared to the greenhouse LCC (decrease in LCC of 0.1% and 0.2% for the greenhouse with a concrete slab and soil floor, respectively).

Table 6.1: Present-value costs, residual value, NS, and change in LCC for the greenhouse models.

Floor type	Insulation location and thickness	Energy cost	Incremental initial investment cost	Capital replacement cost	Residual value	NS	Change in LCC
Concrete slab	BCGH (no insulation)	$1,582,202	$0	$84,949	$25,586	-	-
	Vertical perimeter	$1,579,716	$912	$84,949	$25,586	$1,575	-0.1%
	Vertical perimeter and horizontal floor zones	$1,577,112	$3,192	$84,949	$25,586	$1,899	-0.1%
	Vertical perimeter and horizontal floor plus crop zones	$1,577,726	$12,311	$84,949	$25,586	-$7,835	0.3%
Soil floor	BCGH (no insulation)	$1,567,120	$0	$84,949	$25,586	-	-
	Vertical perimeter	$1,564,725	$912	$84,949	$25,586	$1,483	-0.1%
	Vertical perimeter and horizontal floor zones	$1,560,546	$3,192	$84,949	$25,586	$3,382	-0.2%
	Vertical perimeter and horizontal floor plus crop zones	$1,560,371	$12,311	$84,949	$25,586	-$5,562	0.2%

6.7.3 Impact of Insulation on Energy Consumption

Table 6.2 gives the annual lighting electricity use and fuel consumed for heating. The BCGH with the soil floor consumed 0.7% more electricity for lighting than the concrete floor BCGH due to the higher solar absorptance of soil compared to concrete. Meanwhile, the increased thermal energy storage in the soil caused heating energy use to decrease by 2.9%. It is interesting to note that for the concrete greenhouse, the heating energy use was lowest for the case of perimeter and floor zone insulation (natural gas use of 61,466 m^3 yr^{-1}), whereas it slightly increased to 61,519 m^3 yr^{-1} when crop zone insulation was also employed. This demonstrates how, in certain cases, the use of ground insulation can be detrimental to energy conservation efforts because it reduces the potential for passive solar heating. For the designs that achieved the highest NS, heating energy was reduced by 0.6% for the greenhouse with a concrete slab and 1.0% for the soil floor. Therefore, employing ground insulation produced negligible energy savings and economic benefit for the location that was investigated. It should be noted that a single insulation thickness was selected for this study. The analysis could be repeated for different thicknesses of EPS insulation to identify the optimal level.

Table 6.2: Energy consumption for the greenhouse models.

Floor type	Insulation level	Lighting electricity consumption (kWh yr^{-1})	Natural gas consumption for heating (m^3 yr-1)
Concrete slab	BCGH (no insulation)	114,971	61,903
	Vertical perimeter	114,971	61,690
	Vertical perimeter and horizontal floor zones	114,971	61,466
	Vertical perimeter and horizontal floor plus crop zones	114,971	61,519
Soil floor	BCGH (no insulation)	115,755	60,105
	Vertical perimeter	115,755	59,900
	Vertical perimeter and horizontal floor zones	115,755	59,541
	Vertical perimeter and horizontal floor plus crop zones	115,755	59,526

6.8 Conclusion

This chapter demonstrates how the combination of integrated thermal-daylight energy analysis and life cycle cost analysis can be employed to compare envelope designs for greenhouses. To the best of the author's knowledge, it is the first time that a 3D ground heat transfer model was used to compare floor envelope designs for a greenhouse that controls light to a consistent daily integral, based on local climatic and economic conditions.

The methodology was applied to determine the most cost-effective ground insulation design for a greenhouse located in Ottawa, Ontario, Canada. Two types of floor designs were investigated (concrete slab and unfinished soil floor) and the insulation installation configurations were vertical around the perimeter and horizontal beneath the footprint. The portion of total heat loss that occurred through the ground was approximately 4% and permutations in ground insulation design reduced heating energy consumption by up to 1%. The greenhouses produced a higher NS when insulation was applied to both the perimeter and the surface beneath the floor zone then when it was applied to the perimeter alone. Meanwhile, adding insulation beneath the crop zone was not a viable option because it increased the LCC. In all cases, the improvement in economic performance was small (NS below $4,000 and reduction in life cycle under 0.2%). Therefore, a design with perimeter insulation may be the best option because it uses the least amount of material resources and provides some cost savings in addition to frost protection, reduced risk of condensation and improved thermal comfort for the crops.

The development of a 3D ground heat transfer model (that would ideally be compatible with commercially available simulation tools such as TRNSYS and EnergyPlus) which can simultaneously handle vertical perimeter insulation (for both basements and slab on grade), horizontal insulation and wing insulation would be useful for comparing all possible ground insulation configurations. Combined energy and life cycle cost analysis is valuable for determining optimal envelope designs that are capable of lowering energy consumption, improving economics and enhancing greenhouse durability.

CHAPTER 7: CONCLUSION

7.1 Summary

This thesis demonstrates how the combination of integrated thermal-daylight energy analysis and life cycle cost analysis can be employed to design the envelope of greenhouses that control light to a consistent daily integral. To the best of the author's knowledge, it is the first time that a design methodology for greenhouses with artificial lighting was developed and used to compare conventional and solar energy generating claddings that are applied to the walls and roof and to evaluate various ground insulation design configurations based on a 3-dimensional ground heat transfer model. The first step of the design methodology consists of performing an integrated thermal-daylighting analysis using the TRNSYS energy simulation software. Once the energy performance of the base case greenhouse and the design alternative(s) have been obtained, life cycle cost analysis was employed to identify the most cost-effective design via the net savings measure of economic performance. The methodology is general and can assist designers in identifying the most cost-effective solution, based on local climatic and economic conditions, from a set of discrete envelope design alternatives that may be applied to each surface of a greenhouse.

The design methodology was applied to evaluate the energy and economic performance of several greenhouse envelope designs through the following three case studies for a mid-latitude (Ottawa, Ontario (45.4°N), Canada) and high-latitude location (Whitehorse, Yukon (60.7°N), Canada): 1) comparison of a glass base case with crystalline silicone semi-transparent photovoltaic (STPV) cladding applied to the roof, whereby various photovoltaic area ratios (10-50%), bifacial STPV (for Ottawa only), two electricity pricing schemes, and present and future efficiencies of photovoltaic and horticultural lighting technology were assessed; 2) comparison of a glass base case with twin-wall polycarbonate and opaque insulation (permanent and movable) on the walls and roof; and 3) evaluation of the most suitable ground insulation design configuration (vertical perimeter and horizontal configurations applied to greenhouses with a concrete slab, unfinished soil and a raft hydroponic system). The main conclusions that can be drawn from the research conducted under this thesis can be summarized by the following points:

- **Comparison of STPV modeling approaches:**
    - It is recommended to use the "effective" STPV model, which combines photovoltaic (PV) cell and clear-glazed portions into an effective layer, for all types of STPV cladding because it has the following advantages over its "separate" counterpart: 1) the PV area ratio (or transparency) can be easily modified by creating predefined custom glazings; 2) inter-reflections of shortwave radiation caused by the closing of a screen are accounted for; 3) it enables detailed modeling of bifacial PV cells that considers the inter-reflections with the screen and; 4) detailed modeling of the convection and longwave radiation heat transfer is possible when a screen is applied.
    - The electrical power generated by the STPV cladding affects the greenhouse energy balance and should be modeled as a heat loss at the STPV surface.
    - For STPV with spaced silicone cells, a reference surface temperature is needed to accurately model temperature-dependent PV electricity generation.
- **Energy analysis of STPV cladding:**
    - The use of PV cladding produced internal shading which increased lighting electricity consumption by up to 84% for Ottawa and 27% for Whitehorse (for the present study with constant electricity pricing). Employing PV cladding also caused the heating energy use to decrease by up to 12% in Ottawa and 7% in Whitehorse, presumably because of the additional heat that is generated by increased supplemental lighting compared to the base case greenhouse.
    - Although STPV cladding increased lighting electricity use, it generated 44% and 21% of the electricity that was consumed for supplemental lighting in the present study and, 107% and 51% in the future projection study, for Ottawa and Whitehorse, respectively. Therefore, in the future, a STPV roof could potentially displace all the greenhouse's electricity needs for supplemental lighting.
    - The use of bifacial PV cells for Ottawa increased solar electricity output by 38% at a 10% PV area ratio and this fraction decreases in a nearly exponential manner to 14% at a 50% PV area ratio, presumably because less light is reflected inside the space at higher PV area ratios.

- The use of light diffusing glazing would improve the distribution uniformity of transmitted daylight and may increase crop growth.

- **Economic analysis of STPV cladding:**
  - Currently, for Ottawa, STPV cladding would not an economically attractive investment when constant electricity pricing is employed. However, reductions in life cycle cost (LCC) of up to 12% (at 50% PV area ratio) were obtained when time-of-use (TOU) electricity rates were available. Bifacial PV only reduced LCC when TOU rates were available and the economic result was better than single-ended STPV for lower PV area rations (10-30%). Therefore, financial incentives such as TOU electricity pricing, feed-in-tariff programs and technology demonstration grants would expedite the deployment of PV greenhouses and contribute to reducing the cost of adopting the new technology. Implementing a carbon tax would generate significant funds that can be valuable for subsidizing promising technologies.
  - For Ottawa, in the future nearly 23% and 37% reductions in LCC were achieved for constant and TOU electricity pricing, respectively. Bifacial PV improves the economic result but only up to 40% PV area ratio.
  - For Whitehorse, the use of STPV cladding could reduce LCC by up to 5%. The economic viability improved at higher PV area ratios and was similar for both the present and future projection studies.
  - The economic result would improve if less expensive double-ended high-pressure sodium fixtures were employed in the present study. However, LED technology has greater potential for increased efficiency in the future.
- **Energy and economic analysis of glass, polycarbonate and opaque insulation:**
  - By redirecting light onto the crops, the use of reflective opaque insulation on the north wall of the greenhouse achieved simultaneous reductions in lighting electricity and heating energy costs in both locations.
  - For Ottawa, the most cost-effective envelope design consists of covering the inside surface of the glass with permanent insulation on the north and east walls, employing polycarbonate on the west wall and glass (base case cladding) on the south wall and the roof (LCC decreased by 5.5%). This alternative greenhouse

design caused the lighting electricity consumption to increase by 4.3%, the amount of natural gas used for heating to decrease by 15.6% and GHG emissions related to energy consumption to decrease by 14.7%.

  - For Whitehorse, the most cost-effective design consists of covering the inside surface of the glass with permanent insulation on all surfaces (LCC decreased by 38.9%). This alternative greenhouse design caused the lighting electricity consumption to increase by 172.6%, the amount of propane used for heating to decrease by 71.2% and GHG emissions related to energy consumption to increase by 15.6%. This outcome of a fully opaque greenhouse (i.e. indoor cultivation) is somewhat unexpected and is a result of the high cost of propane and a relatively low cost for electricity.

- **Energy and economic analysis of ground insulation:**
  - The portion of total heat loss that occurred through the ground was approximately 4% and permutations in ground insulation design reduced heating energy consumption by only approximately 1% for the concrete slab and soil greenhouses and approximately 2% for the raft hydroponic greenhouse.
  - In all cases, the improvement in economic results was small (approximately 0.2% reduction in LCC for Ottawa and a maximum of nearly 2% for Whitehorse).
  - Although the choice to insulate provides little economic benefit, it may be beneficial for secondary purposes such as increasing the durability of the greenhouse structure (freeze-thaw protection), reducing the risk of disease associated with condensation and improving crop growth through favorable root zone temperatures.
- **Sensitivity analysis:**
  - The net savings was found to be greatly influenced by the interior convective heat transfer coefficient modeling parameter and therefore designers should employ experimentally validated correlations whenever possible. By overestimating its value, the predicted net savings could be too optimistic.
  - For the STPV study, the most important economic parameters that currently affect the net savings were the electricity price, heating fuel cost and its escalation rate, and the incremental initial investment cost for STPV cladding. In the future, it

was found that the electricity price and its cost escalation rate would become the parameters that influences the economic outcome most for Ottawa and the electricity price and, heating fuel cost and its escalation rate for Whitehorse.

- An operation parameter that has a significant effect on energy use is the minimum ventilation rate, which by varying from 1 to 4 air changes per hour, was found to increase net savings by only 4% even though heating energy consumption increased by as much 81%.
- The impact of lower energy cost in the future should be carefully evaluated to assess the risk associated with alternative envelope designs. It was found that lower electricity and fuel cost escalation rates could significantly decrease and even nullify the projected net savings. Fortunately, lower energy costs would also reduce greenhouse production expenses, thereby facilitating their adoption and increasing food security.

7.2 Contributions

This thesis provides a systematic study regarding the envelope design of greenhouses that control light to a consistent daily integral. The major contributions are:

- **Developed an integrated thermal-daylight modeling methodology** for greenhouses with artificial lighting using building energy simulation software. The necessary adaptations of the software for modeling greenhouses were described and possible limitations were discussed. The modeling method describes the necessary steps for quantifying the amount of PAR from sunlight that is received by the crop canopy, controlling the supply of artificial lighting, and translating its effects to the thermal energy model.
- **Developed of a methodology for the envelope design** of greenhouses with artificial lighting by combining integrated energy analysis and LCCA. The methodology may be used to identify the most cost-effective design from a set of discrete envelope design alternatives for each surface of the greenhouse (walls, roof and ground).
- **Identified and compared methods for modeling STPV cladding** using building energy simulation software, whereby temperature-dependent electrical efficiency calculations

and the thermal response of the greenhouse to PV electricity generation may be considered.

- **Established methods for modeling 3D ground heat transfer** in greenhouses characterized by a separate crop and floor zones.
- **Demonstrated the use of the proposed design methodology** through relevant case studies in a mid-latitude and high-latitude location. The analyses covered STPV cladding applied to the roof, conventional claddings (glass, twin-wall polycarbonate, and opaque insulation) installed on the walls and roof, and the design of ground insulation.
- **Publication of the research findings in the following scientific journals:**
    - Bambara, J. & Athienitis, A. K. (2019). Energy and economic analysis for the design of greenhouses with semi-transparent photovoltaic cladding. Renewable Energy, 131, 1274-1287.
    - Bambara, J., & Athienitis, A.K. (2018). Energy and economic analysis for greenhouse envelope design. Transactions of the American Society of Agricultural and Biological Engineers, 61(6), 1-16.
    - Bambara, J. & Athienitis, A. K. (2018). Energy and economic analysis for greenhouses ground insulation design. Energies, 11(11), 3218.
- **Presentations and papers in the following conferences:**
    - Bambara, J., & Athienitis, A.K. (2015a). Experimental evaluation and energy modeling of a greenhouse concept with semi-transparent photovoltaics. Energy Procedia, 78, 435-440. Paper presented at the 6th International Building Physics Conference. Torino, Italy.
    - Bambara, J., & Athienitis, A.K., (2015b). Integration of organic waste recycling and greenhouse agriculture. Paper presented at the 4th Climate Change Technology Conference. Montréal, Québec.
    - Bambara, J., & Athienitis, A.K., (2016). Comparison of two modeling approaches for semi-transparent photovoltaic cladding in greenhouses and experimental calibration. Paper presented at the eSim IBPSA-Canada's Biennial Conference. Hamilton, Ontario.

7.3 Recommendations for Future Work

While several advances have been realized over the course of this thesis, further steps are necessary to improve greenhouse envelope design.

- **Experimental validation.** This research focused on the theoretical aspects related the envelope design of greenhouses with artificial lighting. As a second part, future work is needed regarding experimental validation of the energy model and of the assumption that crop growth is unaffected by changes in the envelope design for greenhouses that control light to a consistent daily integral. In theory this assumption is correct because the lighting adjusts to provide the plants with the same amount of PAR photons regardless of the envelope design. However, experimental work is needed to better understand the response of various plants to mixed natural and artificial lighting sources (i.e. growth response to equal PAR but different spectrum). For instance, crop growth has yet to be reported for two greenhouses that control light to a consistent daily integral with different envelope designs (e.g. glass control versus STPV cladding) operating side-by-side (i.e. under the same weather conditions). In addition, to assist designers with the complex task of greenhouse modeling, it would be ideal to have access to experimental measurements (annual weather, climate and growth data recorded at time steps of one hour or less) for typical greenhouse designs and operating conditions. For instance, the interior convective heat transfer coefficient was found to have a significant impact on thermal energy use and validated correlations would be useful to improve the accuracy for predicting energy consumption/generation.
- **Development of a modular platform for greenhouse energy simulation.** There is a need to develop a more universal platform for predicting greenhouse microclimate and crop growth. The platform would ideally have a graphical interface whereby various low-to-high resolution models can be developed/implemented/validated by its users so that designers can conveniently perform both quick scan and detailed analyses. TRNSYS is currently the only platform with a graphical interface where a multizone building model (where the geometry can be defined by drawing it in 3D programs) can be connected to other programs (e.g. CONTAM) and allows the user to incorporate pre-existing models (e.g. HVAC, ground heat transfer) or create their own models (e.g. new Types in

TRNSYS or connection to MATLAB) for co-simulation. A promising new feature in TRNSYS 18.0 integrates dynamic daylight simulation based on DaySIM into the Type 56 multizone building model. Therefore, TRNSYS or software having similar capabilities would be an appropriate platform for further collaboration and expansion into the domain of greenhouse modeling. New features can be implemented into the Type 56 multizone building model to provide the key adaptations needed to model greenhouses. This, in combination with the development of new models (Types) or source code that can be called by a range of external programs, could facilitate the process of sharing knowledge between researchers. Some of the possible improvements to TRNSYS may include:

  - Definition of new surface types in Type 56 for modeling evapotranspiration and condensation.
  - Integration of dynamic conversion factors from sunlight illuminance (lux) to photosynthetic photon flux density (PPFD) based on time of day and eventually separate radiation processing for photosynthetically active radiation (PAR).
  - Modeling and control of horticultural light fixtures, possibly as an internal gain, to include distribution of shortwave radiation/PPFD on the crop/interior surfaces and the heat and mass transfers to the airnode.
  - Improve the Type 56 model to enable detailed radiation calculations for glazing and screens that transmit longwave radiation (e.g. PE film) to exterior boundary surfaces (e.g. sky, ground) and provide the option for a second screen.
  - Demonstration of connectivity with CONTAM for modeling photosynthesis (CO_2) and interaction with the mass and energy fluxes.

- **Screens made of flexible STPV** could roll up and generate solar electricity when they are drawn. This would address the inherent disadvantage of STPV cladding which is not able to be withdrawn in periods of low light. Research is also needed to develop organic STPV that has a long lifespan. This technology has significant potential because it can generate electricity from the wavelengths that are less useful for crop growth.
- **STPV for two-to-three-season greenhouses/crop shelters** may produce solar electricity year-round even when crop production ceases (in the winter) and could reduce the problem of peak electricity demand in summer. The STPV would be particularly suitable for providing shading to crops that prefer low levels of light (e.g. baby leafy greens) and

crops that can be grown in summer and preserved (e.g. cannabis). It is likely that lower PV area ratios would result in the greatest benefit. Further experimental and numerical work combined with economic analysis is needed to identify promising designs.

- **Combination of greenhouses and anaerobic digesters** to improve the overall efficiency compared to both systems installed separately (Fig. 2.13). Both anaerobic digester and greenhouse heating energy consumption can be reduced by upgrading greenhouse surplus air thermal energy using heat pumps, storing it inside the thermally massive digester, and using it to heat the greenhouse at a later point (e.g. at night). Most importantly, research into developing methods for recycling the nutrients contained in organic waste and the optimal reuse of these finite resources for supporting agriculture is needed.
- **Integration of renewable energy, agriculture and organic resource recycling sectors**. Future work is needed to optimize the operation of these combined systems (Fig. 7.1). Several key technologies are at their early stages of development and would greatly benefit from financial incentives to accelerate their deployment. For instance, funds generated from a carbon tax could be used to subsidize renewable energy infrastructure (e.g. solar/wind electricity generation and power-to-gas) and a tax on unhealthy food (e.g. sugar, which carries a heavy hidden cost on the medicare system) could be used to assist the next generation of farmers so that they can earn a decent living while promoting integration with organic resource recycling and clean energy infrastructure.

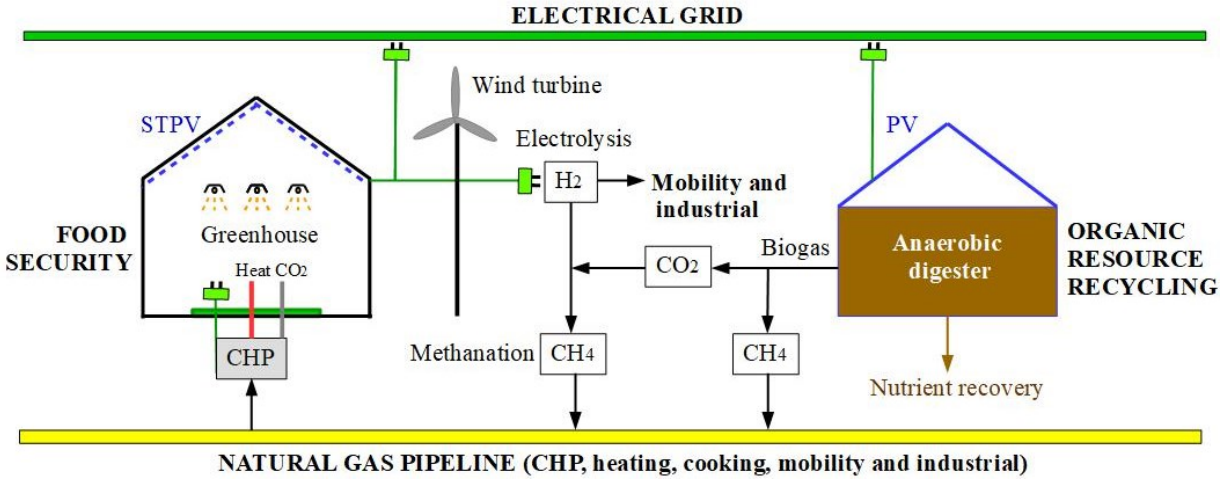

Figure 7.1: Integration of renewable energy, agriculture and organic resource recycling infrastructure.

REFERENCES

Adams, S., Warwick, H.R.I., Hargreaves, D. and Jacobson, R. (2007). An initial investigation into the potential for using sealed greenhouse technologies in the UK. Project number: PC 256 Project leader: CT Pratt.

AGC. (2018). AGC Chemicals. https://www.agcchem.com/documentation/brochures-literature/specialty-materials/25-f-clean-brochure/file

AGi32. (2018). Lighting Analysts. http://docs.agi32.com/AGi32/Content/adding_calculation_points/PPFD_Concepts.htm

Agrithermic. (2018). https://agrithermic.fr/en/a-light-transmission-module-for-photovoltaic-greenhouses-into-enerserre/

Ahamed, M. S., Guo, H., & Tanino, K. (2018). A quasi-steady state model for predicting the heating requirements of conventional greenhouses in cold regions. Information processing in agriculture, 5(1), 33-46.

Ahamed, M. S., Guo, H., & Tanino, K. (2018). A quasi-steady state model for predicting the heating requirements of conventional greenhouses in cold regions. Information processing in agriculture, 5(1), 33-46.

Albright, L. D. (2005). A commercially viable controlled environment agriculture spinach production system. Final report. The New York State Energy Research and Development Authority. Cornell University, New York, USA.

Albright, L. D. (1990). Environment control for animals and plants. American Society of Agricultural Engineers.

Albright, L. D., Both, A. J., & Chiu, A. J. (2000). Controlling greenhouse light to a consistent daily integral. Transactions of the ASAE, 43(2), 421.

Al-Helal, I. M., & Abdel-Ghany, A. M. (2011). Energy partition and conversion of solar and thermal radiation into sensible and latent heat in a greenhouse under arid conditions. Energy and Buildings, 43(7), 1740-1747.

Al-Kayssi, A. W. (2002). Spatial variability of soil temperature under greenhouse conditions. Renewable energy, 27(3), 453-462.

Allen, R. G., Pereira, L. S., Raes, D., & Smith, M. (1998). Crop evapotranspiration-Guidelines for computing crop water requirements-FAO Irrigation and drainage paper 56. Fao, Rome, 300(9), D05109.

Andolsun, S. (2012). Comparison of DOE-2.1 with EnergyPlus and TRNSYS for ground coupled residential buildings in hot and humid climates stage 3. Energy Systems Laboratory.

Andrews, R., & Pearce, J. M. (2011). Environmental and economic assessment of a greenhouse waste heat exchange. Journal of Cleaner Production, 19(13), 1446-1454.

ANSYS. (2018). Fluent. https://www.ansys.com/products/fluids/ansys-fluent

Aroca-Delgado, R., Pérez-Alonso, J., Callejón-Ferre, Á. J., & Velázquez-Martí, B. (2018). Compatibility between crops and solar panels: an overview from shading systems. Sustainability, 10(3), 743.

ASAE. (2003). Heating, ventilating and cooling greenhouses. ANSI/ASAE EP406.4 JAN03. St. Joseph, MI: ASAE.

Athienitis, A. (1998). Building Thermal Analysis. MathSoft Inc.

Athienitis, A. K. (2007, June). Design of a solar home with BIPV-thermal system and ground source heat pump. In 2nd SBRN and SESCI 32nd Joint Conference.

Attar, I., Naili, N., Khalifa, N., Hazami, M., & Farhat, A. (2013). Parametric and numerical study of a solar system for heating a greenhouse equipped with a buried exchanger. Energy conversion and management, 70, 163-173.

Bailera, M., Lisbona, P., Romeo, L. M., & Espatolero, S. (2017). Power to gas projects review: Lab, pilot and demo plants for storing renewable energy and CO2. Renewable and Sustainable Energy Reviews, 69, 292-312.

Bailey, B. J. (1983, August). Limiting the relative humidity in insulated greenhouses at night. In III International Symposium on Energy in Protected Cultivation, 148, 411-420.

Bambara, J., & Athienitis, A. (2015a). Experimental evaluation and energy modeling of a greenhouse concept with semi-transparent photovoltaics. Energy Procedia, 78, 435-440.

Bambara, J., & Athienitis, A. (2015b). Integration of organic waste recycling and greenhouse agriculture CCTC Paper Number 1570094359.

Bambara, J., & Athienitis, A. (2016). Comparison of two modeling approaches for semi-transparent photovoltaic cladding in greenhouses and experimental calibration. eSim Conference Proceedings. Ontario, Canada.

Barbera, E., Sforza, E., Vecchiato, L., & Bertucco, A. (2017). Energy and economic analysis of microalgae cultivation in a photovoltaic-assisted greenhouse: Scenedesmus obliquus as a case study. Energy, 140, 116-124.

Bartok, J. W. (2001). Energy conservation for commercial greenhouses (NRAES-3). Natural Resource, Agriculture and Engineering Service. Ithica, USA.

Bastien, D. (2015). Methodology for enhancing solar energy utilization in solaria and greenhouses (Doctoral dissertation, Concordia University).

Bernstad, A., & la Cour Jansen, J. (2011). A life cycle approach to the management of household food waste–a Swedish full-scale case study. Waste management, 31(8), 1879-1896.

Berroug, F., Lakhal, E. K., El Omari, M., Faraji, M., & El Qarnia, H. (2011). Thermal performance of a greenhouse with a phase change material north wall. Energy and Buildings, 43(11), 3027-3035.

Beshada, E., Zhang, Q., & Boris, R. (2006). Winter performance of a solar energy greenhouse in southern Manitoba. Canadian Biosystems Engineering, 48(5), 1-8.

BOC. (2016). Renewal of the inflation-control target. Bank of Canada, http://www.bankofcanada.ca/wp-content/uploads/2016/10/background_nov11.pdf; 2016

BOC. (2017). Selected historical interest rates - bank rate - V122530 - Jan. 1935. Bank of Canada, http://www.bankofcanada.ca/wp-content/uploads/2010/09/selected_historical_v122530.pdf; 2017

BOC. (2018). Annual exchange rates for 2017. Bank of Canada (BOC), https://www.bankofcanada.ca/rates/exchange/annual-average-exchange-rates/

Bot, G. P. (1983). Greenhouse climate: from physical processes to a dynamic model (Doctoral dissertation, Wageningen University).

Brault, D., Gueymard, C., Boily, R., & Gosselin, A. (1989). Contribution of HPS lighting to the heating requirements of a greenhouse. Paper-American Society of Agricultural Engineers (USA).

Brechner, M., Both, A. J., & Staff, C. E. A. (1996). Hydroponic lettuce handbook. Cornell Controlled Environment Agriculture, 504-509.

Businger, J. A. (1963). The glasshouse (greenhouse) climate. Physics of Plant Environment, WR Van Wijk, Ed. (North Holland Publishing Co., Amsterdam).

Campen, J. B., Bot, G. P. A., & De Zwart, H. F. (2003). Dehumidification of greenhouses at northern latitudes. Biosystems Engineering, 86(4), 487-493.

Canadian Solar. (2016). Dymond - Double-glass PV module product datasheet. Canadian Solar Inc., http://www.canadiansolar.com/fileadmin/user_upload/downloads/datasheets/v5.4/Canadian_Solar-Datasheet-CS6KPFG_1650x992_Dymond_v5.4en.pdf

Carlini, M., & Castellucci, S. (2010). Modelling and simulation for energy production parametric dependence in greenhouses. Mathematical Problems in Engineering, 2010.

Carlini, M., Honorati, T., & Castellucci, S. (2012). Photovoltaic greenhouses: comparison of optical and thermal behaviour for energy savings. Mathematical Problems in Engineering, 2012.

Castellano, S. (2014). Photovoltaic greenhouses: evaluation of shading effect and its influence on agricultural performances. Journal of Agricultural Engineering, 45(4), 168-175.

Castellano, S., Santamaria, P., & Serio, F. (2016). Solar radiation distribution inside a monospan greenhouse with the roof entirely covered by photovoltaic panels. Journal of Agricultural Engineering, 47(1), 1-6.

Cengal, Y. A. (2007). Heat and Mass Transfer: A Practical Approach, 3rd ed. New York, USA. McGraw-Hill.

Chau, J., Sowlati, T., Sokhansanj, S., Preto, F., Melin, S., & Bi, X. (2009). Economic sensitivity of wood biomass utilization for greenhouse heating application. Applied Energy, 86(5), 616-621.

Chen, Y. (2013). Methodology for design and operation of active building-integrated thermal energy storage systems (Doctoral dissertation, Concordia University).

Chong, W. T., Naghavi, M. S., Poh, S. C., Mahlia, T. M. I., & Pan, K. C. (2011). Techno-economic analysis of a wind–solar hybrid renewable energy system with rainwater collection feature for urban high-rise application. Applied Energy, 88(11), 4067-4077.

Chou, S. K., Chua, K. J., Ho, J. C., & Ooi, C. L. (2004). On the study of an energy-efficient greenhouse for heating, cooling and dehumidification applications. Applied energy, 77(4), 355-373.

Climax Conseils. (2014). Personnel communications with Jacques Thériault, Quebec, Canada.

Cohen, S., & Fuchs, M. (1999). Measuring and predicting radiometric properties of reflective shade nets and thermal screens. Journal of agricultural engineering research, 73(3), 245-255.

Cossu, M., Ledda, L., Urracci, G., Sirigu, A., Cossu, A., Murgia, L., ... & Yano, A. (2017). An algorithm for the calculation of the light distribution in photovoltaic greenhouses. Solar Energy, 141, 38-48.

Cossu, M., Murgia, L., Ledda, L., Deligios, P. A., Sirigu, A., Chessa, F., & Pazzona, A. (2014). Solar radiation distribution inside a greenhouse with south-oriented photovoltaic roofs and effects on crop productivity. Applied Energy, 133, 89-100.

Cossu, M., Yano, A., Li, Z., Onoe, M., Nakamura, H., Matsumoto, T., & Nakata, J. (2016). Advances on the semi-transparent modules based on micro solar cells: First integration in a greenhouse system. Applied energy, 162, 1042-1051.

Crawley, D. B., Hand, J. W., Kummert, M., & Griffith, B. T. (2008). Contrasting the capabilities of building energy performance simulation programs. Building and environment, 43(4), 661-673.

Crazy-leds. (2018). https://crazy-leds.com/lighting-metrics-par-ppf-ppfd-photon-efficiency

Cuce, E., Harjunowibowo, D., & Cuce, P. M. (2016). Renewable and sustainable energy saving strategies for greenhouse systems: A comprehensive review. Renewable and Sustainable Energy Reviews, 64, 34-59.

Curry, N., & Pillay, P. (2015). Integrating solar energy into an urban small-scale anaerobic digester for improved performance. Renewable Energy, 83, 280-293.

Darrach, M. (2014). Statistical overview of the canadian vegetable industry 2013. Retrieved from the Agriculture and Agri-Food Canada website: http://www. agr. gc. ca/resources/prod/doc/pdf/st_ovrv_veg_2013_eng. pdf

De Cloet. (2018). http://www.decloetgreenhouse.com/venlo

De Cotret F.R. (2011). Inauguration du méthaniseur couplé d'une serre hydroponique de la Laiterie Charlevoix. http://gaiapresse.ca

De Zwart, H.F. (1996). Analyzing energy-saving options in greenhouse cultivation using a simulation model. Thesis Agricultural Universisty of Wageningen. Publication 96-5 IMAG-DLO. ISBN 90-5485-533-9.

dela Cruz, N. E., Aganon, C. P., Patricio, M. G., Romero, E. S., Lindain, S. A., & Galindez, J. L. (2006, October). Production of Organic Fertilizer from Solid Waste and its Utilization in

Intensive Organic-Based Vegetable Production and for Sustaining Soil Health and Productivity. In International Workshop on Sustained Management of the Soil-Rhizosphere System for Efficient Crop Production and Fertilizer Use (Vol. 16, p. 20).

Deloitte. (2017). Oil and gas price forecast. Deloitte Inc., https://www2.deloitte.com/ca/en/pages/resource-evaluation-and-advisory/articles/deloitte-canadian-price-forecast.html

Deru, M., Judkoff, R., & Neymark, J. (2003). Whole building energy simulation with a three-dimensional ground-coupled heat transfer model. ASHRAE Transactions, 109(1), 557-565.

Despommier, D. (2011). The vertical farm: controlled environment agriculture carried out in tall buildings would create greater food safety and security for large urban populations. Journal für Verbraucherschutz und Lebensmittelsicherheit, 6(2), 233-236.

DisTech. (2018). Personnel communications with Steeve Fournier, Quebec, Canada.

Dobos, A. P. (2014). PVWatts version 5 manual (No. NREL/TP-6A20-62641). National Renewable Energy Laboratory, Colorado, USA.

DOE. (2014). 8.2 Engineering Reference: The Encyclopedic Reference to EnergyPlus Calculations. US Department of Energy. EnergyPlus. https://energyplus.net/

DOE. (2015). WINDOW 7.3. Department of energy, USA, https://windows.lbl.gov/software/window/7/index_7_3_4.html

Dorais, M. (2003, October). The use of supplemental lighting for vegetable crop production: light intensity, crop response, nutrition, crop management, cultural practices. In Canadian Greenhouse Conference (Vol. 9).

Dueck, T. A., Poudel, D., Janse, J., & Hemming, S. (2009). Diffuus licht-wat is de optimale lichtverstrooiing? (No. 308). Wageningen UR Glastuinbouw.

Dupont. (2014). Ionomer-based encapsulants for photovoltaics product datasheet. Dupont, http://www.dupont.com/content/dam/dupont/products-and-services/solar-photovoltaic-materials/solar-photovoltaic-materials-landing/documents/DEC-DuPont-Ionomer-Based-Encapsulants-for-PV.pdf

Dzakovich, M. P., Gómez, C., & Mitchell, C. A. (2015). Tomatoes grown with light-emitting diodes or high-pressure sodium supplemental lights have similar fruit-quality attributes. HortScience, 50(10), 1498-1502.

ePHOTOzine. (2018). https://www.ephotozine.com/article/guide-to-colour-temperature-4804

ECCC. (2016). National Inventory Report 1990-2014: Greenhouse Gas Sources and Sinks in Canada. Environment and Climate Change Canada (ECCC); 2016.

Egigian-Nicholas, C. (2013). Integrating greenhouse facilities with AD bioenergy. BioCycle, 54(3), 40-43.

Elings, A., Kempkes, F. L. K., Kaarsemaker, R. C., Ruijs, M. N. A., van de Braak, N. J. & Dueck, T. A. (2005). The energy balance and energy-saving measures in greenhouse tomato cultivation. Acta Horticulturae 691, 67-74.

Elings, A. & Marcelis, L. (2010). Temperatuurregeling in komkommer, met gebruik van het INTKAM gewasmodel. Accessible via http://edepot.wur.nl/22639

Elmhirst, J. (2006). Crop profile for greenhouse tomato in Canada. Agriculture and Agri-Food Canada. Retrieved from www.publications.gc.ca/collections/collection_2009/agr/A118-10-24-2006E.pdf

Emmott, C. J., Röhr, J. A., Campoy-Quiles, M., Kirchartz, T., Urbina, A., Ekins-Daukes, N. J., & Nelson, J. (2015). Organic photovoltaic greenhouses: a unique application for semi-transparent PV?. Energy & environmental science, 8(4), 1317-1328.

Emphase. (2015). https://enphase.com/sites/default/files/Vine%20Fresh%20Produce%20%282%29.pdf

Enbridge. (2017). Large volume rates. Enbridge Inc., https://www.enbridgegas.com/businesses/accounts-billing/gas-rates/large-volume-rates/rate-6.aspx

Environment Canada. (2013). Technical document on municipal solid waste organics processing, ISBN: 978-1-100-21707-9.

EPA. (2008). Environmental Protection Agency, Technology characterization: reciprocating engines. CHP partnership program, Energy and Environmental Analysis Inc.

Escobedo, J. F., Gomes, E. N., Oliveira, A. P., & Soares, J. (2011). Ratios of UV, PAR and NIR components to global solar radiation measured at Botucatu site in Brazil. Renewable Energy, 36(1), 169-178.

ESP-r. (2018). http://www.esru.strath.ac.uk/Programs/ESP-r.htm

Ewing, D. (2018). https://amadeintheshade.com/2016/02/understanding-heat-reduction-and-window-films/

Fatnassi, H., Poncet, C., Bazzano, M. M., Brun, R., & Bertin, N. (2015). A numerical simulation of the photovoltaic greenhouse microclimate. Solar Energy, 120, 575-584.

Fazlil-Ilahil, W. F. (2009). Evapotranspiration models in greenhouse (Doctoral dissertation, Wageningen University).

Fitz-Rodríguez, E., Kubota, C., Giacomelli, G. A., Tignor, M. E., Wilson, S. B., & McMahon, M. (2010). Dynamic modeling and simulation of greenhouse environments under several scenarios: A web-based application. Computers and electronics in agriculture, 70(1), 105-116.

Fu, R., Feldman, D. J., Margolis, R. M., Woodhouse, M. A., & Ardani, K. B. (2017). US solar photovoltaic system cost benchmark: Q1 2017 (No. NREL/TP-6A20-68925). National Renewable Energy Lab.(NREL), Golden, CO (United States).

Fuller, S., & Petersen, S. (1996). Life-cycle costing manual for the federal energy management program, NIST Handbook 135 (No. Handbook (NIST HB)-135).

Ganguly, A., & Ghosh, S. (2011). Performance analysis of a floriculture greenhouse powered by integrated solar photovoltaic fuel cell system. Journal of Solar Energy Engineering, 133(4), 041001.

Ganguly, A., Misra, D., & Ghosh, S. (2010). Modeling and analysis of solar photovoltaic-electrolyzer-fuel cell hybrid power system integrated with a floriculture greenhouse. Energy and buildings, 42(11), 2036-2043.

Garzoli, K. (1989). Energy efficient greeenhouses. In: III Energy Saving in Protected Cultivation. ISHS, pp. 53–62.

Gebhart, B. (1961). Surface temperature calculations in radiant surroundings of arbitrary complexity—for gray, diffuse radiation. International Journal of Heat and Mass Transfer, 3(4), 341-346.

Gebhart. B. (1971). Heat Transfer. 2nd ed. New York, USA. McGraw-Hill.

Ghosal, M. K., Tiwari, G. N., & Srivastava, N. S. L. (2004). Thermal modeling of a greenhouse with an integrated earth to air heat exchanger: an experimental validation. Energy and Buildings, 36(3), 219-227.

Gotham Greens. (2018). http://gothamgreens.com/our-farms/

Grant, A., Johnstone, C., & Kelly, N. (2008). Urban wind energy conversion: The potential of ducted turbines. Renewable Energy, 33(6), 1157-1163.

Gravita. (2018). https://gavita.com/retail/products/gavita-pro-line-classic/gavita-pro-1000-de/

Gravita. (2016). Personnel communications with Amber Piech, Ontario, Canada.

Green, M.A., Emery, K., Hishikawa, Y., Warta, W., Dunlop, E. D. (2015). Solar cell efficiency tables (Version 45). Progress in photovoltaics: Research and applications; 23(1): 1-9.

Grow lights. (2018). http://growlights.ca/

Guardian. (2017). Clear float glass product datasheet. Guardian glass, http://www.me.en.sunguardglass.com/cs/groups/sunguardme/documents/native/gi_005564.pdf

Guerrero-Lemus, R., Vega, R., Kim, T., Kimm, A., & Shephard, L. E. (2016). Bifacial solar photovoltaics–A technology review. Renewable and sustainable energy reviews, 60, 1533-1549.

Gupta, M. J., & Chandra, P. (2002). Effect of greenhouse design parameters on conservation of energy for greenhouse environmental control. Energy, 27(8), 777-794.

Handbook, A. F. (2009). American society of heating, refrigerating and air-conditioning engineers. Inc.: Atlanta, GA, USA.

Harbick, K., & Albright, L. D. (2016, May). Comparison of energy consumption: greenhouses and plant factories. In VIII International Symposium on Light in Horticulture 1134 (pp. 285-292).

Harnett, R. (1975). Study of glasshouse type and orientation. Acta Horticulturae 46, 209‑216.

Harnois (2018). http://www.harnois.com/en/

Harnois. (2017). Personnel communications with Simon Desforges, Quebec, Canada.

Hellickson, M., Walker, J. (1983). Ventilation of agricultural structures.

Hemming, S., Kempkes, F., van der Braak, N., Dueck, T. and Marissen, N. (2006a). Greenhouse cooling by NIR-reflection. Acta Horticulturae. 719: 97-106.

Hemming, S., van der Braak, N., Dueck, T., Jongschaap, R. and Marissen, N. (2006b). Filtering natural light by the greenhouse covering using model simulations-more production and better plant quality by diffuse light? Acta Horticulturae. 711, 105-110

Hemming, S., Sapounas, A., de Zwart, H. F., Ruijs, M. N. A., & Maaswinkel, R. H. M. (2010). Design of a sustainable innovation greenhouse system for Turkey (No. GTB-1009). Wageningen UR Greenhouse Horticulture.

Hemming, S., Kempkes, F.L.K. and Mohammadkhani, V. (2011). New glass coatings for high insulating greenhouses without light losses - energy saving, crop production and economic potentials. Acta Horticulturae. 893: 217-226.

Henninger, J. H. (1984). Solar absorptance and thermal emittance of some common spacecraft thermal-control coatings (No. NASA-RP240400-1121). National Aeronautics and Space Administration, District of Columbia, USA.

Hepbasli, A. (2013). Low exergy modelling and performance analysis of greenhouses coupled to closed earth-to-air heat exchangers (EAHEs). Energy and Buildings, 64, 224-230.

Hernández, R., & Kubota, C. (2014). Growth and morphological response of cucumber seedlings to supplemental red and blue photon flux ratios under varied solar daily light integrals. Scientia Horticulturae, 173, 92-99.

Hill, J. M. (2006). Dynamic modeling of tree growth and energy use in a nursery greenhouse using Matlab and Simulink. Masters of Engineering. Agricultural and Biological Engineering. Cornell University.

Hiller, M. D., Beckman, W. A., & Mitchell, J. W. (2000). TRNSHD—a program for shading and insolation calculations. Building and Environment, 35(7), 633-644.

Hortilux. (2018). https://eyehortilux.com/grow-lights/

Hottel, H. C. (1976). A simple model for estimating the transmittance of direct solar radiation through clear atmospheres. Solar energy, 18(2), 129-134.

Hussain, M. I., Ali, A., & Lee, G. H. (2015). Performance and economic analyses of linear and spot Fresnel lens solar collectors used for greenhouse heating in South Korea. Energy, 90, 1522-1531.

Hydronov. (2018). https://hydronov.com/

IEC. (2011). International Electrotechnical Commission (IEC). Photovoltaic module performance testing and energy rating - Part 1: Irradiance and temperature performance measurements and power rating IEC 61853-1; 2011.

Illumitex. (2016). PowerHarvest W series product datasheet. Illumitex Inc., https://illumitex.com/wp-content/uploads/2016/10/PowerHarvestW_Spec10.16.pdf

Illumitex. (2018). Personal communications with Joel Enns. Ontario, Canada.

Ingham, R. E., Trofymow, J. A., Ingham, E. R., & Coleman, D. C. (1985). Interactions of bacteria, fungi, and their nematode grazers: effects on nutrient cycling and plant growth. Ecological monographs, 55(1), 119-140.

Isofoil. (2018). https://www.isolofoam.com/english/isofoil

Jackson, H.A. & Darby, D.E. (2006). Greenhouse Ventilation. Canada Service Plan. M-6704.

Jin, C., Du, S., Wang, Y., Condon, J., Lin, X., & Zhang, Y. (2009). Carbon dioxide enrichment by composting in greenhouses and its effect on vegetable production. Journal of Plant Nutrition and Soil Science, 172(3), 418-424.

Jolliet, O. (1994). HORTITRANS, a model for predicting and optimizing humidity and transpiration in greenhouses. Journal of Agricultural Engineering Research, 57(1), 23-37.

Kadowaki, M., Yano, A., Ishizu, F., Tanaka, T., & Noda, S. (2012). Effects of greenhouse photovoltaic array shading on Welsh onion growth. Biosystems Engineering, 111(3), 290-297.

Kapsis, K. (2016). Modelling, design and experimental study of semi-transparent photovoltaic windows for commercial building applications (Doctoral dissertation, Concordia University).

Katsoulas, N., & Kittas, C. (2011). Greenhouse crop transpiration modelling. In Evapotranspiration-From Measurements to Agricultural and Environmental Applications. InTech.

Kittas, C., Katsoulas, N., & Bartzanas, T. (2012). Greenhouse climate control in mediterranean greenhouses. Cuadernos de Estudios Agroalimentarios (CEA), (3), 89-114.

Kittas, C., Karamanis, M., & Katsoulas, N. (2005). Air temperature regime in a forced ventilated greenhouse with rose crop. Energy and buildings, 37(8), 807-812.

Klein, S. A., Duffie J. A., Mitchell, J. C., Kummer, J. P., Thornton, J. W., Bradley, D. E., . . . Kummert, M. (2014). TRNSYS 17. Volume 4. Mathematical Reference. Solar Energy Laboratory, University of Wisconsin-Madison, Wisconsin, USA.

Kompogas. (2007). Anaerobic digestion of source segregated biowastes – case study, University of Glamorgan, United Kingdom.

Kozai, T. (2005). Closed systems with lamps for high quality transplant production at low costs using minimum resources. In Photoautotrophic (sugar-free medium) Micropropagation as a New Micropropagation and Transplant Production System (pp. 275-311). Springer, Dordrecht.

Kozai, T., Niu, G., & Takagaki, M. (Eds.). (2015). Plant factory: an indoor vertical farming system for efficient quality food production. Academic Press.

Kubo. (2018). Kubo Group. https://www.kubogroup.nl/en/ultra-clima

Kusuda, T., & Achenbach, P. R. (1965). Earth temperature and thermal diffusivity at selected stations in the United States (No. NBS-8972). National Bureau of Standards Gaithersburg MD.

Laate, E. A. (2013). The economics of production and marketing of greenhouse crops in Alberta. Alberta Agriculture and Rural Development, Alberta, Canada.

Lawand, T. A., Alward, R., Saulnier, B., & Brunet, E. (1975). The development and testing of an environmentally designed greenhouse for colder regions. Solar Energy, 17(5), 307-312.

Leckner, M., & Zmeureanu, R. (2011). Life cycle cost and energy analysis of a net zero energy house with solar combisystem. Applied Energy, 88(1), 232-241.

Lee, C. S., Costola, D., Swinkels, G. L. A. M., & Hensen, J. L. M. (2012). On the use of building energy simulation programs in the performance assessment of agricultural greenhouses. In Proceedings of the 1st Asia Conference of the International Building Performance Simulation Association. Shanghai, China (pp. 1-8).

Lorenzo, P., Sanchez-Guerrero, M. C., Medrano, E., Garcia, M. L., Caparros, I., Coelho, G., & Giménez, M. (2004). Climate control in the summer season: a comparative study of external mobile shading and fog system. Acta horticulturae.

Lufa farms. (2018). https://montreal.lufa.com/en/blog/articles/the-times-are-changin

Lumigrow. (2018). LED growers' guide for vine crops. Lumigrow. Retrieved from www.lumigrow.com/applied-researches/led-growers-guide-vine-crops/

Lychnos, G., & Davies, P. A. (2008, October). A solar powered liquid-desiccant cooling system for greenhouses. In International Workshop on Greenhouse Environmental Control and Crop Production in Semi-Arid Regions 797 (pp. 95-109).

Manzano, A. (2007). Gasification of greenhouse residues for obtaining electrical energy in the south of Spain: localization by GIS. Interciencia, 32(2), 131-136.

Marceau, M. L., & VanGeem, M. G. (2008). Solar reflectance values for concrete. Concrete international, 30(08), 52-58.

Marszal, A. J., Heiselberg, P., Jensen, R. L., & Nørgaard, J. (2012). On-site or off-site renewable energy supply options? Life cycle cost analysis of a net zero energy building in Denmark. Renewable energy, 44, 154-165.

MATLAB. (2018). https://www.mathworks.com/products/matlab.html

Max, J. F., Reisinger, G., Hofmann, T., Hinken, J., Tantau, H. J., Ulbrich, A., ... & Schurr, U. (2012). Glass–film-combination: Opto-physical properties and energy saving potential of a novel greenhouse glazing system. Energy and Buildings, 50, 298-307.

McAdams, W. H. (1959). Heat Transmission, 3rd ed. New York, USA. McGraw-Hill.

McCree, K. J. (1972). Test of current definitions of photosynthetically active radiation against leaf photosynthesis data. Agricultural Meteorology, 10, 443-453.

McDonald, J. (2004). Fuel Heat Values. Originally published by CSTN, http://www.veoliawatertech.com/crownsolutions/ressources/documents/2/21901,Water-pp147.pdf

McHenry, M. P. (2009). Agricultural bio-char production, renewable energy generation and farm carbon sequestration in Western Australia: Certainty, uncertainty and risk. Agriculture, Ecosystems & Environment, 129(1-3), 1-7.

Minuto, G., Bruzzone, C., Tinivella, F., Delfino, G., & Minuto, A. (2009). Fotovoltaico sui tetti delle serre per produrre anche energia. Suppl L'Inform Agrario, 65(10), 16–9.

Mitalas, G. P., & Arseneault, J. G. (1970). Fortran IV program to calculate z-transfer functions for the calculation of transient heat transfer through walls and roofs. National Research Council Canada, Division of Building Research.

Modak S. (2011). Advancing USA agriculture with ultra-clean CHP and CO_2 fertilization for greenhouses. US Clean Heat & Power Association. CHP Forum.

Mukezangango J. (2017). Statistical overview of the Canadian vegetable industry 2016. Retrieved from the Agriculture and Agri-Food Canada website: http://www.agr.gc.ca/resources/prod/doc/pdf/VegRep_2016-eng.pdf

Müller, G., Jentsch, M. F., & Stoddart, E. (2009). Vertical axis resistance type wind turbines for use in buildings. Renewable Energy, 34(5), 1407-1412.

National geographic. (2018). https://news.nationalgeographic.com/news/2014/07/140717-japan-largest-indoor-plant-factory-food/

Nawalany, G., Bieda, W., Radoń, J., & Herbut, P. (2014). Experimental study on development of thermal conditions in ground beneath a greenhouse. Energy and Buildings, 69, 103-111.

NEB. (2017). Energy conversion tables. National Energy Board (NEB). Government of Canada, https://www.neb-one.gc.ca/nrg/tl/cnvrsntbl/cnvrsntbl-eng.html

Nelson, J. A., & Bugbee, B. (2014). Economic analysis of greenhouse lighting: light emitting diodes vs. high intensity discharge fixtures. PloS one, 9(6), e99010.

Nelson, J. A., & Bugbee, B. (2015). Analysis of environmental effects on leaf temperature under sunlight, high pressure sodium and light emitting diodes. PloS one, 10(10), e0138930.

Ontario Hydro. (2017). Ontario Hydro Rates, http://www.ontario-hydro.com/current-rates

Ozgener, O. (2010). Use of solar assisted geothermal heat pump and small wind turbine systems for heating agricultural and residential buildings. Energy, 35(1), 262-268.

Papadopoulos, A. P., & Hao, X. (1997). Effects of three greenhouse cover materials on tomato growth, productivity, and energy use. Scientia Horticulturae, 70(2-3), 165-178.

Peng, J., Curcija, D. C., Lu, L., Selkowitz, S. E., Yang, H., & Mitchell, R. (2016). Developing a method and simulation model for evaluating the overall energy performance of a ventilated semi-transparent photovoltaic double-skin facade. Progress in Photovoltaics: Research and Applications, 24(6), 781-799.

Perez, R., Stewart, R., Seals, R., & Guertin, T. (1988). The development and verification of the Perez diffuse radiation model (No. SAND-88-7030). Sandia National Labs., Albuquerque, NM (USA); State Univ. of New York, Albany (USA). Atmospheric Sciences Research Center.

Philips. (2012). Philips Electronics. Philips LED Lighting in horticulture. Netherlands.

Philips. (2018). Calculux. http://www.lighting.philips.cz/podpora/podpora-vyrobku/calculux

Pieters, J. G., & Deltour, J. M. (1997). Performances of greenhouses with the presence of condensation on cladding materials. Journal of Agricultural Engineering Research, 68(2), 125-137.

Pietzsch, M., & Meyer, J. (2007, October). Use of reject heat from biogas power plants for greenhouse heating. In International Symposium on High Technology for Greenhouse System Management: Greensys2007 801 (pp. 719-724).

Pinho, P., Hytönen, T., Rantanen, M., Elomaa, P., & Halonen, L. (2013). Dynamic control of supplemental lighting intensity in a greenhouse environment. Lighting Research & Technology, 45(3), 295-304.

Pinho, P., Jokinen, K., & Halonen, L. (2012). Horticultural lighting–present and future challenges. Lighting Research & Technology, 44(4), 427-437.

Piscia, D., Montero, J. I., Baeza, E., & Bailey, B. J. (2012). A CFD greenhouse night-time condensation model. Biosystems Engineering, 111(2), 141-154.

Plas-Tech. (2016), Personnel communications with Jeanette Easter. Ontario, Canada.

Polygal. (2018). Clear versus polymatte polycarbonate product datasheet (PLM-US-1209-01). Polygal Inc. http://www.polygal-northamerica.com/wp-content/uploads/2016/04/Polymatte.pdf

Polysolar. (2018). http://www.polysolar.co.uk/documents/PS-CT%20Transparent%20Technical%20Specification%20sheet.pdf

Rath, T. (1992). Einsatz wissensbasierter Systeme zur Modellierung und Darstellung von gartenbautechnischem Fachwissen am Beispiel des hybriden Expertensystems HORTEX. Thesis University of Hannover, Germany.

Reagan, J. A., & Acklam, D. M. (1979). Solar reflectivity of common building materials and its influence on the roof heat gain of typical southwestern USA residences. Energy and Buildings, 2(3), 237-248.

Reinhart, C. F., & Walkenhorst, O. (2001). Validation of dynamic RADIANCE-based daylight simulations for a test office with external blinds. Energy and buildings, 33(7), 683-697.

RETScreen. (2013). Clean Energy Project Analysis Software. Version 4. Ministry of Natural Resources, Canada.

Robinson, L. (2009). Numerical and experimental study of semi-transparent photovoltaics integrated into commercial building facades (Doctoral dissertation, Concordia University).

Rousse, D. R., Martin, D. Y., Thériault, R., Léveillée, F., & Boily, R. (2000). Heat recovery in greenhouses: a practical solution. Applied Thermal Engineering, 20(8), 687-706.

Roy, J. C., Boulard, T., Kittas, C., & Wang, S. (2002). Convective and ventilation transfers in greenhouses, Part 1: the greenhouse considered as a perfectly stirred tank. Biosystems Engineering, 83, 1-20.

RSMeans. (2016). RSMeans assemblies cost data. The Gordian Group. Rockland, Massachusetts, USA.

RSMeans. (2017). RSMeans building construction cost data. The Gordian Group. Rockland, Massachusetts, USA.

RSMeans. (2018). RSMeans electrical cost data. The Gordian Group. Rockland, Massachusetts, USA; 2018.

Runkle, E. & Both, A. (2011). Greenhouse energy conservation strategies. Michigan State University – Extension Bulletin. 3160.

Sablani, S. S., Goosen, M. F. A., Paton, C., Shayya, W. H., & Al-Hinai, H. (2003). Simulation of fresh water production using a humidification-dehumidification seawater greenhouse. Desalination, 159(3), 283-288.

Sanford, S. (2011). Reducing greenhouse energy consumption—An overview. Energy, 3907(01).

Sapounas, A. A., Bartzanas, T., Nikita-Martzopoulou, C., & Kittas, C. (2008). Aspects of CFD modelling of a fan and pad evaporative cooling system in greenhouses. International Journal of Ventilation, 6(4), 379-388.

Schröder, P., & Hanrahan, P. (1993, September). On the form factor between two polygons. In Proceedings of the 20th annual conference on Computer graphics and interactive techniques (pp. 163-164). ACM.

Seginer, I. (1997). Alternative design formulae for the ventilation rate of greenhouses. Journal of Agricultural Engineering Research, 68(4), 355-365.

Sethi, V. P. (2009). On the selection of shape and orientation of a greenhouse: Thermal modeling and experimental validation. Solar Energy, 83(1), 21-38.

Sharpe, T., & Proven, G. (2010). Crossflex: Concept and early development of a true building integrated wind turbine. Energy and Buildings, 42(12), 2365-2375.

Shutterstock. (2018). https://www.shutterstock.com

Sinclair, R. (2006). An analysis of resource recovery opportunities in Canada and the projection of greenhouse gas emissions implications, National Resources Canada.

SketchUp. (2015). http://www.sketchup.com/

Skoplaki, E., & Palyvos, J. A. (2009). On the temperature dependence of photovoltaic module electrical performance: A review of efficiency/power correlations. Solar energy, 83(5), 614-624.

Solutia. (2010). Saflex® PA41 solar PVB encapsulant product datasheet. Solutia Inc., https://www.saflex.com/pdf/2009%20Product%20Bulletin%20PA41.pdf

Sonneveld, P. J., Swinkels, G. L. A. M., Campen, J., Van Tuijl, B. A. J., Janssen, H. J. J., & Bot, G. P. A. (2010). Performance results of a solar greenhouse combining electrical and thermal energy production. Biosystems engineering, 106(1), 48-57.

Sonneveld, P. J., Swinkels, G. L. A. M., Van Tuijl, B. A. J., Janssen, H. J. J., Campen, J., & Bot, G. P. A. (2011). Performance of a concentrated photovoltaic energy system with static linear Fresnel lenses. Solar Energy, 85(3), 432-442.

Speedling. (2018). Raft hydroponic tray Model TR338DA. Speedling, http://www.speedling.com/eps-and-hort/trays/

Speetjens, S. L., Hemming, S., Wang, D., & Tsay, J. (2012). Design of a vegetable greenhouse system for subtropical conditions in Taiwan (No. 1189). Wageningen UR Greenhouse Horticulture.

Stanghellini, C., & de Jong, T. (1995). A model of humidity and its applications in a greenhouse. Agricultural and Forest Meteorology, 76(2), 129-148.

Stathopoulos, T., Alrawashdeh, H., Al-Quraan, A., Blocken, B., Dilimulati, A., Paraschivoiu, M., & Pilay, P. (2018). Urban wind energy: Some views on potential and challenges. Journal of Wind Engineering and Industrial Aerodynamics, 179, 146-157.

Statistics Canada. (2007). Waste management industry survey: Business and government sectors 2004, Catalogue no. 16F0023X, Ottawa.

Statistics Canada. (2010). Greenhouse, sod and nursery industries. 22-202-X.

Statistics Canada. (2017). Average hourly wages of employees by selected characteristics and occupation, unadjusted data, by province (monthly for Ontario). Statistics Canada, http://www.statcan.gc.ca/tables-tableaux/sum-som/l01/cst01/labr69k-eng.htm

Statistics Canada. (2018). Total greenhouse area in use and mushrooms, historical data. https://www150.statcan.gc.ca/t1/tbl1/en/cv.action?pid=3210015901

Stephenson, D. G., & Mitalas, G. P. (1971). Calculation of heat conduction transfer functions for multi-layers slabs. Air Cond. Engrs. Trans;(United States), 77.

Sturm, B., Maier, M., Royapoor, M., & Joyce, S. (2014). Dependency of production planning on availability of thermal energy in commercial greenhouses–A case study in Germany. Applied Thermal Engineering, 71(1), 239-247.

Sultan, M., El-Sharkawy, I. I., Miyazaki, T., Saha, B. B., & Koyama, S. (2014). Experimental study on carbon based adsorbents for greenhouse dehumidification. Evergreen, 1(2), 5-11.

Sun Well. (2018). Semi-transparent photovoltaic modules. Sun Well Solar. http://www.sunwellsolar.com/sws/homepage/htmlhomepage/download/SunWellSolar_Semi_DM.pdf

Sun Works. (2007). Building integrated agriculture: Opportunities for urban CEA. Innovations in Agriculture Conference. New York Sun Works. Syracuse, NY, USA.

Svensson. (2011). Climate and screen management. AB Ludvig Svensson, Netherlands, <http://www.ludvigsvensson.com/storage/ma/cb93c101d682438aaf50d8bd2a079704/edd5182a086f4f3994d24a018eec4eb7/pdf/3/Climate%20and%20screen%20management_Turkey_Tomatoes_English.pdf

Tantau, H. J., Meyer, J., Schmidt U., & Bessler B. (2011). Low energy greenhouse - a system approach. Acta Horticulturae. 893:75-84.

Tchamitchian, M., Martin-Clouaire, R., Lagier, J., Jeannequin, B., & Mercier, S. (2006). SERRISTE: A daily set point determination software for glasshouse tomato production. Computers and Electronics in Agriculture, 50(1), 25-47.

Teitel, M., Levi, A., Zhao, Y., Barak, M., Bar-lev, E., & Shmuel, D. (2008). Energy saving in agricultural buildings through fan motor control by variable frequency drives. Energy and Buildings, 40(6), 953-960.

TESS. (2012). Component libraries for the TRNSYS simulation environment. Thermal Energy System Specialists (TESS), http://www.tess-inc.com

TESS. (2017). Personnel communications with the Thermal Energy System Specialists (TESS) Technical Support Team. Wisconsin, USA.

Thomas, R. B. (1978). The use of specularly-reflecting back walls in greenhouses. Journal of Agricultural Engineering Research, 23(1), 85-97.

Tianhua, L., Ying, W., & Meng, W. (2012). To discusses the sunlight greenhouse of light-dimmer based on the electrochromic technology. Journal of Agricultural Mechanization Research, 8, 021.

Tiwari, G. N., & Gupta, A. (2002). A comparison in performance of greenhouses with various shapes: a parametric study. International journal of ambient energy, 23(3), 136-148.

Tong, G., Christopher, D. M., & Li, B. (2009). Numerical modelling of temperature variations in a Chinese solar greenhouse. Computers and electronics in agriculture, 68(1), 129-139.

TRANSSOLAR. (2005). TRNSYS 17. Volume 5. Multizone Building modeling with Type 56 and TRNBuild. Solar Energy Laboratory, University of Wisconsin-Madison, Wisconsin, USA.

TRANSSOLAR. (2018). http://www.trnsys.de/download/de/T18_flyer_Daylight_en.pdf; http://sel.me.wisc.edu/trnsys/features/trnsys18_0_updates.pdf

Ureña-Sánchez, R., Callejón-Ferre, Á. J., Pérez-Alonso, J., & Carreño-Ortega, Á. (2012). Greenhouse tomato production with electricity generation by roof-mounted flexible solar panels. Scientia Agricola, 69(4), 233-239.

Ushio. (2018). https://www.ushio.com/files/specifications/hilux-gro-grow-lamps.pdf

Usmani, J. A., Tiwari, G. N. & Chandra, A. (1995). Performance characteristic of a greenhouse integrated biogas system. Energy conservation and management. Center for energy studies, Indian Institute of Technology, Delhi India.

Vadiee, A. (2011). Energy Analysis of the Closed Greenhouse Concept. (Doctoral dissertation, KTH School of Industrial Engineering and Management).

Van den Bulck, N., Coomans, M., Wittemans, L., Hanssens, J., & Steppe, K. (2013). Monitoring and energetic performance analysis of an innovative ventilation concept in a Belgian greenhouse. Energy and Buildings, 57, 51-57.

Vanthoor, B. H. E. (2011). A model-based greenhouse design method. (Doctoral dissertation, Wageningen University).

Vanthoor, B. H., Gazquez, J. C., Magan, J. J., Ruijs, M. N., Baeza, E., Stanghellini, C., ... & de Visser, P. H. (2012a). A methodology for model-based greenhouse design: Part 4, economic evaluation of different greenhouse designs: A Spanish case. biosystems engineering, 111(4), 336-349.

Vanthoor, B. H., Stigter, J. D., van Henten, E. J., Stanghellini, C., de Visser, P. H., & Hemming, S. (2012b). A methodology for model-based greenhouse design: Part 5, greenhouse design optimisation for southern-Spanish and Dutch conditions. Biosystems engineering, 111(4), 350-368.

Viessmann. (2017). Viessmann Manufacturing Company. Gas-fired condensing boiler product datasheets, https://www.viessmann.ca/content/dam/vi-brands/CA/pdfs/commercial/vitocrossal_200-cm2_sm_gw6b_tdm.pdf/_jcr_content/renditions/original.media_file.inline.file/vitocrossal_200-cm2_sm_gw6b_tdm.pdf; https://www.viessmann.ca/content/dam/vi-brands/CA/pdfs/commercial/vitocrossal_200-cm2_lg_gw6b_tdm.pdf/_jcr_content/renditions/original.media_file.inline.file/vitocrossal_200-cm2_lg_gw6b_tdm.pdf

Von Elsner, B., Briassoulis, D., Waaijenberg, D., Mistriotis, A., Von Zabeltitz, C., Gratraud, J., ... & Suay-Cortes, R. (2000). Review of structural and functional characteristics of greenhouses in European Union countries, part II: typical designs. Journal of agricultural engineering research, 75(2), 111-126.

Wall, M. (1995). A design tool for glazed spaces. Part 1: Description (No. CONF-950624-). American Society of Heating, Refrigerating and Air-Conditioning Engineers, Inc., Atlanta, GA (United States).

Westbooke. (2018). http://westbrooksystems.com/

Westbrook. (2017). Personnel communications with Les Van Egmond, Ontario, Canada

Wuhu. (2017). Low iron glass patterned tempered solar panel photovoltaic glass. Wuhu Yaohua Glass Gardening Co. Ltd., http://yh-glass.en.made-in-china.com/product/wNVQBbsOPthX/China-3-2-4mm-Low-Iron-Glass-Patterned-Tempered-Solar-Panel-Photovoltaic-Glass.html

Yang, S. H., & Rhee, J. Y. (2013). Utilization and performance evaluation of a surplus air heat pump system for greenhouse cooling and heating. Applied Energy, 105, 244-251.

Yang, S. H., Lee, C. G., Lee, W. K., Ashtiani, A. A., Kim, J. Y., Lee, S. D., & Rhee, J. Y. (2012). Heating and cooling system for utilization of surplus air thermal energy in greenhouse and its control logic. Journal of Biosystems Engineering, 37(1), 19-27.

Yano, A., Furue, A., Kadowaki, M., Tanaka, T., Hiraki, E., Miyamoto, M., ... & Noda, S. (2009). Electrical energy generated by photovoltaic modules mounted inside the roof of a north–south oriented greenhouse. Biosystems engineering, 103(2), 228-238.

Yano, A., Kadowaki, M., Furue, A., Tamaki, N., Tanaka, T., Hiraki, E., ... & Noda, S. (2010). Shading and electrical features of a photovoltaic array mounted inside the roof of an east–west oriented greenhouse. Biosystems engineering, 106(4), 367-377.

YEC. (2011). Rate Schedules, Yukon Electrical Company (YEC) and Yukon Energy, http://www.atcoelectricyukon.com/Rates-and-Regulations/Documents/YECL%20YEC%20Rate%20Schedules%20Aug%201%202017%20FINAL.pdf

YER. (2016). Summary of Yukon electrical rates (YER), www.housing.yk.ca/pdf/ElectricalRates.pdf

YRFP. (2018). Yukon retail fuel prices (YRFP), http://www.energy.gov.yk.ca/fuel.html

Yucel, K. T., Basyigit, C., & Ozel, C. (2003, June). Thermal insulation properties of expanded polystyrene as construction and insulating materials. In 15th Symposium in Thermophysical Properties (pp. 54-66).

Zhang, Y., Mahrer, Y., & Margolin, M. (1997). Predicting the microclimate inside a greenhouse: an application of a one-dimensional numerical model in an unheated greenhouse. Agricultural and forest meteorology, 86(3-4), 291-297.

Zhu, X. G., Long, S. P., & Ort, D. R. (2008). What is the maximum efficiency with which photosynthesis can convert solar energy into biomass?. Current opinion in biotechnology, 19(2), 153-159.

Zolnier, S., Lyra, G. B., & Gates, R. S. (2004). Evapotranspiration estimates for greenhouse lettuce using an intermittent nutrient film technique. Transactions of the ASAE, 47(1), 271.

Zwart systems. (2018). http://www.zwartsystems.ca/systems/humidification

ZWE. (2013). Zero Waste Energy (ZWE) LLC, Project case studies, Lafayette, California.

APPENDIX A: Values of Greenhouse Design Parameters

Table A.1: Parameter values of different materials/components used in the greenhouse model.

Material/component	Parameter	Symbol	Value	Reference
Window frame	Frame fraction	F_{fr}	10%	Assumed
	Solar reflectance	ρ_{fr}	0.6	Assumed
Thermal shading screen (60% shade)	Solar transmittance	τ_{TSS}	0.31	Cohen and Fuchs (1999)
	Solar reflectance (both sides)	ρ_{TSS}	0.48	
	Emissivity	ε_{TSS}	0.03	
	Fraction of absorbed SWR that is convected to airnode	F_{conv_TSS}	50%	Assumed
	Additional thermal resistance	R_{TSS}	0.161 m^2 C W^{-1}	Calculated from Athienitis (1998)
	Irradiance above which TSS closes	I_{TSS}	700 W m^{-2}	Svensson (2011)
	Outside air temperature below which TSS closes	T_{TSS}	20°C	
Crop canopy	Target DLI	DLI	17 mol m^{-2} day^{-1}	Albright (2000)
	Maximum total photoperiod	PP_{max}	24 hr day^{-1}	Albright (2005)
	PAR absorptance	α_{c_PAR}	0.9	Nelson and Bugbee (2015)
	NIR absorptance	α_{c_NIR}	0.3	
	Emissivity	ε_c	0.95	
	Fraction of incident SWR converted to latent heat flux	F_{ET}	40%	Zolnier et al. (2004)
	Evapotranspiration constant	ET_{cst}	20 W m^{-2}	
	Solar reflectance	ρ_c	0.4	Calculated Eq. (3.10)
Concrete floor	Thickness	l_{con}	0.1 m	Assumed
	Specific heat	c_{p_con}	1 kJ kg^{-1} °C^{-1}	TRANSSOLAR (2005)
	Density	ρ_{con}	1400 kg m^{-3}	
	Thermal conductivity	k_{con}	1.13 W m^{-1} °C^{-1}	
	Emissivity	ε_{con}	0.9	
	Solar reflectance	ρ_{con}	0.5	Marceau and VanGeem (2008)
EPS ground insulation (Chapter 4 and 5)	Thickness	l_{ins_gnd}	25 mm	Assumed
	Thermal conductivity	k_{ins}	0.036 W m^{-1} °C^{-1}	Yucel et al. (2003)
EPS ground insulation (Chapter 6)	Thickness	l_{ins}	50 mm	Assumed
	Thermal conductivity	k_{ins}	0.036 W m^{-1} °C^{-1}	Yucel et al. (2003)
	Specific heat	c_{p_ins}	1.5 kJ kg^{-1} °C^{-1}	
	Density	ρ_{ins}	20 kg m^{-3}	
	Depth of vertical perimeter insulation	D_{per_ins}	0.61 m	Assumed
Foil-faced EPS insulation	Thickness	l_{ins}	75 mm	Assumed
	Thermal conductivity	k_{ins}	0.036 W m^{-1} °C^{-1}	Yucel et al. (2003)

(permanent and movable used in Chapter 5)	Emissivity	ε_{ins}	0.03	Henninger (1984)
	Solar reflectance	ρ_{ins}	0.8	
Exterior ground cover	Solar reflectance	ρ_{gnd}	0.5	Handbook (2009)
	Emissivity	ε_{gnd}	0.9	
Artificial lights (high intensity LED)	Electric power rating	E_{AL_r}	565 W	Illumitex (2016)
	Fixture PPF	PPF_{AL}	1000 µmol s^{-1}	
	Fixture PE	PE_{AL}	1.77 µmol J^{-1}	Calculated from Eq. (3.15)
	Electrical efficiency	η_{AL}	40%	Pinho et al. (2012)
	Maximum AL photoperiod	PP_{AL}	12 hr day^{-1}	Assumed
	PPFD on crop surface	$PPFD_{AL}$	394 µmol m^{-2} s^{-1}	Calculated Eq. (3.13)
	Lifespan	P_{AL}	50,000 hr	Illumitex (2016)
Solar radiation	PAR fraction	F_{PAR}	0.5	Escobedo et al. (2011)
	NIR fraction	F_{NIR}	0.5	
	Photon efficiency (PAR)	PE_{sol}	4.6 µmol J^{-1}	Calculated from Eq. (3.12)
	Irradiance at STC	I_{STC}	1000 W m^{-2}	IEC (2011)
Heating	Setpoint temperature	T_{sp}	20°C	Albright (2005)
	Energy value of natural gas	EV_{gas}	37 MJ m^{-3}	NEB (2017)
	Boiler efficiency	η_{boil}	95%	Viessmann (2017)
Ventilation	Minimum ventilation rate	ACH_{min}	1 hr^{-1}	Climax Conseils (2014)
	Maximum ventilation rate	ACH_{max}	60 hr^{-1}	Jackson and Darby (2000)
Air	Specific heat	c_{p_a}	1.012 kJ kg^{-1} $°C^{-1}$	TRANSSOLAR (2005)
	Density	ρ_a	1.204 kg m^{-3}	
Water	Latent heat of vaporization	h_{v_W}	2454 kJ kg^{-1}	
GHG emissions	Electricity emission factor	EF_{elec}	0.05 kg eCO_2 kWh^{-1}	ECCC (2016)
	Natural gas emission factor	EF_{gas}	1.89 kg eCO_2 m^{-3}	
STPV	Thermal conductance	C_{STPV}	109 W m^{-2} $°C^{-1}$	Calculated from STPV thickness and thermal conductivity (Table 4.1)
	Emissivity	ε_{STPV}	0.9	Assumed
	Temperature coefficient	β_{pv}	0.41% $°C^{-1}$	Canadian Solar (2016)
	Wiring losses	L_w	2%	Dobos (2014)
	Inverter efficiency	η_{inv}	96%	
	PV cell temperature at STC	T_{STC}	25°C	IEC (2011)
Soil layer beneath concrete slab (Chapter 4 and 5)	Thickness	l_{soil}	0.7 m	Assumed
	Specific heat	c_{p_soil}	0.84 kJ kg^{-1} $°C^{-1}$	TRANSSOLAR (2005)
	Density	ρ_{soil}	3200 kg m^{-3}	
	Thermal conductivity	k_{soil}	2.42 W m^{-1} $°C^{-1}$	

Soil (Chapter 6)	Depth of arable soil layer	D_{soil_ar}	0.7 m	Assumed
	Depth of ground zone and far-field distanced	D_{soil}	10 m	Assumed
	Smallest control volume size	CV_{min}	0.1 m	Assumed
	Specific heat	c_{p_soil}	0.84 kJ kg^{-1} $°C^{-1}$	TRANSSOLAR (2005)
	Density	ρ_{soil}	3200 kg m^{-3}	
	Thermal conductivity	k_{soil}	2.42 W m^{-1} $°C^{-1}$	
	Emissivity	ε_{soil}	0.9	Cengal (2007)
	Solar reflectance	ρ_{soil}	0.75	Reagan and Acklam (1979)
	Deep earth temperature	T_{de_soil}	5.9°C	RETScreen (2013)
	Amplitude of surface temperature	Amp	15.3°C	
	Time shift	ts	32 d	Klein et al. (2014)
Air coupling (Chapter 6)	Air mass flow rate between airnodes	m_{cpl}	100,000 kg hr^{-1}	Assumed
Constants	Stefan-Boltzmann constant	σ	5.67 10^{-8} W m^{-2} K^{-4}	
	Avogadro's constant	N	6.022 10^{23} photons $mole^{-1}$	
	Planck's constant	h_p	6.63 10^{-34} J s	
	Speed of light	c	3 10^{8} m s^{-1}	
	Timestep	Δt	0.25 hr	Assumed

APPENDIX B: Values of Greenhouse LCCA Parameters

Table B.1: Values of the cost data used in the LCCA.

Parameter	Symbol	Value	Reference
Base date	B	2017	
Study period	n	25 yr	Assumed
Nominal discount rate	D	2.8%	Average value from BOC (2017) between 1996 and 2016
Inflation rate	I	2%	Target rate set by BOC (2016)
Real discount rate	d	0.8%	Calculated from Eq. (3.35)
Installed cost of greenhouse structure per unit area	C_{stru_tot}	346.82 \$ m^{-2}	RSMeans (2016, 2017); Westbrook (2017)
Installed cost of HVAC system per unit area	C_{HVAC_tot}	61.74 \$ m^{-2}	Laate (2013)
Installed cost of AL system per unit area	C_{AL_tot}	360.29 \$ m^{-2}	Illumitex (2018); RSMeans (2018)
Average electricity price	C_{el}	0.12 \$ kWh^{-1}	Average electricity price (includes consumption and power demand) and average cost escalation rate from Ontario Hydro. (2017) between 2006 and 2016.
Electricity cost escalation rate	e_{el}	7.3%	
Natural gas price	C_{gas}	0.23 \$ m^{-3}	Enbridge (2017)
Natural gas cost escalation rate	e_{gas}	5.9%	The cost escalation rate was obtained from Deloitte (2017) between 2017 and 2024
Artificial light fixture price per Watt	C_{AL}	1.61 \$ W^{-1}	Illumitex (2018)
Forecasted future (end of study period) artificial light fixture price per Watt	C_{AL_FF}	0.28 \$ W^{-1}	Assumed
Fixture cost escalation rate	e_{AL}	-6.8%	Calculated from Eq. (4.44)
Maximum fixture lifespan	P_{AL_max}	15 yr	Assumed
Hourly wage for electrician	HW	25 \$ hr^{-1}	Statistics Canada (2017)
Labor time per fixture replaced	p	0.3 hr	Assumed
Lifespan of glass, ground/permanent /movable insulation and STPV	P_{glass}; P_{ins}; P_{STPV}	25 yr	Assumed
Lifespan of polycarbonate	P_{poly}	15 yr	Polygal (2018)
Lifespan condensing boiler	P_{boil}	15 yr	Assumed
Cost of glass	C_{glass_mat}	35 \$ m^{-2}	Harnois (2017)
Cost of polycarbonate	C_{poly_mat}	45 \$ m^{-2}	Plas-Tech (2016)
Labor cost for polycarbonate replacement	$C_{poly\_lab\_repl}$	83 \$ m^{-2}	The labor cost to replace polycarbonate is assumed to be 50% more than the installation cost provided by Plas-Tech (2016)
EPS insulation cost (Chapter 5)	C_{ins_mat}	9.76 \$ m^{-2} (75mm)	RSMeans (2017)
EPS insulation cost (Chapter 6)	C_{ins_mat}	6.51 \$ m^{-2} (50mm)	

EPS insulation installation cost	C_{ins_inst}	5.76 \$ m^{-2} (50 and 75mm)	
Movable EPS insulation annual installed plus removal cost	C_{mov_lab}	11.52 \$ m^{-2}	Adding and removing movable insulation assumed to be double EPS installation cost
TSS cost	C_{TSS_mat}	14.1 \$ m^{-2}	Westbook (2017)
TSS installation cost	C_{TSS_inst}	14.5 \$ m^{-2}	
Condensing boiler cost	C_{boil_mat}	102.1-125.1 \$ kW^{-1}	For a thermal output range of 188-501 kW (Viessmann, 2017; DisTech, 2018)
Condensing boiler installation cost	C_{boil_inst}	204.2-250.3 \$ kW^{-1}	Taken as twice the equipment cost (DisTech, 2018)
Condensing boiler replacement cost	$C_{boil\_lab\_repl}$	306.3-375.4 \$ kW^{-1}	Taken as 50% more than the installation cost
Incremental initial investment for STPV glazing	ΔC_{pv_mat}	0.85 \$ W^{-1}	Fu et al. (2017)
Incremental installation price per Watt for STPV glazing	ΔC_{pv_inst}	0.15 \$ W^{-1}	
Inverter lifespan	P_{inv}	15 yr	Assumed
Inverter price per Watt	C_{inv_mat}	0.18 \$ W^{-1}	Fu et al. (2017)
Inverter installation price per Watt	C_{inv_inst}	0.05 \$ W^{-1}	
Initial investment cost of greenhouse	*Inv* (Chapter 4 and 5)	\$ 714,300	Calculated from Eq. (4.53)
	Inv (Chapter 6)	\$ 712,700 (concrete floor)	Calculated in Chapter 4 but without ground insulation
		\$ 655,200 (soil floor)	Calculated in Chapter 4 but without ground insulation and concrete slab
		\$ 666,700 (raft hydroponic)	Calculated in Chapter 4 but without ground insulation and concrete slab only on floor zones

APPENDIX C: Comparison of Two Modeling Approaches for STPV Cladding and Experimental Calibration[4]

C.1 Comparison of Two Modeling Approaches for Semi-Transparent Photovoltaic Glazing

STPV cladding can be modeled for energy simulation purposes by creating custom window and/or walls assemblies. Crystalline silicon STPV modules consists of a frame, clear-glazed and PV cell portions whereas thin-film and organic STPV modules have a frame and a semi-transparent glazed portion. Fig. C.1 illustrates the two methods, termed the "separate" and "effective" STPV models, that can be used for modeling STPV glazing, in this case using TRNSYS 17.2 simulation software (Klein et al., 2014). The separate STPV model considers distinct treatment of the PV cell area, clear-glazed area, and frame. The PV cell area is modeled as an exterior wall that surrounds a window comprised of a clear glazing and frame (Fig. C.1a). The effective STPV model considers the combination of PV cell and clear-glazed portions into an effective layer. The optical properties of the effective STPV layer are calculated using an area-weighted approach based on the clear-glazed portion and opaque portion covered by PV cells (Fig. C.1b).

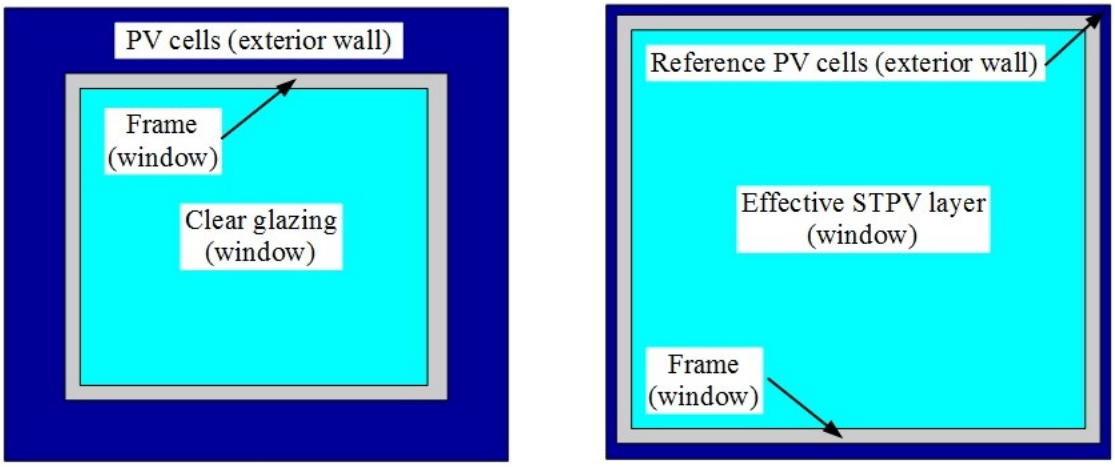

Figure C.1: (a) Schematic showing the defined surfaces for the separate STPV mode; (b) The effective STPV model.

[4] This Appendix contains a part of the paper that was submitted and presented at the eSim Conference held in Hamilton, Canada – 3-6th May, 2016 (Bambara and Athienitis, 2016).

Fig. C.2 depicts how the custom window created for the STPV glazing combines the PV cell and clear-glazed portions into an effective glazing.

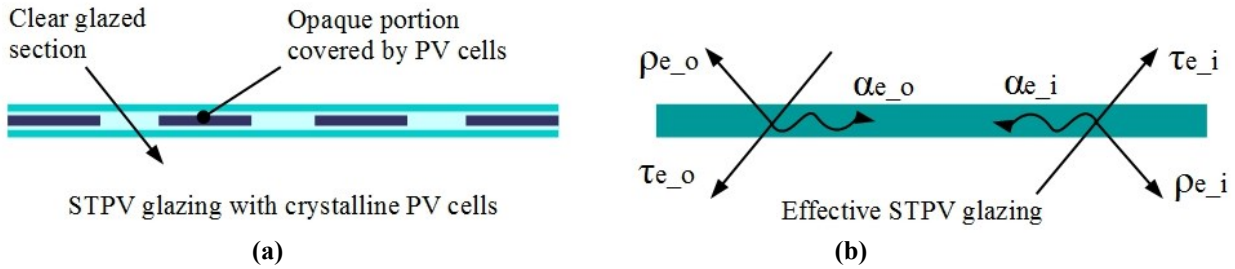

Figure C.2: (a) Schematic of the multilayer STPV glazing; and (b) the effective STPV glazing.

It is recommended to use the effective STPV model for all types of STPV cladding (crystalline-silicon, thin-film, and organic) because it has the following advantages over its separate counterpart:

- **Modifying the PV area ratio:** The PV area ratio (or transparency) can be easily modified using the effective STPV model. Custom windows representing STPV modules of various PV area ratios (and possibly multi-glazed STPV) can be created in Window 7.3 (DOE, 2015) at the beginning of a project. It is then easy to change the STPV design for various surfaces in the building model (including the option of selecting a clear glazed window instead of STPV). For the separate STPV model, the geometry must be modified in SketchUp (2015) to increase or decrease the portion of the wall covered by PV cells, and then re-imported into TRNBuild, which is a tedious process.
- **Inter-reflections:** Inter-reflections of shortwave radiation caused by the closing of a blind are accounted for by the effective STPV model. This is particularly important in greenhouse applications where interior blinds are commonly used. In addition, the effective STPV model allows a blind to be closed over the entire window area (comprised of PV cells, glazing and frame). For the separate STPV model, the blind can only be applied to the glazed surface (which excludes the PV cells), and reflection/absorption of shortwave radiation on the PV cells cannot be considered.
- **Bifacial PV cells:** A detailed modeling of bifacial PV cells that considers the inter-reflections of the blinds is possible using the effective STPV model. The closing of the blind causes much of the sunlight to be reflected on the interior side of the bifacial solar

cell, resulting in increased electric power output compared to when the blind is not in use. The separate STPV model can be employed to model single-glazed bifacial PV cells that do not use a blind.

- **Convection and longwave radiation heat transfer:** Detailed modeling of the convection and longwave radiation heat transfer is possible when a thermal screen is applied. The effective STPV model enables a thermal screen (modeled as a blind which closes at night) to be drawn across the entire window area (comprised of PV cells, glazing and frame). This allows for the consideration of the detailed modeling of convection, and most importantly, longwave radiation (Type 56 multi-zone building model allows for us to specify the emissivity of the blind material). The separate STPV model cannot apply the thermal screen over the PV cell wall. A possible solution for considering the additional thermal resistance of the blind is to adjust the interior CHTC, but this does not account for the emissivity of the thermal screen.

C.2 Experimental Calibration of a Semi-Transparent Photovoltaic Cladding Model

Experimental setup

The Concordia University Paul Fazio Solar Simulator - Environmental Chamber (SSEC) laboratory is an indoor research facility designed to emulate outdoor weather conditions (solar radiation, exterior air temperature, wind, etc.). It therefore provides a fully controlled and monitored environment for research, development, and testing of solar energy applications and advanced building envelopes. A 4.65 m^2 experimental greenhouse concept integrated with STPV cladding (2.37 m x 1.96 m x 2.03 m) was built (Fig. C.3). Six 58-Watt STPV modules measuring 1.18 m x 0.67 m each (45.5% PV cells, 49.2% clear glazing and 5.3% framing) are used to cover one of the walls.

During testing, the greenhouse is placed inside the environmental chamber, which is maintained at an air temperature of between 6-9°C (Fig. C.4). Then, the solar simulator lampfield is activated to transmit shortwave radiation through the environmental chamber (EC) windows and onto the STPV wall of the experimental greenhouse. The lampfield uses a set of six metal halide global lamps, with a total peak power output of 27.6 kW. The lampfield produces a dense multiline spectrum of rare earth metals similar to the air mass 1.5 spectrum defined by EN

60904-3. This provides a spectral distribution very close to natural sunlight and fulfils the specifications of relevant standards EN 12975:2006 and ISO 9806-1:1994. The lamps can also be individually moved on 2 axes and dimmed, offering the possibility to illuminate test surfaces of different sizes with variable degrees of irradiance intensity. In this experiment, an average irradiance of 1038 W m^{-2} was provided on the STPV wall with a distribution uniformity of 86%. Irradiance is measured by a pyranometer, mounted on an X-Y collector scanner with an accuracy of ± 5% of the reading. Two fans are used to mix the air within the greenhouse.

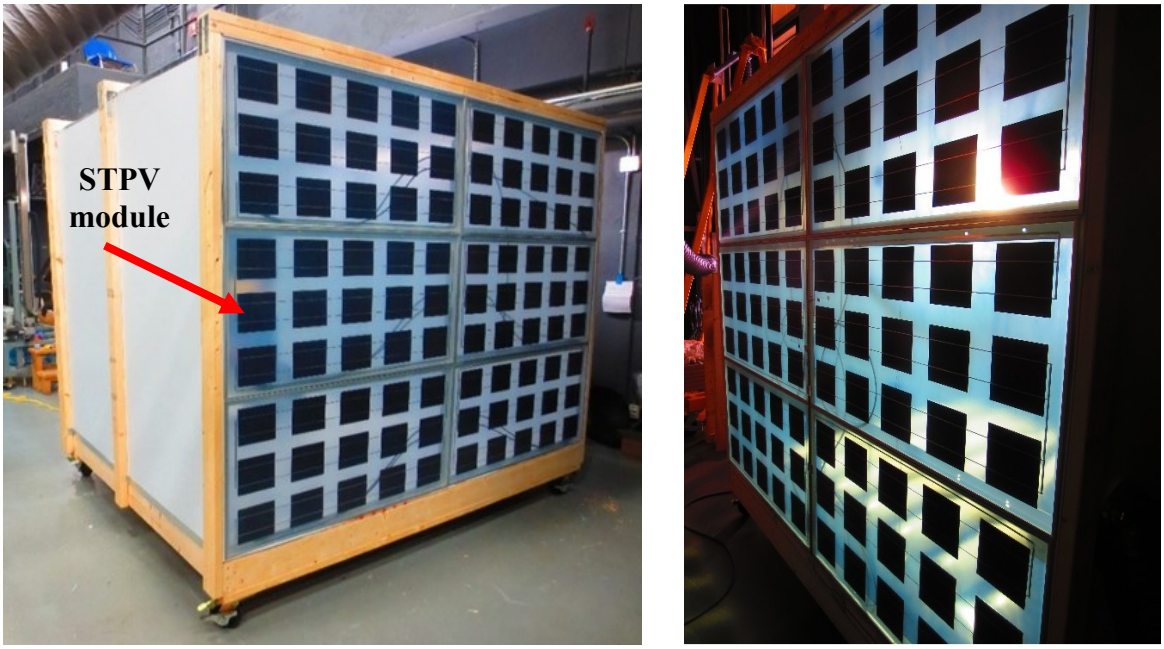

(a) (b)

Figure C.3: (a) Photo of the experimental greenhouse concept from the exterior and; (b) the interior.

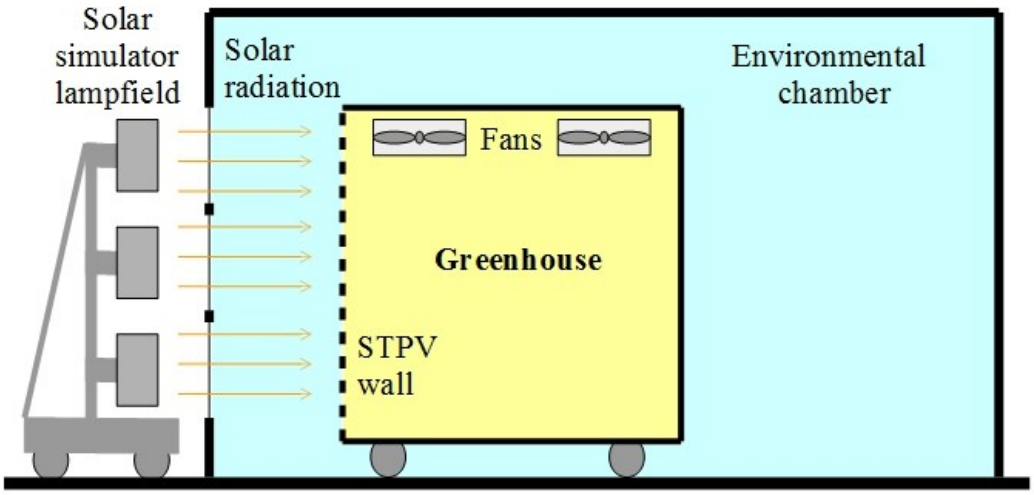

Figure C.4: Experimental setup inside the SSEC laboratory.

The STPV cladding is made of 156 mm square polycrystalline-silicon PV cells, encapsulated between 3.2 mm low-iron patterned (diffusing) clear glass on the exterior and a polyvinyl fluoride film on the interior. The framing consists of aluminum approximately 4 mm thick. The walls and roof are made of 4 mm extruded polypropylene sheets that are fastened to a 38 mm x 89 mm softwood framing located on the exterior. The floor is constructed of 38 mm x 140 mm softwood joists that are covered by 19 mm plywood, with 4 mm extruded polypropylene sheets used as the interior finish. The experiment is mounted on wheels which elevate it by approximately 150 mm above the floor level. The walls, floor, and roof are painted black with a matte finish.

The greenhouse air temperature and PV cell surface temperatures were measured using T-Type thermocouples with an accuracy of ± 0.3°C. Air temperatures were taken as the average of 15 thermocouples (five equally placed along the height, located at ¼, ½ and ¾ of the greenhouse depth from the centerline of the PV wall), and the six PV cell temperatures were measured on the interior surface of the center PV cell of each SPTV module. The average EC air temperature and interior surface temperatures were also measured for the lampfield windows, front, back, side walls, roof, and floor. The rate of direct current (DC) electric energy generated by the six STPV modules (wired in series) was determined by measuring the produced current and voltage (IV) using an IV curve tracer (DS-100C by Daystar inc.). The error in measured voltage is the larger of ± 0.5% of reading or ± 0.028 Volts. The error in measured current is the

larger of ± 0.5% of reading or ± 0.045 Amps. An electronic load (eload) device (N3300A by Agilent) was used to consume the electricity generated by the PV. The eload was configured to allow the STPV panels to operate at the maximum power point measured by the IV tracer.

The data acquisition system is made up of one CompactRIO device fabricated by National Instruments. The CompactRIO chassis uses NI 9211 thermocouple input modules to convert the analogue voltage signal from the sensor into a storable digital signal. The CompactRIO device was connected to a desktop computer running National Instruments' LabVIEW software. A program running inside LabVIEW was designed to provide a real-time graphical display and to record data on the computer's hard drive. The data was sampled every 10 seconds and recorded as one-minute averages.

The experimental testing began when the greenhouse air temperature was in equilibrium with the EC air. The mixing fans and the solar simulator lampfield were simultaneously turned on. Two hours into the experiment, the PV modules were disconnected from the eload for a period of 30 minutes so that the effect of the PV electric power output on the thermal performance could be assessed. Approximately 3 hours into the experiment, the solar simulator lampfield was turned off.

Modeling and simulation

An energy model of the experimental greenhouse was developed using TRNSYS 17.2 simulation software (Klein et al., 2014). Based on the need to calibrate an energy model using experimental measurements, a short time-step of one minute is selected for the simulations. Fig. C.5 illustrates the major energy fluxes considered in the greenhouse model.

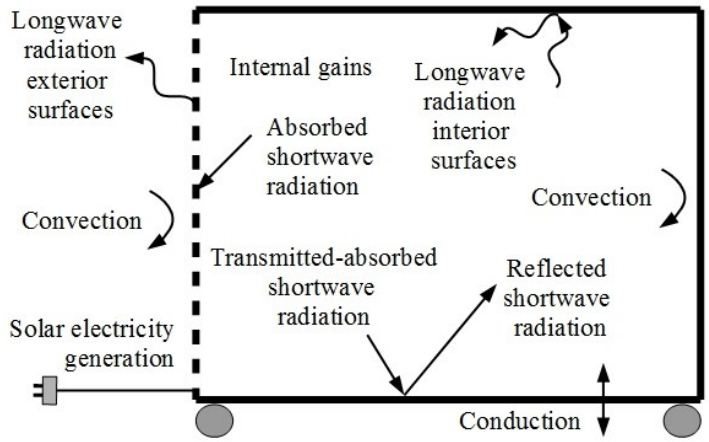

Figure C.5: Schematic showing energy fluxes considered in the greenhouse model.

The mass balance for the greenhouse airnode is not considered, because there is no ventilation and infiltration are neglected (all joints were sealed with silicone, and a door with continuous weather stripping was used). The terms used in Eq. (C.1-C.5) are defined in section 4.5.

The energy balance for the greenhouse airnode (*i*) can be written as:

$$X_{th} \cdot \rho_a \cdot c_{p\_a} \cdot V_i \cdot (\partial T_i / \partial t) = Q_{conv} + Q_{gains} \quad \text{(C.1)}$$

The energy balance for a given inside surface (*si*, walls, roof and floor) can be given by:

$$0 = Q_{cond} + Q_{conv\_si} + Q_{swr\_si} + Q_{lwr\_si} \quad \text{(C.2)}$$

The energy balance for a given outside surface (walls, roof and floor) can be defined as:

$$0 = Q_{cond} + Q_{conv\_so} + Q_{lwr\_so} \quad \text{(C.3)}$$

As described in the previous section, the STPV wall is modeled using two different approaches, termed the separate and effective STPV models, for comparison. The energy balance for the inside surface of the glazed portion (clear glazed for the separate model and effective layer for the effective model) or walls (extruded polypropylene or PV cell wall) is expressed as:

$$0 = Q_{lwr\_si} + Q_{cond} + Q_{conv\_si} \quad \text{(C.4)}$$

The energy balance for the outside surface of the glazed portion or walls is described by:

$$0 = Q_{lwr\_so} + Q_{cond} + Q_{conv\_so} - E_{pv} \quad \text{(C.5)}$$

where E_{pv} is the electricity generated by the exterior surface of either the PV cell wall used in the separate model or the effective layer used in the effective model.

Modeling key assumptions

Conduction: Type 56 multi-zone building model uses the ASHRAE transfer function method to solve the transient conduction heat transfer through opaque envelope components (TRANSSOLAR, 2005). The thermal capacitance of the window (glazing and frame), PV cell wall, and extruded polypropylene is ignored. One-dimensional steady state heat conduction is computed by Eq. (4.7). The thermal conductance of the glazing (clear glazing, PV cell wall, and effective STPV layer) and frame is estimated to be 232 W m^{-2} °C^{-1}. The thermal conductance of the extruded polypropylene was measured to be 11.3 W m^{-2} °C^{-1} using heat flow meter (436) by Netzsch. The thermal mass of the plywood that was installed on the floor is considered with thermal conductance, specific heat, and density estimated to be 7.9 W m^{-2} °C^{-1}, 1200 J kg^{-1} °C^{-1}, and 800 kg m^{-3}, respectively. The edge effects and framing are ignored in the model.

Convection: The convection heat flux between an inside surface and the air is calculated by Eq. (4.8). Similarly, the convection heat flux between an outside surface and the air is calculated by Eq. (4.11). The interior CHTC is estimated to be 10 W m^{-2} °C^{-1} for the walls (opaque and STPV), roof, and floor. The exterior CHTCs are estimated to be 8 W m^{-2} °C^{-1} for the walls and roof, and 5 W m^{-2} °C^{-1} beneath the floor.

Longwave radiation: Detailed radiation heat transfer calculations are performed by considering the radiation exchange of a given surface with all other viewing surfaces. Longwave radiation heat flux between two surfaces is given by Eq. (4.13). For longwave radiation exchange on exterior surfaces, the viewing surfaces include the average EC interior surface temperatures (for all surfaces except the STPV wall) and the area-weighted average EC interior lampfield wall and window temperature (for the STPV wall). Type 56 enables detailed radiation calculations for building geometries that are convex. Sketchup is used to create three-dimensional data of the building, then the view factor matrices (for interior surfaces) are generated in TRNBuild, and the longwave radiation heat transfer is calculated using the so-called Gebhart-factor (Gebhart, 1961, 1971). The emissivity for the interior and exterior surfaces of the extruded polypropylene and PV

cells, and the exterior surface of the floor, are assumed to be 0.9. The emissivity of the clear glazing and aluminum frame are assumed to be 0.84 and 0.77, respectively.

Shortwave radiation: The shortwave radiation produced by the solar simulator lampfield is modeled as a diffuse radiation that is incident on the STPV wall because of the patterned glass. The measured average irradiance of 1038 W m^{-2} is used in the model. For a detailed treatment of shortwave diffuse radiation including multi-reflection, the view factor matrices and so-called Gebhart-factor are used. The absorptance of shortwave radiation on the interior surface of the extruded polypropylene (black paint), clear glazing, frame, and interior surface of the PV cells is assumed to be 0.9, 0.05, 0.15, and 0.3, respectively. The absorptance-transmittance of the exterior surface of the portion of STPV that is covered by PV cells is assumed to be 0.85. The average transmittance of the clear-glazed portion was measured to be 0.77.

Internal gains: The sensible heat gains (Q_{gains} in W) considered in the model are equal to the heat produced by two air mixing fans, written as:

$$Q_{gains} = E_{fan} \tag{C.6}$$

where E_{fan} is the power of the two mixing fans, measured to be 66.7 W each using a handheld Watt-meter.

PV electric power: The electric power produced by the PV affects the surface energy balance, and therefore it is modeled as a heat loss equal to the measured rate of DC electric power output (E_m in W), given by:

$$E_m = V_m \cdot I_m \tag{C.7}$$

where

V_m is the measured voltage (V)
I_m is the measured current (A).

The error in the reported electric power (ΔE_m in W) is estimated by:

$$\Delta E_m = E_m \cdot \sqrt{(\Delta V_m/V_m)^2 + (\Delta I_m/I_m)^2} \tag{C.8}$$

where

ΔV_m is the error in measured voltage (V)

ΔI_m is the error measured current (A).

The measured electrical efficiency of the STPV string (η_m in %) is defined by:

$$\eta_m = E_m / \left(G_m \cdot A_{pv}\right) \quad \text{(C.9)}$$

where

G_m is the measured incident shortwave radiation (W m^{-2})

A_{pv} is PV cell area defined by Eq. (C.12).

The error in the reported electrical efficiency ($\Delta\eta_m$ in %) is calculated by:

$$\Delta\eta_m = \eta_m \cdot \sqrt{(\Delta E_m/E_m)^2 + (\Delta G_m/G_m)^2 + \left(\Delta L_{pv}/L_{pv}\right)^2 + \left(\Delta W_{pv}/W_{pv}\right)^2} \quad \text{(C.10)}$$

where

ΔG_m is the error measured incident shortwave radiation (W m^{-2})

ΔL_{pv} is the error in measuring the length of PV cells (m)

L_{pv} is the length of PV cells (m)

ΔW_{pv} is the error in measuring the width of PV cells (m)

L_{pv} is the width of PV cells (m).

The minimum measured value of irradiance over the STPV wall (926.5 W m^{-2}) is used for PV electric energy calculations because it dictates the current produced by the STPV modules that were wired in series.

The theoretical temperature-dependent rate of DC electric energy generated by the PV surface (E_{PV} in W) is computed as (Skoplaki and Palyvos, 2009):

$$E_{pv} = G_m \cdot A_{pv} \cdot \eta_{STC} \cdot \left(1 - \beta_{pv} \cdot \left[T_{pv} - T_{STC}\right]\right) \quad \text{(C.11)}$$

where

η_{STC} is the electrical efficiency of the PV module at STC (dimensionless)

β_{PV} is the PV module temperature coefficient (% °C^{-1})

T_{pv} is the inside surface temperature of the PV cells (°C)

T_{STC} is the PV cells temperature at STC (°C).

The effect of the wiring losses is not considered.

Custom windows: The program Window 7.3 (DOE, 2015) is used to generate thermal and optical properties for custom window assemblies, comprised here of a single glazing and frame. The separate STPV model considers a clear glazing and frame, whereas the effective STPV model considers the effective STPV layer (PV cells and clear glazing) and frame. The output data of Window 7.3 is then used to define a new window in TRNBuild. Type 56 calculates the amount of shortwave radiation that is absorbed and transmitted by the glazing (here it includes the diffuse component and its reflections). It is assumed that the shortwave radiation transmitted through the STPV wall is diffuse. Energy storage in the glazing and frame are neglected.

This effective STPV glazing is specified as a custom window in Type 56, where the glazed portion (comprised of a clear glazing and PV cell portion) is modeled as an effective layer whose optical properties depend on the PV area ratio (area-weighted approach based on the clear-glazed portion and opaque portion covered by PV cells). The effective transmittance and reflectance of the effective STPV glazing, for shortwave radiation directed from outside to inside and vice versa, are calculated from Eq. (4.25-4.29). The PV area ratio (F_{pv}) is 0.48, the transmittances of the clear glazing for the exterior and interior sides (τ_{g_so} and τ_{g_si}) are 0.77, the PV reflectance for the exterior side (ρ_{pv_so}) is 0.15 and interior side (ρ_{pv_si}) is 0.7 and, the clear glazing reflectance for the exterior and interior sides (ρ_{g_so} and ρ_{g_si}) is 0.18. Based on Eq. (4.25-4.28), the transmittance of the effective STPV layer in both directions is 0.4, and the exterior and interior reflectance are 0.1 and 0.36, respectively. The effective absorptance for each side of the glazing is given by Eq. (4.29). The exterior and interior absorptance of the effective STPV layer are 0.5 and 0.24, respectively. The obtained effective transmittance and reflectance are then used to create a custom glazing in Window 7.3. The PV electric power output can be calculated in the same way as for the separate STPV model (Eq. C.11) using a PV cell area (A_{pv} in m^2) equal to:

$$A_{pv} = F_{pv} \cdot \left(A_{STPV} - A_{fr}\right) \tag{C.12}$$

where

F_{pv} is the PV area ratio (dimensionless)
A_{STPV} is the STPV glazing area (m^2)
A_{fr} is the frame area (m^2).

A similar modeling approach can be used to consider thin-film and organic STPV cladding, using transparency instead of the PV area ratio.

Perimeter wall: Type 56 requires that at least 1% of a surface be defined as a wall (i.e. maximum 99% window). This wall surface is modeled as a PV cell (same as for the separate model) and may serve as a reference for calculating the temperature-dependent electric power output.

Results and Discussion

The DC voltage across and the current through the STPV string (six STPV modules wired in series) was measured to be 36.80 ± 0.18 Volts and 6.08 ± 0.05 Amps, respectively (measured just before disconnecting them from the eload). The electric power output is 224.4 ± 2.0 Watts (Eq. (C.7-C.8)), and the electrical efficiency of the STPV string is calculated to be 11.1 ± 0.56 % (Eq. (C.9-C.10)).

Fig. C.6 shows that the solar simulator radiation causes the average PV cell temperature to rise by 44°C and reach a steady state temperature of 50.4°C in approximately one hour. It also provides a comparison of the measured average PV cell temperature with those obtained using both STPV models. It is found that the separate STPV model is in good agreement (±1°C) with the measured results, whereas the effective STPV model underestimates the PV surface temperature by approximately 10°C. This result is expected because the effective STPV layer is semi-transparent and has a lower absorptance (0.5) than the PV cells modeled as an opaque wall (0.85). The main consideration is whether this has an impact on the greenhouse air temperature. This will be evaluated later.

Based on these measurements, the theoretical rate of electric energy generated by the STPV string is found to be 224.1 and 235.7 Watts, for the separate and effective STPV models, respectively (Eq. (C.11)), with an input of 0.125 for the PV module electrical efficiency and of

0.0046 for the temperature coefficient [35]. Thus, the "standard" STPV model provides an accurate estimation of the electric power output (0.1% lower), whereas the effective STPV models overestimate it by 5.1%. The approach that was selected to avoid overestimating electric power output when using the effective STPV model is to define the wall around the STPV window (representing 1% of total surface area) as an exterior wall comprised of PV cells. This provides the same PV cell surface temperature as the separate STPV model (confirmed from the model results and therefore not presented here) and could be used as a reference for calculating a more realistic electric power. Since the greenhouse air temperature is nearly identical for both STPV models, it is assumed that the PV cell temperature would also be the same. It should be noted that this approach is only valid for STPV modules using crystalline-silicon PV cells. For thin-film and organic STPV modules, the effective STPV model provides a valid surface temperature for estimating electric power output (i.e. separate STPV model is not applicable).

Fig. C.6 also shows that when the STPV string is disconnected from the eload, the measured average PV cell temperature increases by 4.4°C (from 50.4 to 54.8°C). This demonstrates the importance of accounting for electric power production in the PV surface (PV wall and effective STPV layer) energy balance. Moreover, the effect of not considering the thermal capacitance of the STPV surface can be observed from the sharp rise/decay in the modeled surface temperature compared to the experimental measurements.

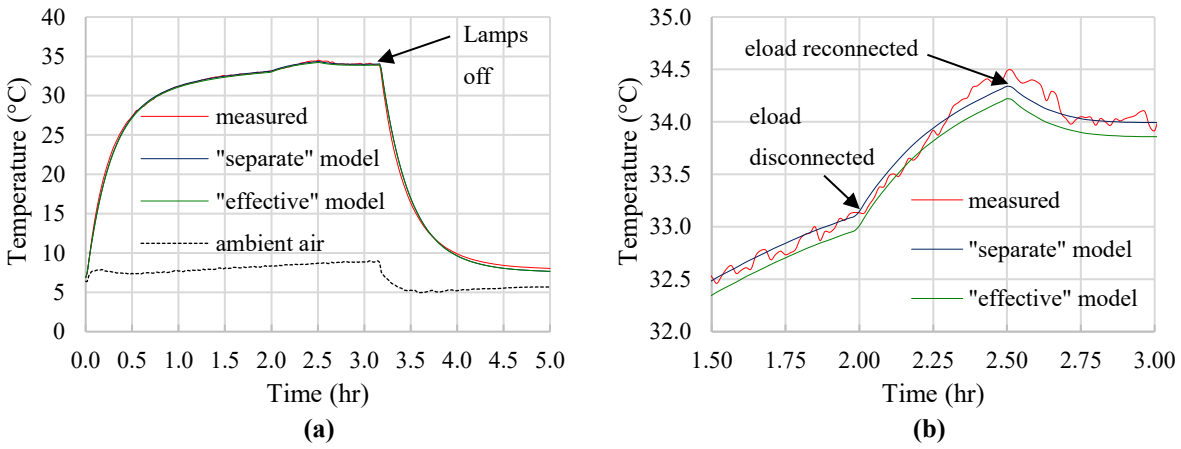

Figure C.6: (a) Comparison of measured average PV cell temperature with those obtained using both STPV models; (b) close-up of the period when the PV modules are disconnected from the eload.

Fig. C.7 shows that the solar simulator radiation causes the greenhouse air temperature to rise by 26.2°C and reach a steady state temperature of 33.1°C in approximately one hour. It also provides a comparison of the measured average greenhouse air temperature with those obtained using both STPV models. The results indicate that good agreement (±1°C) exists between the measured and modeled results when an air capacitance multiplication factor of eight is used in the model. Most importantly, no noticeable difference can be observed between the predictions obtained from the separate and effective STPV models. This suggests that, despite discrepancies in the PV surface temperature predictions, the effective STPV model accurately represents shortwave radiation transmitted by the STPV modules.

Moreover, the greenhouse air temperature increased by 1.4°C (from 33.1 to 34.5°C) when the STPV modules were disconnected from the eload. This confirms that electric power production should be accounted for in the energy balance of the PV surface (PV wall of the separate STPV model and effective STPV layer) because it also affects the predicted greenhouse air temperature.

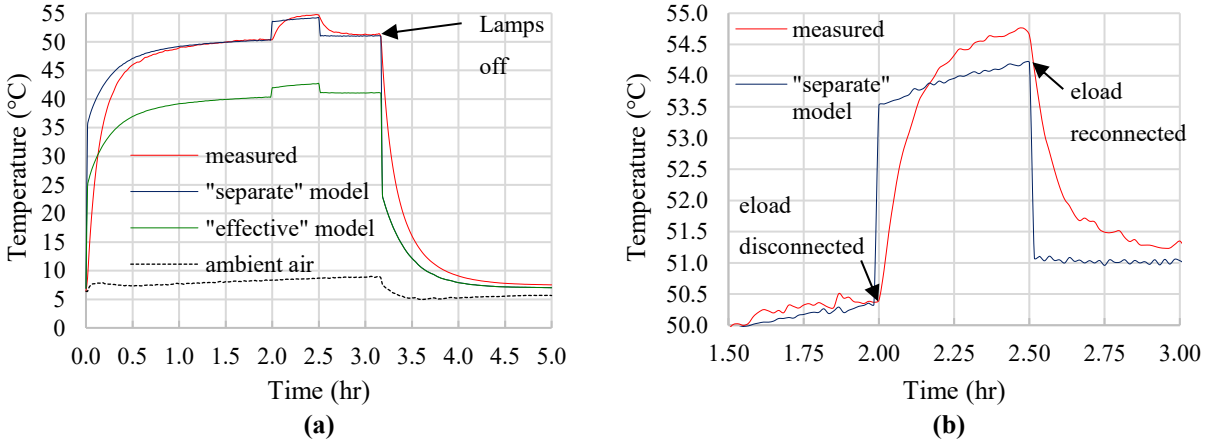

Figure C.7: (a) Comparison of measured average greenhouse air temperature with predictions using both STPV models; (b) close-up of the period when the PV modules are disconnected from the eload.

Based on these results, it is found that both STPV models can be used to accurately predict the air temperature inside a greenhouse equipped with crystalline-silicon STPV modules. However, the reference PV cell temperature should be used to accurately predict the temperature-dependent electric power output when the effective STPV model is selected.

APPENDIX D: Analysis of Bifacial PV and Effect of Time-of-use Electricity Pricing for Ottawa, Canada

D.1 Greenhouse Characteristics

The analysis for Ottawa was repeated using bifacial PV cells and time-of-use (TOU) electricity pricing.

D.2 Energy Analysis

The methodology for the daylighting, artificial lighting control and thermal modules is the same as described in section 4.5, except for those presented below.

Modeling key assumptions

Electricity pricing: In this study, two scenarios are considered for the lighting control. The first employs constant electricity price whereby the supplemental lighting is activated after sunset. The second scenario considers TOU electricity pricing whereby it is desired to provide supplemental lighting during the off-peak period to reduce electricity costs. The TOU scheme is also advantageous for increasing revenues from solar electricity generation, which is produced and sold back to the grid at mid-peak and on-peak rates. This scenario divides each weekday into three electricity prices (off-peak, mid-peak, on-peak) which change for the summer and winter periods. Weekends use the off-peak rate. As shown in Table D.1, the off-peak period is from 7pm-7am, and this is when artificial lighting is supplied, as needed.

Table D.1: Schedule of TOU electricity pricing (Ontario Hydro, 2017).

Season	Off-peak	Mid-peak	On-peak
Summer (May 1st - October 31st)	7pm-7am and weekends	7am-11am; 5pm-7pm	11am-5pm
Winter (November 1st - April 31st)		11am-5pm	7am-11am; 5pm-7pm

Windows: The area-weighted effective solar optical properties are the same for the inside and outside of the bifacial STPV glazing.

Solar electricity generation: The electricity generated by the PV affects the energy balance of the STPV surface and is modeled as a heat loss. The rate of electricity generation from the inside surface of the STPV roof is estimated using (Skoplaki and Palyvos, 2009):

$$E_{pv\_si} = I_{pv\_si} \cdot F_{pv} \cdot \left(A - F_{fr} \cdot A\right) \cdot \eta_{STC} \cdot \left(1 - \beta_{pv} \cdot \left[T_{pv\_so} - T_{STC}\right]\right) \cdot (1 - L_w) \cdot \eta_{inv} \qquad \text{(D.1)}$$

The effect of solar incidence angle on electricity generation is not considered. In order to determine the solar electricity generation from the inside surface of the bifacial cells, the solar radiation that is incident on the inside surface of the STPV glazing is required. The TRNSYS simulation provides as output the solar radiation being absorbed on a surface ($Q_{swr\_pv\_si}$ in kJ hr^{-1}) and so based on this, the solar radiation incident on the inside surface of the STPV glazing (I_{pv_si} in W m^{-2}) is calculated from:

$$I_{pv\_si} = Q_{swr\_pv\_si} / \left(3.6 \cdot \alpha_{pv\_si} \cdot \left[A - F_{fr} \cdot A\right]\right) \qquad \text{(D.2)}$$

where

α_{pv_si} is the solar absorptance of the inside surface of the PV cells

the factor 3.6 serves to convert units kJ hr^{-1} to W.

Then, this is used to determine the rate of electricity generation from the interior bifacial side using Eq. (D.1). The annual electric energy generated by the STPV cladding is determined from:

$$E_{pv\_yr} = \sum_{\Delta t=0}^{365 \cdot 24/\Delta t} \left[\Delta t \cdot \left(E_{pv\_so} + E_{pv\_si}\right)/10^3\right] \qquad \text{(D.3)}$$

where the factor 10^3 serves to convert units W to kW.

Values of greenhouse design parameters

The values of the greenhouse design parameters are the same as in section 4.5, except the solar reflectance of PV cell portion for both sides is now the same to reflect bifacial PV cells ($\alpha_{pv\_si} = \alpha_{pv\_so} = 0.089$).

D.3 Economic Analysis

The methodology for the economic analysis is the same as described in section 4.6, except for those presented below.

LCCA key assumptions

The current incremental cost for the bifacial STPV glazing and the TOU electricity pricing is given in Table D.2. Bifacial PV modules are assumed to cost 50% more that their single sided counterparts.

Table D.2: Values of the cost data used in the LCCA.

Parameter		Symbol	Value	Reference
Average TOU electricity price	Off-peak	C_{el_op}	0.087 \$ kWh^{-1}	Electricity price includes consumption and power demand (Ontario Hydro, 2017)
	Medium-peak	C_{el_mp}	0.132 \$ kWh^{-1}	
	On-peak	C_{el_p}	0.18 \$ kWh^{-1}	
Incremental initial investment for bifacial STPV glazing		ΔC_{bipv_mat}	1.28 \$ W^{-1}	Assumed

D.4 Results and Discussion

Electricity consumption for artificial lighting

The simulation results for energy consumption/generation of the BCGH and PVGH are given in Table D.3 and D.4 for the present and future projection studies, respectively. As expected, the lighting electricity consumption was equivalent for the constant and TOU electricity rates because both control the DLI to the same target value. Fig. D.1 shows the lighting electricity consumption for the various STPV designs employed in the present and future projection study. Higher PV area ratios increased the lighting electricity consumption compared to the BCGH by a minimum of 26.7% for the bifacial STPV with 10% PV area ratio, and by a maximum of 128.0% for bifacial STPV with 50% PV area ratio. This increase was near linear and comparatively similar to the BCGH for both the single-sided and bifacial STPV up to PV area ratio of approximately 20%. The lighting electricity used for bifacial STPV was always higher than that of single-sided STPV because less light is reflected onto the crops from the interior side the PV cells (compare to thr highly reflective PV cell backsheet that was specified for single-sided STPV). Consequently, more artificial lighting is required to compensate for the lower amount of reflected sunlight. Above a PV area ratio of about 30%, the lighting electricity consumed for bifacial STPV increased at a higher rate than that of single-sided STPV. Moreover, it was found that improving the efficiency of the lighting fixtures (future projection study) reduced lighting electricity consumption by 44.7% in all cases.

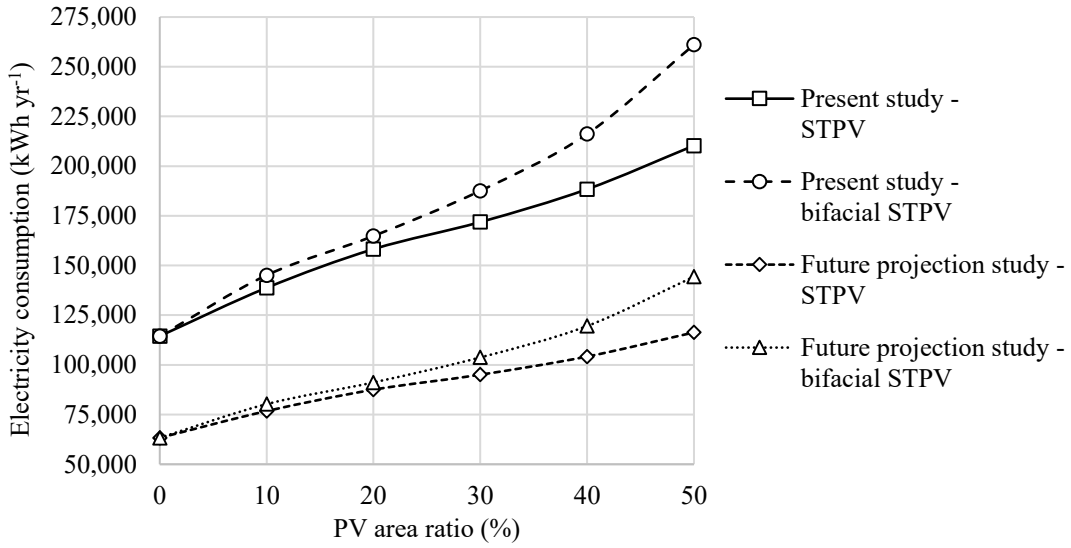

Figure D.1: Annual electricity consumption for artificial lighting.

Table D.3: Greenhouse energy consumption/generation in the present study.

Roof envelope design	Constant electricity price			TOU electricity price		
	AL electricity consumption (kWh yr^{-1})	PV electricity generation (kWh yr^{-1})	Gas consumption (m^3 yr^{-1})	AL electricity consumption (kWh yr^{-1})	PV electricity generation (kWh yr^{-1})	Gas consumption (m^3 yr^{-1})
BCGH	114,475	-	62,783	114,475	-	62,650
STPV 10%	138,766	18,354	60,328	138,766	18,354	60,212
STPV 20%	158,224	36,717	58,733	158,224	36,717	58,606
STPV 30%	171,857	55,088	57,811	171,857	55,088	57,671
STPV 40%	188,381	73,467	56,812	188,381	73,467	56,663
STPV 50%	210,318	91,850	55,260	210,318	91,850	55,096
bifacial STPV 10%	145,087	25,153	59,759	145,087	25,152	59,638
bifacial STPV 20%	164,834	46,253	58,383	164,834	46,253	58,251
bifacial STPV 30%	187,597	66,099	56,936	187,597	66,099	56,788
bifacial STPV 40%	216,143	85,377	55,296	216,143	85,376	55,132
bifacial STPV 50%	261,049	104,632	52,778	261,049	104,630	52,604

Table D.4: Greenhouse energy consumption/generation in the future projection study.

Roof envelope design	Constant electricity price			TOU electricity price		
	AL electricity consumption (kWh yr^{-1})	PV electricity generation (kWh yr^{-1})	Gas consumption (m^3 yr^{-1})	AL electricity consumption (kWh yr^{-1})	PV electricity generation (kWh yr^{-1})	Gas consumption (m^3 yr^{-1})
BCGH	63,316	-	66,372	63,316	-	66,367
STPV 10%	76,751	24,924	65,014	76,774	24,924	65,008
STPV 20%	87,513	49,863	64,007	87,513	49,863	64,000
STPV 30%	95,054	74,812	63,521	95,054	74,812	63,509
STPV 40%	104,193	99,774	62,986	104,193	99,774	62,971
STPV 50%	116,326	124,742	61,987	116,326	124,741	61,963
bifacial STPV 10%	80,247	34,259	64,659	80,247	34,259	64,653
bifacial STPV 20%	91,169	62,946	63,874	91,169	62,945	63,865
bifacial STPV 30%	103,759	89,926	63,075	103,759	89,925	63,060
bifacial STPV 40%	119,548	116,137	62,191	119,548	116,136	62,167
bifacial STPV 50%	144,385	142,327	60,679	144,385	142,326	60,641

Electricity generation from STPV cladding

Tables D.3 and D.4 confirm the expected result that electricity generation from the STPV cladding is not influenced by the constant and TOU electricity rates. Fig. D.2 illustrates how solar electricity generation increased linearly with the PV area ratio. The PV cladding on the roof generated a minimum of 27.1 kWh m^{-2} yr^{-1} (present study with bifacial STPV of 10% PV area ratio) and a maximum of 153.2 kWh m^{-2} yr^{-1} (future projection study with bifacial STPV of 50% PV area ratio) of renewable electricity. It was found that improving the PV electrical efficiency from 17% (present study) to 23% (future projection study) increased electricity production by approximately 36% in all cases.

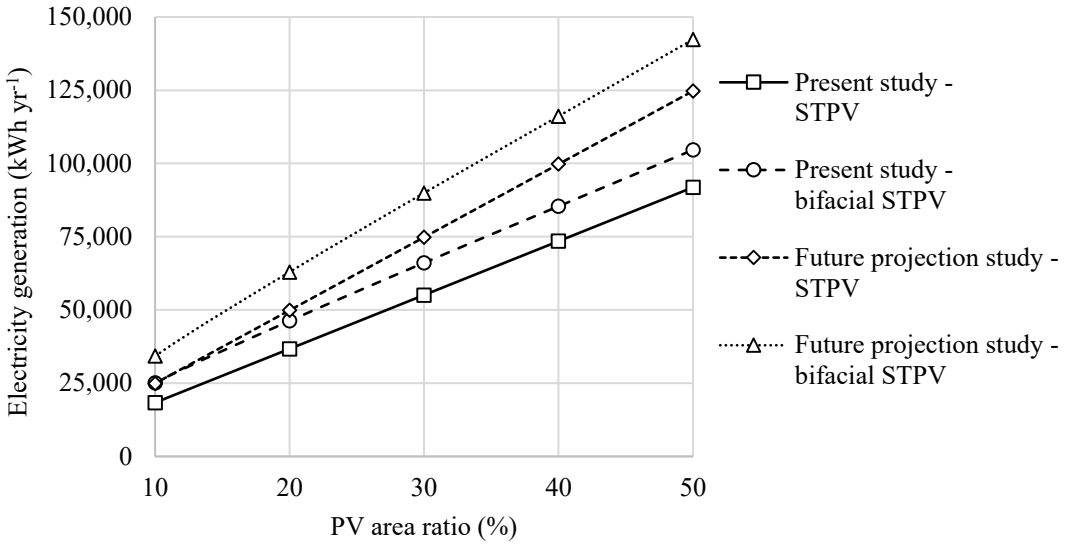

Figure D.2: Electricity generation from STPV cladding.

Fig. D.3 shows how the solar electricity generated from the bifacial interior PV cells decreased in a nearly exponentially manner as the PV area ratio increased. The bifacial PV cells increased solar electricity generation by 37.5% at a PV area ratio of 10% compared to only 14.1% at a PV area ratio of 50%. A possible explanation is that, as the PV area ratio increased, the availability of light that is reflected onto the interior STPV surface became increasingly lower. It is likely that the electricity generated by the bifacial PV cells could be increased by adopting more advanced TSS control strategies. In this study, the TSS closes when the exterior global horizontal irradiance is above a user-specified maximum value, regardless of the STPV design. Since less sunlight is transmitted at higher PV area ratios, the exterior irradiance value that causes the TSS to close could be increased with the PV area ratio. This would allow more sunlight to be transmitted and reflected by the inside surface of the STPV cladding, and thus provide a more favorable comparison to designs with lower PV area ratios.

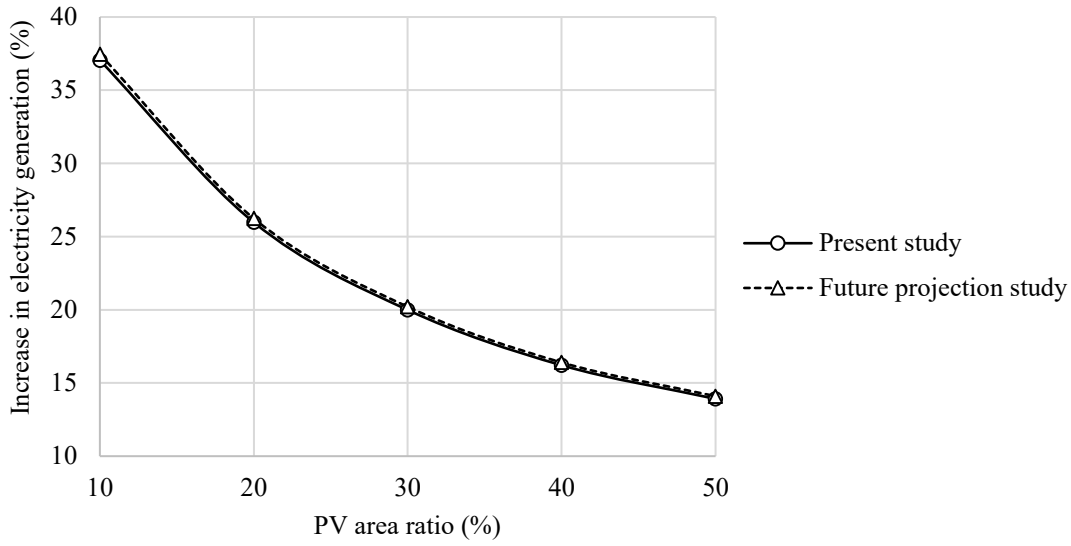

Figure D.3: Electricity production increase for bifacial STPV compare to single-sided.

Net electricity consumption/generation

Fig. D.4 shows the difference in the electricity consumption (lighting and PV electricity) between the PVGH and BCGH. The results for the present study indicated that the greenhouse with bifacial STPV did not produce enough solar electricity to compensate for the increased use of lighting electricity that is provoked by the STPV shading. In the best case, the greenhouse with 20% PV area ratio consumed 4,106 kWh yr^{-1} more than the BCGH. However, when the efficiency of artificial lighting and PV technology increased to their future projection values, the PVGH always consumed less electricity (between 17,328-61,257 kWh yr^{-1}) than the BCGH. Therefore, the energy balance is sensitive to the efficiency of PV and lighting technology. The produced solar electricity can be stored for later use (e.g. power-to-gas) or exported to the grid to contribute to the supply renewable energy and potentially help reduce peak demand.

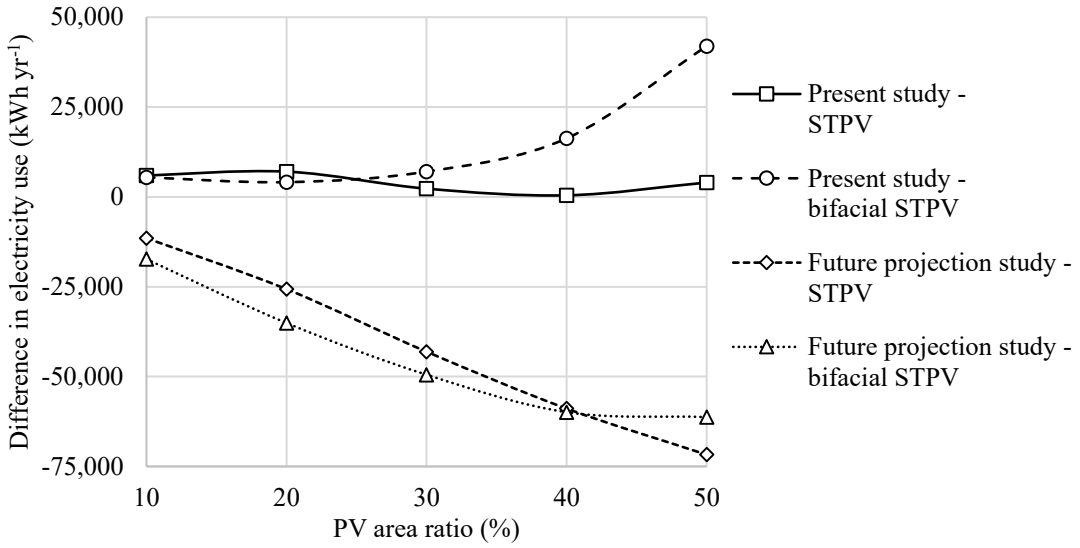

Figure D.4: Difference in electricity consumption (for lighting minus PV generation) between the PVGH and BCGH (negative indicates PVGH consumes less electricity than BCGH).

Fig. D.5 gives the fraction of consumed lighting electricity that was offset by electricity generated from the STPV roof. For the present study, the bifacial STPV roof generated between 17.3-40.1% of the electricity that was consumed for supplemental lighting, whereas 42.7-98.6% of the electricity needs could be produced in the future when horticulture lighting and PV efficiencies are higher. This fraction was higher for bifacial STPV compared to single-sided STPV until a PV area ratio of approximately 40%, above which the trend was inversed. These results demonstrate that the STPV roof has the potential to displace nearly all the greenhouse's electricity needs for supplemental lighting.

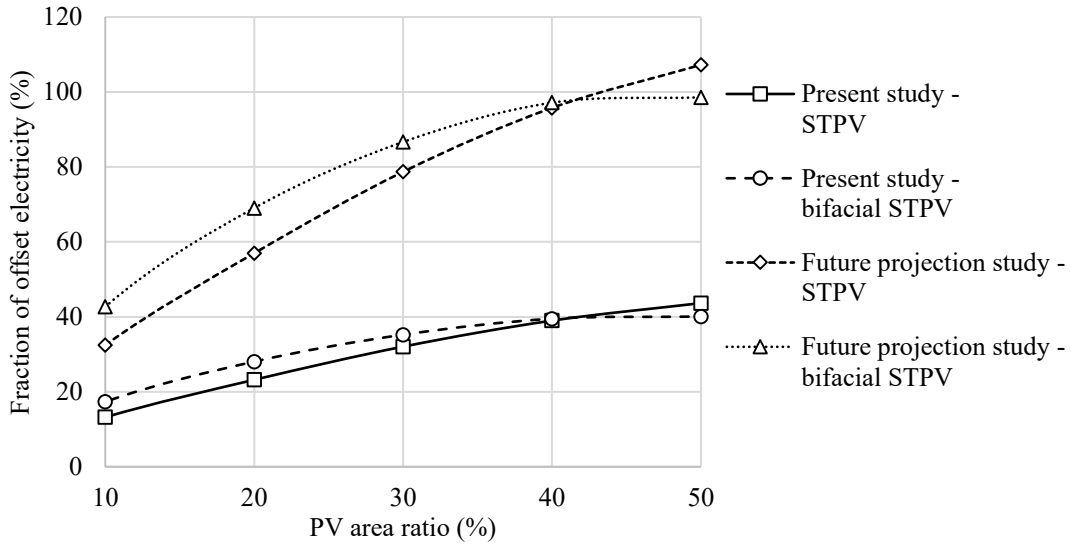

Figure D.5: Fraction of electricity consumed for artificial lighting that is offset by electricity generated from STPV.

Natural gas consumption

Fig. D.6 presents the natural gas consumed for heating for the various STPV designs considered in the current and future projection studies. The heating energy consumption decreased in a nearly linear manner with increasing PV area ratios by a minimum of 4.8% (10% PV area ratio) and a maximum of 15.9% (50% PV area ratio) for bifacial STPV in the present study. Moreover, natural gas use increased by 5.9-15.3% in the future projection study compared to the present study because increasing artificial light fixture efficiency reduced the portion of electricity that is converted to heat and consequently the "free-heating" effect on the greenhouse air. Furthermore, Tables D.3 and D.4 show how that natural gas consumption was slightly lower for the case with TOU electricity pricing because supplemental lighting was operated later into the night, when heating energy demand is higher.

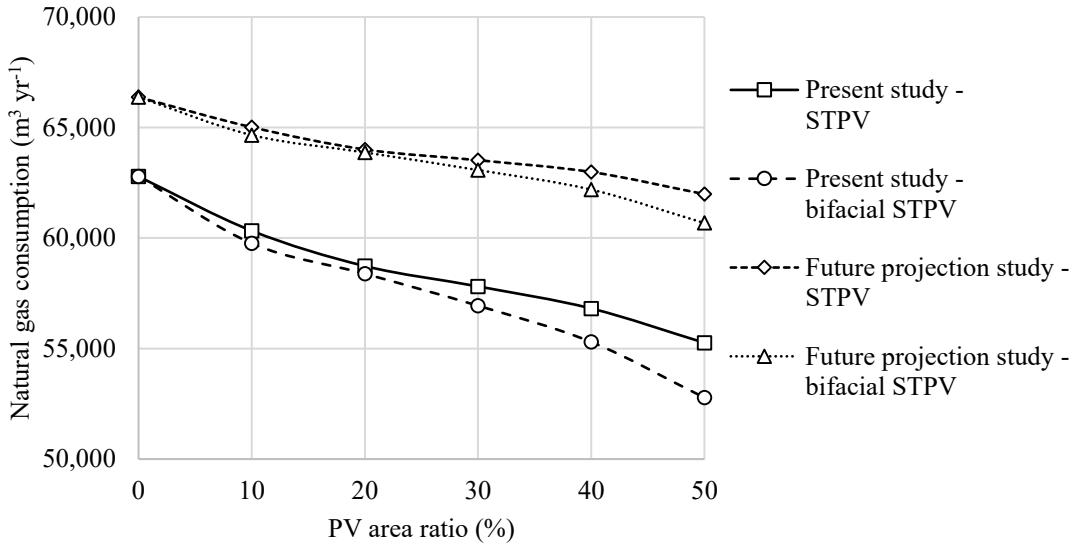

Figure D.6: Natural gas consumption for heating.

Life cycle energy cost

Tables D.5 and D.6 present the life cycle energy cost obtained for the various PVGH designs considered in the present and future projection studies, respectively. A PVGH can only be economically viable when its life cycle energy costs are lower than that of the BCGH. The life cycle energy cost decreased in all cases except the following cases which occurred in the present study and using constant electricity pricing: 1) for single-sided STPV of 10% and 20% PV area ratio; and 2) for bifacial STPV of 10%, 40% and 50% PV area ratio.

Net savings and change in life cycle cost

For bifacial STPV in the present study (Table D.5), the economic results range from a 13.8% increase in LCC (net loss of $326,373) at 50% PV area ratio using constant electricity pricing to a 7.4% reduction in LCC (net savings of $158,303) at 40% PV area ratio using TOU electricity pricing. For the future projection study (Table D.6), a reduction in LCC was achieved for all the bifacial STPV designs. The smallest reduction in LCC was 5.8% and occurred at 10% PV area ratio using constant electricity pricing whereas the LCC was reduced by as much as 35.4% at 50% PV area ratio using TOU electricity pricing. Therefore, the economic situation is evolving towards increased viability of STPV claddings and there may be significant potential for them to reduce LCC the in the future.

Fig. D.7 provides the net savings that were achieved for the various PVGH designs considered in the present study. For the case of constant electricity pricing, the results indicate that installing STPV cladding would produce a financial loss of between $12,450 and $326,373 over its lifespan. In other words, a PVGH installed in the present with constant electricity pricing would increase life cycle cost between 0.8-13.8%. The incurred loss was minimal at a PV area ratio of 40% for single-sided STPV ($12,450) and 20% for bifacial STPV ($31,050). For bifacial STPV, the economic viability decreased as the PV area ratio increased whereas it was nearly constant for single-sided STPV. Therefore, STPV cladding would not be an economically attractive investment at current efficiencies of horticultural lighting and PV technology and when constant electricity rates are the only option that is available. However, when TOU electricity pricing exists, STPV became a cost-effective investment (even at current efficiencies of technology) and reduced LCC by 1.5-11.7% (net savings of $32,694-249,382). The net savings for single-sided STPV increased with the PV area ratio (maximum net savings for TOU electricity pricing occurred at the highest PV area ratio that was tested) whereas for bifacial STPV, net savings reached a maximum value of $158,304 at a PV area ratio of 40%. These results suggest that at current efficiencies of technology, STPV cladding can be an economically attractive envelope design if favorable electricity tariff schemes such as TOU pricing exist. Furthermore, the deployment of STPV cladding could be further accelerated with additional financial incentives such as technology demonstration grants and electricity feed-in-tariff programs.

Fig. D.8 presents the net savings of the PVGH for the future projection study. For constant electricity pricing, the LCC decreased by 3.8-22.8% (net savings of $75,186-454,893), whereas for TOU electricity pricing, reductions of 6.9-37.0% (net savings of $127,881-689,579) were achieved. For all the PVGH design alternatives investigated, the net savings increased with the PV area ratio except for the case of bifacial STPV using constant electricity pricing at a PV area ratio of 50%. Therefore, for bifacial STPV and constant electricity pricing, the LCC reduction was greatest (17.9%) at a PV area ratio of 40%. For the case of TOU electricity pricing, net savings increased in a near linearly manner with the PV area ratio for the single-sided STPV whereas its rate of growth was decreasing for bifacial STPV. The net savings for bifacial STPV were higher than single-sided STPV until a PV area ratio of approximately 35% for the constant pricing and 45% for the TOU electricity pricing. Interestingly, the optimal PV

area ratio was found to be 40% (net savings of $357,543, 17.9% decrease in LCC) for bifacial STPV using constant electricity pricing.

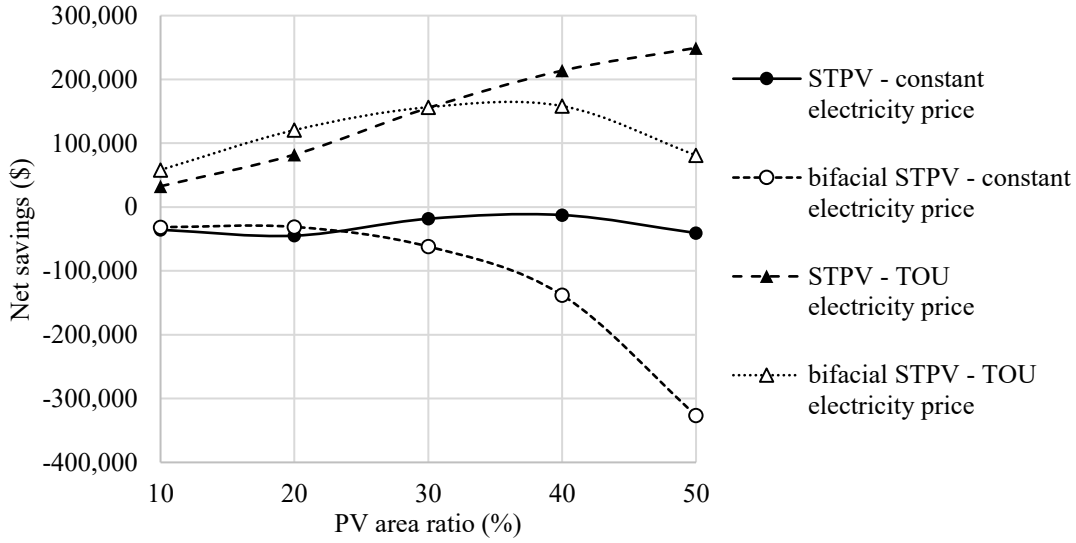

Figure D.7: Net savings achieved by integrating STPV cladding on the greenhouse roof - present study.

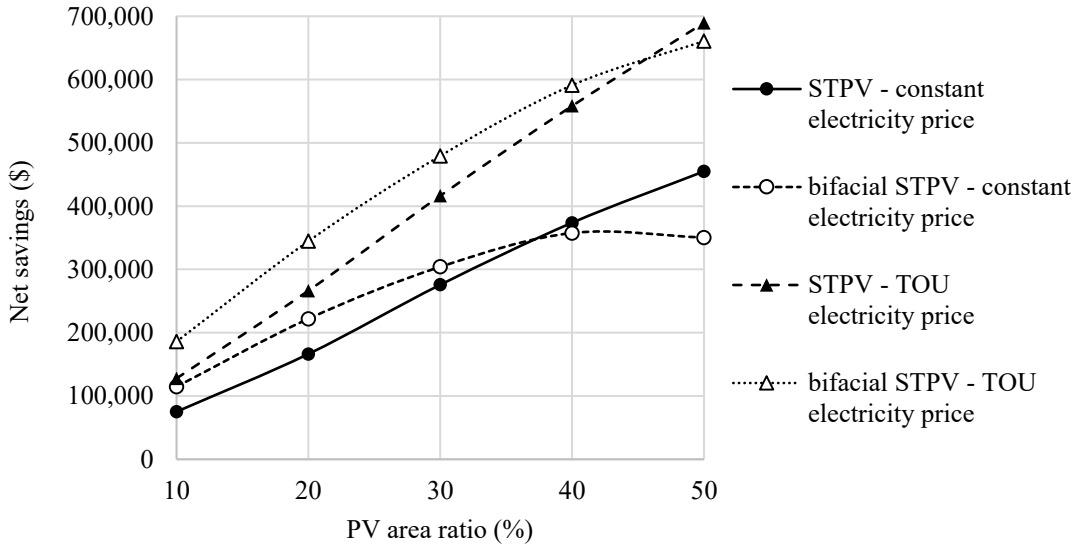

Figure D.8: Net savings achieved by integrating STPV cladding on the greenhouse roof – future projection study.

Table D.5: Present-value costs, residual value, net savings, and change in life cycle cost - present study.

Electricity price	Roof envelope design	Energy cost	Initial investment cost	Capital replacement cost	Residual value	Net savings	Change in LCC
Constant	BCGH	$1,588,749	$0	$84,949	$25,586	-	-
	STPV 10%	$1,604,584	$17,483	$87,856	$26,287	-$35,525	1.5%
	STPV 20%	$1,594,180	$34,967	$90,764	$26,989	-$44,811	1.9%
	STPV 30%	$1,547,967	$52,450	$93,672	$27,690	-$18,287	0.8%
	STPV 40%	$1,522,440	$69,934	$96,580	$28,392	-$12,450	0.5%
	STPV 50%	$1,530,954	$87,417	$99,487	$29,093	-$40,654	1.7%
	bifacial STPV 10%	$1,594,365	$23,596	$87,856	$26,287	-$31,418	1.3%
	bifacial STPV 20%	$1,568,196	$47,191	$90,764	$26,989	-$31,050	1.3%
	bifacial STPV 30%	$1,573,162	$70,787	$93,672	$27,690	-$61,818	2.6%
	bifacial STPV 40%	$1,623,442	$94,382	$96,580	$28,392	-$137,900	5.8%
	bifacial STPV 50%	$1,786,113	$117,978	$99,487	$29,093	-$326,373	13.8%
TOU	BCGH	$1,351,762	$0	$84,949	$25,586	-	-
	STPV 10%	$1,299,378	$17,483	$87,856	$26,287	$32,694	-1.5%
	STPV 20%	$1,230,146	$34,967	$90,764	$26,989	$82,237	-3.9%
	STPV 30%	$1,137,285	$52,450	$93,672	$27,690	$155,409	-7.3%
	STPV 40%	$1,059,199	$69,934	$96,580	$28,392	$213,805	-10.1%
	STPV 50%	$1,003,932	$87,417	$99,487	$29,093	$249,382	-11.7%
	bifacial STPV 10%	$1,267,691	$23,596	$87,856	$26,287	$58,270	-2.7%
	bifacial STPV 20%	$1,179,520	$47,191	$90,764	$26,989	$120,639	-5.7%
	bifacial STPV 30%	$1,117,846	$70,787	$93,672	$27,690	$156,511	-7.4%
	bifacial STPV 40%	$1,090,252	$94,382	$96,580	$28,392	$158,304	-7.4%
	bifacial STPV 50%	$1,141,536	$117,978	$99,487	$29,093	$81,218	-3.8%

Table D.6: Present-value costs, residual value, net savings, and change in life cycle cost - future projection study.

Electricity price	Roof envelope design	Energy cost	Initial investment cost	Capital replacement cost	Residual value	Net savings	Change in LCC
Constant	BCGH	$1,247,596	$0	$46,968	$14,146	-	-
	STPV 10%	$1,145,772	$23,654	$50,902	$15,095	$75,186	-3.8%
	STPV 20%	$1,027,912	$47,308	$54,836	$16,045	$166,406	-8.3%
	STPV 30%	$891,914	$70,962	$58,770	$16,994	$275,766	-13.8%
	STPV 40%	$767,240	$94,616	$62,704	$17,943	$373,801	-18.7%
	STPV 50%	$659,509	$118,270	$66,638	$18,892	$454,893	-22.8%
	bifacial STPV 10%	$1,097,916	$31,923	$50,902	$15,095	$114,772	-5.8%
	bifacial STPV 20%	$955,784	$63,847	$54,836	$16,045	$221,996	-11.1%
	bifacial STPV 30%	$838,747	$95,770	$58,770	$16,994	$304,125	-15.2%
	bifacial STPV 40%	$750,420	$127,693	$62,704	$17,943	$357,543	-17.9%
	bifacial STPV 50%	$722,668	$159,617	$66,638	$18,892	$350,388	-17.6%
TOU	BCGH	$1,117,328	$0	$46,968	$14,146	-	-
	STPV 10%	$962,809	$23,654	$50,902	$15,095	$127,881	-6.9%
	STPV 20%	$797,627	$47,308	$54,836	$16,045	$266,423	-14.3%
	STPV 30%	$621,020	$70,962	$58,770	$16,994	$416,391	-22.3%
	STPV 40%	$452,423	$94,616	$62,704	$17,943	$558,350	-29.9%
	STPV 50%	$294,555	$118,270	$66,638	$18,892	$689,579	-37.0%
	bifacial STPV 10%	$896,397	$31,923	$50,902	$15,095	$186,023	-10.0%
	bifacial STPV 20%	$702,901	$63,847	$54,836	$16,045	$344,611	-18.5%
	bifacial STPV 30%	$533,215	$95,770	$58,770	$16,994	$479,389	-25.7%
	bifacial STPV 40%	$386,566	$127,693	$62,704	$17,943	$591,130	-31.7%
	bifacial STPV 50%	$281,944	$159,617	$66,638	$18,892	$660,844	-35.4%

APPENDIX E: Energy and Economic Analysis of STPV Cladding for Whitehorse, Canada

E.1 Greenhouse Characteristics

The analysis of Chapter 4 was repeated for Whitehorse, Yukon (60.7°N, high-latitude, 6,915 heating degree-days), Canada.

E.2 Energy Analysis

The methodology for the daylighting, artificial lighting control and thermal modules is the same as described in section 4.5, except for those presented below.

Weather data: The ground temperature (beneath the soil layer) was defined as an annual sinusoidal function with an assumed mean value of 0°C for Whitehorse, with an amplitude of 2°C and the minimum temperature occurring on the 90th day of the year. For the analysis at peak heating design conditions, no solar radiation, a wind speed of 10 m s^{-1}, exterior air relative humidity of 20%, exterior air temperatures of -35.3°C, sky temperatures of -63°C (calculated with Type 575 with no cloud cover), and ground temperature of -2°C were selected for Whitehorse (RETScreen, 2013).

Thermal energy consumption: For Whitehorse, it is assumed that liquified propane is used to fire the condensing boiler. The annual propane consumption (m_{prop_yr} in L yr^{-1}) is equal to:

$$m_{prop\_yr} = 10^3 \cdot Q_{heat\_yr} / \left(EV_{prop} \cdot \eta_{boil}\right) \quad \text{(E.1)}$$

where EV_{prop} is the energy value of propane (MJ m^{-3}) equal to 25.5 MJ L^{-1} (McDonald, 2004).

E.3 Economic Analysis

The methodology for the economic analysis is the same as described in section 4.6, except for those presented in Table E.1.

Table E.1: Values of the cost data used in the LCCA for Whitehorse.

Parameter	Symbol	Value	Reference
Installed cost of greenhouse structure per unit area	C_{stru_tot}	354.08 \$ m^{-2}	RSMeans (2016, 2017)
Installed cost of AL system per unit area	C_{AL_tot}	340.24 \$ m^{-2}	Illumitex (2018); RSMeans (2018)
Initial investment cost of greenhouse	Inv	\$ 702,400	Calculated from Eq. (4.53)
Average electricity price	C_{el}	0.15 \$ kWh^{-1}	Electricity price (includes consumption and power demand) above 20,000 kWh $month^{-1}$ from (YER, 2016) is used; cost escalation rate calculated from (YEC, 2011; YER, 2016) between 2011-17
Electricity cost escalation rate	e_{el}	2.1%	
Propane price	C_{prop}	1.24 \$ L^{-1}	YRFP (2018)
Propane cost escalation rate	e_{prop}	5.9%	The cost escalation rate was obtained from (Deloitte, 2017) between 2017 and 2024 (propane value assumed to be the same as natural gas)
EPS insulation cost	C_{ins_mat}	11.28 \$ m^{-2}	RSMeans (2017)
EPS insulation installation cost	C_{ins_inst}	4.18 \$ m^{-2}	
Movable EPS insulation annual installed plus removal cost	C_{mov_lab}	8.36 \$ m^{-2}	Adding and removing movable insulation assumed to be double EPS installation cost

E.4 Results and Discussion

Electricity consumption for artificial lighting

Table E.2 gives the energy consumption/generation for Whitehorse. It was found that electricity consumption increased in a near linear manner with increased PV area rations. In both the present and future projection studies, a PV area ratio of 50% increased lighting electricity consumption by 26.7% compared to the BCGH. The increased efficiency of lighting technology decreased electricity consumption by 44.7% in all cases.

Table E.2: Greenhouse energy consumption/generation for Whitehorse.

Roof envelope design	Present			Future		
	AL electricity consumption (kWh yr^{-1})	PV electricity generation (kWh yr^{-1})	Propane consumption (L yr^{-1})	AL electricity consumption (kWh yr^{-1})	PV electricity generation (kWh yr^{-1})	Propane consumption (L yr^{-1})
BCGH	265,510	-	129,547	146,853	-	144,049
STPV 10%	284,679	13,824	126,626	157,455	18,766	141,972
STPV 20%	299,882	27,655	124,504	165,864	37,542	140,500
STPV 30%	310,788	41,490	123,355	171,896	56,324	139,812
STPV 40%	322,231	55,331	122,197	178,225	75,114	139,117
STPV 50%	336,484	69,174	120,228	186,108	93,908	137,716

Electricity generation from STPV cladding

For Whitehorse, the PV roof surface generated a minimum solar electricity generation of 14.9 kWh m^{-2} yr^{-1} (present study with single-sided STPV of 10% PV area ratio) and a maximum of 101.1 kWh m^{-2} yr^{-1} (future projection study with single-sided STPV of 50% PV area ratio) (Table E.2). It was found that improving the PV electrical efficiency from 17% (present study) to 23% (future projection study) increased electricity production by approximately 36% in all cases.

Net electricity consumption/generation

The results for the present study indicated that the PVGH did not produce enough solar electricity to compensate for the increased use of lighting electricity that is provoked by the STPV shading (Fig. D.4). In the best case, the greenhouse with a PV area ratio of 40% consumed 1,390 kWh yr^{-1} more than the BCGH. However, when the efficiency of artificial lighting and PV technology increased to their future projection values, the PVGH always consumed less electricity (between 8,164-54,653 kWh yr^{-1}) than the BCGH. For Whitehorse, PV electricity generation could provide 4.9-20.6% of lighting electricity requirements in the present study whereas 11.9-50.5% was achieved in the future projection study.

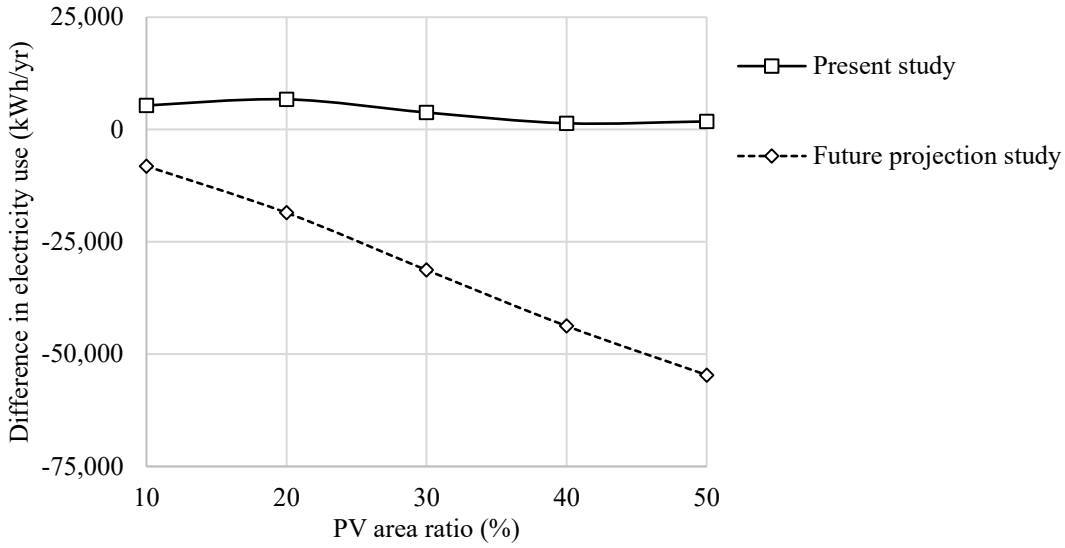

Figure E.1: Difference in electricity consumption (for lighting minus PV generation) between the PVGH and BCGH (negative indicates PVGH consumes less electricity than BCGH) for Whitehorse.

Propane consumption

The heating energy consumption decreased in a nearly linear manner with increasing PV area ratios by a minimum of 1.4% for the single-sided STPV with a 10% PV area ratio in the future projection study, and by a maximum of 7.2% for single-sided STPV with a 50% PV area ratio in the present study (Table E.2). Moreover, propane use increased by 11.2-14.5% in the future projection study compared to the present study due to the lower amount of heat that is dissipated from fixtures of higher efficiency.

Life cycle energy cost

The life cycle energy cost for all the PVGH designs were always inferior to those of the BCGH. This indicates that net savings are possible.

Net savings and change in life cycle cost

Table E.3 presents the LCCA components for the various PVGH designs considered in the present and future projection studies. For all PVGH designs, increasing the PV area ratio lowered the LCC. In both the present and future projection studies, the LCC was reduced by approximately 1.3% (net savings slightly over $140,000) for STPV of 10% PV area ratio and

4.8% (net savings slightly of approximately $500,000) for STPV of 50% PV area ratio. Unlike for Ottawa, increasing the efficiency of PV and horticultural lighting technology in the future projection study did not improve the economic benefit. This is likely because the decrease in life cycle energy cost that could be achieved from lower lighting electricity use and higher PV electricity generation (achieved by employing higher efficiency technology in the future) was counteracted by the resulting increase in propane consumed for heating (which carries a relatively high cost in Whitehorse, compared to electricity).

Table E.3: Present-value costs, residual value, net savings, and change in life cycle cost for Whitehorse.

Study	Roof envelope design	Energy cost	Initial investment cost	Capital replacement cost	Residual value	Net savings	Change in LCC
Present	BCGH	$9,324,452	-	$84,949	$25,586	-	-
	STPV 10%	$9,164,698	$17,483	$87,856	$26,287	$140,064	-1.4%
	STPV 20%	$9,037,469	$34,967	$90,764	$26,989	$247,603	-2.5%
	STPV 30%	$8,952,233	$52,450	$93,672	$27,690	$313,150	-3.1%
	STPV 40%	$8,868,766	$69,934	$96,580	$28,392	$376,927	-3.7%
	STPV 50%	$8,746,852	$87,417	$99,487	$29,093	$479,152	-4.8%
Future	BCGH	$9,706,721	-	$46,968	$14,146	-	-
	STPV 10%	$9,539,830	$23,654	$50,902	$15,095	$140,252	-1.3%
	STPV 20%	$9,401,108	$47,308	$54,836	$16,045	$252,335	-2.4%
	STPV 30%	$9,301,032	$70,962	$58,770	$16,994	$325,772	-3.1%
	STPV 40%	$9,201,827	$94,616	$62,704	$17,943	$398,338	-3.8%
	STPV 50%	$9,065,144	$118,270	$66,638	$18,892	$508,382	-4.9%

Comparison of energy consumption/generation between both design locations

Table E.4 provides a comparison of the energy consumption and generation between Ottawa and Whitehorse. As expected, lighting electricity consumption was higher, and PV electricity generation was less due to lower daylight availability, and heating energy consumption increased due to the colder climate in Whitehorse compared to Ottawa. For the present and future projection studies, the lighting electricity consumption was 60.0-131.9% higher in Whitehorse. Thermal energy consumption for heating increased by 42.2-53.1% in Whitehorse. PV electricity generation decreased by 24.7% in Whitehorse for all cases.

Table E.4: Change in energy consumption/generation between Ottawa and Whitehorse.

Roof envelope design	Present			Future		
	Lighting electricity consumption (kWh yr^{-1})	Heating energy consumption (GJ yr^{-1})	PV electricity generation (kWh yr^{-1})	Lighting electricity consumption (kWh yr^{-1})	Heating energy consumption (GJ yr^{-1})	PV electricity generation (kWh yr^{-1})
BCGH	131.9%	42.2%	-	131.9%	49.6%	-
STPV 10%	105.2%	44.7%	-24.7%	105.2%	50.5%	-24.7%
STPV 20%	89.5%	46.1%	-24.7%	89.5%	51.3%	-24.7%
STPV 30%	80.8%	47.1%	-24.7%	80.8%	51.7%	-24.7%
STPV 40%	71.1%	48.2%	-24.7%	71.1%	52.2%	-24.7%
STPV 50%	60.0%	49.9%	-24.7%	60.0%	53.1%	-24.7%

APPENDIX F: Sensitivity of Net Savings to Economic Parameter Values for Chapter 4

It is impossible to know for certain what the price of energy, materials, labor and equipment will actually be over the next 25 years or so. To identify the critical input values in the LCCA, several parameters were individually varied by ±5 and ±10% and plotted against the resulting percent changes in net savings. When one variable is modified, all others remain at their default values.

The following results are for Ottawa, Canada. Fig. F.1 and F.2 provide the results for the present and future projection studies, respectively, for the case of a greenhouse equipped with single-sided STPV of 50% PV area ratio and using the constant electricity price. Based on Fig. F.1, the critical input values (which provoke a change in NS greater than ±2% when varied by ±10%) to LCCA include the energy (electricity and heating fuel) price and its cost escalation rate, and the incremental initial investment for STPV. A 10% increase in the natural gas price, natural gas cost escalation rate, electricity price, electricity cost escalation rate and incremental initial investment for STPV caused the net savings to change by 19.1%, 17.3%, -6.8%, -7.9% and -13.7% respectively. In all cases and for both locations, varying the replacement cost of artificial lights did not affect the net savings because, for all cases studied except one, they were replaced at the maximum fixture lifespan (15 years) rather than the bulb lifespan (50,000 hr).

In the future (Fig. F.2), the critical input values (which provoke a change in NS greater than ±2% when varied by ±10%) to the LCCA include the electricity price and its cost escalation rate. A 10% increase in the electricity price and its cost escalation rate caused the net savings to change by -8.7% and 13.8% respectively. Changes in the natural gas price, natural gas cost escalation rate and the incremental initial investment for STPV had a negligible (<2%) effect on the economic result. Therefore, in the future, the importance of the incremental initial investment cost for STPV will diminish compared to the life cycle energy costs.

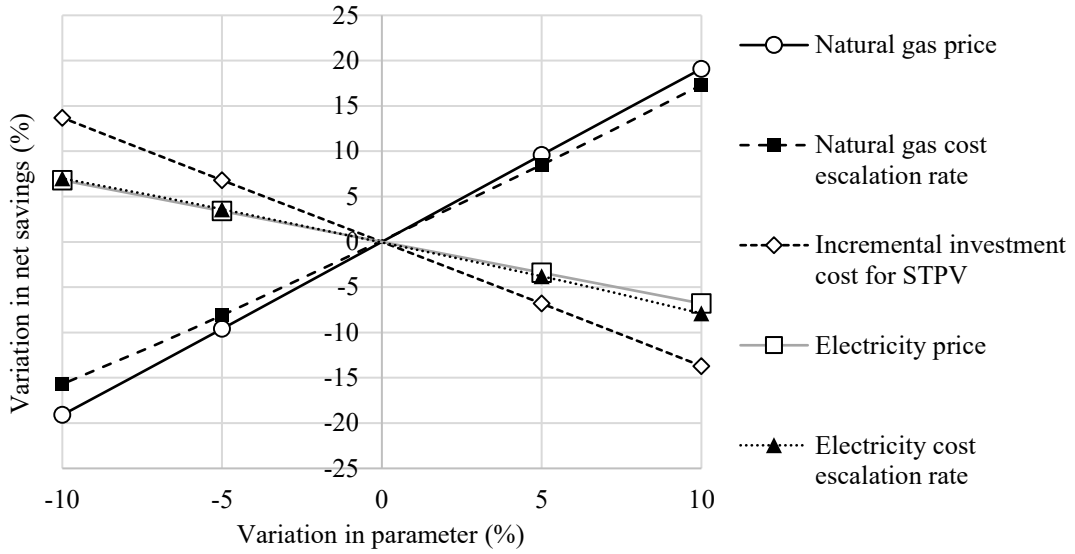

Figure F.1: Sensitivity analysis for the present study for Ottawa - variation in net savings given percent change in parameter (single-sided STPV; 50% PV area ratio; constant electricity price).

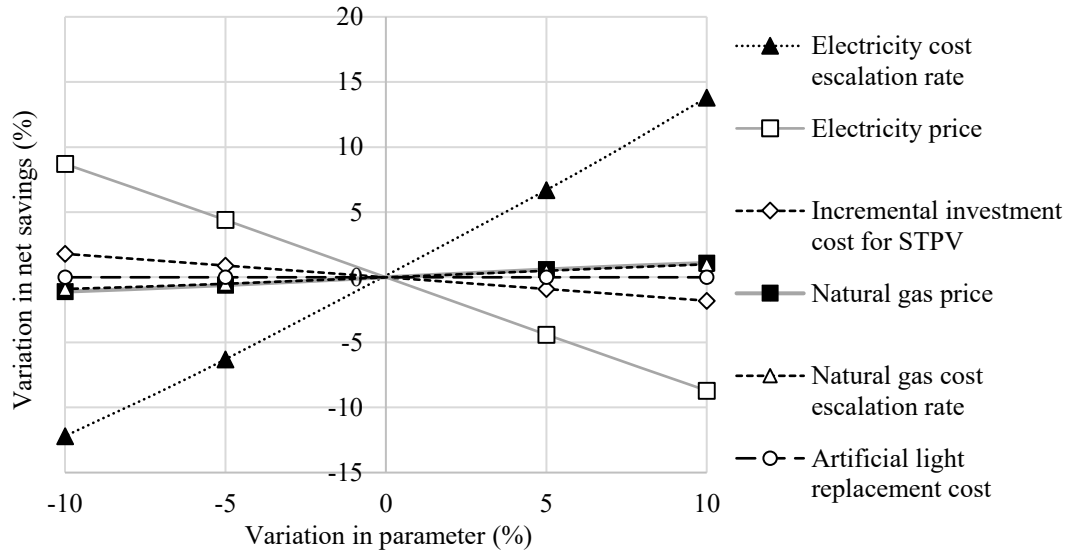

Figure F.2: Sensitivity analysis for the future projection study for Ottawa - variation in net savings given percent change in parameter (single-sided STPV; 50% PV area ratio; constant electricity price).

The following results are for Whitehorse, Canada. Figs. F.3 and F.4 provide the results for the present and future projection studies, respectively, for the case of a greenhouse equipped with single-sided STPV of 50% PV area ratio and using the constant electricity price. Based on Fig. F.3, the critical input values (which provoke a change in NS greater than ±2% when varied

by ±10%) to the LCCA include the propane price and its cost escalation rate. A 10% increase in the propane price and its cost escalation rate caused the net savings to change by 12.2% and 11.1% respectively. Changes in the electricity price, electricity cost escalation rate and the incremental initial investment for STPV had a negligible (<2%) effect on the economic result.

In the future (Fig. F.4), the critical input values (which provoke a change in NS greater than ±2% when varied by ±10%) to the LCCA include the propane price and its cost escalation rate and the electricity price. A 10% increase in the propane price, the propane cost escalation rate and the electricity rate caused the net savings to change by 7.8%, 7.1% and 4.8%, respectively. Changes in the electricity cost escalation rate and the incremental initial investment for STPV had a negligible (<2%) effect on the economic result.

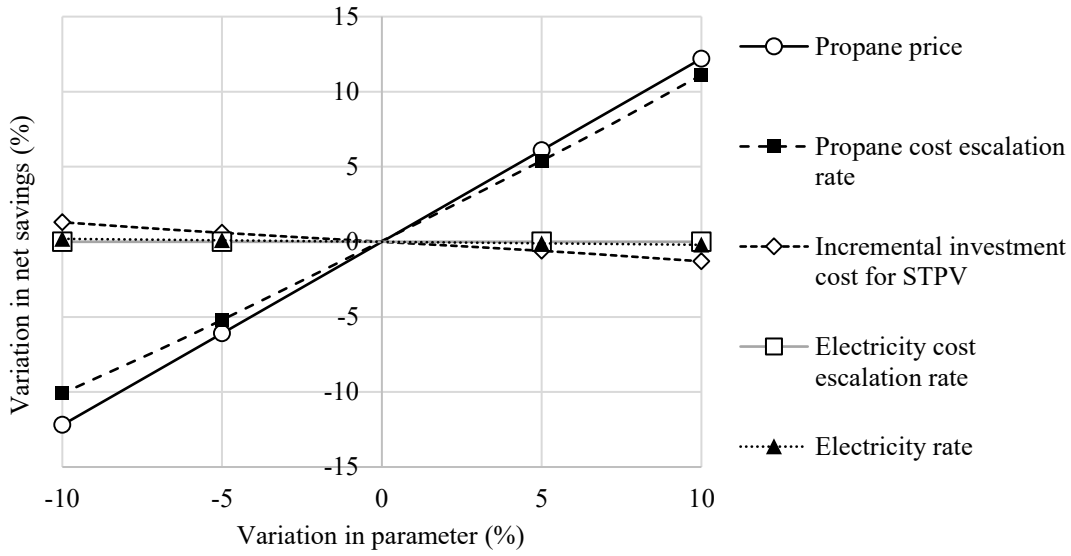

Figure F.3: Sensitivity analysis for the present study for Whitehorse - variation in net savings given percent change in parameter (single-sided STPV; 50% PV area ratio; constant electricity price).

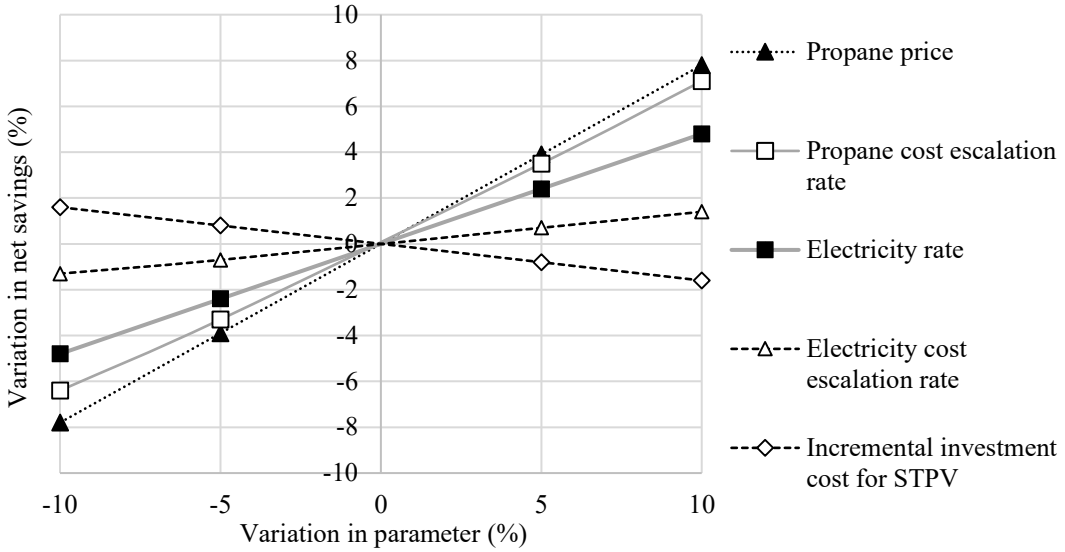

Figure F.4: Sensitivity analysis for the future projection study for Whitehorse - variation in net savings given percent change in parameter (single-sided STPV; 50% PV area ratio; constant electricity price).

There is usually less uncertainty about material and labor cost and the price of energy because their current costs are specified at the base date. Therefore, it may be advisable to spend additional effort on determining the degree of uncertainty associated with the energy cost escalation rate. The future price of fuel (natural gas, propane) and fuel-based electricity generation is unknown and volatile. So long as these resources are obtained from fossil deposits, the price can be expected to increase in the long term. However, as the cost of renewable energy (e.g. solar and wind) continues its rapid decline and promising technology such as power-to-gas matures (e.g. high temperature electrolysis and biological methanation), fossil fuels will be gradually replaced with renewable synthetic/biological fuels. Consequently, a decrease in the cost of fossil fuel-based energy (fuel and electricity) can be expected in the future. A comparison of the impact of various fuel cost escalation rates on the economic result was conducted, assuming the future price of energy will be lower than the values employed in this study. Table F.1 provides the change in net savings that would results from having a fuel cost escalation rate of 2%, 0% and -2% for the present study. The percent change is calculated for the case of a greenhouse equipped with single-sided STPV of 50% PV area ratio and using the constant electricity price. For Ottawa, a lower natural gas cost escalation rate could decrease the net savings by up to 140.2%. For Whitehorse, a lower propane cost escalation rate could decrease

the net savings by up to 79.5%. Therefore, the impact of lower fuel cost in the future has a significant impact on net savings and should be carefully evaluated to assess the risk associated with the proposed alternative envelope designs.

Table F.1: Effect of predicted energy cost escalation rate on net savings.

		Fuel cost escalation rate		
		2%	0%	-2%
Change in net savings	Ottawa	-90.9%	-119.4%	-140.2%
	Whitehorse	-51.5%	-67.7%	-79.5%

APPENDIX G: Comparison of Glass, Polycarbonate and Opaque Cladding for Whitehorse, Canada

G.1 Greenhouse Characteristics

The analysis of Chapter 5 was repeated for Whitehorse, Yukon (60.7°N, high-latitude, 6,915 heating degree-days), Canada.

G.2 Energy Analysis

The methodology for the daylighting, artificial lighting control and thermal modules is the same as described in section 5.5 and Appendix E.

G.3 Economic Analysis

The methodology for the economic analysis is the same as described in section 5.6 and additional details are provided Appendix E.

G.4 Results and Discussion

Table G.1 provides the availability of solar radiation for the greenhouse surfaces for Whitehorse. The analysis of the surfaces will be in the order: north, west, east walls, south walls, and roof (although the south wall receives more solar radiation than the roof, it was decided to perform the analysis for the walls first followed by the roof).

Table G.1: Annual incident solar radiation on greenhouse surfaces.

Surface	north wall	east wall	west wall	south wall	roof
Incident solar radiation (GJ m^{-2} yr^{-1})	1.21	2.62	2.59	3.76	3.65

The present-value costs, residual value, NS (in $CAD 2017), and change in LCCA for the AGH and BCGH in Whitehorse are provided in Table G.2. Table G.3 gives the annual energy consumption (lighting electricity and fuel consumed for heating) and the annual GHG emissions related to energy consumption for Whitehorse. Like Ottawa, the lighting electricity consumption in Whitehorse increased for all AGH designs except when permanent and movable insulation was applied to the north wall and the case with permanent insulation on the north wall plus polycarbonate on the west wall. This demonstrates how the use of reflective opaque insulation on the north wall can redirect light onto the crops and simultaneously achieve reductions in

electricity and heating energy consumption. For the north wall, the use of permanent insulation decreased LCC by 4.7% (net savings of $486,205). For the west wall, the use of permanent insulation (in addition to being employed on the north wall) decreased LCC by 9.1% (net savings of $952,483). For the east wall, the use of permanent insulation (in addition to being employed on the north and west walls) decreased LCC by 13.5% (net savings of $1,408,571). For the south wall, the use of permanent insulation (in addition to being employed on the north, west and east walls) decreased LCC by 18.2% (net savings of $1,895,812). For the roof, the use of permanent insulation (in addition to being employed on all the walls) decreased LCC by 38.9% (net savings of $4,054,463). Therefore, the the most cost-effective design for Whitehorse consists of covering all inside surfaces of the glass with permanent insulation. This AGH design caused the lighting electricity consumption to increase by 172.6% (from 265,510 kWh yr^{-1} to 723,823 kWh yr^{-1}), the amount of propane used for heating to decrease by 71.2% (from 134,886 m^3 yr^{-1} to 38,844 m^3 yr^{-1}) and GHG emissions related to energy consumption to increase by 15.6% (320,545 kg_{CO_2} yr^{-1} to 370,675 kg_{CO_2} yr^{-1}). A possible explanation for why a plant factory (no sunlight, only artificial lighting) type grow operation was found to be the most economically viable design is the fact that it achieves by far the lowest heating energy use (38,844 L yr^{-1} of propane compared to 134,886 L yr^{-1} for the BCGH) combined with the high cost of heating fuel in that remote location. Under these circumstances, it would be recommended to compare the LCC of the glazed greenhouse with added insulation to that of a warehouse type building. Moreover, the possibility of having multi-level crop production (e.g. on shelves) could be examined so that heating energy and building footprint could be further reduced.

In Yukon, most of the electricity is generated hydro and diesel whereas heating is typically produced from the combustion of fossil fuels such as propane. The results show that in all cases studied except one, the decrease in GHG emissions from reduced propane use outweighs the increase in emissions from higher electricity consumption. It is interesting to note that the only case where GHG emissions related to energy consumption increased compared to the BCGH is for the most cost-effective envelope design (15.6% increase for the AGH design with all surfaces covered with permanent insulation). This demonstrates how envelope design based on economic and environmental concerns do not always go hand in hand. However, GHG emissions related to energy consumption will gradually decrease as fossil fuels are replaced with renewable power and carbon-neutral fuels that are derived from them.

Table G.2: Present-value costs, residual value, net savings, and change in life cycle cost for Whitehorse.

	Energy costs	Initial investment costs	O&MR costs	Capital replacement cost	Residual value	Net Savings	Change in LCC
Base case	$9,659,922	-	-	$84,949	$25,586	-	-
N wall permanent insulation	$9,175,183	-$1,466	-	$84,949	$25,586	$486,205	-4.7%
N wall movable ins.	$9,448,884	$1,258	$21,098	$84,949	$25,586	$188,681	-1.8%
N wall polycarbonate	$9,366,041	$1,116	-	$94,176	$25,892	$283,843	-2.7%
NW walls permanent ins.	$8,710,371	-$2,932	-	$84,949	$25,586	$952,483	-9.1%
N walls permanent ins.; W wall movable ins.	$8,967,672	-$208	$21,098	$84,949	$25,586	$671,359	-6.4%
N walls permanent ins.; W wall poly.	$8,891,460	-$350	-	$94,176	$25,892	$759,890	-7.3%
NWE walls permanent ins.	$8,255,749	-$4,398	-	$84,949	$25,586	$1,408,571	-13.5%
NW walls permanent ins.; E wall movable ins.	$8,503,035	-$1,673	$21,098	$84,949	$25,586	$1,137,462	-10.9%
NW walls permanent ins.; E wall poly.	$8,428,069	-$1,816	-	$94,176	$25,892	$1,224,747	-11.8%
NWES walls permanent ins.	$7,820,947	-$34,214	-	$59,734	$22,995	$1,895,812	-18.2%
NWE walls permanent ins.; S wall movable ins.	$8,028,416	-$31,489	$21,098	$59,734	$22,995	$1,664,521	-16.0%
NWE walls permanent ins.; S wall poly.	$7,967,430	-$31,632	-	$68,961	$23,300	$1,737,826	-16.7%
NWES walls and roof permanent ins.	$5,667,853	-$77,966	-	$105,403	$30,469	$4,054,463	-38.9%
NWES walls permanent ins.; Roof movable ins.	$6,230,075	-$55,279	$175,694	$31,677	$20,111	$3,357,229	-32.2%
NWES walls permanent ins.; Roof movable ins. (6 months)	$5,683,434	-$55,279	$175,694	$31,677	$20,111	$3,903,870	-37.5%
NWES walls permanent ins.; Roof poly	$6,209,630	-$24,923	-	$136,579	$25,542	$3,423,541	-32.9%

Table G.3: Energy consumption and associated GHG emissions for Whitehorse.

	Lighting electricity consumption (kWh yr^{-1})	Propane consumption (L yr^{-1})	Peak thermal energy demand (kW)	Lighting electricity CO_2 emissions (kge_{CO_2} yr^{-1})	Propane CO_2 emissions (kge_{CO_2} yr^{-1})	Total CO_2 emissions (kge_{CO_2} yr^{-1})	Change in CO_2 emissions
Base case	265,510	134,886	361	114,170	206,375	320,545	-
N wall permanent insulation	263,651	127,304	349	113,370	194,775	308,145	-3.9%
N wall movable ins.	264,519	131,598	349	113,743	201,345	315,088	-1.7%
N wall polycarbonate	265,676	130,197	349	114,241	199,202	313,443	-2.2%
NW walls permanent ins.	269,311	119,506	337	115,804	182,844	298,647	-6.8%
N walls permanent ins.; W wall movable ins.	265,221	123,890	337	114,045	189,552	303,597	-5.3%
N walls permanent ins.; W wall poly.	265,428	122,663	336	114,134	187,674	301,808	-5.9%
NWE walls permanent ins.	275,880	111,805	325	118,628	171,062	289,690	-9.6%
NW walls permanent ins.; E wall movable ins.	270,840	116,098	325	116,461	177,630	294,091	-8.3%
NW walls permanent ins.; E wall poly.	271,335	114,870	325	116,674	175,750	292,425	-8.8%
NWES walls permanent ins.	298,890	103,253	313	128,523	157,978	286,500	-10.6%
NWE walls permanent ins.; S wall movable ins.	288,067	107,323	313	123,869	164,204	288,072	-10.1%
NWE walls permanent ins.; S wall poly.	280,465	106,892	313	120,600	163,544	284,144	-11.4%
NWES walls and roof permanent ins.	723,823	38,844	218	311,244	59,431	370,675	15.6%
NWES walls permanent ins.; Roof movable ins.	326,858	75,953	218	140,549	116,208	256,757	-19.9%
NWES walls permanent ins.; Roof movable ins. (6 months)	390,892	62,711	218	168,083	95,948	264,032	-17.6%
NWES walls permanent ins.; Roof poly.	328,593	75,505	266	141,295	115,522	256,817	-19.9%

Comparison of energy consumption between both design locations

A comparison of energy use between both design locations shows that the BCGH in Whitehorse consumed 131.9% more electricity for lighting and 42.8% more thermal energy for heating compared to the BCGH in Ottawa. For the BCGH in both locations, approximately 55% of the total energy consumed for heating occurred at night.

APPENDIX H: Sensitivity Analysis for Chapter 5

The parameters related to energy modeling, greenhouse operation and economics may not be well known at the early stages of design. Therefore, an analysis of the impact of varying some of the key parameters is conducted hereafter.

H.1 Sensitivity of Net Savings to Energy Model Input Parameter Values

The energy model input parameters to be considered are those that significantly impact energy consumption and whose value carries considerable uncertainty. The ground temperature and the interior, and to a lesser the extent the exterior, convective heat transfer coefficients are a good example because they significantly influence predicted heating energy and their values are not well known. Therefore, the analysis was repeated using model parameter values that would result in higher/extreme heating energy use. A lower ground temperature (0°C instead of 10±2°C), an interor CHTC (20 W m^{-2} $°C^{-1}$) representing high-mixing of greenhouse air using horizontal airflow fans and an exterior CHTC (43.7 W m^{-2} $°C^{-1}$) representative of windy conditions (approximately 10 m s^{-1}) were selected for the analysis. For Ottawa, the lower ground temperature increased the heating energy consumption by 6.4% for the BCGH and 7.7% for the AGH design with the highest net savings. Since the net savings were only reduced by 0.4%, this accuracy of this parameter is negligible with respect to the economic outcome. Moreover, a higher exterior CHTC increased the heating energy consumption by 2.8% for the BCGH and 2.3% for the AGH design with the highest net savings. This caused the net savings to increase by 5.1% which is relatively small. A higher interior CHTC increased the heating energy consumption by 118.6% for the BCGH and 109.5% for the AGH design with the highest net savings. This caused the net savings to increase by 124.1%. Therefore, the inside CHTC is a modeling parameter that greatly influences both the predicted heating energy consumption and the economic outcome. By overestimating its value, the predicted net savings could be too optimistic. Consequently, efforts should focus on accurately determining this parameter for the specific envelope material and geometry and according to the airflow patterns that exist inside the greenhouse.

H.2 Sensitivity of Net Savings to Operation Parameter Values

An operation parameter that has a large impact on energy use and whose value is not well-established at early stages of design is the nighttime ventilation rate. This minimum ventilation rate can vary significantly. In some cases, condensation on the inside glazing is enough to dehumidify the inside air and avoid nighttime ventilation altogether. However, in most cases, a minimum ventilation rate, which typically varies between 1-4 ACH, is provided (Jackson and Darby, 2006; Climax Conseils, 2014). In this study, a ventilation rate of 1 ACH was selected but it is desired to determine how higher ventilation rates would impact the heating energy use and more importantly, the net savings. In Ottawa, a higher ventilation rate of 4 ACH increased the heating energy consumption by 69.3% for the BCGH and 81.2% for the AGH design with the highest net savings. Meanwhile, the net savings only increased by 3.8%. Therefore, even though the assumed ventilation rate greatly impacts the heating energy use, the effect on net savings is small. A possible explanation for this result is the comparative nature of the net savings. Moreover, the analysis for the movable insulation was conducted for a four-month installation period, which may not be the optimal amount of time. Installing the insulation for a six-month period was assessed to verify whether the incurred decrease in heating energy cost could justify the increased lighting electricity cost caused by blocking the sunlight in the early spring and late fall seasons. In Whitehorse, the results for a six-month installation period of rooftop movable insulation indicates that the economic result improved (net savings of $3,903,870 compared to $3,357,229 for a four-month period) but it was still inferior (albeit very close) to the design with permanent insulation (net savings of $4,054,463). Therefore, the installation period for movable insulation should be carefully assessed when compared to static envelope design alternatives.

H.3 Sensitivity of Net Savings to Economic Parameter Values

It is impossible to know for certain what the price of energy, materials, labor and equipment will actually be over the next 25 years or so. To identify the critical input values in the LCCA, several parameters were individually varied by ±5 and ±10% and plotted against the resulting percent changes in net savings. When one variable is modified, all others remain at their default values. Based on Figs. H.1, H.2 and H.3, the critical input values (which provoke a change in NS greater than ±1% when varied by ±10%) to in the LCCA include the energy

(electricity and heating fuel) price and its cost escalation rate, the cost for the condensing boiler, and the installation cost of movable insulation. Varying the replacement cost of artificial lights did not affect the net savings because, for all cases studied except one, they were replaced at the maximum fixture lifespan (15 years) rather than the bulb lifespan (50,000 hr). The AGH design with the highest net savings in Whitehorse (all surfaces have permanent insulation) was the only one to cause the light fixture replacement period to fall below 15 years (replacement required after 11.4 years) and therefore sensitivity analysis to its cost escalation rate was assessed.

For Ottawa, a 10% increase in the natural gas price, natural gas cost escalation rate, electricity price, electricity cost escalation rate, cost for the condensing boiler and the installation cost of movable insulation caused the net savings to change by 9.0%, 8.2%, -2.8% and -3.2%, 4.3% and 32.5% respectively (Fig. H.1 and H.2). Although the percentage for the movable insulation installation cost is high, the obtained net savings was low ($8,933 for north wall with movable insulation compared to $131,143 for the AGH with the highest net savings) and so is the absolute value of the increase that is produced. Changes in the material and installation cost of insulation, polycarbonate and TSS had a negligible (<1%) effect on the economic results. For Whitehorse, a 10% increase in the propane price, propane cost escalation rate, electricity price and electricity cost escalation rate caused the net savings to change by 14.9%, 13.5%, -5% and -1.4%, respectively (Fig. H.3). Changes in the condensing boiler cost and the initial cost of artificial lighting had a negligible (<1%) effect on the economic results whereas it was unaffected by 10% fluctuations in the insulation material and installation cost.

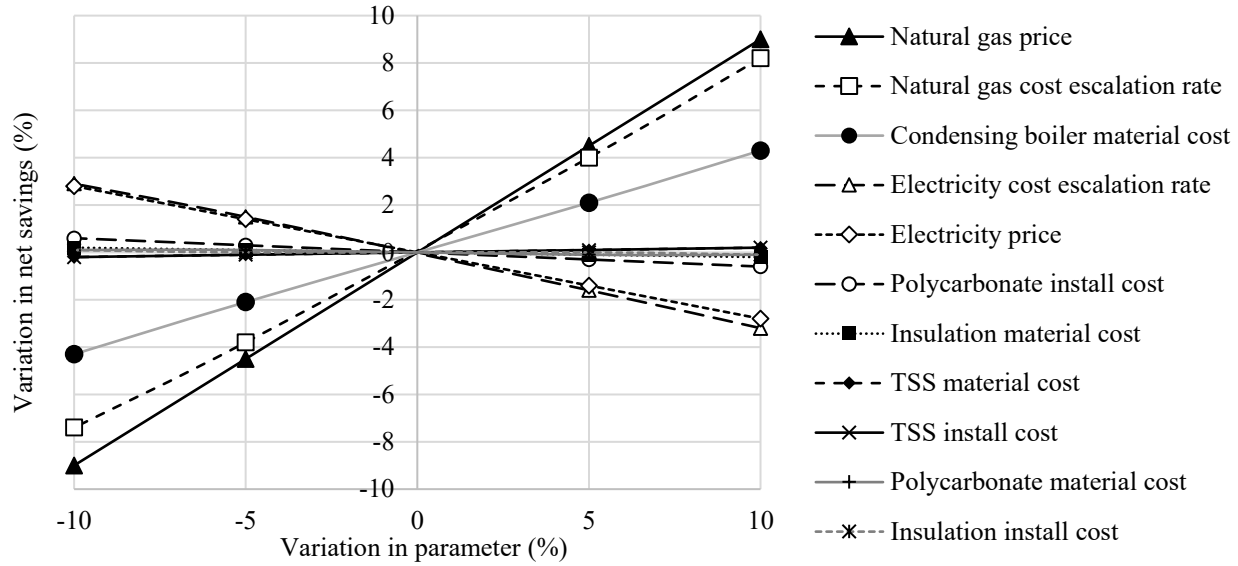

Figure H.1: Sensitivity analysis for percentage change in NS given percent change in parameter – AGH design with highest net savings for Ottawa.

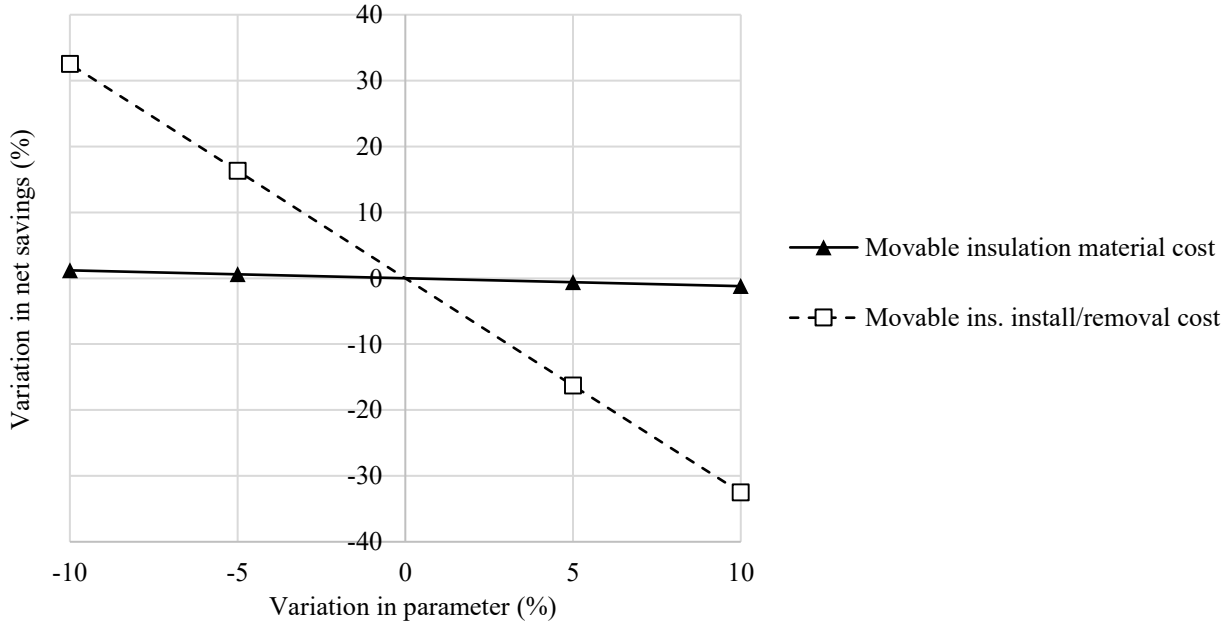

Figure H.2: Sensitivity analysis for percentage change in NS given percent change in parameter - north wall movable insulation for Ottawa.

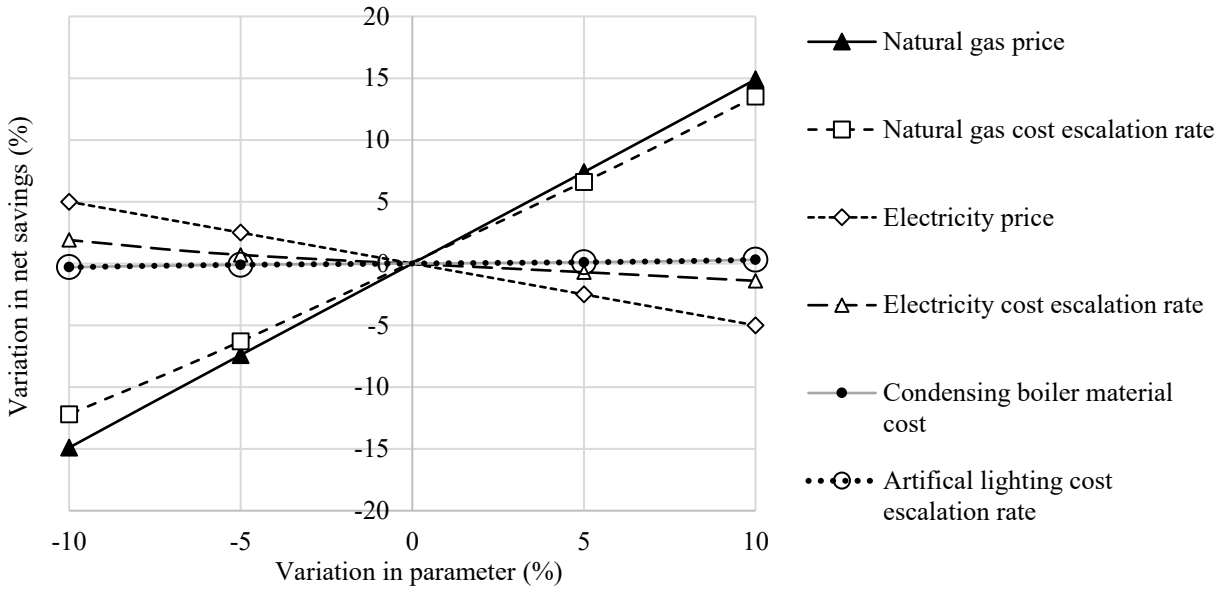

Figure H.3: Sensitivity analysis for percentage change in NS given percent change in parameter - AGH design with highest net savings for Whitehorse.

There is usually less uncertainty about material and labor cost and the price of energy (electricity, natural gas, propane) because their current costs are specified at the base date. Therefore, it may be advisable to spend additional effort on determining the degree of uncertainty associated with the electricity and fuel cost escalation rates. The impact of various energy escalation rate scenarios on the economic results was performed. Table H.1 provides to change in net savings that would results from having a fuel cost escalation rate of 2%, 0% and -2%. The percent change is based on the AGH design with the highest net savings compared to the BCGH. For Ottawa, a lower natural gas cost escalation rate could decrease the net savings by up to 58.6%. For Whitehorse, a lower propane cost escalation rate could decrease the net savings could by up to 96.8%. Therefore, the renewable energy transition could have a disruptive impact on the net savings outcome and deserves careful examination to assess the risk associated with alternative envelope designs.

Table H.1: Effect of predicted energy cost escalation rate on net savings.

		Fuel cost escalation rate		
		2%	0%	-2%
Change in net savings	Ottawa	-38.0%	-49.9%	-58.6%
	Whitehorse	-62.7%	-82.4%	-96.8%

APPENDIX I: Energy and Economic Analysis of Ground Insulation for Raft Hydroponic Greenhouse

I.1 Greenhouse Characteristics

The analysis of Chapter 6 was repeated for a greenhouse that grows leafy greens vegetables in a raft hydroponic system. As shown in Fig. I.1, in a raft system, plants grow in floating planting trays with the roots submerged in nutrient rich water (typically 0.25-0.3 m deep) (Albright, 2005). Trays with seedlings are loaded at one end of the greenhouse and the finished trays are harvested at the other.

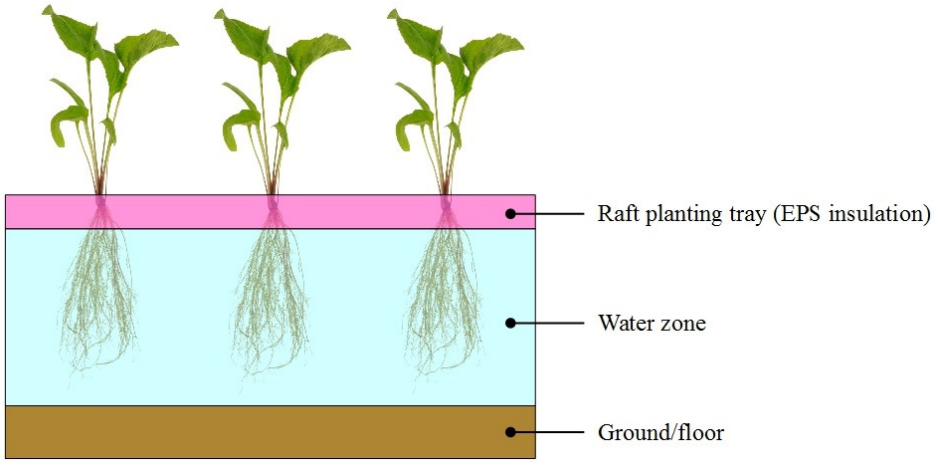

Figure I.1: Cross section of raft hydroponic growing system.

I.2 Energy Analysis

The methodology for the daylighting, artificial lighting control and thermal modules is the same as described in section 6.5, except for those presented below.

To model the water zone, another thermal zone is added below the ground surface of the crop zone. The Type 56 multi-zone building model is intended to be used to model air zones. However, other fluids such as water can be modeled when they are well-mixed, and the appropriate thermal capacitance and interior convective and radiative heat transfer characteristics are specified. The top surface of the water zone consists of typical raft trays made from EPS (with assumed uniform thermal properties that are identical to EPS thermal insulation boards) (Speedling, 2018) and the bottom surface is specified as a thin soil layer (25 mm thick) this is

directly in contact with the discretized ground zone below. Fig. I.2 shows the two thermal zones and the four airnodes that define the raft hydroponic greenhouse.

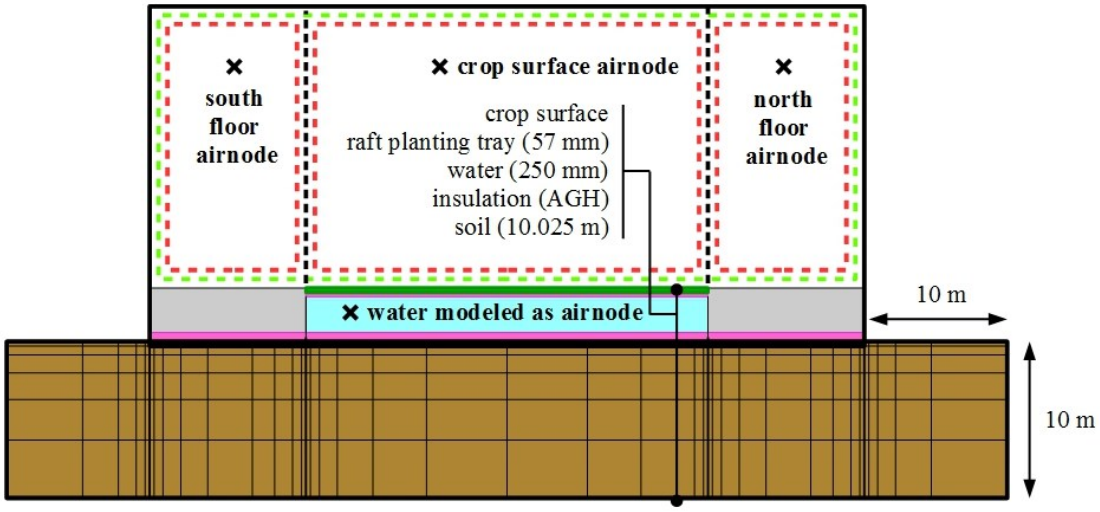

Figure I.2: Raft hydroponic greenhouse with discretized ground zone.

Fig. I.3 illustrates the major mass and energy fluxes that are considered in the raft hydroponic greenhouse model.

The energy balance for the additional water airnode is written as:

$$\rho_w \cdot c_{p\_w} \cdot V_w \cdot (\partial T_w / \partial t) = Q_{conv\_si\_w} + Q_{heat\_w} + Q_{cool} \quad \text{(I.1)}$$

where

ρ_w is the density of water (kg m^{-3})

c_{p_w} is specific heat of water at constant pressure (kJ kg^{-1} °C^{-1})

V_w is the volume of the water zone (m^3)

∂T_w is the rate of change of the water zone temperature (°C)

$Q_{conv\_si\_w}$ is the energy flux due to convection (W)

Q_{heat_w} is the energy flux from auxiliary heating (W).

Q_{cool} is the energy flux from auxiliary cooling (W).

The energy balance for the top surface of the water airnode (raft planting tray surface that is in contact with water) and for the bottom surface of the water airnode is expressed as:

$$0 = Q_{cond} + Q_{conv\_si\_w} \quad \text{(I.2)}$$

The mass balance of the water zone is not presented because evaporation is neglected.

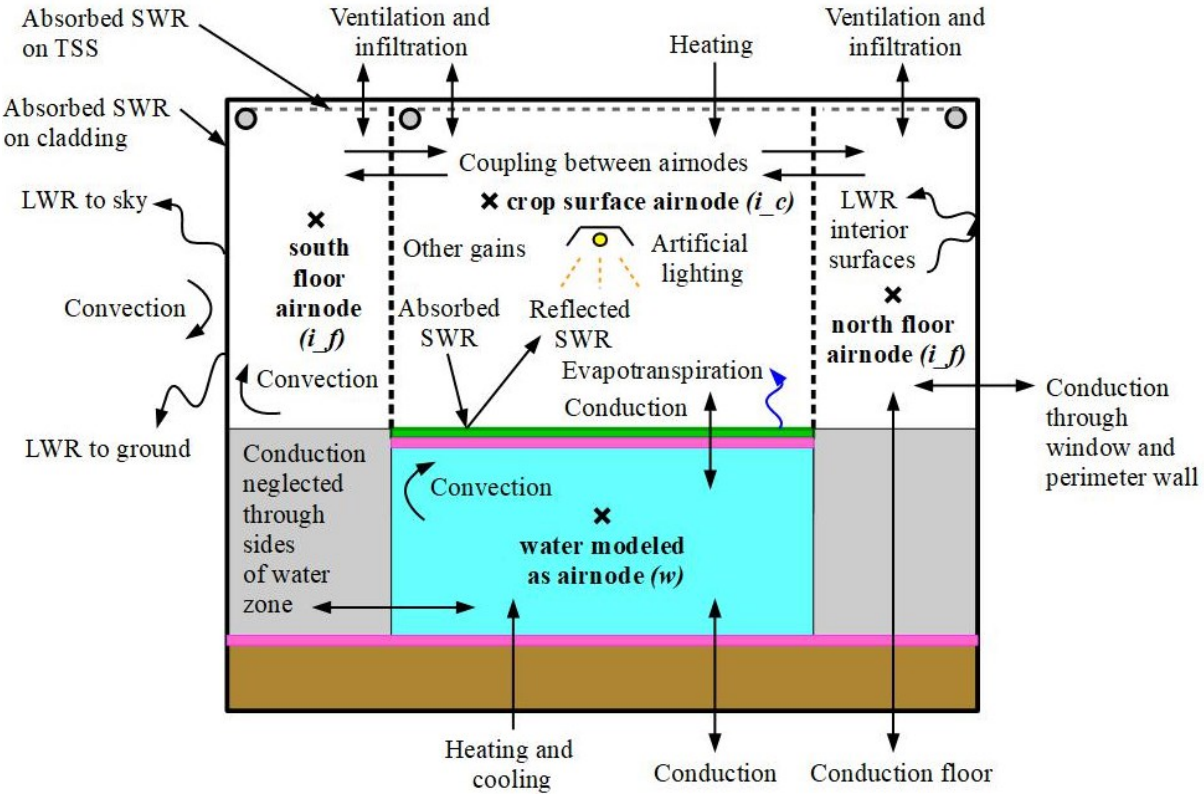

Figure I.3: Schematic showing the mass and energy fluxes considered in the raft hydroponic greenhouse model.

Modeling key assumptions

Water zone: The convection heat flux between the inside surfaces of the water zone and the water ($Q_{conv\_si\_w}$ in W) is calculated by:

$$Q_{conv\_si\_w} = h_w \cdot A_{si} \cdot (T_{si} - T_w) \quad \text{(I.3)}$$

where

h_w is the inside surface convective heat transfer coefficient (W m^{-2} °C^{-1})

T_w is water temperature (°C).

To calculate the inside CHTC, the type of convection must first be established. Since there is some recirculation of water inside the water zone, forced convection exists. The type of forced convection is determined from the Reynolds number (Re_w) which is calculated as:

$$Re_w = \left(\rho_w \cdot V_{avg} \cdot D_{h\_w}\right)/\mu_w \tag{I.4}$$

where

V_{avg} is the average velocity of water flowing through the water zone (m s^{-1})

D_{h_w} is hydraulic diameter (m)

μ_w is dynamic viscosity of water (kg m^{-1} s^{-1}).).

where

$$V_{avg} = WCH \cdot (D_w \cdot L_w \cdot W_w)/(3600 \cdot D_w \cdot L_w) \tag{I.5}$$

where

WCH is the number of changes per hour of recirculating water (hr^{-1})

D_w is the water zone depth (m)

L_w is the water zone length (E-W direction) (m)

W_w is the water zone width (N-S direction) (m)

the factor 3600 serves to convert units hr to s.

$$D_{h\_w} = 4 \cdot (D_w \cdot L_w)/[2 \cdot (D_w + L_w)] \tag{I.6}$$

The Reynolds number is calculated to be 1909 using the assumed recirculation water flow value (Table I.1) and since it is below 2300, the flow is laminar. Then, the Nusselt number (Nu) is obtained using analytical values for laminar flow in rectangular tubes (Cengal, 2007). The inside surface CHTC (h_w in W m^{-2} °C^{-1}) can then be computed from:

$$h_w = (k_w \cdot Nu)/D_h \tag{I.7}$$

The heat transfer from the perimeter walls of the water zone are neglected by specifying a high thermal resistance. Radiative heat transfer within the water zone is neglected.

Thermal energy consumption: In raft hydroponic systems, the temperature of the water is carefully controlled. For optimal growth conditions, heating is typically applied to maintain the water above 24°C and cooling to keep it below 26°C (Albright, 2007). In this study, the water was heated to the same temperature as the air (20°C) to enable comparison between both greenhouses (concrete slab/soil floors and raft hydroponic system). However, a simulation will also be performed for the optimal heating setpoint temperature of 24°C for comparison purposes. The output of the TRNSYS simulation provides the cooling power at each timestep (Q_{cool} in kJ hr^{-1}) that is required to maintain the desired setpoint temperature. The annual thermal energy consumption for cooling (Q_{cool_yr} in GJ yr^{-1}) is expressed as:

$$Q_{cool\_yr} = \sum_{\Delta t=0}^{365\cdot 24/\Delta t}(Q_{cool} \cdot \Delta t/10^6) \quad \text{(I.8)}$$

where the factor 10^6 serves to convert units kJ to GJ.

When cooling is provided by an electric chiller, the electricity consumption (E_{cool_yr} in kWh yr^{-1}) is computed as:

$$E_{cool\_yr} = \left(10^6 \cdot Q_{cool\_yr}\right)/(3600 \cdot COP) \quad \text{(I.9)}$$

where

COP is the chiller coefficient of performance (dimensionless)
the factor 10^6 serves to convert units kJ to GJ
the factor 3600 serves to convert units hr to s.

The chiller size was estimated based on the maximum cooling energy obtained from the TMY energy simulations.

Table I.1 provides the additional parameters used in the raft hydroponic model.

Table I.1: Parameter values for the greenhouse model.

Material/component	Parameter	Symbol	Value	Reference
Water zone	Length	L_W	30.48 m	Assumed
	Width	W_W	24.384 m	Assumed
	Depth	D_w	250 mm	Albright (2005)
	Hydraulic diameter	D_{h_w}	0.504 m	Calculation from Eq. (I.6)
	Flow rate (recirculation)	WCH	0.5 /hr	Assumed
	Thermal conductivity	k_W	0.607 W m^{-1} °C^{-1}	Cengal (2007)
	Density	ρ_W	997 kg m^{-3}	
	Specific heat	c_{p_W}	4.2 kJ kg^{-1} °C^{-1}	
	Dynamic viscosity	μ_w	$0.891 \cdot 10^{-3}$ kg m^{-1} s^{-1}	
	Nusselt number	Nu	8.24	
	Inside CHTC	h_w	9.9 W m^{-2} °C^{-1}	Calculated from Eq. (I.7)
	Heating setpoint temperature	$T_{sp\_heat\_w}$	20°C	Albright (2005)
	Cooling setpoint temperature	$T_{sp\_cool\_w}$	26°C	
	Thermal resistance of vertical walls around perimeter	R_w	17.6 m^2 °C W^{-1}	Assumed
Raft planter trays* (EPS)	Thickness	l_{ins_r}	57 mm	Speedling (2018)
Chiller	Coefficient of performance	COP	4	Kozai (2005)

* thermal properties same as for ground insulation

I.3 Economic Analysis

The methodology for the economic analysis is the same as described in section 6.6.

I.4 Results and Discussion

The present-value costs, residual value, net savings, and change in life cycle cost for the raft hydroponic AGH and BCGH are provided in Table I.2 for Ottawa. Table I.3 gives the annual lighting electricity use and fuel consumed for heating for Ottawa.

For the raft hydroponic greenhouse, the economic results were improved (net savings of $2,959 and decrease in LCC of 0.1%) when perimeter insulation is applied. When horizontal floor zone insulation is added, the net savings decreased from $2,959 to $673. Therefore, the use of perimeter and floor zone insulation decreased net savings compared to perimeter alone. Therefore, the case of perimeter and crop zone insulation was assessed next and found to be the most cost-effective design (net savings of $4,942 and 0.2% decrease in LCC). The case of

perimeter and floor plus crop zone insulation is shown for reference (net savings of $4,399). However, since the use of floor insulation was found to decrease net savings compared to perimeter alone, it can be predicted that it would not be as cost effective as the case without floor insulation and could be rejected as a viable design permutation without needing to perform calculations. Although this analysis provided insight into the most cost-effective greenhouse ground insulation design in Ottawa, the net savings are negligible compared to the greenhouse LCC (decrease in LCC of 0.1%). For the designs that achieved the highest net savings, heating energy was reduced by 1.9%.

Table I.2: Present-value costs, residual value, net savings, and change in life cycle cost for the greenhouse models for Ottawa.

Floor type	Insulation location and thickness	Energy cost	Incremental initial investment cost	Capital replacement cost	Residual value	Net savings	Change in LCC
Raft hydroponic	BCGH (no insulation)	$1,648,469	$0	$84,949	$25,586	-	-
	50 mm vertical perimeter	$1,644,598	$912	$84,949	$25,586	$2,959	-0.1%
	50 mm vertical perimeter and horizontal floor zones	$1,644,604	$3,192	$84,949	$25,586	$673	-0.03%
	50 mm vertical perimeter and horizontal floor plus crop zones	$1,631,759	$12,311	$84,949	$25,586	$4,399	-0.2%
	50 mm vertical perimeter and horizontal crop zone	$1,633,495	$10,031	$84,949	$25,586	$4,942	-0.2%

Table I.3: Energy consumption and greenhouse models for Ottawa.

Floor type	Insulation level	Lighting electricity consumption (kWh yr^{-1})	Natural gas consumption for heating (m^3 yr^{-1})
Raft hydroponic	BCGH (no insulation)	114,971	67,588
	50 mm vertical perimeter	114,971	67,256
	50 mm vertical perimeter and horizontal floor zones	114,971	67,257
	50 mm vertical perimeter and horizontal floor plus crop zones	114,971	66,155
	50 mm vertical perimeter and horizontal crop zone	114,971	66,304

APPENDIX J: Energy and Economic Analysis of Ground Insulation for Whitehorse, Canada

J.1 Greenhouse Characteristics

The analysis of Chapter 6 was repeated for Whitehorse, Yukon (60.7°N, high-latitude, 6,915 heating degree-days), Canada.

J.2 Energy Analysis

The methodology for the daylighting, artificial lighting control and thermal modules is the same as described in section 6.5 and Appendix I, except for those presented in Table J.1.

Table J.1: Parameter values for the greenhouse model.

Material/component	Parameter	Symbol	Value	Reference
Soil	Deep earth temperature	T_{de_soil}	-1 °C	RETScreen (2013)
	Amplitude of surface temperature	*Amp*	15.8 °C	

J.3 Economic Analysis

The methodology for the economic analysis is the same as described in section 5.6 and Appendix I, except for those presented in Table J.2.

Table J.2: Values of the cost data used in the LCCA.

Parameter	Symbol	Value	Reference
EPS insulation cost	C_{ins_mat}	7.52 \$ m^{-2}	RSMeans (2017)
EPS insulation installation cost	C_{ins_inst}	4.18 \$ m^{-2}	
Initial investment cost of greenhouse	*Inv*	\$ 691,500 (concrete slab)	Calculated in Chapter 4 but without ground insulation
		\$ 636,600 (unfinished soil)	Calculated in Chapter 4 but without ground insulation and concrete slab
		\$ 647,600 (raft hydroponic)	Calculated in Chapter 4 but without ground insulation and concrete slab only on floor zones

J.4 Results and Discussion

The average heat loss pathways for the BCGH with a concrete slab in January, were determined to be: 20.4% for infiltration, 21.2% for ventilation, 36.8% from the roof, 17.6% from the walls and 4.0% from the ground. These results are from sunset to sunrise because the ground

becomes a source of heat gain when sunlight exists. The portion of the envelope heat loss (walls, roof and ground) that occurred through the ground was approximately 7%.

The present-value costs, residual value, net savings, and change in life cycle cost for AGH and BCGH are provided in Table J.3 and Table J.4 gives the annual lighting electricity use and fuel consumed for heating.

For Whitehorse, all three greenhouse designs provided increased net savings as the area covered by insulation increased. This is presumably due to the cold climate which increases the viability of adding insulation. The highest net savings of $67,544, $68,184 and $197,433 (0.7%, 0.7% and 1.9% decrease in LCC) were achieved when vertical perimeter and horizontal floor plus crop zone insulation was applied to the concrete slab, soil floor and raft hydroponic greenhouses, respectively. For the greenhouses with a concrete slab and soil floor, the net savings increased the most (139.5% from $23,400 to $56,044 for concrete slab and 177.3% from $21,448 to $59,477 for the soil floor) when floor zone insulation was added to the design with perimeter insulation. For the raft hydroponic greenhouse, the greatest net savings increase of 285.6% (from $51,202 to $197,433) was obtained when crop zone insulation was added to the design with perimeter and floor zone insulation whereas it only increased by 29.3% when floor zone insulation was added to the design with perimeter insulation. This highlights how heat transfer to the ground is high for a water zone and adding insulation becomes particularly beneficial. Meanwhile, the impact of adding crop zone insulation (to the design with perimeter and floor zone insulation) only improved net savings by 20.5% and 14.6% for the greenhouses with a concrete slab and soil floor, respectively. These observed changes in net savings are directly related to the effect of added insulation on the amount of propane that was consumed for heating (and hence the life cycle energy cost). For instance, for the raft hydroponic greenhouse, installing insulation beneath the crop zone (in addition to the perimeter and floor zone) decreased propane consumption nearly four times more than was achieved when insulation was employed on the perimeter and floor zone. Moreover, cooling of the raft hydroponic water zone was not required for any of the studied cases.

For the designs that achieved the highest net savings, heating energy was reduced by 1.0%, 1.0% and 2.5% for Whitehorse, for the concrete slab, soil floor and raft hydroponic

greenhouses respectively. Therefore, employing ground insulation does not produce significant energy savings or economic benefit.

Table J.3: Present-value costs, residual value, net savings, and change in life cycle cost for the greenhouse models for Whitehorse.

Floor type	Insulation location and thickness	Energy cost	Incremental initial investment cost	Capital replacement cost	Residual value	Net savings	Change in LCC
Concrete slab	BCGH (no insulation)	$8,981,774	$0	$84,949	$25,586	-	-
	50 mm vertical perimeter	$8,957,504	$870	$84,949	$25,586	$23,400	-0.2%
	50 mm vertical perimeter and horizontal floor zones	$8,922,687	$3,043	$84,949	$25,586	$56,044	-0.6%
	50 mm vertical perimeter and horizontal floor plus crop zones	$8,902,490	$11,739	$84,949	$25,586	$67,544	-0.7%
Soil floor	BCGH (no insulation)	$8,837,627	$0	$84,949	$25,586	-	-
	50 mm vertical perimeter	$8,815,309	$870	$84,949	$25,586	$21,448	-0.2%
	50 mm vertical perimeter and horizontal floor zones	$8,775,106	$3,043	$84,949	$25,586	$59,477	-0.6%
	50 mm vertical perimeter and horizontal floor plus crop zones	$8,757,704	$11,739	$84,949	$25,586	$68,184	-0.7%
Raft hydroponic	BCGH (no insulation)	$9,551,836	$0	$84,949	$25,586	-	-
	50 mm vertical perimeter	$9,511,352	$870	$84,949	$25,586	$39,614	-0.4%
	50 mm vertical perimeter and horizontal floor zones	$9,497,591	$3,043	$84,949	$25,586	$51,202	-0.5%
	50 mm vertical perimeter and horizontal floor plus crop zones	$9,342,663	$11,739	$84,949	$25,586	$197,433	-1.9%

Table J.4: Energy consumption and greenhouse models for Whitehorse.

Floor type	Insulation level	Lighting electricity consumption (kWh yr^{-1})	Propane consumption for heating (L yr^{-1})
Concrete slab	BCGH (no insulation)	265,800	124,074
	50 mm vertical perimeter	265,800	123,687
	50 mm vertical perimeter and horizontal floor zones	265,800	123,133
	50 mm vertical perimeter and horizontal floor plus crop zones	265,800	122,812
Soil floor	BCGH (no insulation)	266,667	121,718
	50 mm vertical perimeter	266,667	121,363
	50 mm vertical perimeter and horizontal floor zones	266,667	120,723
	50 mm vertical perimeter and horizontal floor plus crop zones	266,667	120,446
Raft hydroponic	BCGH (no insulation)	265,800	133,145
	50 mm vertical perimeter	265,800	132,501
	50 mm vertical perimeter and horizontal floor zones	265,800	132,282
	50 mm vertical perimeter and horizontal floor plus crop zones	265,800	129,817

APPENDIX K: Sensitivity Analysis for Chapter 6

K.1 Sensitivity of Net Savings to Energy Model Input Parameter Values

The energy model input parameters to be considered are those that significantly impact energy consumption and whose value carries considerable uncertainty. In this study, the floor surface interior CHTC and the interior surfaces of the water zone in the raft hydroponic greenhouse will be assessed because they may have a significant impact on predicted heating energy and their values are not well known.

Therefore, the analysis was repeated using model parameter values that would result in higher/extreme heating energy use. An interior ground surface CHTC value of 20 W m^{-2} $°C^{-1}$ (representing high-mixing of greenhouse air using horizontal airflow fans) and water zone value of 100 W m^{-2} $°C^{-1}$ was selected for the comparison. Table K.1 presents the results for the greenhouse with a concrete slab and Table K.2 is for the raft hydroponic greenhouse. For the greenhouse with a concrete slab, a higher CHTC increased the heating energy consumption by 13.7% for the BCGH and 13.3% for the AGH design with the highest net savings. Although its effect on heating energy use is relatively small, the net savings increased significantly (190.8%). For the raft hydroponic greenhouse, a higher water zone CHTC increased the heating energy consumption by 9.5% for the BCGH and 7.8% for the AGH design with the highest net savings. Again, although its effect on heating energy use is relatively small, the net savings is highly impacted and increased by 202.9%. Therefore, the inside floor surface and water zone CHTC is a modeling parameter that greatly influences the economic result. By overestimating its value, the predicted net savings could be too optimistic. Consequently, efforts should focus on accurately determining this parameter for the specific ground cover and water/airflow patterns that exist inside the greenhouse.

Table K.1: Effect of ground surface CHTC for the greenhouse with a concrete slab for Ottawa.

Item	Insulation level	Internal calculation of CHTC	CHTC increased to 20 W m^{-2} $°C^{-1}$	% Change
Natural gas consumption for heating (m^3 yr^{-1})	BCGH	61,903	70,359	13.7%
	50 mm vertical perimeter and horizontal floor plus crop zones	61,466	69,611	13.3%
Net savings	50 mm vertical perimeter and horizontal floor plus crop zones	$1,899	$5,521	190.8%

Table K.2: Effect of water zone surface CHTC for raft hydroponic greenhouse for Ottawa.

Item	Insulation level	CHTC of 9.9 W m^{-2} $°C^{-1}$	CHTC increased to 100 W m^{-2} $°C^{-1}$	% Change
Natural gas consumption for heating (m^3 yr^{-1})	BCGH	61,903	67,788	9.5%
	50 mm vertical perimeter and horizontal floor plus crop zones	61,466	66,239	7.8%
Net savings	50 mm vertical perimeter and horizontal floor plus crop zones	$1,899	$5,752	202.9%

K.2 Sensitivity of Net Savings to Operation Parameter Values

To enable fair comparison between the three greenhouse designs, the heating setpoint temperature for the water zone in the raft hydroponic greenhouse was selected to be the same as the air setpoint temperature (20°C). However, the ideal water heating setpoint temperature is approximately 24°C (Albright, 2005). Table K.3 presents the effect of increasing the setpoint temperature on the heating energy use and economic result. A higher water setpoint temperature increased the thermal energy consumption by 12.2% for the BCGH and 10.1% for the AGH design with the highest net savings. Meanwhile, the net savings increased by 365.8%, which is very significant in relative terms. However, since the net savings was low ($1,899), the increased value ($8,844) in absolute terms remains relatively low.

Moreover, the fraction of total thermal energy that is used to heat the water zone was found to be 7.9% for the BCGH and 6.6% for the AGH design with the highest net savings. Therefore, the added insulation caused a relative decrease of 16.5% for the fraction of thermal energy needed to heat the water. Increasing the water heating setpoint temperature was found to increase this percentage of total heating by approximately 43% for both the BCGH and AGH design.

Table K.3: Effect of raft hydroponic greenhouse water heating setpoint temperature on thermal energy use and net savings for Ottawa.

Item	Insulation level	Water heating setpoint temperature			Portion of total heating for water zone		
		20°C	24°C	% Change	20°C	24°C	% Change
Natural gas consumption for heating (m^3 yr^{-1})	BCGH	61,903	69,478	12.2%	7.9%	11.3%	43.0%
	50 mm vertical perimeter and horizontal floor plus crop zones	61,466	67,663	10.1%	6.6%	9.5%	43.9%
Net savings	50 mm vertical perimeter and horizontal floor plus crop zones	1,899	8,844	365.8%	-		

K.3 Sensitivity of Net Savings to Economic Parameter Values

It is impossible to know for certain what the price of energy, materials, labor and equipment will actually be over the next 25 years or so. To identify the critical input values in the LCCA, several parameters were individually varied by ±5 and ±10% and plotted against the resulting percent changes in net savings. When one variable is modified, all others remain at their default values. Fig. K.1 and K.2 provide the results for the envelope design with highest net savings for the greenhouse with concrete floor in Ottawa and Whitehorse, respectively. Based on Fig. K.1, the critical input values (which provoke a change in NS greater than ±1% when varied by ±10%) in the LCCA for Ottawa include the natural gas price, natural gas cost escalation rate, the discount rate, and the insulation material and installation cost. A 10% increase in the natural gas price, natural gas cost escalation rate, discount rate, insulation material and installation cost caused the net savings to change by 26.8%, 24.3%, -11.0%, -8.9% and -7.9%, respectively. For all cases and both locations, the electricity price and cost escalation does not impact net savings because the electricity consumption for lighting is not affected by design permutations of the ground envelope for a given greenhouse design. For all cases and both locations, varying the replacement cost of artificial lights did not affect the net savings because, for all cases studied, they were replaced at the maximum fixture lifespan (15 years) rather than the bulb lifespan (50,000 hr).

Based on Fig. K.2, the critical input values (which provoke a change in NS greater than ±1% when varied by ±10%) in the LCCA for Whitehorse include the propane price and its cost escalation rate. A 10% increase in the propane price and its cost escalation rate caused the net

savings to change by 11.7%, 10.7% respectively. Changes in the insulation material and installation cost had a negligible (<1%) effect on the economic results. Although the percentage decrease is less for Whitehorse, the absolute change in net savings is more in that location because of the higher value of net savings that was obtained ($1,899 in Ottawa versus $67,544 in Whitehorse).

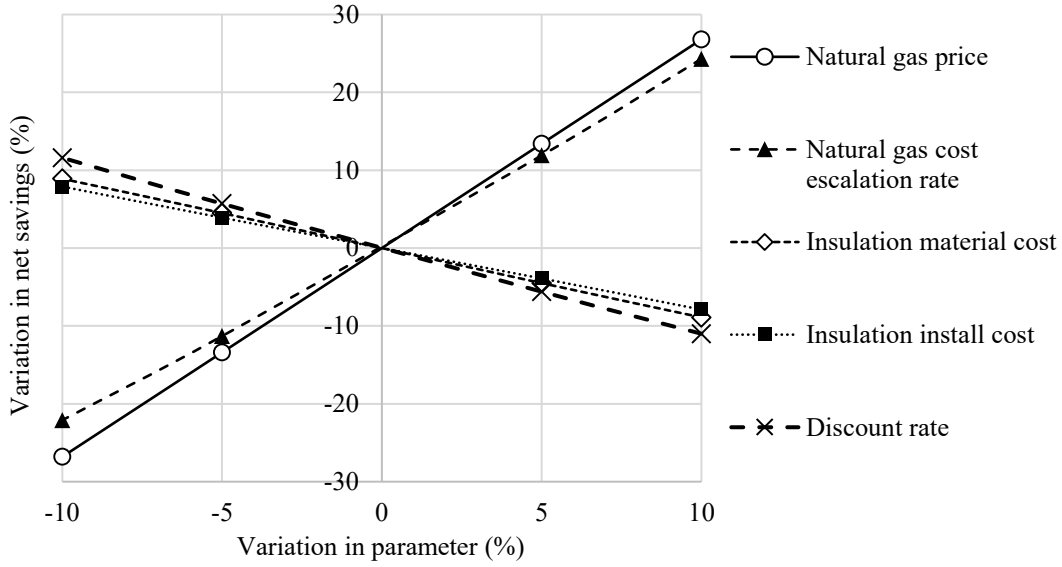

Figure K.1: Sensitivity analysis for percentage change in NS given percent change in parameter – Envelope design with highest net savings for greenhouse with concrete floor for Ottawa.

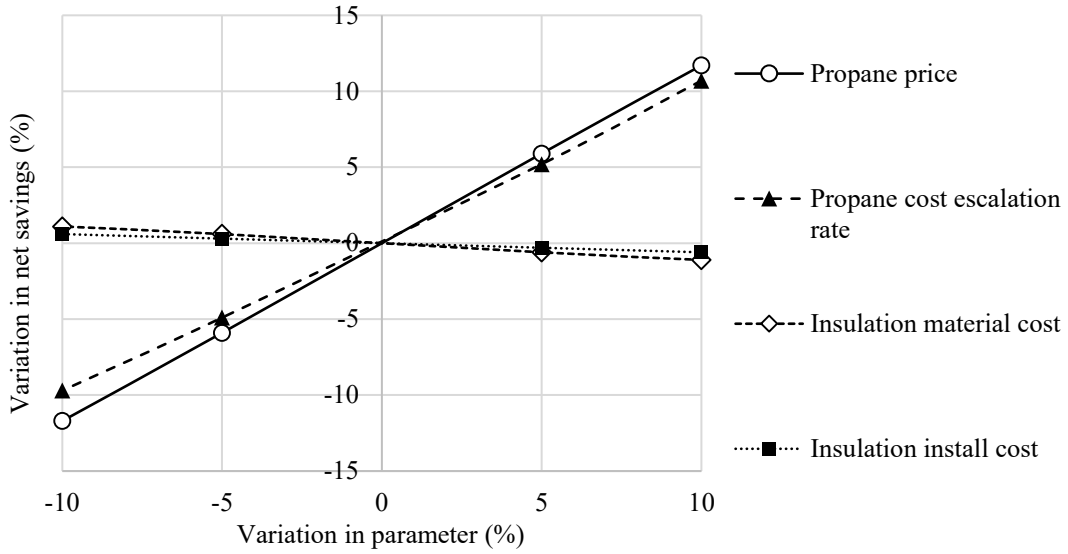

Figure K.2: Sensitivity analysis for percentage change in NS given percent change in parameter – Envelope design with highest net savings for greenhouse with a concrete slab for Whitehorse.

There is usually less uncertainty about material and labor cost and the price of energy because their current costs are specified at the base date. Therefore, it may be advisable to spend additional effort on determining the degree of uncertainty associated with the energy cost escalation rate. A comparison of the impact of various fuel cost escalation rates on the economic result was conducted, assuming the future price of energy will be lower than the values employed in this study. Table K.4 provides the change in net savings that would results from having a fuel cost escalation rate of 2%, 0% and -2%. The percent change is calculated for the greenhouse with a concrete slab for the AGH design with the highest net savings, compared to the BCGH. For Ottawa, a lower natural gas cost escalation rate could decrease the net savings by up to 174.3%. For Whitehorse, a lower propane cost escalation rate could decrease the net savings by up to 76.3%. Therefore, the impact of lower fuel cost in the future should be carefully evaluated to assess the risk associated with the proposed alternative envelope designs.

Table K.4: Effect of predicted energy cost escalation rate on net savings.

		Fuel cost escalation rate		
		2%	0%	-2%
Change in net savings	Ottawa	-113%	-148.4%	-174.3%
	Whitehorse	-49.5%	-65.0%	-76.3%

APPENDIX L: Comparison of the Energy Performance for a Greenhouse and a Vertical Farm with Semi-Transparent Photovoltaics[5]

A simulation study is performed to compare the solar energy generation and thermal energy consumption of a conventional greenhouse and a vertical farm concept employing STPV. The vertical farm carries the advantage of using less space and will likely consume less energy for heating in winter. However, a vertical construction will have less roof area and hence it is expected that less solar energy generation would result.

L.1 Design Details

Two closed greenhouse designs for the production of leafy greens in the urban environment were compared for energy performance (Fig. L.1). The base case is a single story 4000 m^2 greenhouse, whereas the alternative design is a four-storey vertical farm with a footprint of 1000 m^2 (both have a total area of 4000 m^2). The roof and east, south and west walls are all covered with STPV (60% PV cells, 30% glass and 10% framing). The north wall consists of clear glazing. The analysis is repeated for single (τ = 84.7%; U=250 W m^{-2} °C^{-1}) and double (τ = 72.6%; U=1.8 W m^{-2} °C^{-1}) STPV. The floor consists of 100 mm concrete. The plants are grown on eight stacked shelves 0.8 m wide with 0.4 m vertical spacing and 1 m horizontal spacing between rows. LED grow lights are used to provide 11 mol m^{-2} day^{-1} on the total crop production area of 14,080 m^2 (Philips, 2012).

L.2 Energy Modeling

An energy model was created to compare the two greenhouse design options. The details for the energy and mass transfer are reported in Bambara and Athienitis (2015a).

[5] Bambara, J., & Athienitis, A. (2015a). Experimental evaluation and energy modeling of a greenhouse concept with semi-transparent photovoltaics. Energy Procedia, 78, 435-440. (this Appendix contains a part of the paper that was submitted and presented at the 6th International Building Physics Conference held in Torino, Italy – 14-17th June, 2015)

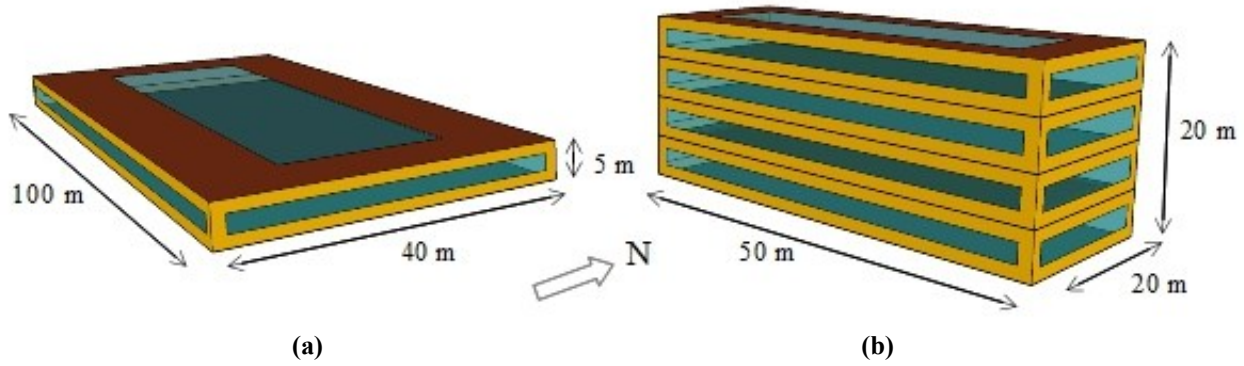

Figure L.1: (a) Cross section showing the horizontal greenhouse; and (b) vertical farm.

L.3 Results and Discussion

Annual simulations of the model were performed using hourly typical meteorological year data for Montreal, Canada. Fig. L.2 compares the monthly heating (+) and cooling (-) energy demand of the greenhouse and vertical farm for single (Fig. L.2a) and double-glazed (Fig. L.2b) STPV cladding. For each month, it is found that the vertical farm consumes less heat than the greenhouse (up to 40.1%). During the summer, the greenhouse requires more cooling than the vertical farm, whereas during the spring and fall, the opposite occurs. When the exterior air temperature is below the greenhouse setpoint, free cooling should be provided using a heat exchanger with the exterior air.

Table L.2 presents the annual energy consumption and electrical energy generation for the greenhouse and vertical farm. The simulation results are provided for both single-glazed and double-glazed STPV cladding for comparison. It is found that the vertical farm consumes 31.3% and 18.3% less heating energy than the greenhouse for the single- and double-glazed STPV cladding, respectively. The vertical farm consumes less heat because it has 30% less surface area exposed to the exterior than the greenhouse does. The use of double-glazing reduces the annual demand for heating by 76.1% for the greenhouse and 71.5% for the vertical farm.

For the cooling energy demand, the difference between both designs is much smaller. It is found that the vertical farm consumes 5.5% more cooling than the greenhouse using the single-glazed STPV, and 1.5% less cooling using the double-glazed STPV. The use of double glazing

increases the annual demand for cooling by 35.2% for the greenhouse and 26.3% for the vertical farm.

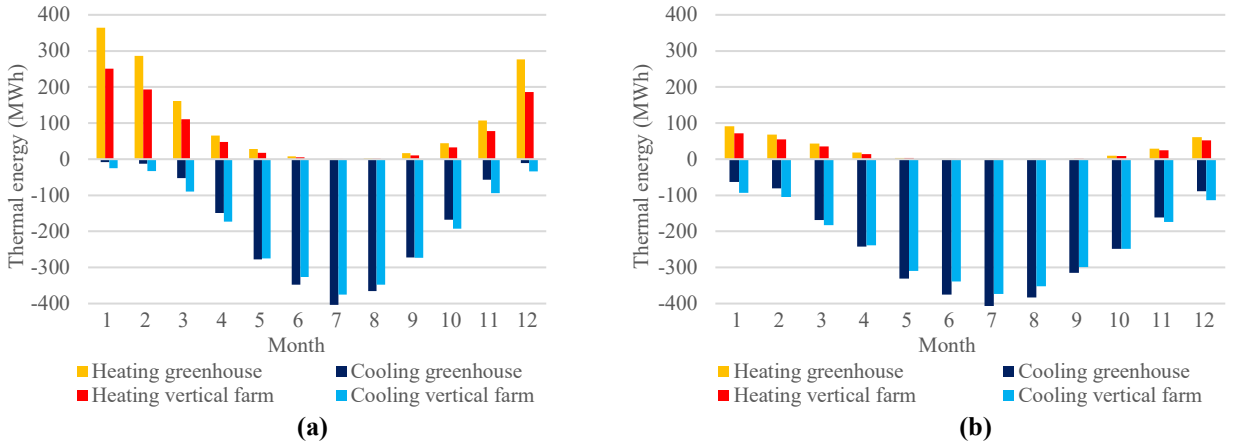

Figure L.2: (a) Thermal energy demand for the greenhouse and vertical farm using single glazed STPV; and (b) double glazed STPV.

Table L.1: Annual energy consumption and production (MWh yr^{-1}) for the greenhouse (GH) and vertical farm (VF).

Envelope material	Heating energy			Cooling energy			PV electricity			Electric energy
	GH	VF	Var.	GH	VF	Var.	GH	VF	Var.	
Single glazed STPV	1362.0	935.4	31.3%	2123	2239.0	5.4%	570.9	289.5	49.3%	3460.2
Double glazed STPV	325.6	266.2	18.3%	2870.9	2828.1	1.5%	572.2	289.9	49.3%	3460.2
Variation	76.1%	71.5%	-	35.2%	26.3%	-	0.2%	0.1%	-	-

The solar electricity generated by the greenhouse is nearly double that of the vertical farm. This is a result of the greenhouse having a roof area four times greater than the vertical farm. The use of single and double STPV has a negligible impact on the solar electricity generation. It is found that the STPV cladding can produce 16.5% of the annual electricity required to operate the greenhouse and 8.4% to operate the vertical farm.

APPENDIX M: Integration of Organic Waste Recycling and Greenhouse Agriculture[6]

M.1 Abstract

The objective of this paper is to determine the potential for using organic waste to operate greenhouses in Canada. TRNSYS was used to perform annual energy simulations of a 4,000 m^2 greenhouse. Results indicate that 9.1 million wet tonnes yr^{-1} organic waste could be used to operate 1.12 million m^2 of new greenhouse agriculture area while producing 1,072 GWh yr^{-1} and 2,070 GWh yr^{-1} of exportable electrical and thermal energy, respectively. This research addresses the imminent problems of food and energy security, while at the same time offering promising solutions to the urgent issues of climate change and local food production.

M.2 Introduction

Concerns around waste management are growing, led by a lack of available landfill sites, the increasing costs of disposal, and the environmental degradation produced by current practices. Organic waste, consisting mainly of municipal wastes (food scraps and yard waste), farming wastes (livestock manure and agriculture residues) and sewage sludge, is the largest contributor to the waste stream, and must therefore be at the centre of strategies for waste reduction, reuse and recycling. Biological treatment using anaerobic digestion (i.e. the breakdown of organic waste by bacteria in the absence of oxygen), followed by composting, has been shown to be an effective way to recycle organic waste. With the Canadian government's objective of increasing the rate of recycled organic waste from approximately 20% today, we are thus presented with a unique opportunity to rethink the design of Organic Waste Recycling (OWR) facilities before they are built (Statistics Canada, 2007).

Ideally, OWR facilities should be designed to treat both municipal and farming organic waste streams together. This method, known as co-digestion, carries numerous advantages: 1) we gain great economies of scale compared to treating the wastes separately; 2) the energy production and operational stability of the biological process is improved; and 3) high-quality fertilizer suitable for greenhouse agriculture can be produced, allowing for essential nutrients

[6] The contents of this Appendix were presented and submitted as a paper at the 4th Climate Change and Technology Conference held in Montreal, Canada – May 25-27th, 2015 (Bambara and Athienitis, 2015b).

such as phosphorus, nitrogen and potassium to be recycled. Farming wastes, in particular livestock manures, significantly contribute to environmental degradation. Yet despite this, OWR facilities today are generally designed to treat municipal waste separately from farming waste, and there are currently no plans for the combined treatment of both streams.

Co-digestion facilities can also be combined with greenhouses to integrate waste management and agricultural goals. This carries immense promise owing to several benefits: 1) the energy and fertilizer produced by the OWR facility can be used to operate a greenhouse, thereby saving resources; 2) great economies of scale can be achieved in the purchase of the greenhouses' mechanical and HVAC equipment; and 3) greater efficiency is gained in the material and energy flow between the greenhouse and OWR facility. Today, there are only a few examples where greenhouses are combined with OWR. The Swiss biogas company Kompogas has built one such facility, where tomatoes are grown inside an adjacent greenhouse using energy and fertilizer from the OWR process (Kompogas, 2007).

Fig. M.1 shows how OWR outputs satisfy all the requirements for operating the greenhouse. The greenhouse's organic waste is treated by the OWR facility, which can be achieved most efficiently with the greenhouse located on-site. By converting approximately 50% of the waste's volatile solids into energy in the form of biogas, the anaerobic digestion process reduces the volume of the organic waste by about 30% (Environment Canada, 2013). The produced biogas can be burned in a CHP engine to produce electricity, heat, carbon dioxide and water. Carbon dioxide can be supplemented to the greenhouse to accelerate crop growth and improve crop quality. The residual organic waste, or digestate, is then composted at thermophilic temperature to obtain a pathogen-free compost fertilizer.

This research aims to identify optimal methods for combining greenhouses with co-digestion facilities and to determine the potential for building such facilities in Canada. The energy produced from the organic waste would be entirely used to operate the OWR process and the integrated greenhouses during peak winter design conditions. It is assumed that all of the produced biogas would be combusted in a CHP engine, and that the electricity and thermal energy not used by the greenhouses would be exported to the grid and used for district heating.

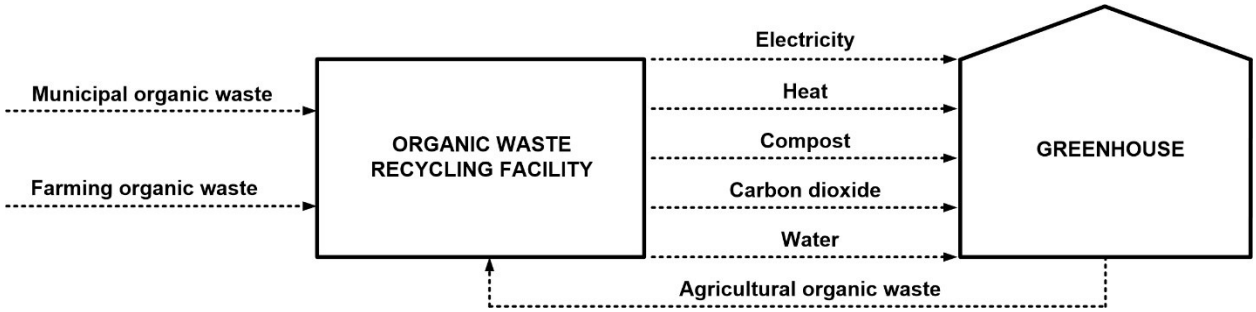

Figure M.1: Integration of OWR and greenhouse agriculture.

M.3 Organic Waste Inventory and Outputs

An important design consideration is the mixture of organic wastes that would produce a high-quality compost fertilizer suitable for greenhouse agriculture. A feedstock mixture consisting of 75% municipal organic waste (food scraps and yard waste) and 25% livestock manure would provide a fertilizer with the adequate carbon and macronutrient content (dela Cruz et al., 2006). The analysis assumes that all of the available municipal organic waste would be treated by these facilities, and that a portion of the total livestock manure would be co-digested in order to obtain the desired mixture. Table M.1 shows the amount of municipal organic waste generated per province, $M_{municipal}$ (Sinclair, 2006). Based on this, the amount of livestock manure, M_{manure}, required for the co-digestion mix is:

$$M_{manure} = \frac{M_{municipal}}{1 - f_{manure}} - M_{municipal} \tag{M.1}$$

where f_{manure} is the fraction of manure in the mix (25%) (dela Cruz et al., 2006).

The methane production rate from organic waste, $V_{methane}$, is determined using:

$$V_{methane} = f_{dry} \cdot f_{solids} \cdot S_{\deg raded} \cdot Y_{methane} \cdot \left(M_{municipal} + M_{manure}\right) \tag{M.2}$$

where f_{dry} is dryness of the waste (27%), f_{solids} is the solids:minerals ratio (90:10), $S_{destroyed}$ is the anaerobic degradation efficiency (50%) and $Y_{methane}$ is the theoretical yield of methane (0.5 Nm^3 methane per kg of dry organic solids degraded obtained by stoichiometry, $C_5H_7NO_2$ (average elemental formula for biomass) + 3 H_2O → 2.5 CH_4 + 2.5 CO_2 + NH_3, i.e. 0.35 kg CH_4 or 0.5 Nm^3CH_4 kg^{-1} dry organic solid degraded).

The amount of compost produced is assumed to be 40% of the input organic waste (ZWE, 2013).

Table M.1 shows the amount of organic waste (in wet tonnes) treated by co-digestion and the methane and compost production for each province. The co-digestion of 9.1 million wet tonnes yr^{-1} of organic waste in Canada would produce 546.8 million m^3 yr^{-1} of methane and 3.6 million tonnes yr^{-1} of compost.

Table M.1: Inventory of wastes, energy and fertilizer production.

Provinces	Percent of total waste generation	Food scraps and yard waste (tonnes yr^{-1})	Livestock manure (tonnes yr^{-1})	Total organic waste (tonnes yr^{-1})	Methane production (m^3 yr^{-1})	Compost production (tonnes yr^{-1})
Maritimes	5%	312,322	104,107	416,429	24,985,760	166,572
Quebec	27%	1,819,837	606,612	2,426,449	145,586,960	970,580
Ontario	37%	2,503,665	834,555	3,338,220	200,293,200	1,335,288
Manitoba	4%	274,010	91,337	365,347	21,920,800	146,139
Saskatchewan	4%	290,047	96,682	386,729	23,203,760	154,692
Alberta	12%	846,993	282,331	1,129,324	67,759,440	451,730
British Columbia	12%	788,787	262,929	1,051,716	63,102,960	420,686
Total	100%	6,835,661	2,278,554	9,114,215	546,852,880	3,645,686

The electrical and thermal power (Q_{elec} and $Q_{thermal}$) produced by the combustion of methane in a CHP engine is given by:

$$Q_{elec} = V_{methane} \cdot HV_{methane} \cdot \eta_{elec} \tag{M.3}$$

$$Q_{thermal} = V_{methane} \cdot HV_{methane} \cdot \eta_{thermal} \tag{M.4}$$

where, $HV_{methane}$ is the median heating value of methane, 37 MJ m^{-3}, and η_{elec} is the electrical efficiency (35%) and $\eta_{thermal}$ is the thermal efficiency (45%) of the CHP engine, based on the performance reported by manufacturers (EPA, 2008).

The electrical and thermal power consumed by the OWR facility is assumed to be 5% and 10% of the biogas production, respectively (Bernstad and la Cour Jansen, 2011). The exportable power available for operating greenhouses, Q_{elec_export} and $Q_{thermal\_export}$, is determined by subtracting the power produced from the power consumed by the OWR facility. Table M.2

shows how OWR in Canada could produce 192,481 kW and 224,561 kW of electrical and thermal power, respectively, that could be used to operate the greenhouses.

Table M.2: Electrical and thermal power production and use by the OWR facility.

Provinces	Peak electrical power production [kW]	Peak thermal power production [kW]	Peak electrical power use [kW]	Peak thermal power use [kW]	Exportable electrical power [kW]	Exportable thermal power [kW]
Maritimes	10,260	13,192	1,466	2,931	8,794	10,260
Quebec	59,784	76,865	8,541	17,081	51,244	59,784
Ontario	82,249	105,748	11,750	23,500	70,499	82,249
Manitoba	9,002	11,573	1,286	2,572	7,716	9,002
Saskatchewan	9,528	12,251	1,361	2,722	8,167	9,528
Alberta	27,825	35,775	3,975	7,950	23,850	27,825
British Columbia	25,913	33,316	3,702	7,404	22,211	25,913
Total	224,561	288,721	32,080	64,160	192,481	224,561

M.4 Greenhouse Details

This section covers the design, modeling and control of the greenhouse that would be integrated with the OWR facility. The greenhouses would operate using the available energy from the organic waste recycling process. In order to calculate the potential greenhouse area, its peak electrical and thermal energy requirements must first be determined.

Greenhouse design

Fig. M.2 illustrates the 4,000 m² greenhouse that was selected for the analysis. The envelope consists of air-filled double-glazing (72.6% solar transmittance at normal incidence angle; the U-value found using the program Windows 7.3 is U=2.91 W m^{-2} °C^{-1} for the walls and U=3.45 W m^{-2} °C^{-1} for the roof) with 10% framing (U=4 W m^{-2} °C^{-1}). There is a 0.8 m high wall around the greenhouse perimeter composed of concrete 0.15 m thick with rigid insulation (U=1 W m^{-2} °C^{-1}) on the exterior. The floor consists of a concrete slab 0.1 m thick.

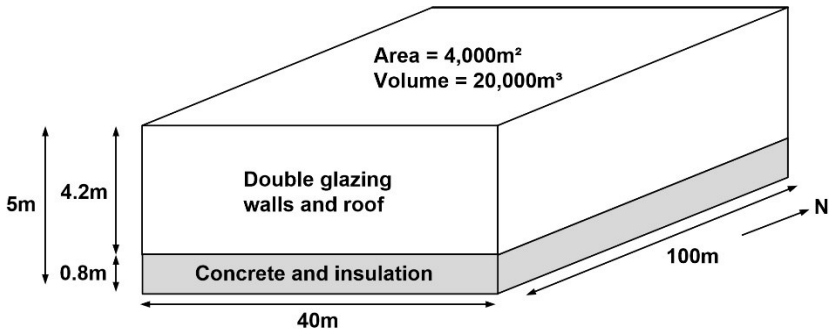

Figure M.2: Greenhouse geometry and dimensions.

Greenhouse energy modeling

TRNSYS 17.2 is the simulation environment used for the transient simulation of the greenhouse. The details for the energy and mass transfer are reported in Bambara and Athienitis (2015b).

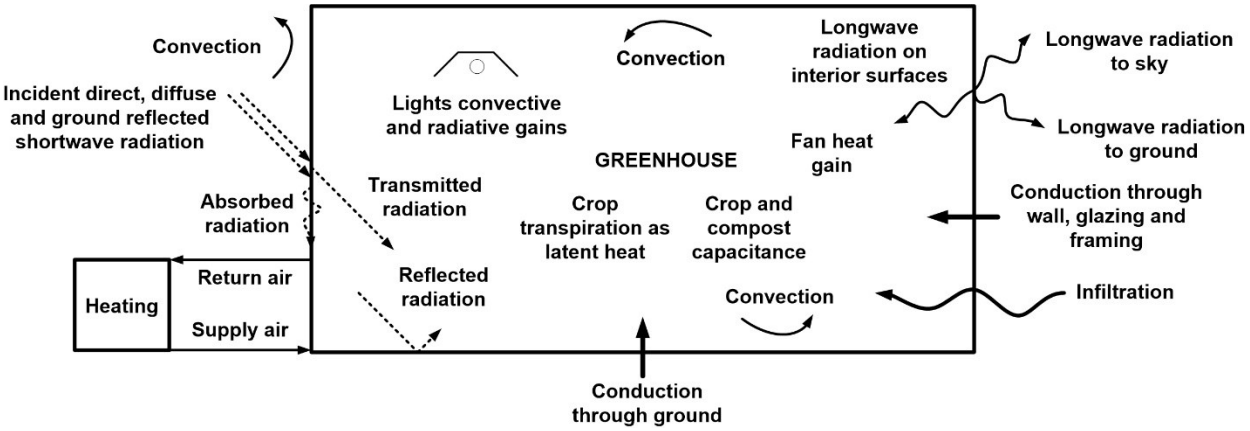

Figure M.3: Energy transfer mechanisms considered for the greenhouse model.

Greenhouse climate control

Exterior air is delivered to the greenhouse in order to regulate temperature and humidity. Fig. M.4 provides details on the greenhouse climate control strategies. The ventilation system design consists of under-channel ducted air distribution which has been proven to increase ventilation efficiency by delivering fresh air directly to the plants (Van den Bulck et al., 2013). This technique uses blowers to push conditioned air through flexible plastic ducts positioned beneath suspended growth channels. Ventilation air is supplied by a fan (20 W m^{-2}) at a rate of 120 kg hr^{-1} m^{-2} and at a heating setpoint temperature of 18°C, with between 5-100% consisting

of fresh exterior air, depending on the exterior environmental conditions (Adams et al., 2007). When the exterior air temperature is above 18°C, the supply air is 100% exterior air, whereas when the exterior air temperature is below 0°C and there is no sun, the supply air consists of its minimum value of 5% exterior air. For exterior air temperatures between 0-18°C, the ventilation rate is calculated using linear algorithms based on the exterior temperature and horizontal solar radiation. A heat exchanger (type 760) is used to transfer heat from the exhaust air stream to the exterior air stream. A sensible heat transfer efficiency of 75% is assumed.

Thermal screens are used to reduce night heat loss. The movable screens increase the thermal resistance of the greenhouse envelope by 0.125 m^2 $°C^{-1}$ W^{-1} and is activated during the night when the ambient air temperature is below 5°C. Blinds are used to reduce overheating inside the greenhouse. Two movable blinds of 50% and 75% transmittance are activated when the ambient air temperature is above 10°C and the total horizontal irradiance is above 400 W m^{-2} and 600 W m^{-2}, respectively.

Artificial lighting is provided by high-pressure sodium lights with an intensity of 150 W m^{-2}. The lights are on for 16 hr day^{-1} (5am-9pm) from December to February, and for 12 hr day^{-1} from October to November and March to April (lights are off during hours of peak solar radiation from 12pm-4pm). The lights are off from May to September. It is assumed that 10% of the light's energy is convected to the air node and 90% is emitted as radiation. The latent heat due to evapotranspiration is assumed to be equal to the rate of irrigation water supplied to the plants, which ranges from 0.04-0.4 kg hr^{-1} m^{-2} depending on the level of solar radiation (Climax Conseils, 2014).

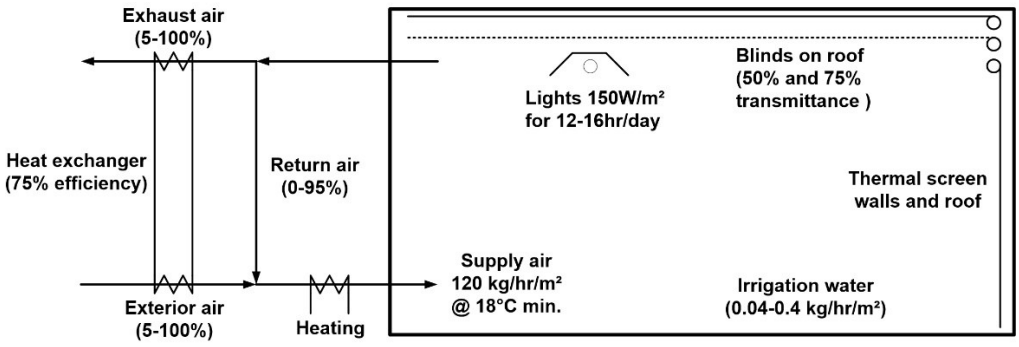

Figure M.4: Greenhouse climate control details.

M.5 Results and Discussion

Greenhouse climate during peak design conditions

Energy simulations were performed for both a warm sunny day and a cold winter day in order to verify that the greenhouse temperature is maintained within a suitable range for crop production. Hottel's clear sky model (Hottel, 1976) was used to calculate the incident solar radiation on the greenhouse surfaces. An exterior relative humidity of 90% and a wind speed of 0.5 m s^{-1} and 10 m s^{-1} were selected for the summer and winter days, respectively. Fig. M.5 shows the results for the daily variation in greenhouse air temperature and the defined peak exterior air temperatures and total horizontal solar radiation levels. The minimum and maximum greenhouse air temperature is found to be 15°C and 43°C for the winter and summer design day, respectively. The peak summer greenhouse air temperature is too high for most plants. However, the analysis did not consider the effect of cooling the greenhouse, which can be achieved using excess heat from the CHP engine to drive an absorption chiller.

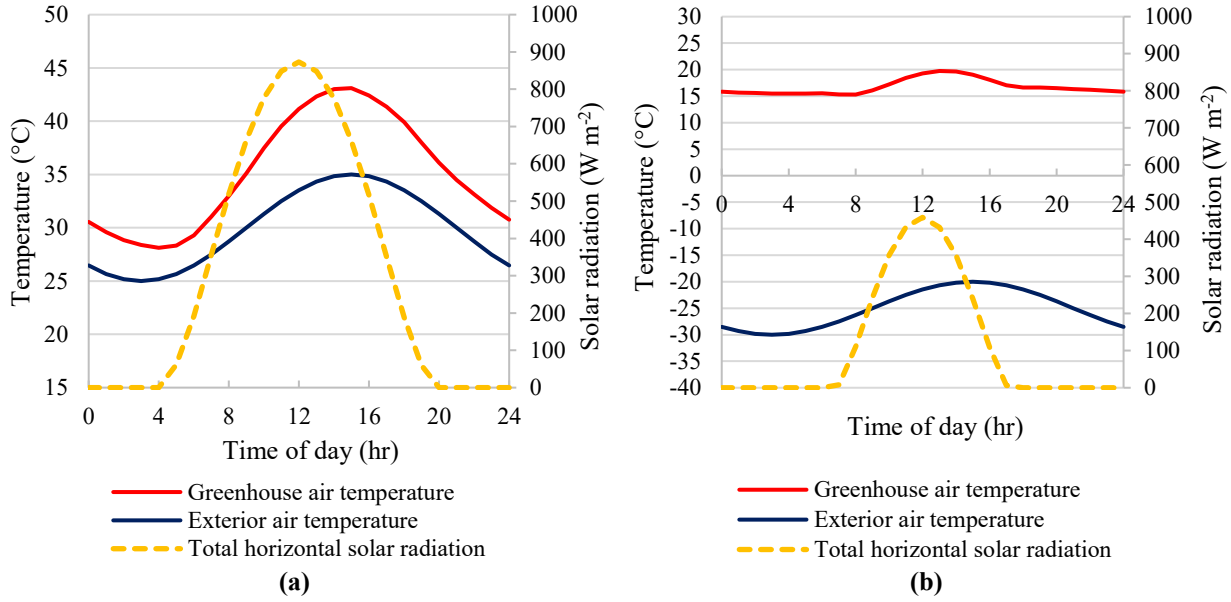

Figure M.5: (a) Daily greenhouse air temperature during peak winter; and (b) summer design conditions.

New greenhouse agriculture area and net energy production

The new greenhouse agriculture area that could be operated from the organic waste's energy is determined by assuming that either all the electrical or thermal power produced would be consumed by the greenhouse during the peak winter design condition. Based on the energy model for the 4,000 m^2 greenhouse, the peak electrical and thermal power demand during the winter design day ($Q_{elec\_m^2}$ and $Q_{thermal\_m^2}$) is 0.17 and 0.20 kW m^{-2}, respectively. The greenhouse area that could be operated with the energy from the organic waste is dictated by either its electrical or thermal power demand and is calculated using the following equation:

$$A_{GH} = \min\left[\frac{Q_{elec\_export}}{Q_{elec\_m^2}}, \frac{Q_{thermal\_export}}{Q_{thermal\_m^2}}\right] \quad \text{(M.5)}$$

Electrical and thermal energy will be available to export to the grid, except during peak winter conditions. In order to determine the amount of energy that could be exported, annual energy simulations for the greenhouse using typical meteorological year data is required. The energy consumed by the greenhouse would vary across Canada, and a representative city for each province was therefore selected for the energy simulations. For each hour of simulation, the electrical and thermal power required to operate the greenhouse area in each province (Q_{GH_elec} and $Q_{GH\_thermal}$) is recorded. The net electrical and thermal energy available for export (E_{elec_net} and $E_{thermal\_net}$) is given by:

$$E_{elec\_net} = \sum_{t=0}^{8760} \Delta t \cdot \left(Q_{elec\_export} - Q_{GH\_elec}\right) \quad \text{(M.6)}$$

$$E_{thermal\_net} = \sum_{t=0}^{8760} \Delta t \cdot \left(Q_{thermal\_export} - Q_{GH\_thermal}\right) \quad \text{(M.7)}$$

Table M.3 shows that 1.12 million m^2 of new greenhouse agriculture area could be operated with the energy produced by the selected organic waste in Canada. The net electrical energy that could be exported to the grid is 1,072 GWh yr^{-1}, and the thermal energy available for district heating would be 2,070 GWh yr^{-1}.

Table M.3: New greenhouse area and net energy production.

Provinces and representative city for energy simulations	New greenhouse agriculture area (m^2)	Net electrical energy production (GWh yr^{-1})	Net thermal energy production (GWh yr^{-1})
Maritimes (Halifax)	51,301	49	96
Quebec (Montreal)	298,920	285	551
Ontario (Toronto)	411,244	393	766
Manitoba (Winnipeg)	45,008	43	79
Saskatchewan (Saskatoon)	47,642	45	84
Alberta (Edmonton)	139,124	133	252
British Columbia (Vancouver)	129,564	124	242
Total	1,122,803	1,072	2,070

M.6 Conclusion

This paper presented a design for the optimal recycling and reuse of organic waste for greenhouse agriculture, while energy modeling and simulations highlight the untapped potential of implementing such technologies across Canada. The co-digestion of municipal organic waste (food scraps and yard waste) and livestock manure would provide energy, carbon dioxide, water and high-quality compost suitable for greenhouse agriculture. The results show that 1.12 million m^2 of new greenhouse agriculture area could be operated in Canada with the energy produced by the recycling of 9.1 million tonnes yr^{-1} of organic wastes. In addition, 1072 GWh yr^{-1} of electrical energy could be exported to the grid, and 2070 GWh $yr^{-1}$of thermal energy would become available for district heating.

This research addresses the imminent problems of food and energy security, while at the same time offering a promising solution to addressing the urgent issues of climate change and local food production. The remainder of Canada's organic wastes that are not considered in this study may be anaerobically co-digested in a similar fashion to reduce human impact on the environment and provide stable and renewable energy infrastructure. The concept of integrating OWR and food production remains a widely unexplored topic, and it is hoped that other researchers and developers will be inspired by this work to advance the science further.